DEVELOPMENT OF AN ELASTO-PLASTIC ANALYTICAL MODEL FOR DESIGN OF GROUTED ROCK BOLTS IN TUNNELS WITH PARTICULAR REFERENCE TO POOR ROCK MASSES

A THESIS SUBMITTED TO
THE GRADUATE SCHOOL OF NATURAL AND APPLIED SCIENCES
OF
MIDDLE EAST TECHNICAL UNIVERSITY

BY

REZA RANGSAZ OSGOUI

IN PARTIAL FULFILLMENT OF THE REQUIREMENTS
FOR
THE DEGREE OF DOCTOR OF PHILOSOPHY
IN
MINING ENGINEERING

JANUARY 2007

Approval of the Graduate School of Natural and Applied Sciences.

Prof. Dr. Canan Özgen
Director

I certify that this thesis satisfies all the requirements as a thesis for the degree of Doctor of Philosophy.

Prof. Dr. Celal Karpuz
Head of Department

This is to certify that we have read this thesis and that in our opinion it is fully adequate, in scope and quality, as a thesis for the degree of Doctor of Philosophy.

Prof. Dr. Celal Karpuz
Supervisor

Examining Committee Members:

Prof. Dr. Hasan Gercek (ZKU, MINE) _____

Prof. Dr. Celal Karpuz (METU, MINE) _____

Prof. Dr. Resat Ulusay (HU, GEO) _____

Assoc.Prof. Dr. Levent Tutluoglu (METU, MINE) _____

Assoc.Prof. Dr. Aydin Bilgin (METU, MINE) _____

I hereby declare that all information in this document has been obtained and presented in accordance with academic rules and ethical conduct. I also declare that, as required by these rules and conduct, I have fully cited and referenced all material and results that are not original to this work.

Name, Last name: REZA RANGSAZ OSGOUI

Signature:

ABSTRACT

DEVELOPMENT OF AN ELASTO-PLASTIC ANALYTICAL MODEL FOR DESIGN OF GROUTED ROCK BOLTS IN TUNNELS WITH PARTICULAR REFERENCE TO POOR ROCK MASSES

Rangsaz Osgoui, Reza

Ph.D., Department of Mining Engineering

Supervisor: Prof. Dr. Celal Karpuz

January, 2007, 223 Pages

The analysis presented in this thesis provides a methodology for grouted bolts design, based on empirical and analytical methods. Hence, the main objectives of this thesis are to offer practical means for better characterisation of poor to very poor rock masses, to better predict support pressure, and to develop an elasto-plastic analytical model for design of grouted bolts in tunnels excavated in such rock masses.

To improve the applicability of the GSI (Geological Strength Index) in poor to very poor rock masses, using Broken Domain Structure (BSTR), Structure Rating (SR), and Intact Core Recovery (ICR), some modifications have been offered, resulting in the Modified-GSI. Applying rock-load height concept and Modified-GSI, an approach to estimate support pressure has been developed. The main advantage of this approach is its applicability in squeezing ground and anisotropic stress conditions. Numerical modelling was carried out in order to adjust the proposed support pressure equation.

Considering convergence reduction approach, an elasto-plastic model based on the latest version of Hoek- Brown failure criterion has been developed for a more effective and practical grouted bolt design. The link between empirical approach and elasto-plastic solution makes it possible to reach more realistic and appropriate bolting pattern design. In this way, the need for the redesign procedure in the convergence reduction approach is eliminated. The results of the proposed elastic-plastic solution have been compared with a numerical model using $FLAC^{2D}$, and a reasonable agreement was observed. The practical application of the developed methodology is depicted by an analysis of a case study in Turkey.

Keywords: Elasto-Plastic Solution, Grouted Rock Bolt Design, Poor Rock Masses, Support Pressure, Tunnelling.

ÖZ

ZAYIF KAYALARDA AÇILAN TÜNELLERDE ÇİMENTOLU KAYA SAPLAMASI TASARIMI İÇİN ELASTO- PLASTİK ANALİTİK BİR MODEL GELİŞTİRİLMESİ

Rangsaz Osgoui, Reza

Doktora, Maden Mühendisliği Bölümü

Tez Yöneticisi: Prof. Dr. Celal Karpuz

Ocak 2007, 223 Sayfa

Bu tezde sunulan analiz; ampirik ve analitik metodlara dayanarak çimentolu kaya saplama tasarımı için bir metodoloji sağlamaktadır. Bu nedenle tezin ana amaçları; zayıf-çok zayıf kaya kütlelerini pratik anlamda daha iyi nitelendirmek, tahkimat basıncını daha iyi tahmin etmek ve bu tip kaya kütlelerinde açılan tünellerde çimentolu kaya saplamalarının tasarımı için elastik-plastik çözümsel bir model geliştirmektir.

Zayıf-çok zayıf kaya kütlelerinde JDİ (Jeolojik Dayanım İndeksi)'nin uygulanabilirliğini geliştirmek için Kırılmış Kaya Yapısı (KYP), Yapısal Puanlama (YP), ve Sağlam Korot Verimi (SKV) parametreleri kullanılarak bazı değişiklikler önerilmiş ve JDİ modifiye edilmiştir. Kaya yükü yüksekliği kavramı ve Modifiye JDİ uygulanarak tahkimat basıncını hesaplamak için bir yaklaşım geliştirilmiştir. Bu yaklaşımın ana avantajı, sıkışmış zemin ve anizotropik gerilme durumlarında uygulanabilir olmasıdır. Önerilen tahkimat basıncı denklemini ayarlamak için sayısal modelleme çalışmaları yapılmıştır.

Konverjans İndirgeme yaklaşımı göz önüne alınarak; Hoek-Brown yenilme kriterinin son durumu esas alınarak, daha etkin çimentolu kaya saplama tasarımını yapabilmek için bir elastik-plastik model geliştirilmiştir. Ampirik yaklaşım ve elastik-plastik çözüm arasında sağlanan bu bağlantı aracılığı ile, daha gerçekçi ve daha uygun kaya saplama tasarımına ulaşmak mümkün olabilmektedir. Böylelikle, konverjans indirgeme yaklaşımındaki tekrar tasarım işlemi ihtiyacı ortadan kalkmaktadır. Önerilen elastik-plastik çözümün sonuçları, FLAC^{2D} kullanarak bulunan sayısal model sonuçları ile karşılaştırılmış ve kabul edilebilir bir uyuşma gözlemlenmiştir. Ayrıca geliştirilen metodoloji, Türkiye'de pratik bir durumda da uygulanmıştır.

Anahtar Kelimeler: Elasik-Plastik Çözüm, Çimentolu Kaya Saplama Tasarımı, Zayıf Kaya Kütlesi, Tahkimat Basıncı, Tünelcilik.

To My Family and in memory of my dear Professor: late Erdal Ünal

IN MEMORY OF MY ESTEEMED PROFESSOR

A great amount of this research work was conducted under the supervision of the Late Professor **Erdal Ünal** at the Middle East Technical University.

Writing in memory of my honored supervisor is unbelievably difficult. How I should present the PhD thesis without who was always supporting me monetarily and spiritually has been an obsession since his missing.

During my PhD curriculum, I had been attracted impression by Professor Ünal and I had been working as his teaching assistant. Not only he was my supervisor but he also was my intimate friend. No time I remember that I was alone when he was alive. In any step of my PhD study and life in Turkey, he always helped endlessly. His guidance, encouragement, and enthusiastic support throughout my graduate program are gratefully appreciated. The most important was that he taught me how to live with humanity.

But for him, this PhD thesis would not have been achieved. I am sure that his soul would be happy for the completion of my PhD thesis.

ACKNOWLEDGEMENTS

I wish to express my sincerest gratitude to Prof. Dr. Celal Karpuz for his kind supervision, invaluable suggestions, friendship and help towards the completion of my dissertation.

I would like to express my sincere appreciation to Assoc. Prof. Dr. Levent Tutluoglu for his steady helps and remarkable contributions during my PhD study period. I was impressed of his effectual rock mechanics courses, of which I learned deeply. His notable contributions in mathematical treatments of elastic-plasticity in Chapter 5 and in doctorate committee have been fully appreciated.

I have to express my appreciation to Prof. Dr. Hasan Gercek for his invaluable suggestions and critical comments on final thesis manuscript and for serving on doctorate committee.

I wish to extend my sincerest gratitude and thanks to Prof. Dr. Resat Ulusay, Assoc. Prof. Dr. Aydin Bilgin for their suggestions, comments guidance and valuable contributions during various stages of the research and for serving on doctorate committee.

My special gratitude and appreciation is extended to Prof. Dr. Sebastiano Pelizza, Prof. Dr. Daniele Peila of the Turin University of Technology (Politecnico di Torino) for their invitation and scholarship for post-graduate study and Prof. Dr. Pierpaolo Oreste for his considerable supervision in numerical modelling in Chapter 6. Also I have to thank Dr. Oggeri for his kindness and help in Italy.

My greatest debt is to Dr. Carlos Carranza-Torres of University of Minnesota for his noticeable suggestions and comments on Chapter 5.

And, I want to thank Acar Insaat A.S. Company for financial support during my work on Malatya Tunnel Project.

I would like to express my heartfelt gratitude to the Mining Engineering Department of METU for given permission to my Post-graduate study in Italy.

I am most grateful to all my fellow graduate students at the Mining Engineering Department for their extreme friendship and understanding since 2001.

I have to express my deepest appreciation to my lovely friends Sinem Sener and Levent Ergene for their endless kindness, support and friendship in Turkey. They treated me like real sister and brother.

A special gratitude must be gone to my real mentor, Arman Kocal who was always found in assistance. Thanks for his help in preparation of the final thesis volumes.

My thanks also go to secretariat and staff of the Mining Engineering Department of METU for their kind-heartedly help and support.

I am grateful to all my mentors in Turkey especially in METU Sport Center and METU Campus for their intimacy, friendship, and sympathy toward me. To whom I confess I love Turkey so much.

Finally, I wish to express my sincere gratitude to my dear family for their continuing love and support. I would not have achieved this goal without their patience, understanding and encouragement. To whom, I dedicate this thesis.

TABLE OF CONTENTS

ABSTRACT iv
ÖZ vi
ACKNOWLEDGEMENTS x
LIST OF TABLES xvi
LIST OF FIGURES xviii
LIST OF SYMBOLS xxiii
INTRODUCTION 1
1.1 General Description 1
1.2 Statement of the Problem 2
1.3 Objective of the Thesis 2
1.4 Procedures used in the Thesis 4
1.5 Organization of the thesis 6
2 LITERATURE SURVEY 7
2.1 Introduction 7
2.2 Grouted bolts 8
2.3 Failure of grouted bolts 9
2.4 Grouted bolts design methods 10
2.4.1 Empirical design methods 10
2.4.2 Analytical design methods 11
2.4.3 Numerical design methods 14
2.5 Summary and backbone of the proposed model 17
3 CHARACTERIZATION OF POOR AND VERY POOR ROCK MASSES USING MODIFIED-GEOLOGICAL STRENGTH INDEX "MODIFIED-GSI" 18
3.1 Introduction 18
3.2 Need for modifying Geological Strength Index (GSI) for poor rock mass 19
3.2.1 GSI development and improvement within last 10 years 19
3.2.2 Deficiency and inadequacy of the existing GSI charts 20
3.2.3 Modification and recuperation of the existing GSI charts 20
3.3 Methods of estimating Modified-GSI for poor and very poor rock masses 23
3.4 Methods of determining the parameters used in empirically proposed approach for characterizing the poor and very poor rock masses 26

3.5 Poor and very poor rock mass geometry indicators used in the Modified-GSI 26
3.5.1 Determination of the parameters associated with degree of jointing (blockiness or interlocking) 27
3.5.1.1 Broken Structural Domain (BSTR) indicator 27
3.5.1.2 Determination of the Rock Quality Designation (RQD) 30
3.5.1.3 Block size (volume) 30
3.5.1.4 Volumetric joint count (J_v) 31
3.5.1.5 Correlation between RQD, J_v and V_b 34
3.5.1.6 Determination of the Structure Rating (SR) 38
3.5.2 Poor and very poor rock mass joint condition indicators 39
3.6 Poor and very poor rock mass strength envelope 41
3.6.1 Hoek - Brown failure criterion 42

4 SUPPORT PRESSURE (ROCK LOAD) ESTIMATION FOR TUNNELS IN POOR AND VERY POOR ROCK MASSES 45

4.1 Introduction 45
4.2 Squeezing-prone ground condition 46
4.2.1 Support pressure and squeezing ground condition 49
4.2.1.1 Empirical approaches 50
4.3 Newly proposed approach 56
4.3.1 Support pressure (rock-load) function 56
4.3.2 Rock- load height concept 58
4.3.3 Geomechanical parameters used in calculating support pressure 61
4.3.3.1 Geological Strength Index (GSI) estimation 61
4.3.3.2 The effect of the disturbance factor 61
4.3.3.3 The effect of intact rock strength 63
4.4 Comparison of the support pressure with the estimates of Barton's Q-system 65
4.5 Analytical and numerical approaches for rock-load height estimates 68
4.5.1 Comparison of the rock-load heights obtained from the proposed empirical approach with those determined by closed-form solutions for circular tunnels 69
4.5.1.1 Plastic zone around a circular tunnel 69
4.5.2 Comparison of the rock-load heights obtained from the proposed approach with those determined by numerical methods for arch-shaped and rectangular tunnels 70
4.5.2.1 Configuration of the numerical models 71
4.5.2.2 Analysis and interpretation of the results 73
4.5.2.3 Correction factor for horizontal to vertical stress ratio 85

5 DEVELOPMENT OF A NEW ANALYTICAL ELASTO-PLASTIC SOLUTION FOR BOTH UNSUPPORTED AND REINFORCED TUNNEL 87

5.1 Introduction 87
5.2 Definition of the problem 88

5.3 Method of solution 88
5.4 Yield criterion 91
5.5 Flow rule of plasticity and the plastic potential 93
5.6 Stresses in the plastic zone 98
5.7 Stresses in the outer elastic zone 100
5.8 Radius of the plastic zone 101
5.9 Strains and displacement analysis 102
5.9.1 Strains in elastic zone 102
5.9.2 Strains in the plastic zone 102
5.9.2.1 Determination of the elastic strains in the plastic zone 103
5.9.2.2 Determination of the plastic strains in the plastic zone 103
5.9.2.3 Radial displacement field 104
5.10 Stress distribution along fully grouted bolts 106
5.11 Influence of bolting on strength parameters and bolt density parameter 108
5.12 Concept of equivalent material approach (equivalent strength parameters) 110
5.13 Rock stabilization through effective material strength parameters 111
5.14 Influence of bolt length on tunnel wall stability 116
5.15 Concept of equivalent plastic zone 117
5.15.1 Determination of the Equivalent Plastic Zone Category I 117
5.15.1.1 Zone 1 : $r_i < r < r_e^*$ 119
5.15.1.2 Zone 2 : $r_e^* < r < \rho$ 119
5.15.1.3 Zone 3 : $\rho < r < (r_i + L_b)$ 120
5.15.1.4 Zone 4 : $r > (r_i + L_b)$ 120
5.15.1.5 Equivalent Plastic Zone (EPZ) 121
5.15.2 Determination of the Equivalent Plastic Zone Category II 121
5.15.3 Determination of the Equivalent Plastic Zone Category III 122
5.16 Practical application of the proposed elasto-plastic solution 123
5.17 Influence of grouted bolts on tunnel stability 128
5.18 The effect of the bolt density on stresses and displacement field 130
5.19 Normalized convergence ratio 132
5.19.1 Normalized convergence ratio as a design tool 133
5.20 Influence of bolt length on tunnel convergence 134
5.21 Use of displacement control (convergence reduction) approach for design 139
5.22 Comparison with empirical design methods 142
5.23 Correlation between Support pressure and rock-bolt density parameter 143
5.24 Summary of advantages of proposed elasto-plastic analytical model and its contribution to the grouted bolts design 148

6 NUMERICAL VERIFICATION OF THE PROPOSED ELASTO-PLASTIC SOLUTION 150

6.1 Introduction 150
6.2 Numerical model of unsupported tunnel 150

6.3 Grouted rock-bolt numerical simulation and numerical model of reinforced tunnel 156
6.3.1 Axial behaviour 157
6.3.2 The shear behaviour of the grout annulus 158
6.3.2.1 Correlation between bond cohesive strength "Sbond" of FLAC and λ of the bolt density parameter of the analytical model 162

7 CRITICAL DISCUSSIONS AND FIELD VERIFICATION OF THE DEVELOPED MODEL 167

7.1 Implication of the Modified-GSI 167
7.2 Implication of the support pressure function 167
7.3 Implication of the proposed elastic-plastic analytical model 169
7.4 Implications of the advancing tunnel face 171
7.5 Implication of numerical modelling 173
7.6 Field verification of proposed empirical and elasto-plastic analytical approaches (A case study: the rock reinforcement design applied to No: 7 Malatya Railroad Tunnel in Turkey) 173
7.6.1 Application of the proposed empirical approach to characterize the rock mass 175
7.6.2 Application of the proposed elasto-plastic model to design of reinforcement 176

8 CONCLUSIONS AND RECOMMENDATIONS 180

REFERENCES 182

APPENDICES

APPENDIX A 195

APPENDIX B 199

Determination of the Equivalent Plastic Zone Category II 199
Zone 1 : $r_i < r < \rho$ 199
Zone 2 : $\rho < r < r_e^*$ 200
Zone 3 : $r_e^* < r < r_i + L_b$ 201
Zone 4 : $r > (r_i + L_b)$ 201
Equivalent Plastic Zone (EPZ) 202
Determination of the Equivalent Plastic Zone Category III 203
Zone 1 : $r_i < r < \rho$ 203
Zone 2 : $\rho < r < (r_i + L_b)$ 204
Zone 3 : $(r_i + L_b) < r < r_e^*$ 205
Zone 4 : $r > r_e^*$ 206
Equivalent Plastic Zone (EPZ) 206

APPENDIX C 209

APPENDIX D 215

CURRICULUM VITAE 222

LIST OF TABLES

Table 3-1 Classification of the block volume related to particle size (volume) and BSTR suggested by Palmström (1995, 2000) and modified for this study. Key: N /A (Not Applicable) 32
Table 3-2 Descriptive terms corresponding to block size and intervals of Jv originally suggested by ISRM (1981) and modified for this thesis study 34
Table 3-3 Joint condition index (Ijc) ratings for using in Modified-GSI 41
Table 3-4 Approximate equations for normalized principal stress relationships of Hoek Brown failure criterion used for poor and very poor rock masses. Key: $\sigma_{1n} = \sigma_1/\sigma_{ci}$, $\sigma_{3n} = \sigma_3/\sigma_{ci}$, and σ_{ci} is the uniaxial compressive strength of the intact rock 44
Table 4-1 Summary of various empirical approaches for support pressure estimation 48
Table 4-2 Terzaghi's rock-load classifications for squeezing ground condition (Terzaghi, 1946) 49
Table 4-3 The degree of squeezing ground condition in terms of the strength factor (Jethwa *et al.*1981), key: σ_{cm} : rock mass strength 51
Table 4-4 The squeezing class of rock mass in terms of strength factor (SF) (Aydan *et al*., 1993, 1996 and Palmström, 1995) 52
Table 4-5 The degree of squeezing ground condition in terms of the strength factor (ISRM, 1981 and Barla, 1995) 52
Table 4-6 The degree of squeezing ground condition (Bhasin & Grimstad 1996) . 53
Table 4-7 The squeezing ground classes in terms of critical strain concept 54
Table 4-8 The degree of squeezing ground condition in terms of strength factor or the competency factor (Palmström, 1995) 55
Table 4-9 Suggested values for squeezing ground condition correction factors (S_q) used in empirical approach (adopted and modified from Hoek & Marinos, 2000 and Singh *et al*. 1997) 56
Table 4-10 Modified guidline for estimating disturbance factor (D), which originally suggested by Hoek *et al.* (2002) 62
Table 4-11 A comparison between support pressure values of Q-system and proposed approach with the specified assumption. 66
Table 4-12 Fixed and variable parameters used in numerical parametric studies .. 73
Table 5-1 Yield and potential functions used in the various tunnel elasto-plastic models. Key : ψ = dilation angle, ϕ = internal friction angle 95
Table 5-2 Input parameters used in the practical example 124
Table 5-3 Input parameters used in this example 130
Table 5-4 Rock mass properties used in the parametric study on influence of grouted bolt length on tunnel convergence, key : ψ=0° 135

Table 5-5 Rock mass properties used in example corresponding to displacement control approach 140
Table 5-6 The influence of bolt density parameter β on tunnel convergence 141
Table 5-7 Recommended grouted bolt densities for a reinforced tunnel of 2.5 m radius for different rock classes (field stress = 15 MPa, grouted bolt diameter = 32 mm), key: the use of bolt couplings for installation of long bolts in small diameter tunnel must be applied 143
Table 5-8 Engineering specifications of grouted bolts (MAI-bolts or Self Drilling Anchor) used in this study (after Atlas Copco, 2004) 145
Table 6-1 The results of pull-out test in different rock mass quality used in the parametric study of FLAC analysis (TUSC, 2006). 161
Table 6-2 Cohesive strength of the grout used in the grouted rock bolts 161
Table C-1 Spreadsheet implementing the proposed elasto-plastic solution 209

LIST OF FIGURES

Figure 1-1 The comparison between methodology of grouted bolt design used in this study and other models 3
Figure 1-2 Methodology for grouted bolts design 5
Figure 2-1 Rheological model of a reinforced jointed rock mass (Pande & Gerrard, 1983) 16
Figure 2-2 Idealized equivalent material property approach (Duan, 1991) 16
Figure 3-1 The original GSI chart introduced by Hoek (1994) and Hoek & Brown (1997). 21
Figure 3-2 An example of existing quantitative GSI charts and its inadequacy in characterizing the poor and very poor rock mass (Cai *et al*. 2003). 22
Figure 3-3 Modified-GSI chart introduced for this study 24
Figure 3-4 Flow chart showing the proposed approach for characterizing poor and very poor rock masses 25
Figure 3-5 Various types of Broken Structural Domain (BSTR), METU's Rock Mechanics Laboratory 28
Figure 3-6 Core-box surveying for No:7 Malatya Railway tunnel project. Various types of BSTR are marked, METU's Rock Mechanics Laboratory, (Osgoui & Ünal, 2005b) 28
Figure 3-7 A typical core-box including BSTR (Palmström, 2005a) 29
Figure 3-8 Various types of BSTR 29
Figure 3-9 The variation of volumetric joint count with the joint density 37
Figure 3-10 The correlation between average number of discontinuities per meter of a scan-line survey (λ_d) and volumetric joint count (Jv) with different approaches. 38
Figure 3-11 The relationship between structure rating (SR) and the Volumetric Joint Count (Jv), suggested in this study. 40
Figure 4-1 New concept for estimation of support pressure in rock tunnels 46
Figure 4-2 The relationship between the strain and strength factor to indicate the degree of squeezing ground condition (Hoek & Marinos, 2000) 54
Figure 4-3 The variation of support pressure as a function of GSI for different roof spans 59
Figure 4-4 Rock-load height concept 60
Figure 4-5 The variation of rock loads (support pressure) as a function of disturbance factor "*D*" for different rock mass classes 62
Figure 4-6 Suggested post- failure characteristics for different quality rock masses by Hoek & Brown (1997) and modified in terms of strength reduction factors in this study 64
Figure 4-7 A comparison between support pressure values of Q-system and proposed approach 67

Figure 4-8 The relationship between Equivalent Rock-load Heights (ERH) and Modified-GSI. Note that the Index R indicates that in some solutions the residual strength parameters were taken into consideration. (Note that some elasto-plastic solutions are overlapped) 70
Figure 4-9 The meshes used for the arch-shaped tunnel by Finite Difference Method (FDM) (below) and Finite Element Method (FEM) (above) in an infinite Hoek- Brown medium. 72
Figure 4-10 Representation of failure height to rock-load height ratio (hf/ht) with in-situ stress ratio (k) for various rock mass quality (GSI) and spans in arch-shaped tunnels 74
Figure 4-11 Representation of failure height to rock-load height ratio (hf/ht) with in-situ stress ratio (k) for various rock mass quality (GSI) and spans in rectangular tunnels 75
Figure 4-12 The variation of rock-load height with stress ratio (k) for an arch-shaped tunnel with width of 10m if GSI=20. As seen, the greater stress ratio (k), the bigger rock-load height expect for k=0.5. 77
Figure 4-13 The variation of rock-load height with stress ratio (k) for a rectangular tunnel with width of 10m if GSI=45. As seen, the greater stress ratio (k), the bigger rock-load height expect for k=0.5. 78
Figure 4-14 A representation showing the decreasing the failure height with improving rock mass quality for an arch-shaped tunnel of 5m wide excavated in a hydrostatic condition of in-situ stress. 79
Figure 4-15 A representation showing the decreasing the failure height with improving rock mass quality for a rectangular tunnel of 5m wide excavated in a hydrostatic condition of in-situ stress. 80
Figure 4-16 The variation of the failure height with roof span for different value of stress ratio (k) for poor rock mass GSI=20 in arch-shaped tunnel. 82
Figure 4-17 The variation of the failure height with roof span for different value of stress ratio (k) for fair rock mass GSI=45 in arched-shape tunnel. 83
Figure 4-18 The variation of the failure height with roof span for different value of stress ratio (k) for good quality rock mass GSI=85 in arch-shaped tunnel. 83
Figure 4-19 The variation of the failure height with roof span for different value of stress ratio (k) for poor rock mass GSI=20 in a rectangular-shaped tunnel. ... 84
Figure 4-20 The variation of the failure height with roof span for different value of stress ratio (k) for fair rock mass GSI=45 in a rectangular shaped tunnel. 84
Figure 4-21 The variation of the failure height with roof span for different value of stress ratio (k) for good quality rock mass GSI=85. 85
Figure 4-22 Suggested value for stress correction factor (C_s) used in proposed formula (h_f: failure height by numerical method, h_t; rock-load height by empirical approach). 86
Figure 5-1 Definition of the model 89
Figure 5-2 Hoek-Brown failure criterion for intact rock (curve a) and rock masses with decreasing values of GSI (curves b and c) (Carranza- Torres, 2004) 92
Figure 5-3 Peak and residual failure envelopes considered for the generalized Hoek-Brown failure criterion for the problem in Figure 5.1 (Carranza- Torres, 2004) 93
Figure 5-4 Hoek-Brown yield function, Mohr-Coulomb plastic potential, and plastic strain increment relationship in this study (Ogawa & Lo, 1987) 97

Figure 5-5 Stress-strain regime for a rock obeying elastic-britlle-plastic behaviour (Brown *et al*. 1983) 98
Figure 5-6 Stress distribution model for grouted bolts (Xueyi, 1983; Indraratna & Kaiser, 1990a) 107
Figure 5-7 Fully reinforced circular excavation and equilibrium considerations for bolt-ground interaction (Indraratna & Kaiser, 1990a) 109
Figure 5-8 Creation of the Equivalent Plastic Zone around the circular tunnel reinforced by grouted bolts, considering equivalent material concept..... 112
Figure 5-9 Variation of the equivalent strength parameter (m*) of Hoek-Brown failure criterion with β..... 113
Figure 5-10 Variation of the equivalent strength parameter (s*) of Hoek-Brown failure criterion with β..... 113
Figure 5-11 Variation of the equivalent compressive strength (σ_{ci}*) with β 114
Figure 5-12 Increase of strength parameters by reinforcing the rock using grouted bolts, considering the equivalent material concept. Key: $\Delta\sigma_3$: confining action of grouted rock bolts in the plastic (post- peak) zone. 114
Figure 5-13 The effect of grouted bolts on the Ground Reaction Curve (GRC) (Indraratna & Kaiser, 1990a ; Oreste, 2003)..... 116
Figure 5-14 Categorization of the extent of the yielding (plastic zone) (Indraratna & Kaiser, 1990a, b) 118
Figure 5-15 Stress field around the unsupported tunnel surface..... 125
Figure 5-16 Distribution of the tangential and radial stresses obtained from the proposed elasto-plastic model and Carranza-Torres' solution (2004) 125
Figure 5-17 Displacement field obtained from the proposed elasto-plastic model and Carranza-Torres' solution (2004) 126
Figure 5-18 Ground Reaction Curve (GRC) of unsupported tunnel (natural ground) based on proposed elastic- plastic model 126
Figure 5-19 Radial and tangential stresses distribution near the reinforced tunnel 127
Figure 5-20 Comparison of the tunnel surface displacement for both unsupported and reinforced tunnel cases 127
Figure 5-21 Ground Reaction Curve (GRC) with and without grouted bolts based on proposed elasto-plastic model 128
Figure 5-22 Influence of field stress on tunnel convergence for different magnitude of the bolt density parameter..... 129
Figure 5-23 Stress field near the tunnel for different value of the bolt density parameter β..... 131
Figure 5-24 Displacement field near the tunnel for different value of the bolt density parameter β 132
Figure 5-25 Variation of tunnel convergence with bolt density parameter for 2 m long grouted bolt 134
Figure 5-26 Variation of the tunnel convergence with bolt density parameter for grouted bolts of 1.5 and 3m (Case A) 137
Figure 5-27 Variation of the tunnel convergence with bolt density parameter for grouted bolts of 1.8 and 4m (Case B)..... 138

Figure 5-28 Variation of the bolt density parameter with support pressure (rock load) for different types of grouted bolts in terms of their yield capacity and diameter 145
Figure 5-29 Correlation between the bolt density parameter and support pressure for a tunnel of 2.5 m radius excavated in relatively poor to very poor rock mass (GSI < 40) and undergoing a very high squeezing, $\frac{c_h}{\sigma_v} = 1.5$ 146
Figure 5-30 An informative sketch highlighting the variation of the bolt density parameter β with the square configuration of the bolting of a 2.5m width tunnel with respect to different bolt diameter. The hatched area denotes that the bolting pattern is not practical and economical. 147
Figure 6-1 Model for FLAC analysis of a circular tunnel in an infinite Hoek-Brown medium (quarter symmetry model) 151
Figure 6-2 Quadratic Finite Difference Model adopted in the FLAC 2-D analysis with grid 120 * 120 153
Figure 6-3 Tangential and radial stress filed result from the analytical and numerical methods 154
Figure 6-4 Displacement filed stems from the analytical and numerical methods 154
Figure 6-5 The variation of the displacements with different values of Hoek - Brown constant (*a*). 155
Figure 6-6 Numerical model of reinforced circular tunnel- quarter symmetrical model 157
Figure 6-7 Nomenclature for beam elements (Itasca, 2000) 158
Figure 6-8 Conceptual mechanical representation of fully bonded reinforcement which accounts for shear behaviour of the grout annulus (Itasca, 2000) 159
Figure 6-9 Grout material behaviour for grouted bolts (Itasca, 2000) 160
Figure 6-10 Analytically and numerically calculated tangential and radial stress around the bolted tunnel with different values of grout shear stiffness and bond strength. The stress field of model 2 and analytical solution are to a certain extent compatible. 164
Figure 6-11 Stresses distribution around the bolted tunnel from both analytical and numerical methods 164
Figure 6-12 Analytically and numerically calculated displacement around the bolted tunnel with different values of grout shear stiffness and bond strength. The displacement field of model 2 and analytical solution are well-matched. 165
Figure 6-13 Displacements distribution around the bolted tunnel from both analytical and numerical methods 166
Figure 7-1 Computational steps of the developed model for design of grouted bolts in this thesis 168
Figure 7-2 Profile of radial displacements u_r for an unsupported tunnel in the vicinity of the tunnel face (Osgoui, 2006b). This deformation profile was drawn based on input parameters given in Table 5-2. The upper figure was reproduced from Carranza- Torres & Fairhurst (2000). 172
Figure 7-3 Huge collapse as a result of remarkable amount of convergence in squeezing ground condition in Malatya Railroad Tunnel 174
Figure 7-4 Grouted bolts configuration in Malatya Tunnel 177

Figure 7-5 Predicted tangential and radial stresses around the Malatya Tunnel in both natural and reinforced cases. The radius of yielding for both unsupported and reinforced cases is indicated. 178
Figure 7-6 Predicted displacement (convergence) around the Malatya Tunnel in the absence and presence of grouted bolts 178
Figure A-1 The function $f(x)$ (in blue) is approximated by a quadratic function $P(x)$ (Waner & Costenoble, 2006) 198

LIST OF SYMBOLS

BSTR = Broken Structural Domain

EPZ = Equivalent Plastic Zone

ERH =Equivalent Rock-load Height

FOS = Factor Of Safety

GSI = Geological Strength Index of Hoek-Brown

ICR =Intact Core Recovery

Kbond = grout shear stiffness

Modified - GSI = Modified Geological Strength Index

NATM = New Austrian Tunnelling Method

Q - system = Barton's Rock Quality Index

RMR = Bieniawski's Rock Mass Rating

RQD = Rock Quality Designation

Sbond = cohesive strength of the grout

SF = Strength Factor

SI = normalized tunnel closure

SR = Structure Rating

A = rock bolt cross-section area

a = strength constant of Hoek-Brown failure criterion

a' = residual strength constant of Hoek-Brown failure criterion

B = opening span

C_b = bolt yield capacity

C_g = grout bond cohesive strength in pull-out test

C_m = cohesive strength of the rock mass around the bolt

C_m^* = equivalent cohesion of rock mass

C_s = correction factor for stress ratio

D = disturbance factor

D_{ij}^e = elastic deviatoric strain component

D_n =estimated number of discontinuity sets

d = bolt diameter

E = Young's (elasticity) modulus

F_s = shear force developed in the grout

$F(c)$ = yield function

G = shear modulus

H = tunnel depth below surface

H_q =critical depth for squeezing ground condition

h_f = failure height

h_t = rock-load height

I_{jc} = joint condition index

J_v =volumetric joint count

K = bulk modulus

k =stress ratio

L_b = bolt length

L_d =scanline length

m_i = strength constant of Hoek-Brown failure criterion for intact rock

m_b = strength constant of Hoek-Brown failure criterion

m_b' = residual strength constant of Hoek-Brown failure criterion

m_b^* = equivalent strength constant of Hoek-Brown failure criterion

N_d = number of discontinuities along a scanline

N_ψ = dilation coefficient

P = support pressure (rock load, rock pressure, support load density)

P_i = fictitious support pressure

P_o = far field stress

Q_s =axial load distribution along grouted bolt

$Q(c)$ = plastic potential

r = distance from tunnel center to point of interest

r_b = bolt radius

r_e = radius of plastic (broken, yielding) zone

r_e^* = radius of Equivalent Plastic Zone (EPZ)

r_i = tunnel radius

S_b =average size of block or rock pieces

S_L = longitudinal bolt spacing

S_q = correction factor for squeezing ground condition

S_r =post-peak strength reduction factor

S_s = equal spacing of the square bolting pattern

S_T = transversal (circumferential) bolt spacing

s = strength constant of Hoek-Brown failure criterion

s' = residual strength constant of Hoek-Brown failure criterion

s^* = equivalent strength constant of Hoek-Brown failure criterion

T = tensile force applied in pull-out test

T_m = mean force along bolt

t_f = joint filling thickness

u_b = displacement of the bolt in the pull-out test

u_e =elastic tunnel displacement (convergence)

u_m = displacement at the host rock around the bolt in pull-out test

u_o = initial displacement occurs before bolting

u_r = radial displacement

u_{ri} = displacement (convergence) of unsupported tunnel

u_{ri}^* = displacement (convergence) of reinforced tunnel

u_θ = tangential displacement

u_{ri}^* / u_{ri} = normalized convergence ratio

V_b = block volume

W = opening width

W_c =weathering class

β = bolt density parameter

β_b = block shape factor

$\Delta\sigma_3$ =confining stress due to grouted bolt effect

Δ^e = elastic volumetric component

ΔF^s =incremental axial force in grouted bolt

γ = rock mass unit weight

$\gamma_{r\theta}$ =shear strain in axi-symmetric problem

δ_{ij} = kronecker's delta

ε_1 = maximum principal strain

ε_3 =minimum principal strain

ε_r = radial strain

ε_θ =tangential strain

ε^e =elastic strain

ε^p =plastic strain

ε_θ^t = total tangential strain

ε_θ^e = elastic tangential strain

ε_θ^p = plastic tangential strain

ε_r^e = elastic radial strain

ε_r^p = plastic radial strain

ε_r^t = total radial strain

ε_θ^e = elastic tangential strain increment

ε_θ^p = plastic tangential strain increment

ε_θ^t = total tangential strain

$\dot{\varepsilon}^p{}_{ij}$ = incremental plastic strain in flow rule

λ = friction factor for bolt - grout interface

λ_d =average number of discontinuities counted along a scanline

λ_f = non-negative constant of proportionality in flow rule

ν = Poisson's ratio

ρ = radius of the neutral point of the bolt

σ_1 = maximum principal stress

σ_3 = minimum principal stress

σ_{cm} = unconfined uniaxial rock mass strength

σ_{ci} = uniaxial compressive strength of intact rock

c'_{ci} = residual compressive strength of intact rock

σ_{ci}^{*} = equivalent strength of intact rock

c_h =horizontal in-situ stress

c_v = vertical in-situ stress

c_r = radial stress

c_θ = tangential stress

c_{re} = radial stress at elastic-plastic interface

$c_{\theta e}$ = tangential stress at elastic-plastic interface

c'_{ij} = deviatoric stress component

c_o = volumetric stress component

c_s = axial stress distribution along the bolt

c_{cg} = uniaxial compressive strength of the grout

$\tau_{\lim it}$ = critical shear strength of the grout in pull-out test

τ_{peak} = peak shear strength of the grout in pull-out test

τ_s = shear stress distribution along a grouted bolt

$\tau_{r\theta}$ =shear strain in axi-symmetric problem

φ_m = internal friction angle of the host rock mass in pull-out test

φ_m^{*} = equivalent internal friction angle of the rock mass

φ_g = internal friction angle of grout

ϕ = internal friction angle of rock

ϕ_h = borehole diameter

ψ = dilatancy angle of rock

CHAPTER 1

INTRODUCTION

1.1 General Description

The main objective of any reinforcement system should be to assist the rock mass in supporting itself by building a ground arch and by increasing the strength of the rock mass. Rock bolts can be classified as active or passive. In active rock bolts, a pre-specified load is applied to the rock surface during installation. Tensioned bolts fall into this category. Active bolts are most useful for reinforcing loosened and detached blocks in non-yielding ground to withstand gravity loads. They cannot be activated by ground displacements.

Passive and untentioned grouted bolts develop load as the rock mass deforms. Small displacements are normally sufficient to mobilize axial bolt tension by shear stress transmission from the rock mass to the bolt surface. Grouted bolts are not required to be pre-loaded and regarded as the passive support means if not preloaded. Grouted bolts have been successfully applied in wide range of rock mass quality especially in poor rock mass and found to be often more economical and more effective than active rock bolts. Owing to their grouting effect on improvement of rock mass, grouted rock-bolts have been widely used in tunnelling under difficult ground condition. They are also widely used in mining for the stabilization of roadways, and permanent tunnels. Simplicity of installation, versatility and lower cost of rebars are the further benefits of grouted bolts in comparison to their alternative counterparts.

Grouted rock-bolts become an integral part of the rock mass, thereby restricting the rock mass displacements by internal strengthening. Another function of grouted rock-bolts is ground reinforcement action. Accompanied with injection, grouted rock bolting can be considered as a ground improvement option, whereby the shear strength of the poor quality rock mass can be raised to such an extent that considerable decreases in plastic zone and convergence of tunnel are recorded. Hence, grouted rock bolting is a means capable of modifying the convergence-confinement curve and modifying the value of the radial displacement at the moment of installing the final lining.

In these days, the applicability of the grouted rock bolts has been successfully put into practice in conventional tunnelling methods. However, the use of the grouted rock-bolts has been attracted plausible acceptance in mechanized tunnelling. The use of the transversely installed grouted bolts in open-type TBMs and longitudinally installed ahead of the face in shielded-TBMs has been broadly practiced.

1.2 Statement of the Problem

"The influence of the grouted bolts in improving of the yielded zone around opening has not been clearly understood." Hoek & Brown (1980b).

As is evident from the quotation above, in spite of many achievements made so far, there are still some uncertainties and inconveniences in rock-bolt and rock mass interaction concept, which have to be overcome. Especially, in poor rock masses, undergoing considerable amount of convergence and asqueezing, the effect of the grouted rock-bolts on improving the rock mass and on stability of the openings has not been intuitively recognized. Consequently, an in-depth understanding on the mechanism on how grouted rock-bolts work and improve such a poor rock mass is of great importance.

The reason for difficulty in poor rock mass bolting is believed to be due to complexity of deformational mechanism of such a rock mass, which suggests that a great extent of care has to be taken to model the interaction of rock-bolts and poor to very poor rock masses. When overstressed, poor rock masses undergo plastic failure and radial inward displacement on the opening periphery. This phenomenon is called tunnel convergence (closure). The question here is how the systematically radial grouted rock-bolts can improve the already yielding around the tunnel and how they decrease and control the tunnel convergence?

Even though empirical design methods based on rock mass classification system have been widely used in throughout the whole world, there are stills lots of uncertainties and critics toward them. This is due to the fact that empirical design methods are to some degree inflexible in selecting support systems and they may not provide a sufficiently sensitive guide to properly design the grouted bolts especially for poor rock masses.

1.3 Objective of the Thesis

The objective of this study is to develop an easy, quick, and practical way for reliable design of the grouted bolts without need for numerical techniques. For temporary support design, some engineers rely only on using empirical method while some believe in analytical solutions (elasto-plastic).The developed methodology combines both analytical and empirical approaches to satisfy both concepts.

The main objective of this thesis is to overcome the drawbacks of other models as listed:

I. Complexity and uncertainties in existing rock-bolt and rock mass interaction approaches;
II. Unreliability and inflexibility of the empirical-based design method such as RMR and Q- System, especially in poor quality rock mass;
III. Most recent grouted bolt design methods model the rock bolt and rock independently;
IV. Most of the existing grouted bolt design methods are based on coupling behavior only along the interfaces of bolt itself- grout- host rock; rather than the actual global effect of the bolt on rock mass behaviour as shown in Figure 1-1.
V. For the sake of simplicity, most of the rock-support interaction approaches only take account of the mechanical bolts in their analysis to draw the support confinement curve even if they used grouted bolts;
VI. Most of the present models cannot imply the extent at which ground reaction curve for a reinforced tunnel can be modified as grouted bolts act dependently with rock mass and they become an integral part of deforming rock mass;
VII. Most approaches use numerical techniques to investigate the effect of the grouted bolts on rock mass and the stresses and displacements around the opening.

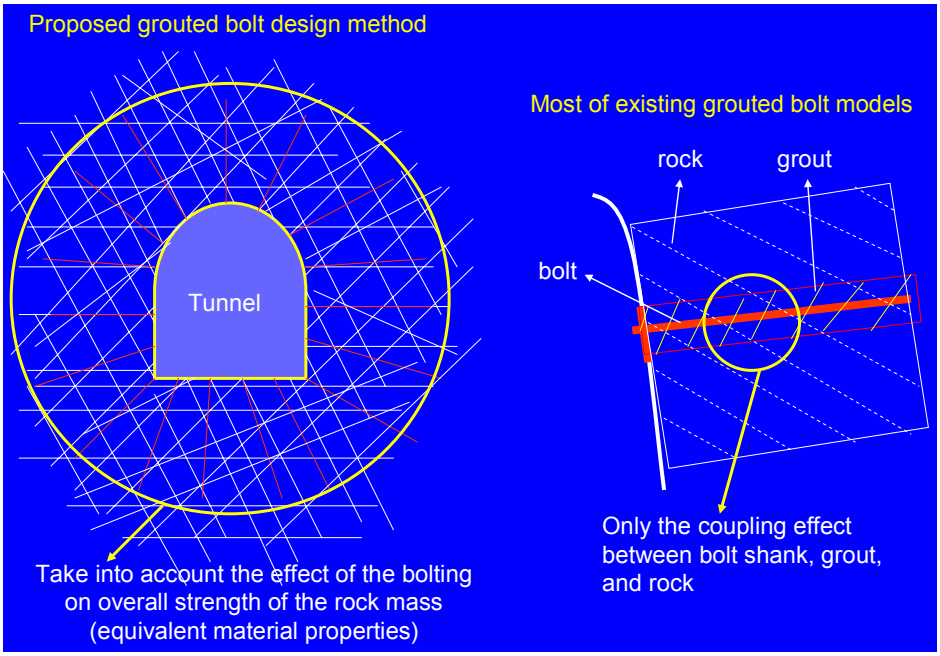

Figure 1-1 The comparison between methodology of grouted bolt design used in this study and other models

Developing a practical way for the design of grouted bolts in poor rock masses firstly lies in characterizing poor rock mass appropriately. The resulting information could be considered as the important input data for the subsequent stages of design procedure, either analytical solution or numerical model. Modified-GSI is regarded as the significant indicator of unfortunate rock mass, which can be then used in estimating rock-load height, support pressure (rock-load), and in elasto-plastic numerical model of the bolted tunnel, thereby culminating in achieving realistic results. By doing these step by step, a methodology for grouted rock-bolt design will be achieved in such a manner that it would embrace both empirical and analytical design methods.

1.4 Procedures used in the Thesis

"Displacement monitoring plays a significant role in the observational (design-as-you-go) approach in tunnelling. In particular, tunnel convergence can be considered as a primary field measurement, because it is not only a readily recordable indicator of the overall ground response, but also its magnitude constitutes a very useful parameter for the evaluation of tunnel stability. Also, it is often not dominated by localized processes like localized rock mass failure. Consequently, the control of convergence can be considered as a key component for the design of underground excavations. Effectiveness of rock-bolts can be, in practice, best assessed in terms of convergence control (reductions)." (Indraratna & Kaiser, 1990b).

The above quotation indicates the importance of convergence control in stability of tunnels. Therefore, an appropriate rock bolt system for reinforcing an opening cannot be achieved unless an alternative method based on convergence control is utulized. The methodology presented in this thesis constitutes an extension of the application of elasto-plasticity in tandem with empirical approach for the design of grouted bolts in tunnels as illustrated in Figure 1-2. It provides an alternative method based on a convergence control approach.

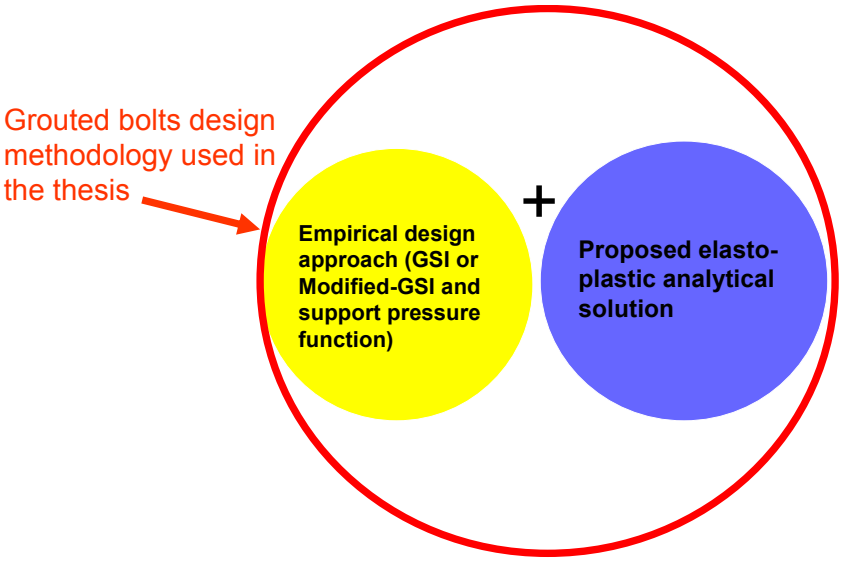

Figure 1-2 Methodology for grouted bolts design

The proposed analytical model considers the influence of bolt-ground interaction, opening size and the bolting pattern on plastic zone and the tunnel convergence. The concept of equivalent material properties (equivalent strength parameters) was defined to describe that the Hoek- Brown residual strength parameters (m_b', s', σ_{ci}', and *a'*) of yielding zone around the tunnel can be uniformly increased due to the effect of grouted bolts. Three categories of yield propagation have been defined and analyzed with respect to the relative location of the plastic zone boundary in contrast to the neutral point of zero shear stress on the bolt. The bolt density parameter (β), a dimensionless quantity that relates friction along the bolt surface, the bolt diameter, the tunnel radius, and the longitudinal and tangential (circumferential) bolt spacing, is incorporated with support pressure to link between the analytical and empirical design approaches and to find the first estimation of the bolt density parameter. It also makes it possible to depict a systematic rock-bolts design for non-circular tunnel shapes.

In order to verify the analytical predictions for both un-reinforced and reinforced tunnels, numerical modelling has been performed with illustrative examples using FLAC^{2D} codes. For simulation of the shear stiffness and cohesive strength of the grout, the typical results of pull-out tests have been used in parametric analysis of FLAC^{2D}. The effect of contrast in stiffness between the rock mass, the grout, and the steel have been also studied to correlate the results. The stresses, displacements, and yielding obtained from the FLAC^{2D} have been compared with those predictions of the developed analytical approach and a good agreement between the results have been observed.

The proposed analytical solution is capable of predicting the ultimate tunnel convergence (at least two tunnel diameters behind the face), where three-dimensional face effects are ignored. It is assumed that the excavated tunnel face is

immediately supported by fully grouted bolts, such that the time-dependent behaviour and loosening can be neglected.

1.5 Organization of the thesis

The scope of this thesis is to examine, both analytically and numerically, the effect of the radial passive rock bolting on a circular tunnel in terms of convergence.

Following the introductory chapter, a comprehensive literature survey on elasto-plastic solutions of tunnels in conjunction with the grouted rock bolts design is presented in Chapter 2. It briefly introduces analytical and numerical approaches of rock-bolt design which have been developed until now.

Chapter 3 provides a new approach to characterize poor and very poor rock masses. Supplemented by some modifications and amendments, the Modified-GSI takes the advantage of utilizing the parameters defining the degree of jointing (degree of blockiness) and discontinuity surface conditions. In order to assist the newly proposed approach, the Broken Structure Domain (BSTR) and Intact Core Recovery (ICR) indicators were defined and embedded into the proposed approach.

In Chapter 4, an empirical approach to estimate the support pressure in tunnels is elucidated. By means of the concept of rock-load height and Modified- GSI, an approach to estimate the support pressure (rock load) for tunnels, especially in poor rock mass, was developed. This approach takes into consideration almost all effective factors on rock-load; namely, the quality of rock mass, the size of opening, the effect of the anisotropy in field stress, the squeezing ground condition, the post-failure behaviour of rock, and the type of excavating.

Chapter 5 deals with the development of the analytical elasto-plastic solution for both unsupported and reinforced tunnel excavated in rock mass that satisfies the latest version of the Hoek-Brown failure criterion proposed in 2002. Firstly, an elasto-plastic solution for the axi-symmetrical problem of an unsupported circular tunnel was developed in order to determine the stresses, displacements, and yielding (plastic) zone. In case of tunnel reinforced by grouted bolts, the proposed model provides the equivalent strength parameter approach based on convergence control. It considers the influence of bolt-ground interaction, tunnel geometry and the pattern of bolts on plastic zone and the tunnel convergence. The introduction of the equivalent plastic zone associated with bolted tunnel is explained and examined in terms of the different magnitude of bolt density parameters and bolt lengths.

In Chapter 6, the results of the analytical model were compared with those from numerical modelling and a reasonable agreement was achieved.

An in depth and critical review of the proposed approach is made in Chapter 7. In addition, the field verification of developed elasto-plastic analytical model and of the proposed empirical approach has been achieved by a practical application in Malatya railroad tunnel in Turkey.

The major conclusions drawn from this research along with the recommendations for further research are summarized in Chapter 8.

CHAPTER 2

LITERATURE SURVEY

Although rock mass reinforcement techniques such as by means of grouted bolts are widespread all over the world, their reinforcement effect has not been fully understood. It is due to complex interaction between grouted bolts and rock mass. The objective of this chapter is to review the general aspects of grouted bolts in conjunction with its reinforcement effect on rock mass using elasto-plastic solutions that have been introduced until now.

2.1 Introduction

The main objective of any support system in an underground opening should be to assist the rock mass in supporting itself by building ground arch and by mobilizing the optimum shear strength of the rock.

In the last decades, due to its effectiveness and flexibility in quite a large variety of geotechnical conditions, rock-bolting has become one of the most dominant support methods in underground constructions, including mining as well as civil engineering applications. If designed properly, openings reinforced by rock-bolts are typically very safe and cost-effective. Structures reinforced by bolts are typically very reliable and long lasting. A variety of bolt types have been developed in order to meet the support needs of different geological and geotechnical conditions together with economical limits. However, due to their effectiveness in poor rock masses, grouted bolts act as an integral part of the rock mass, thereby restricting the rock mass displacement by internal strengthening.

Broadly speaking, laboratory and field experiences, empirical methods based on rock mass classification systems, analytical methods based on rock-support interaction concept (convergence-confinement approach) in tandem with elasto-plastic analysis, and performance assessment are three main methods of designing an effective rock-bolts system. Numerical methods, on the other hand, are capable of modelling those approaches, thereby verifying the reliability of them.

Despite significant progresses, a rational basis for all bolting system designs has not been fully achieved yet. Fortunately, the successful and unsuccessful bolting practices of the last 50 years provide abundant empirical experiences for rock-bolt utilization. Today, more effective bolting systems are being designed by combining of empirical and analytical methods with appropriate amount of case study data.

However, most of them suffer from exact modelling of the bolted rock mass in terms of its degree of improvement. Nevertheless, it is sometimes appropriate to take advantage of numerical approach in rock bolt design. Not only numerical methods do carry out a precise and large-scaled modelling of the real bolting situation but they can also verify the accuracy of analytical models.

2.2 Grouted bolts

Fully grouted bolts are regarded as the passive type of reinforcement action and are most suitable in poor or fractured rock (soft ground) where mechanical anchorage is unsatisfactory. The other main advantage of the grouted bolts is that if local yielding occurs at a position along the bolt length, total failure is prevented since the remaining intact parts will still carry load.

Grouting serves three major purposes (Littlejohn & Bruce, 1975):

I. It bonds the bolt shank to the surrounding ground making the bolt an integral part of the rock mass itself

II. The grout acts as a protective cover for the bolt and prevents or reduces corrosion, and

III. Low viscosity grouts can penetrate cracks that surround the drill hole and improve the rock mass further.

The efficiency of the grouted bolt depends on the shear strength of the bolt-grout interface and the grout-ground interface. Threaded rebar provides an excellent bond with most grout, and cement grouts and organic resin grouts establish a strong bond with most rocks.

In general, most grouts are cement-water based. They should not contain ions that may lead to either corrosion of bolts or deterioration of the cement grout. Grouts must have reasonable workability for efficient injection into drill holes. However, too much water contents may result in excessive shrinkage and reduced strength. Very fine sand or fly ash can be added to reduce shrinkage and increase plasticity. Fluidifiers and retarders are used to maintain workability especially in deep drill holes. Accelerators are used for rapid setting time under unfavorable groundwater conditions. The use of fluidifiers, air entraining agents and anti-bleed agents can effectively reduce the required water content for a given workability, thus producing a higher strength grout although at a higher cost (Littlejohn & Bruce, 1975). A typical mix composition of a cement grout (by weight) my consist of 55 % of Portland cement, 19-22 % of water and a fine sand content of 20 -22 % (water / cement ratio of 0.35 – 0.40). Grouting pressure is generally related to the type of rock mass, inclination and depth of drill holes. Minimum pressure (0.2 MPa) is more than sufficient for 3-5 m drill holes in intact rock but is required for bolting in fractured rock. Grouting pressure must be carefully selected to avoid hydraulic fracture of rock, and for many types of rock they may typically lie in the range 0.3 – 0.7 MPa (Littlejohn & Bruce, 1975).

More recently, the self drilling anchors (MAI-bolts), fully threaded steel bar that can penetrate rock and then be grouted, have been introduced (Atlas Copco, 2004).

These types of grouted bolts are suitable for all types of rock masses especially for poor and very poor rock mass because drill holes are usually closed before installing the bolts and the injection make the ground improved. Using this type of bolts prevents hole collapse and exempts hole from casing.

In brief, the important advantages of using fully grouted bolts are summarized below.

I. In all ground types, grouted anchorage can be ensured.

II. In grouted bolts, the effective bond or anchorage length is equal to the bolt length.

III. Grouted bolts transmit shear stresses much more effectively in both lateral and axial directions, and have a greater axial, bending and shear stiffness. Once activated, they are more effective than other bolts and also are more resistant to shock loads from blasting and earthquakes.

IV. Fully grouted bolts are more resistant to corrosion. In addition, the penetration of grout into cracks reduces permeability and discourages weathering or rock alteration processes in the surrounding rock.

V. Grouted rock bolts act as an integral part of rock mass, improving its strength parameters.

2.3 Failure of grouted bolts

Insufficient grout around bolt shank can result in a reduction of the bolt load capacity and this is a major cause for occasional failure of bolted rock. Accordingly, failure of a few bolts due to poor anchorage can lead to excessive load transfer to the adjacent bolts, sometimes leading to progressive loosening, breaking and bending of bolts. Consequently, the pull-out tests must be performed randomly to assess the anchorage efficiently of the grouted bolts.

There are several ways in which a fully grouted bolt can malfunction (Littlejohn & Bruce, 1975):

I. Yielding of the bolt itself

II. Failure along the bolt - grout interface

III. Fracture within the grout annulus, and

IV. Failure along the grout - rock interface

Yielding of the bolt occurs when the maximum tensile stress at any position along the bolt exceeds the yield stress of steel. If the shear stress developed along the bolt surface exceeds the bond strength (adhesion), pull-out of the bolts occurs as generally observed in the case of smooth rebars. Such failure can be restricted or delayed by profiled bolt surface.

Fracture of the grout annulus or failure along the grout- rock interface can be regarded as premature, if the load capacity of the bolt itself and the bond strength of the bolt-grout interface have not been reached. Excessive shrinkage cracking, high porosity and retarded strength development are some factors responsible for accelerated fracture propagation in the grout annulus. Impaired adhesion at the grout- rock interface can often be the result of inadequately cleaned boreholes, excessively smooth borehole walls or softened rock due to rock alteration.

2.4 Grouted bolts design methods

Modelling the grouted bolts within the rock mass (modelling the reinforcement effect) is a challenging task which is still under development. Different researchers have chosen various approaches to overcome this problem. The challenge comes mainly from finding a practical way to model the actual interaction and effect of grouted bolts inside the rock mass. Nonetheless, a wide range of approaches for reinforcement design has evolved, varying from simple empirical methods to more complex analytical and numerical techniques. In the following sections, the available bolt design methods, which can be classified into three main categories, namely empirical, analytical, and numerical, will be briefly reviewed.

2.4.1 Empirical design methods

In these methods, the suggested bolting patterns are based on other bolting patterns that have been successfully practiced in other cases. Rock mass classification systems such as Bieniawski's RMR (Bieniawski, 1973, 1989) and Barton's Q-system (Barton *et al.* 1974; Grimstad & Barton, 1993) are the main examples of empirical design methods.

The Q-system is such as an empirical method originally based on roughly 200 case records, and therefore, can be conservative. It reflects traditional support methods for advanced tunnel construction technique, which are not always the optimal ones. The Q-system recommends mainly the use of tensioned bolts for poorer rock qualities and intentioned bolts only for good and very good rock. However, in Q-system, for many ground categories, particularly in poor, yielding rock it does not generally recommend the installation of intentioned grouted bolt or Swellex® bolt. The RMR, on the other hand, is applicable to fully grouted bolts in all types of rock. Nonetheless, in poor and yielding rock masses, the RMR system may not provide a sufficiently sensitive guide to appropriately design the grouted bolts in such rock masses. In a recent paper, Palmström and Broch (2006) discuss the uses and misuses of classification systems in great detail. In their conclusion they state:

"Classification systems, and not least the Q-system, may be useful tools for estimating the need for tunnel support at the planning stage, particularly for tunnels in hard and jointed rock masses without overstressing. There are, however, a number of restrictions that should be applied if and when the system is going to be used in other rock masses and in complicated ground conditions. So far such restrictions have not been much discussed in available literature. In this paper a critical evaluation of the parameters that make up the system is carried out.

Potential users of the Q-system should carefully study the limitations of this system as well as other classification systems they may want to apply, before taking them into use." (Palmström and Broch, 2006)

With reference to this important quotation, the need for an alternative reinforcement design method is of great concern. Consequently, this thesis study aims at providing a flexible and practical means for grouted bolt design that can be very useful at the first stage of tunnel design.

2.4.2 Analytical design methods

Analytical axi-symmetric models determining the stresses and deformations around the opening are widely used in the design of tunnel reinforcement due to the computational simplicity. In recent years, their application in designing the reinforcement systems has attracted more interest for researchers. Many analytical formulations based on simple elasticity or elasto-plasticity theory have been developed for the calculation of the ground characteristic curve (convergence-confinement method) and a number of models based on either the Mohr-Coulomb or the Hoek-Brown strength criteria with elastic-perfectly plastic, elastic-brittle plastic, and strain softening material behaviour have been developed. Associated or non-associated flow rules of plasticity are taken into account for determination of the incremental plastic stains in those solutions. Each elasto-plastic problem can be solved either explicitly or implicitly. The former and the latter are termed closed-form (exact) or numerical (approximate) solutions, respectively. A detailed overview of the models proposed in technical literature has been comprehensively presented by Brown *et al.* (1983).

One of the earliest attempts to model the effect of the bolts in stabilizing opening dates back to McNiven & Ewoldsen (1969), who introduced a theoretical approach to model the effect of the singular mechanical rock bolt installed in a circular horizontal tunnel driven in a isotropically elastic and homogeneous material. A pattern of bolts generates a new stress field around the opening that are additive to the present state of stress around the excavation due to far field stresses. The objective of bolting would fall in the fact that the resultant state of stress would be less than the ultimate strength of the rock.

To model one-dimensional resin grouted anchor, Farmer (1975) found a theoretical solution to a circular elastic anchor surrounded by an elastic grout confined by a rigid borehole. He derived a homogeneous linear differential equation describing the distribution of force along the anchor. The decay function is exponential in form. The results of pull-out tests on concrete, limestone and chalk showed good correlation for low axial loads in concrete, but in the weaker limestone and chalk the results were different. The discrepancies could have been ascribed to the lack of a comprehensive model to account for the effect of slip at bolt-grout interface.

Adali & Rosel (1980) introduced an axi-symmetrical elastic model for grouted bolts design in mine tunnels. Unlike elasto-plastic analyses, this model was based on concept implying that the rock mass around the tunnel are only divided into two zones with pure elastic properties.

Papanastassopoulou (1983) developed an analytical approach to model fully grouted bolts installed in arbitrary shaped openings excavated in a homogeneous, isotropic, linearly elastic medium. The assumption of linear shear stress distribution along bolt was another major weakness of this model.

A more realistic analytical treatment of Framer's work was presented by Aydan *et al.* (1985). Although still assuming that the bolt was elastic, an idealized elastic-plastic with strain softening behaviour was adopted for the bolt-grout interface. The results of solving the differential equations for each of the three zones agreed well with the finite element analysis obtained by Hollingshead (1971). In a further development, Aydan (1989) took into account the assumption of an elastic bolt by assuming a bi-linear elasto-plastic behaviour for the bolt and elastic-softening residual plastic behaviour for the grout and rock.

Stille (1983) and Stille *et al.* (1989) presented a closed-form elasto-plastic solution of grouted rock bolts by considering four different approaches of bolt performance which, even though introducing some simplifying assumptions, have proved to be in good agreement with measured data. In these approaches, the analysis of ground reaction curve for a reinforced rock mass with grouted bolts was considered. The region around the tunnel was divided into elastic and plastic zones and an elastic-perfectly plastic behaviour was assumed for bolts. An elasto-plastic rock mass with linear Mohr-Coulomb failure criterion was assumed. The strain in the bolt was assumed to be the same as that of rock and the stiffness of rock mass was modified to allow for bolting. In the plastic rock region, the bolt can yield under high axial strain and the grout can also deform plastically. This work is limited to circular opening under hydrostatic state of stress. Besides, the assumption of perfect bonding in the elastic bolt region and linear shear stress distribution along the bolt are examples of some deficiencies.

Freeman (1978) monitored both the loading process of the rock bolts and the distribution of the shear stress along the bolts, and proposed and defined the neutral point, pick-up length, and anchor length of a rock bolt. According to the results of monitored bolts, the displacement of the rock mass and the rock bolt is considered to be the same at the neutral point, where the shear stress at the interface is zero, while the axial force of the rock bolt attains its maximum.

Following Freeman's research, Yu and Xian (1983) investigated the interaction mechanism of fully grouted bolts around a circular tunnel in a vsico-elastic medium. They suggested an analytical formulation to determine the position of the natural point along the rock bolt. However, the length of the rock bolt was limited and the displacement of the rock mass around a tunnel is assumed as an elastic function.

Indraratna (1987) and Indraratna & Kaiser (1987, 1990a, b) developed another analytical axi-symmetrical approach to model a reinforced circular tunnel in a homogeneous, isotropic medium with fully grouted bolts. Using theory of elasto-plasticity, the equivalent material properties for reinforced ground were calculated and the effect of bolt density and length on stress and displacement fields near the opening was investigated. In this approach, the bolt influence was simulated by a reinforced rock mass with equivalent cohesion and friction angle. Albeit, the analytical model predictions agreed well with the physical model results this

solution was based on some simplifications and came up with major errors, which are listed below:

I. Mohr-Coulomb linear yield criterion

II. Only the cohesion is reduced to the residual value

III. Erroneous calculation of plastic strain in elasto-plastic formulation

Grasso *et al.* (1989a, b) introduced the concept of reinforced rock mass and modeled the bolt action as a fictitious increase in rock cohesion. The reinforced zone is assumed as a whole, and only homogeneous mechanical properties are regarded. This approach was applied, with good results, to the design of the rock tunnels even with poor geotechnical properties.

Oreste (1995, 2002, and 2003), Oreste & Peila (1996), and Peila & Oreste (1995) developed numerical approaches that dealt with the reinforced zone around a tunnel. These approach accounts for the design of passive-rock bolt system based on convergence-confinement concept. In these analyses, the rock bolt was expected to adding an equivalent internal pressure to the tunnel wall. The equivalent internal pressure was originated from the axial force of the rock bolt, which was influenced by the behaviour of rock mass. This model simulated the bolt effect with an overall variation of the rock mass properties, but some difficulties have been encountered in the definition of the new rock mass properties.

Graziani & Ribacchi (1993) analyzed the influence of the presence of a reinforcing element both in the elastic and plastic zone by defining different constitutive laws. The problem was solved using a closed-form solution by introducing a simplified rock mass-strain law, however, two important factors such as the adherence loss at the rock-bolt interface and the flexibility of the bolt plate on the tunnel perimeter were not considered.

Labiouse (1996) developed an axi-symmetrical numerical analysis for the design of ungrouted tensioned bolts. The bolt dimensions and pattern, bolt stiffness, pre-tension load, and delay of installation were taken into account. Since the bolting system could not be considered as an internal support in this approach (i.e. rock mass and the support didn't act independently), a numerically alternative solution was introduced to include the effect of the rock bolts on the ground reaction curve.

Cai *et al.* (2004a, b) introduced an analytical model to describe the interaction behaviour of the rock bolt, the grout medium, and the rock mass. This model is based on improved shear–lag (fiber-loading) theory which is based on consistent deformation concept. They pointed out that any parameter that related to the ground deformation influenced the axial force in the rock bolt. The coupling and decoupling characteristic of the rock bolt interface in pull-out test, uniform deformation of the rock mass and intersecting joints were taken into account in this analysis so as to obtain the realistic value of the axial load in bolt. The position of neutral point was not only related with the length of the rock bolt and the internal radius of tunnel, but also strongly influenced by the properties of the rock mass. The neutral point and maximum axial load in bolt tends to be constant when the anchor length of bolt is long enough, which means that increasing the length of

rock bolt does not improve its effect dramatically under certain conditions. According to the model, the interaction behaviour between the rock bolt and rock mass is described by a parameter determined by the distribution of the interaction stress. The theoretical verifications were done through the measured data in some NATM tunnelling cases even in soft ground. The results obtained were quite compatible with those of Oreste & Peila (1996).

Cai *et al.* (2004c) also presented an axi-symmetrical analysis for bolt design in soft ground based on their previous models. For the rock-bolt and the rock mass interaction analysis, a strain softening behaviour obeying the linear Mohr-Coulomb failure criteria was adopted. Considering the position of the neutral point and the rock bolt length, nine cases were arranged for analysis.

Unlike Stille's approach (1983), which used Mohr-Coulomb failure criterion, Fahimifar & Soroush (2005) adopted the same solution using non-linear Hoek-Brown failure criterion with elastic-plastic with strain softening behaviour. On the basis of the rock-support interaction concept, they developed an alternative solution for the rock mass reinforced by grouted bolts and derived a numerical means to draw the ground reaction curve.

Pelizza *et al*. (2006) investigated a new mechanism of changing the strength parameters of the reinforced ground by rock bolts following the approach of Grasso *et a.l* (1989a, b). In order to realize the proposed hypothesis, theoretical and experimental works were carried out. It was clearly found that the cohesion of strength parameters is only increased by reinforcement of the ground. In other words, the rock bolts have more effects on the increase of cohesion than on internal friction angle.

2.4.3 Numerical design methods

Numerical schemes to model grouted bolts fall into two main categories:

1. Explicit representation of the bolt and
2. Equivalent material approaches.

In the explicit method, the bolt is represented by standard or special elements such as beam truss or bar elements. One of the first attempts to use standard finite elements to model the bolt and grout was done by Coates & Yu (1970). The study was done on the stress distribution around a cylindrical hole in a triaxial stress field together with a loaded anchor (socketed pile) either in tension or compression. The study neglected the presence of the grout and did not allow any yielding. Hollingshead (1971) solved the same problem using a three-phase material (bolt-grout-rock) and allowed penetration of yield zone into the grout wall using an elastic-perfectly plastic criterion for three materials. Nitzsche & Hass (1976) presented an approach to model a system for roof bolts installed in a predefined pattern. The model was used to determine the state of stress due to bolt tensioning.

St John & Van Dillen (1983) proposed a one-dimensional bar element passing through a cylindrical surface to which element representing surrounding material was attached. Three important modes of failure of fully grouted bolts were considered. For axial behaviour, a bi-linear elastic-plastic relation was assumed,

incorporating yielding of the bolt. This model neglects rock stiffness and in-situ effects around the borehole.

Brady & Loring (1988) introduced a finite difference scheme based on St John & Van Dillen's bolt model (St John & Van Dillen, 1983) to evaluate the reinforcement effect in rock mass. Two springs, axial and normal to the direction of the bolt, represented axial and lateral behaviour of the reinforcement. Calculation of the loads generated in the bolt was based on the relative displacement between the rock and a reinforcement node. The equation of motion was solved accounting for the forces generated by the reinforcement.

Peng & Guo (1988) combined the use of boundary element and finite element techniques to analyze the stresses and deformations around a reinforced opening. Boundary elements were used to represent the opening shape as well as the boundary between the bedding planes. The stress distribution along each bolt was determined based on the principal of minimum potential energy. Observed results however showed that the model overestimates the effect of reinforcement due to the assumption of perfect bonding.

An explicit finite element model of the bolt was developed by Aydan (1989). A three dimensional 8-node element (6 nodes in two-dimensional case) consisting of a cylindrical bolt and annulus is attached to the rock. The axial and lateral behaviours of the bolt were modelled, and the response of the grout of the annulus was assumed to be a combination of axial shear (parallel to the bolt axis) as well as a normal response perpendicular to the axis. Good agreement between numerical and analytical approaches was achieved for both elastic-perfectly plastic and elasto-plastic with strain softening behaviour.

In equivalent material approach, on the other hand, the reinforcing element (rock bolt itself) is not treated explicitly; rather, the whole assemblage of joints, rock and reinforcement is treated as a unit which behaves according to the contribution of its components. This can be a suitable method for large scale problems where mesh preparation and element numbers using explicit scheme could be prohibitive.

Pande & Gerrard (1983) used this method and extended the rheological model for jointed rock masses presented by Zienkiewicz & Pande (1977) and applied it for a reinforced medium. The 1-D rheological model consisted of rock material, joint sets and reinforcements all with elasto- viscous- plastic behaviour to represent the reinforced rock mass. The basic concept was to represent elastic, viscous and plastic behaviour of the governing materials by spring, dashpot and slider, respectively. The elasto- visco- plastic model was simulated by a spring (elastic) connected in series with a parallel coupling of a dashpot (viscous) and a slider (plastic). Each joint set was considered to be connected in series, and each reinforcement set in parallel (Figure 2-1). This means that the reinforcement undergos the same strain as the jointed rock mass and share the total stresses with it. The contribution from units are added and distributed over a certain volume of rock mass which is representative of the whole system.

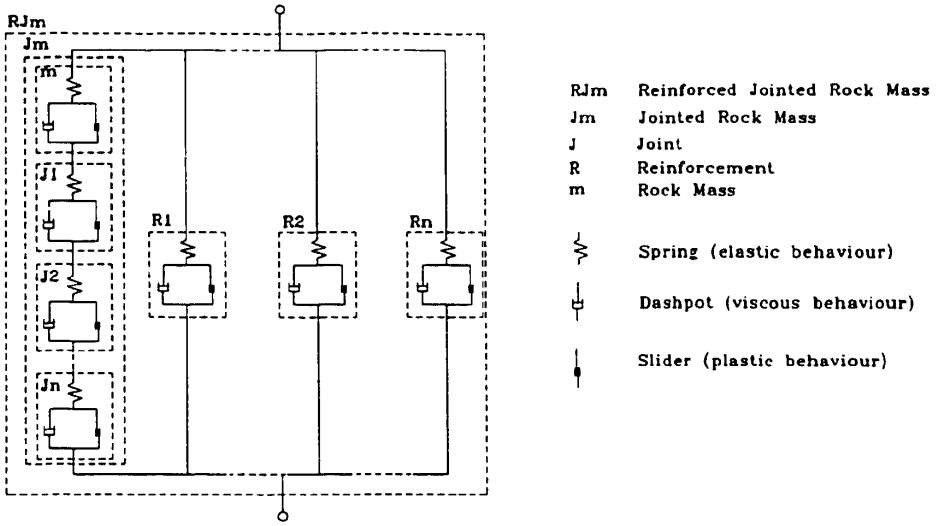

Figure 2-1 Rheological model of a reinforced jointed rock mass (Pande & Gerrard, 1983)

The concept of equivalent material properties approach was first introduced by Pariseau & Duan (1989) and Duan (1991) in numerical modelling application. This idea was to replace a heterogonous borehole assemblage of rock, grout, steel and interfaces by a homogeneous anisotropic material which behaves similar to the original assemblage (Figure 2-2).

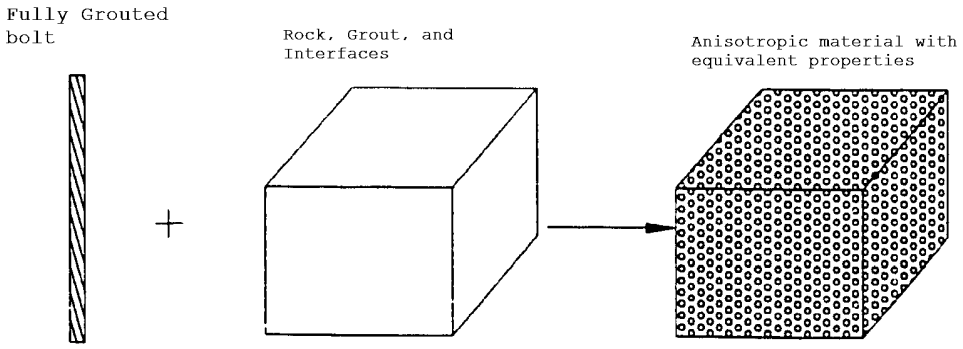

Figure 2-2 Idealized equivalent material property approach (Duan, 1991)

The proposed method was a 3-D approach with an elastic range of deformation for all the materials. To determine the equivalent material properties, a theoretical

approach was used similar to that proposed by Pariseau & Moon (1988) for equivalent elastic moduli of planerly jointed rock mass.

Yamatomi & Amano (1985) examined an axi-symmetrical finite element analysis to determine support capacity of the grouted bolts based on convergence-confinement method. Due to post-peak characteristics of rock mass affecting the deformation modulus and reinforcing effect of the grouted bolts, the finite element analysis was conducted under six conditions of post-failure behaviour. It was the main result of their study that the strain energy stored in the grouted bolts produced the differences between the ground reaction curve with and without the bolting. The support pressure available from the rock-bolts was function of stored strain-energy in bolts. They also modified the elasto-plastic closed-form solution of Brown *et al.* (1983) in order to relate the deduced strain energy to the support pressure.

Atlas Copco (1998) investigated the instability and reinforcement of the tunnel face via numerical modelling in a large cross section highway tunnel in Japan. According to their analysis, the unstable zone behind the tunnel face is limited to 0.5 of the tunnel diameter regardless of rock mass type. In order to stabilize this region, a comparable reinforcement technique using swellex and grouted bolts has been made because the use of shotcrete due to its imperfection in early strength is not reliable. A 2-D discontinuum and a 3-D continuum modelling have been carried out to evaluate the stability of the tunnel face. The early strength of grout material used in bolting and that 30 % of the total displacement occuring at the time of bolt installation at the face has been taken into consideration.

2.5 Summary and backbone of the proposed model

Seeing that the behaviour of reinforcement is quite dependent on how rock mass behaves, the strength parameters of the rock mass around the tunnel can be changed and improved by rock bolting. Consequently, reinforcements affect the behaviour of rock mass by restricting its deformation. This thesis study aims at introducing a new elasto-plastic approach based on equivalent material properties incorporating rock bolts and rock mass dependently. This approach denotes that strength parameter of bolted yielding zone around the tunnel is uniformly increased. It should be noted that this approach is applicable only for homogenous, isotropic rock masses in which at least four joint sets intersect (Hoek & Brown, 1980b). The proposed elasto-plastic model is not valid if a pronounced discontinuity intersects the tunnel or when anisotropic rock mass conditions prevail.

CHAPTER 3

CHARACTERIZATION OF POOR AND VERY POOR ROCK MASSES USING MODIFIED-GEOLOGICAL STRENGTH INDEX "MODIFIED-GSI"

3.1 Introduction

Although there have been a number of rock mass classification or characterization approaches such as Bieniawski's Geomechanics Classification or Rock Mass Rating (RMR) (Bieniawski, 1973, 1976, 1979, 1989), Barton's Q-system (Barton *et al.* 1974, Barton, 2002; Grimstad & Barton, 1993), Palmström's Rock Mass Index RMi (Palmström, 1995, 1996, 2000), Rabcewicz's New Austrian Tunnelling Method (NATM) (Rabcewicz, 1964, 1965), and Hoek's Geological Strength Index (GSI) (Hoek, 1994, Hoek & Brown, 1997), there has not been an emphasis on characterization of the poor rock masses, and their deficiency and inadequacy in characterizing poor rock mass have always been obvious. The inferior input data for analytical and numerical analyses of rock structures in poor and very poor rock mass has always been comprehensible. For example, in the early days of its introduction, RMR classification worked well because most of the problems were in reasonable quality rock masses ($30 < RMR < 70$) under moderate stress conditions. However, it soon became obvious that the RMR system was difficult to apply to rock masses that are of poor and very poor quality as recently reported by Marinos *et al*. (2005). Seeing that the precision of the input data significantly affects the accuracy of the outputs in engineering design, there has been, in fact, a keen interest to develop or improve practical ways for the poor rock mass characterization. It is, therefore, felt herein that there must be an easy handling approach as a tool to aid in poor rock mass characterization.

As the engineering properties of the discontinuities play a primary role in the rating of the classification systems, the accurate determination of the discontinuity properties in a poor and very poor rock mass cannot, in practice, be ascertainable. In opposition to classification systems in which RQD value and joint spacing account for considerable percentages of ratings, these parameters cannot directly be included in the classification or characterization of poor and very poor rock mass because the estimation of the RQD is very difficult and in mostly meaningless. In these cases the maximum percentage of the RQD observed, in most cases, is less than 20%.

3.2 Need for modifying Geological Strength Index (GSI) for poor rock mass

3.2.1 GSI development and improvement within last 10 years

Few attempts have been made to properly characterize poor and very poor rock mass so far. However, with the advent of Geological Strength Index "GSI", it has been a universal rock mass characterization approach capable of characterizing wide spectrum of rock masses and has attracted keen interest in rock mechanics community (Cai *et al.* 2004). In spite of some uncertainties and inadequacies in determining the GSI especially in poor and very poor rock masses, it has found acceptance for characterizing various types of rock masses. In fact, the emergence of the GSI was due to deficiency and inadequacy of the RMR and Q-system in characterizing poor rock mass in such a way as to recuperate the imperfection of them. Nevertheless, after 10 years experiences with using GSI, it has been recognized that it is not capable in characterizing poor to very poor rock mass (RMR < 30).

Hoek (1994) and Hoek & Brown (1997) pointed out that GSI is equal to RMR_{76} without considering the water and discontinuities orientation adjustments. Furthermore, a chart for GSI estimation including rock mass blockiness and rock mass discontinuities properties to simply characterize the rock mass was presented. The original chart used to determine the GSI was mostly based on a descriptive approach, rendering the system somewhat subjective and difficult to use.

The recent form of GSI charts was on account of tunnelling in difficult ground condition in Greece since 1998 by Hoek and Marinos (Hoek *et al*.1998; Marinos & Hoek 2000, 2001). Most recently, Marinos *et al*. (2005) have published an excellent paper putting forward some significant suggestions related with the appropriate selection of the GSI index for a range of rock masses under various conditions. Recommendations on the use of GSI and cases where the GSI is not applicable have been discussed.

In an effort to provide a quantitative means for characterizing jointed rock masses, the original GSI was modified by Sönmez and Ulusay (1999, 2002) and Cai *et al.*(2003, 2004). The former modification used volumetric joint count J_v for determining the structure rating (SR) and used Bieniawski's RMR system for rating the joint surface condition in terms of roughness, weathering and infilling of joint. The latter one, on the other hand, seems to be more beneficial to use in such a manner that a new category of weak rock structure namely; foliated/laminated/ sheared introduced firstly by Hoek *et al.*(1998), Mrinos & Hoek (2000, 2001), Hoek *et al*.(2005) was embedded into GSI chart. They also suggested a 3-D method for estimating block volume and used the RMi system for rating the joint condition. However, the difficulty in evaluating joint condition could not be overcome, because the RMi system is not capable of characterizing the weak rock mass. Marinos *et al*. (2005) have recently acknowledged that the quantifications do not work well in tectonically disturbed rock masses in which the structural fabric has been destroyed. In such rock masses they recommend the use of the original qualitative approach based on careful visual observations. What can be summarized from passage of ten years is that all of the existing amendments are, in fact,

defective in better characterizing poor and very poor rock mass and a need for a modification is of great concern to geologists.

3.2.2 Deficiency and inadequacy of the existing GSI charts

Some of the challenges encountered when applying the GSI lie in its descriptive nature, which manily let the existing GSI charts be at risk especially in poor rock mass. For poor to very poor rock mass characterization, the application of existing GSI charts is hindered by the fact that the use of the GSI for poor to very poor rock masses is to some extent subjective and requires long-term experience (Cai *et al.* 2004).

Although careful consideration has been given to the precise wording for each category and to the relative weights assigned to each combination of structural and surface conditions, the use of the GSI involves some subjectivity (Sönmez & Ulusay, 1999; Cai *et al.* 2004). The obvious deficiency in determining the GSI is in characterizing poor and very poor rock mass where the RMR of a rock mass is below 30 as also reported by Hoek (2004). Therefore, estimation of the GSI value for very poor rock masses needs some special challenges. In addition, long-term experience and sound judgment are required for successfully determining the GSI for a large variety of the rock mass quality ranging from very good to very poor.

The original and the existing GSI charts found in literature are not capable of characterizing poor and very poor rock mass as denoted by N/A in the relevant parts as shown in Figures 3-1 and 3-2. For example, a fair joint condition has been defined for a very poor rock mass like a fully sheared zone, which seems unsound. Besides, existing GSI charts suffer from erroneous intervals of GSI lines. For instance, the line indicating GSI of 50 (fair rock), signifying a fair and good joint condition, can be embedded in the disintegrated category of rock structure or a sheared rock mass structure. It can be, therefore, understood that the existing GSI charts could be no longer used for very poor rock mass and must be adjusted.

3.2.3 Modification and recuperation of the existing GSI charts

In order to overcome such uncertainties and perplexities mentioned and to improve the applicability of GSI usage in poor rock masses, a quantitative supplementary approach has been recommended by incorporating both visual impression and quantitative measures of rock mass. Therefore, what will follows are some modifications and suggestions on the original GSI in such a way as to better characterize poor to very poor rock masses. By adding measurable quantitative input in N/A parts of existing GSI charts, they will be enhanced in characterizing poor rock mass while maintaining its overall simplicity. Further, the new chart is considered as a supplementary means for its counterparts.

The approach is built on the linkage between descriptive geological terms and measurable field parameters such as volumetric joint count (J_v), structure rating (SR), Rock Quality Designation (RQD), broken structure domain (BSTR), intact core recovery (ICR), and discontinuity or joint surface properties.

To set up the Modified-GSI for poor and very poor rock mass, two indicators of weak rock mass; namely, Broken Structure Domain (BSTR) and Joint Condition Index (I_{jc}) are defined. The latter was adopted from the Modified-RMR, which was

developed by Özkan (1995) and Ünal (1996). In addition, eight quantitative or visual parameters are included into the new chart to assist the user. All required information for using in Modified-GSI can readily be obtained from overall field observation, scan-line mapping, and /or core-box surveying.

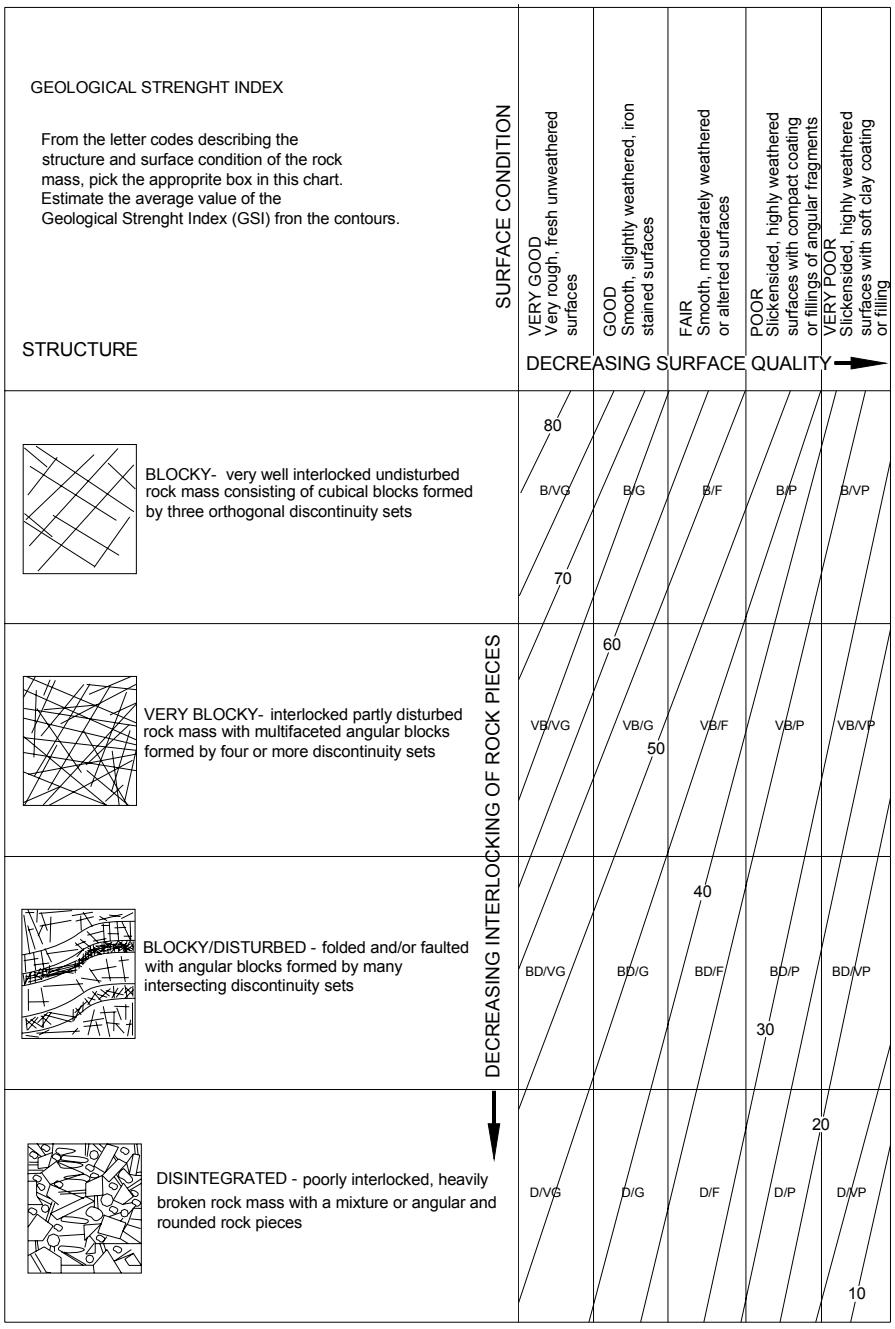

Figure 3-1 The original GSI chart introduced by Hoek (1994) and Hoek & Brown (1997).

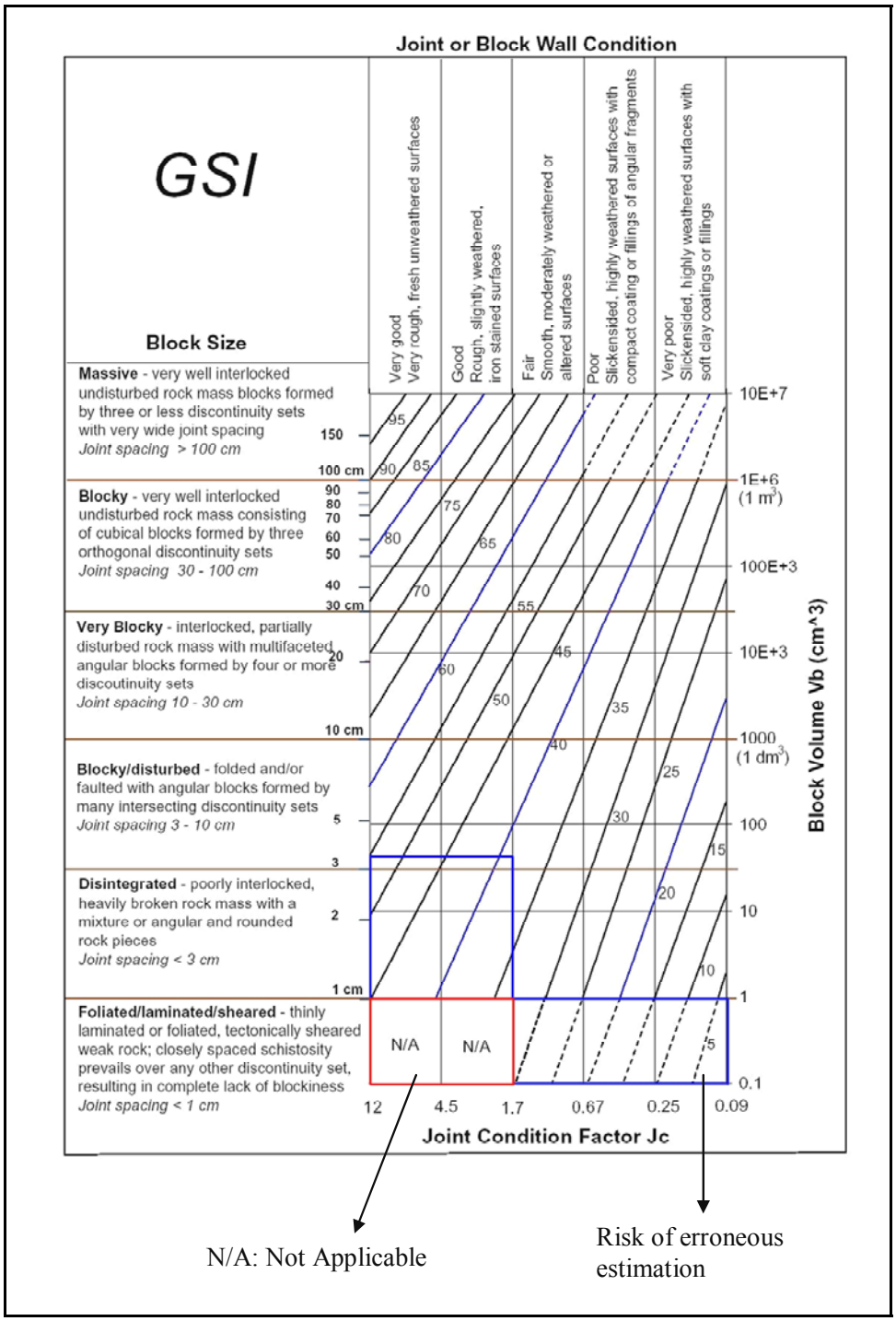

Figure 3-2 An example of existing quantitative GSI charts and its inadequacy in characterizing the poor and very poor rock mass (Cai *et al.* 2003).

For this purpose, a block in the matrix of 2 * 2 of GSI chart is selected in terms of two axes showing the rock mass blockiness (interlocking) and joint surface conditions. As shown in Figure 3-3, the vertical axis of the matrix demonstrates the rock mass geometry parameters. Eight quantitative or visually impressive

parameters are embedded in this axis to assist the user. Joint spacing, joint frequency, volumetric joint count, structure rating, RQD, and block size (volume) are the quantitative indicators whereas the visual definitions can be found by its geological structure namely the type of blockiness of rock mass, ICR, and BSTR. The horizontal axis, on the other side, is assigned for the joint condition. The Modified-GSI (Figure 3-3) ranges between 6 and 27.

Even though there have been quite a few approaches to determine the strength and modulus of rock mass based on GSI, there has not been a practical effort to estimate the support pressure based on GSI in tunnels. It will be one of the thesis topics in Chapter 4.

3.3 Methods of estimating Modified-GSI for poor and very poor rock masses

In the present study, two ways are recommended for estimating GSI value for poor rock mass, however, an alternative is less recommended. It should be noted that the boundary which defines the threshold of poor rock mass is defined at RMR <30. This value was arbitrary chosen, but it has also been considered by others as seen in the literature (Mathis & Page 1995; Morales *et al.* 2004; Hoek 2004; Osgoui & Ünal 2005a, b). Besides, note that for fair to good quality rock mass if RMR > *30* then GSI= RMR. In what follows throughout this study, aforementioned relationships will be employed. The three distinct methods for estimate GSI for poor rock mass are as follow:

1. Using Modified-GSI chart: i.e. Figure 3-3. This method is considered to be more reliable and realistic. It is recommended to use this method.

2. Using regression analysis results: This analysis was carried out in accordance with results obtained from many case studies in the Alpine region undertaken by Morales *et al.* 2004. In order to relate the RMR and GSI for poor and very poor rock mass, only the case studies whose RMR < 30 were taken into account. Regression analysis indicated that the exponential relationship between GSI and RMR yielded a good fit to data. Hence, a new exponential relationship between Rock Mass Rating (RMR) and Geological Strength Index (GSI) was, in turn, suggested by Osgoui & Ünal (2005a) as follow:

$$GSI = 6e^{0.05RMR} \tag{3-1}$$

This correlation has been proved to be compatible with those ascertained from many case studies. The above relation satisfies the intervals of Modified-GSI chart such that the maximum GSI value will be 27 if RMR = 30 and at RMR =0 the minimum value of GSI is 6.

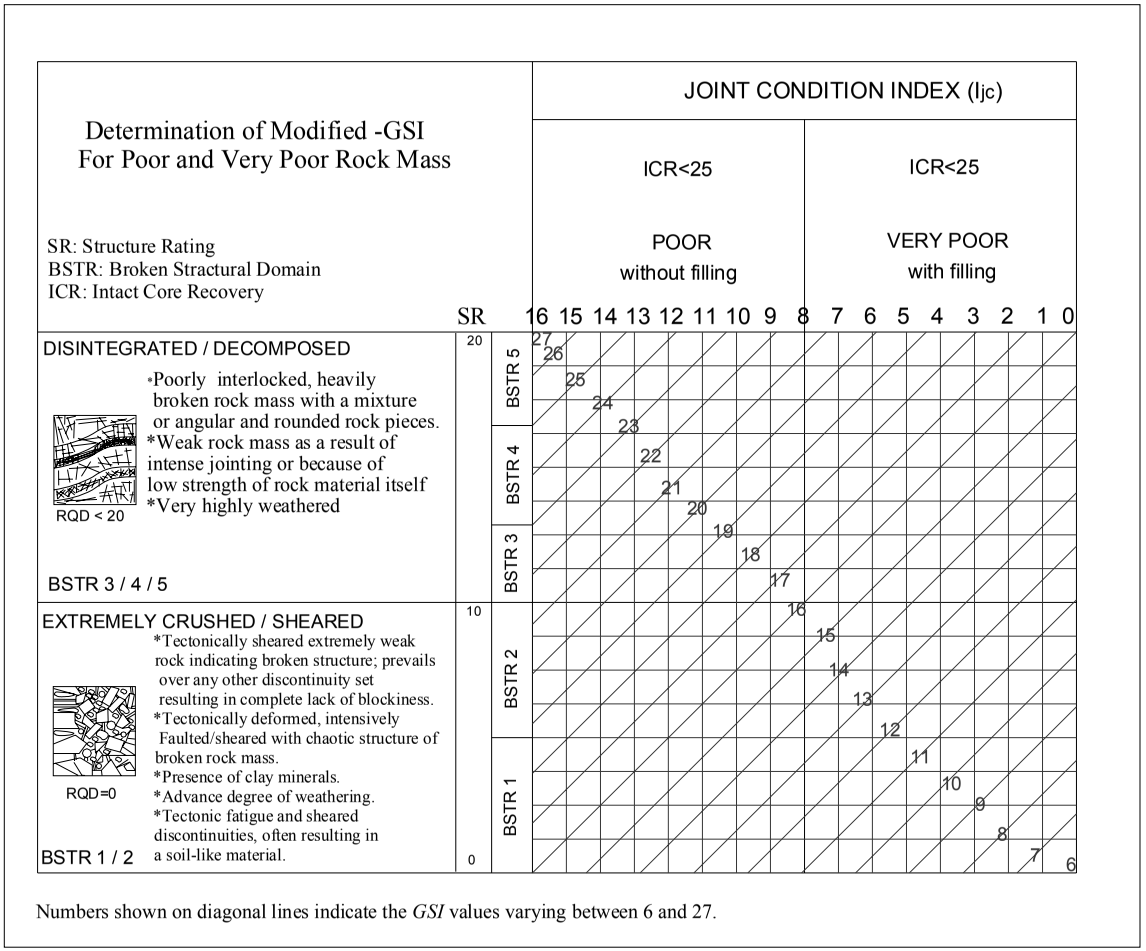

Numbers shown on diagonal lines indicate the *GSI* values varying between 6 and 27.

Figure 3-3 Modified-GSI chart introduced for this study

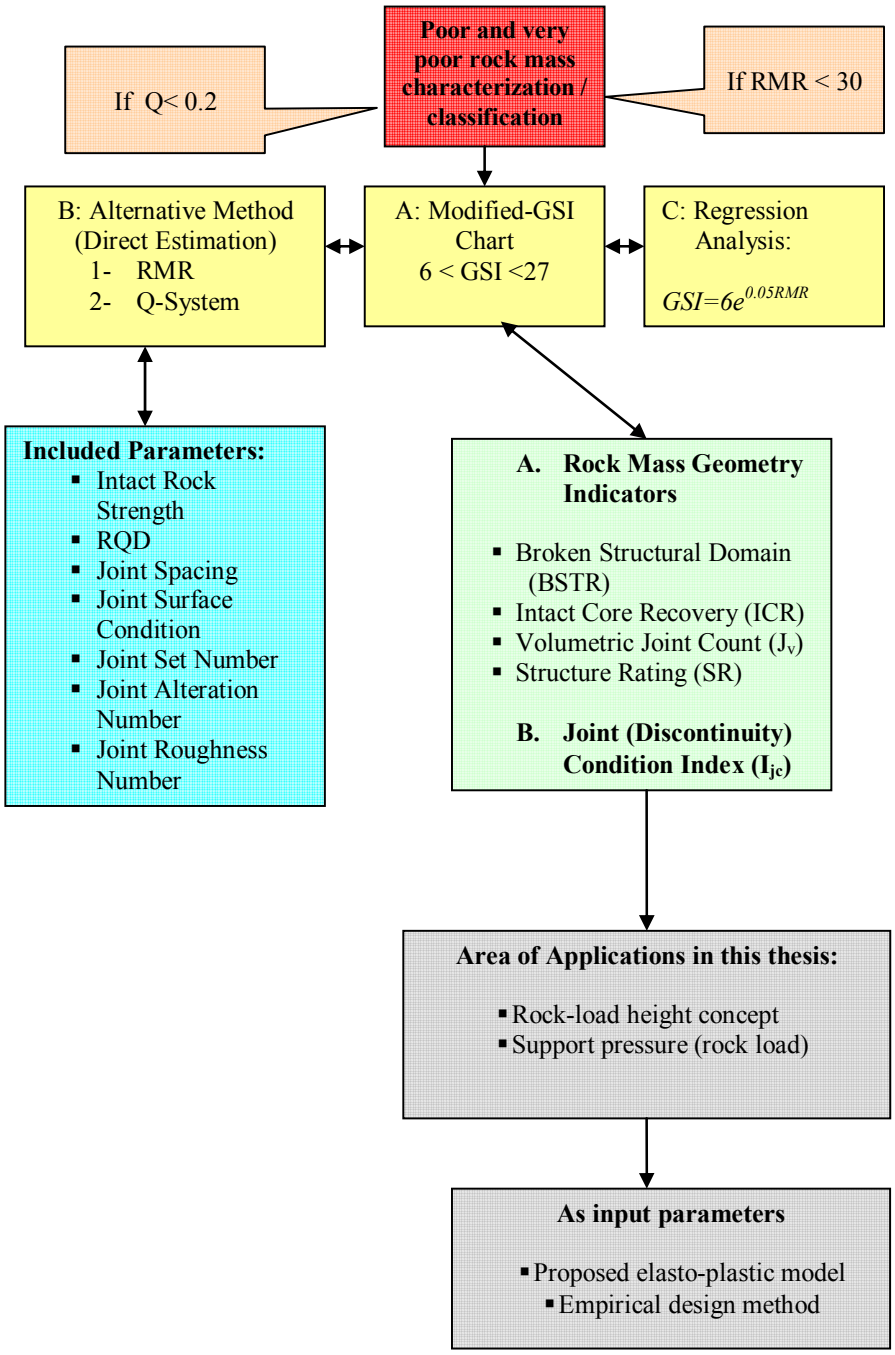

Figure 3-4 Flow chart showing the proposed approach for characterizing poor and very poor rock masses

3. Using alternative method: The alternative way of determining GSI values for quite poor rock masses, not very poor rock, falls within the usual procedure of calculating RMR given by Bieniawski (1973). In this case, the value of the RMR and Q- system that is equal to GSI might be estimated from core box logging not

taking into consideration the effect of the water pressure, the effect of the joint orientation, and the effect of the in-situ stress state (Hoek, 1994). This alternative is not used for very poor rock mass due to meaningless value of RQD.

3.4 Methods of determining the parameters used in empirically proposed approach for characterizing the poor and very poor rock masses

In this part, useful guidelines for calculating the parameters to be used in the Modified-GSI chart (Figure 3-3) are given. As shown in the flowchart of Figure 3-4, five distinguishable stages in estimating Modified-GSI can be as follows:

I. Selecting a method of geological mapping in accordance with availability of the chosen method like: overall field observation, scan-line mapping, core-box surveying, and window mapping technique.

II. Determining the type of Broken Structural Domain (BSTR) to which rock mass is mostly governed and corresponded.

III. Depending on type of geological mapping, estimate some important indicators of rock mass geometry such as: Intact Core Recovery (ICR), Volumetric Joint Count (J_v), Structure Rating (SR).

IV. Given the discontinuity (joint) surface condition, evaluate the roughness, filling, and weathering to obtain Joint Condition Index value (I_{jc}).

V. Using Modified-GSI chart (Figure 3-3), estimate the Modified-GSI for poor and very poor rock mass.

If geological mapping used in Modified-GSI is impossible at the site investigation stage, estimate the GSI value from regression analysis using Equation 3-1.

It is by far the most essential to determine the parameters to be used in aforementioned five steps. In what follows, the methodology of the procedure will be presented.

3.5 Poor and very poor rock mass geometry indicators used in the Modified-GSI

In order to aid in characterizing poor rock mass using Modified-GSI, it is necessary that the parameters included in the proposed approach be known (see Figure 3-3). Those rock mass parameters are readily obtained from site investigation (visual impression and judgments, scan-line mapping) or core-box logging. Depending on the availability of the foregoing methods, users can easily employ the suitable parameters for the Modified-GSI. In what follows, a practical way for determining rock mass indicators used in Modified-GSI is given.

3.5.1 Determination of the parameters associated with degree of jointing (blockiness or interlocking)

3.5.1.1 Broken Structural Domain (BSTR) indicator

Broadly speaking, broken drill-core zones recovered from a very weak rock mass having a length greater than 25 cm are defined as the Broken Structural Domain *(*BSTR*)* (Ünal, 1996, 2002). Various types of BSTR domains can be categorized into 5 groups based on their degree of size and composition. BSTR types included in the Modified-GSI to define the rock-mass structure are demonstrated in Figure 3-5 to Figure 3-8 (Osgoui & Ünal, 2005b). Having recognized the BSTR type, one can distinguish the poor rock mass from very poor rock mass. As can be indicated from Figure 3-5 to Figure 3-8, the poor and very poor rock mass are best characterized by BSTR types. It should be noted that the assignment of only one type of BSTR for a rock medium is not logical; rather, it is suggested to know the types of BSTR governing whole poor rock mass. Otherwise, the assignment of only BSTR 1 / 2 for a domain cannot signify very poor rock mass; rather it stands for a soil material. For the very poor rock mass, it is supposed that a large amount of medium is governed by the BSTR 1 / 2 while poor rock mass is dominantly governed by BSTR 3 /4 /5.

Rock mass governed dominantly by BSTR 3/4/5	POOR ROCK MASS (WEAK ROCK MASS)
Rock mass governed dominantly by BSTR 1/ 2	VERY POOR ROCK MASS (VERY WEAK ROCK MASS)

Figure 3-5 Various types of Broken Structural Domain (BSTR), METU's Rock Mechanics Laboratory

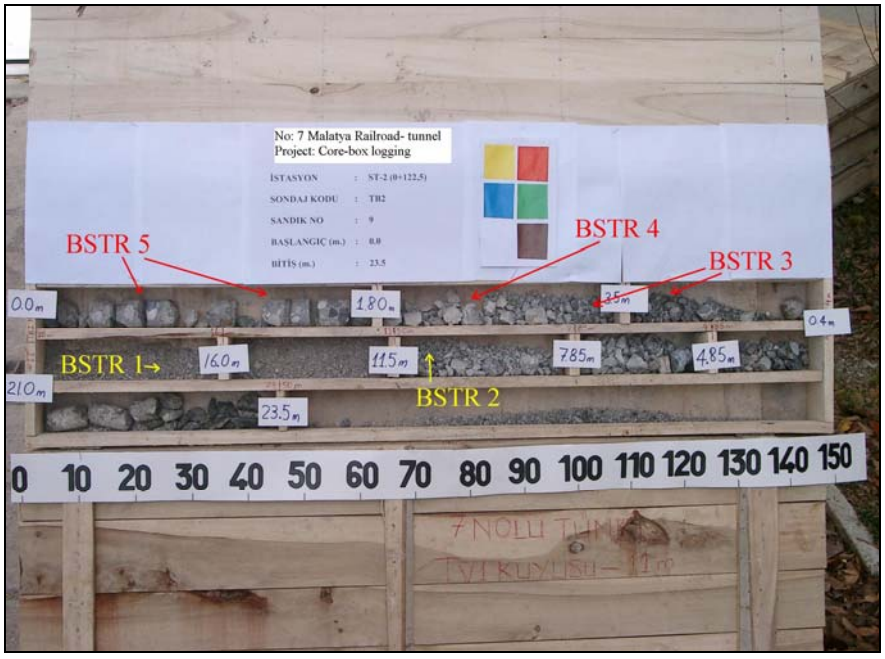

Figure 3-6 Core-box surveying for No:7 Malatya Railway tunnel project. Various types of BSTR are marked, METU's Rock Mechanics Laboratory, (Osgoui & Ünal, 2005b)

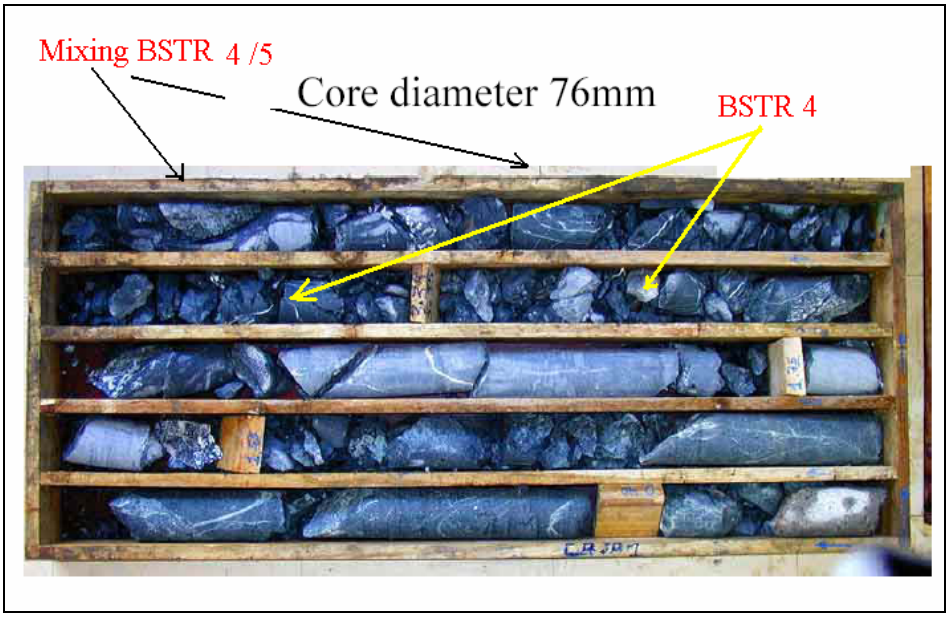

Figure 3-7 A typical core-box including BSTR (Palmström, 2005a)

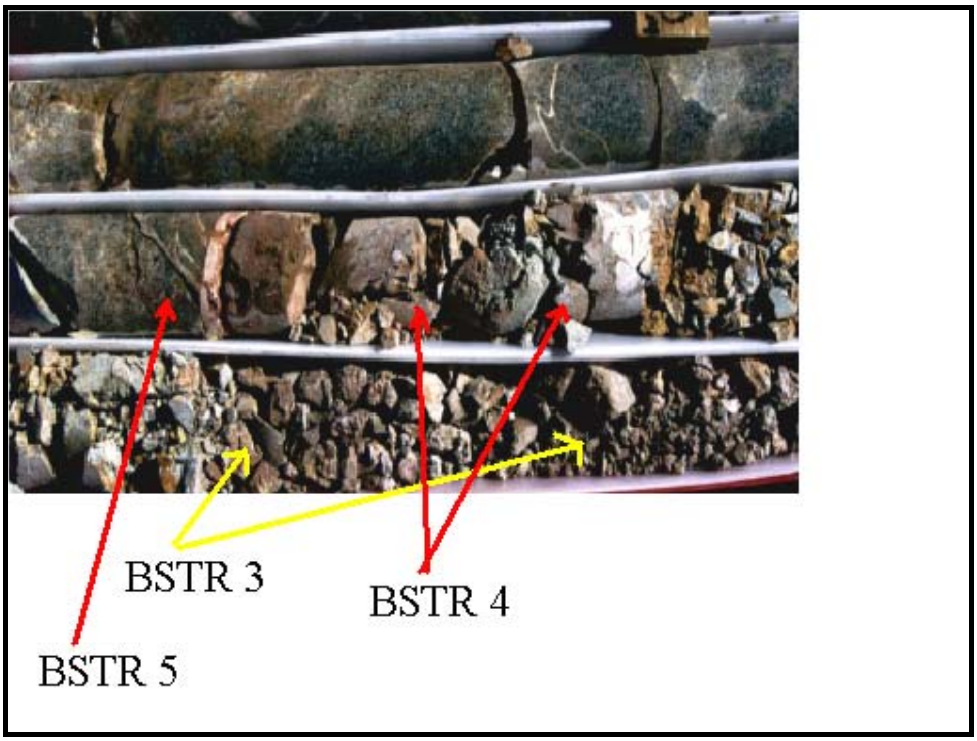

Figure 3-8 Various types of BSTR

This approach can also be regarded as one of the overall observation methods for description of rock mass quality, but it is appropriate that BSTR be described through core-box logging rather than overall rock mass observation.

BSTR 3 / 4/ 5 are assigned for disintegrated- decomposed rock masses while BSTR 1/ 2 signifies the extremely crushed / sheared rock masses.

It is worth noting that the disc types of broken rock cores, denoted to high horizontal stress field, can be categorized into the BSTR type 4.

3.5.1.2 Determination of the Rock Quality Designation (RQD)

Most concerned engineers and more recently Palmström (2001, 2005 a, b), Edelbro (2003), Grenon & Hadjigeorgiou (2003) have pointed out the drawbacks and limitations of RQD. Firstly, RQD value is strongly a function of the borehole orientation; i.e. RQD is directional and gives different RQD values along different directions for the same rock mass. So the rock engineer may be confused as to which one of the values to adopt in quantitative evaluations. Secondly, RQD does not provide good information of core pieces less than 10 cm. Moreover, RQD is not a good parameter in the case of a rock mass with joint spacing close to 10 cm. For instance, if the distance between continuous joints is 105 mm (core length), the RQD value will be 100 % whereas the value of RQD will be 0 if the distance between continuous joints is 95 mm (Palmström, 2005b).

Accordingly, instead of RQD, very susceptible and unreliable in characterizing the rock mass, using other alternatives containing important parameters of rock mass such as block volume and volumetric joint count could, in turn, provide far more reliable and confident results in practice.

In poor and very poor rock masses where the expected value of RQD is low, the two aforementioned disadvantages of RQD are less sensible. In such rock mass due to heavily degree of jointing, the borehole direction is much less sensitive than that of good quality of rock mass. It would be better to say that no matter how the borehole direction is, the obtained cores signify more or less the same results of degree of jointing and fracture frequency. Having defined the BSTR types, one can even evaluate cores with the length of less than 10 cm. Hence, the second drawback of the RQD would be compensated by BSTR types. In the Modified-GSI, the value of RQD less than 20 is assigned for BSTR 3 / 4/ 5 while an RQD equal to zero is recommended for BSTR 1 and 2 (see Figure 3-3).

3.5.1.3 Block size (volume)

Block size is an extremely important indicator of a rock mass. This definition has been flourished over the years in order to overcome the deficiencies and limitations of the RQD in characterizing the rock mass. The block dimensions are determined by joint spacings and the number of joint sets and the persistence of the discontinuities delineating potential blocks (ISRM 1981). Individual or random joints and possibly other planes of weakness may further influence the size and shape of blocks. Impact from rock blasting may also be an influence. Block size can be measured in different ways by simple observation (and measurement) of characteristic blocks, by joint set spacing or by core logging. It is seldom possible

to measure the block size directly because the rock masses having identifiable shape and definable exposure are rarely found in nature (Palmström, 2005b).

Due to a great variety in sizes and shapes of rock blocks, which limited 1-D measuring (scanline mapping) and resulted in complication of direct measurement, other alternatives had to be developed. Therefore, quite a number of indirect approaches have been attracted interest in estimating the degree of jointing associated with rock mass geometry given elsewhere (Palmström 1982, 2005b).

In poor rock masses, due to intensive degree of jointing, weathering, and decomposition the detection of a good rock block representive is very difficult. Therefore, the block volume can be determined in drill cores in cases where the fragments are small enough to be measured in the core, for example where crushed rocks occur like BSTR types 3 and 4. In these casees, it is recommended to measure the block size directly by using core-boxes. From this measurement, the apparent smallest and largest blocks can be obtained. It should be noted that the direct measure of crushed rock pieces volume is not applicable for BSTR type 1, 2, and 3. The various types of BSTR also correlate the block volume (size) where the measuring the rock blocks for very poor rock masses are difficult as outlined in Table 3-1.

3.5.1.4 Volumetric joint count (J_v)

Volumetric joint count J_v is defined as the number of joints intersecting a volume of $1m^3$ of rock mass (Palmström, 1982). In detail, Sönmez & Ulusay (1999) defined J_v as the sum of the number of joints per meter for each joint set present. The volumetric joint count is in general by definition an average measurement for the actual rock mass volume measured, expressing the number of joints occurring in this volume. However, as all joints seldom can be observed (counted) in a volume, J_v is often given as a range from what can be observed (Palmström, 1996).

Table 3-1 Classification of the block volume related to particle size (volume) and BSTR suggested by Palmström (1995, 2000) and modified for this study. Key: N /A (Not Applicable)

Term for density of joints	Term for block size	Block volume (Vb) Palmström (1995)	Block volume (Vb) Palmström (2000)	Term for soil particle	Term for BSTR	Approximate particle volume	BSTR types
				Coarse sand	Sand to Gravel	< 0.5cm^3	1 / 2
				Fine gravel		0.5-10 cm^3	1 / 2
Extremely high	Extremely small	< 10 cm^3	< 30 cm^3	Medium gravel	Small to large size broken material	10-50cm3	3 / 4 / 5
Very high	Very small	10-200 cm^3	30-1000 cm^3	Coarse gravel (some rock cores)		50-100 cm^3	3 / 4 / 5
High	Small	0.2-10 dm^3	1-30 dm^3	Cobbles		0.1-5 dm^3	N /A
Moderate	Moderate	10-200 dm^3	30-1000 dm^3	Boulders		5-100 dm^3	N /A
Low	Large	0.2-10 m^3	1-30 m^3	Blocks		> 0.1 m^3	N /A
Very low	Very large	10-200 m^3	30-1000 m^3				
Extremely low	Extremely large	> 200 m^3	> 1000 m^3				

Sönmez & Ulusay (1999) pointed out that the estimation of the J_v for heavily jointed rock masses and very poor rock masses with no identifiable structural pattern was extraordinary difficult. Since the discontinuities in such rock masses do not introduce considerable differences in their spacing in all directions, they can be assumed as homogeneous and isotropic. Therefore, they recommended the following equation as a practical means for estimation of the number of discontinuities in a rock mass with a volume of $1m^3$:

$$J_v = \lambda_{dx}\lambda_{dy}\lambda_{dz} = \frac{N_{dx}}{L_{dx}} \times \frac{N_{dy}}{L_{dy}} \times \frac{N_{dz}}{L_{dz}} \quad (3\text{-}2)$$

where λ_{dx}, λ_{dy}, and λ_{dz} are the average number of discontinuities counted along the scan-line (L_{dx}, L_{dy}, and L_{dz}) perpendicular to each other or N_{dx}, N_{dy}, and N_{dz} are the number of discontinuities along a scanline with the length of L_{dx}, L_{dy}, and L_{dz}, respectively. In some cases, however, it can be difficult to find exposures along which three scan-line surveys in perpendicular directions can be carried out. In such circumstance, by assuming the rock mass is homogeneous and isotropic the Equation 3-2 can be rewritten in the following form (Sönmez & Ulusay, 1999):

$$J_v = (N_d / L_d)^3 = \lambda^3 \quad (3\text{-}3)$$

Equation 3-3 indicates that, for poor rock masses, the number of joints per $1m^3$ of its volume is independent of the scanline orientation. In other words, it is sufficient to know the number of joints per meter of scanline so as to be able to estimate the volumetric joint count.

For heavily jointed rock mass referred to as the BSTR 3/ 4/ 5, a mixture of angular and rounded rock pieces free from high proportion of fines caused. It can be considered that categorizing such materials as the BSTR 3/ 4/ 5 in the GSI seems to be possible. It is, however, impossible to estimate the number of discontinuity sets in such rock. In order to overcome this difficulty, Sönmez & Ulusay (2002) have recognized that it would be logical and more practical counting the faces of individual rock pieces involved by the BSTR 3/ 4/ 5. For the purpose, by assuming that parallel or nearly parallel surfaces represent the same discontinuity set, such parallel surfaces should be counted once. In the case of a rock piece from a rock mass including three joint sets approximately perpendicular to each others, prismatic blocks with six surfaces are formed and if the parallel surfaces are considered from a single discontinuity set the number of discontinuity sets (D_n) is estimated as 3. While in the case of a tetrahedral rock pieces of which surfaces are not parallel to each others, the number of discontinuity sets is considered as 4. Assuming that BSTR types of rock masses are homogenous and isotropic, the following expression is suggested for the approximate estimation of J_v in conjunction with D_n (Sönmez & Ulusay, 2002):

$$J_v = D_n\left(\frac{1}{S_b}\right) \tag{3-4}$$

where D_n is the estimated number of discontinuity sets as mentioned above and S_b is the average size of the block or rock pieces, which represents average spacing of discontinuities and estimated from the selected pieces of the BSTR 3/ 4/ 5.

The intervals of volumetric joint count J_v in associated with type of rock mass structure are presented in the Table 3-2. As outlined, each interval of J_v is corresponded to a unique description of degree of blockiness (or interlocking) and degree of jointing. Table 3-2 also serves useful information related to rock mass structure used in existing GSI charts. The BSTR types, very important indicator of poor and very poor rock mass used in Modified-GSI chart (Figure 3-3), are pertained to the volumetric joint count intervals.

Table 3-2 Descriptive terms corresponding to block size and intervals of Jv originally suggested by ISRM (1981) and modified for this thesis study

Blockiness Definition	Degree of jointing (density of joints)	Volumetric Joint Count (J_v) (joint/m^3)	Description for GSI(this study)
Exceptionally large blocks	Massive / Intact no joint	< 1	Massive (M)
Large blocks	Weakly jointed	1-3	Blocky (B)
Medium sized block	Moderately jointed	3-10	Very Blocky (VB)
Small blocks	Strongly jointed	10-30	Blocky / Disturbed (BD)
Very small blocks	Very strongly jointed	30-60	Disintegrated/ Decomposed (DD) BSTR 3/4/5
Crushed/ Sheared	Crushed	> 60	Extremely Crushed/Sheared (ECS) BSTR 1/ 2

3.5.1.5 Correlation between RQD, J_v and V_b

The parameters indicating the degree of jointing (blockiness or interlocking) of a rock mass such as RQD, J_v and V_b can be interrelated. As the relation between J_v

and V_b is delineated in three dimensions, their correlation with RQD (one-dimension) has been an increasing pursuit. . The two important indicators, J_v and V_b, exhibiting the block size can be combined in order to provide good information of the block geometry. The type and shape of the block play a significant role in the relationship between J_v and V_b. Depending on the type and shape of the rock block, Palmström (1995, 1996) has pertained the block volume V_b and the volumetric joint count J_v as:

$$V_b = \beta_b \times J_v^{-3} \tag{3-5}$$

where β_b is the block shape factor.

Based on analysis of the results carried out by Şen & Eissa (1991), the block shape factor is of great importance in such a way as to have the most influential role in calculating and inter-correlating the block volume and volumetric joint count precisely. The most basic relationship between J_v and V_b in the form of hyperbolic function for three joint sets was suggested by Şen & Eissa (1991):

$$J_v = \frac{1}{V_b}\left(\frac{1}{\lambda_{dx}\lambda_{dy}} + \frac{1}{\lambda_{dy}\lambda_{dz}} + \frac{1}{\lambda_{dz}\lambda_{dx}} \right) \tag{3-6}$$

where λ_{dx}, λ_{dy}, and λ_{dz} are the average number of discontinuities along x, y, and z directions. Both correlations, i.e. Equations 3-5 and 3-6 indicate a reverse relationship between the block size and the volumetric joint count. With increasing in number of joints within unit of rock mass, the size of rock block decreases.

The indirect estimate of the volumetric joint count J_v was firstly put forwarded by Palmström (1982). The following simple expression between RQD and J_v was presented as follows:

$$RQD = 115 - 3.3\, J_v \quad \text{for } J_v < 4.5 \text{ then } RQD = 100 \quad \text{for } J_v > 35 \text{ then } RQD = 0 \tag{3-7}$$

Reaaranged in terms of RQD, the value of J_v can be readily worked out:

$$J_v = (115 - RQD)/3.3 \tag{3-8}$$

At times, the Equation 3-7 yields RQD values of more than 100, which is not plausible although it is recognized the Equation was not meant to be used outside the RQD limits. For instance, if $J_v = 3$, the Equation 3-7 gives RQD=105. If used within the validity range, $8 < J_v < 24$, as suggested by Şen & Eissa (1991), Equation 3-7 can be used reliably in estimating the order of magnitude of volumetric RQD

when borehole data are unavailable. Şen & Eissa (1992) reached to a conclusion indicating that the RQD is not related to J_v linearly as it stands in the literature; conversely, the relation is non-linear. However, the pre-existing linear equation (i.e. Equation 3-7) approximates the non-linear relation. More recently, Palmström (2005b) has recognized these deficiencies and obscurities of the Equation 3-7. According to data obtained form core logging of 223 m long core drill-hole in gneiss quarry mine, a poor connection between RQD and J_v was reported when using Equation 3-7. He introduced a new correlation between volumetric joint count J_v and RQD as follows:

$$RQD = 110 - 2.5\,J_v \qquad for\ \ 4 < J_v < 44 \tag{3-9}$$

Equation 3-9 is understood to probably give a more appropriate average correlation than Equation 3-7. By rewriting Equation 3-9, the value of J_v is obtained as.

$$J_v = (110\text{-}RQD)/\,2.5 \tag{3-10}$$

Compared with the Priest & Hudson's (1976) linear Equation $RQD=110.4-3.68\lambda$ (Priest & Hudson, 1976), which is applicable in the range of the $6 < \lambda_d < 16$, the linear Equations 3-7 and 3-9 are understood to be comparable as Bieniawski (1973) stated that the relation between fracture frequency (i.e. λ_d) and RQD is linear. It can also be evident that RQD is related with joint frequency in one and three dimension.

Substituting Equations 3-7 and 3-9 into Priest & Hudson's (1976) non-linear equation $RQD = 100e^{-0.1\lambda}(0.1\lambda_d + 1)$ (Priest & Hudson, 1976), the new formulations in estimating the value of volumetric joint count J_v (3-D) in terms of the average number of joints per meter λ_d (1-D) will be introduced as follows:

$$J_v = 34.85 - 30.30e^{-0.1\lambda_d}(0.1\lambda_d + 1) \tag{3-11}$$

$$J_v = 44 - 40e^{-0.1\lambda_d}(0.1\lambda_d + 1) \tag{3-12}$$

The main advantage of Equations 3-11 and 3-12 is to roughly estimate the J_v through λ_d, rather than RQD. Where the estimate of RQD is difficult due to its limitations and constrains, the correlation between J_v and λ_d could be more practical.

Based on results obtained from core–box logging of poor rock mass in TUPRAG open-pit gold mine (Kisladag Project) in Turkey, a new statistically relationship between joint frequency (number of joint per meter λ_d in 1-D) and volumetric joint count J_v in 3-D has been developed as follows and shown in Figure 3-9.

$$J_v = 10.41 \ln(\lambda_d) - 6.84 \quad (3\text{-}13)$$

$$\lambda_d = \exp\left(\frac{J_v + 6.84}{10.4}\right)$$

For poor (BSTR 3 /4 / 5) and very poor rock mass (BSTR 1 / 2), the volumetric joint count J_v varies between 30-60 and 60-100, respectively (ISRM, 1981; Sönmez & Ulusay, 1999).

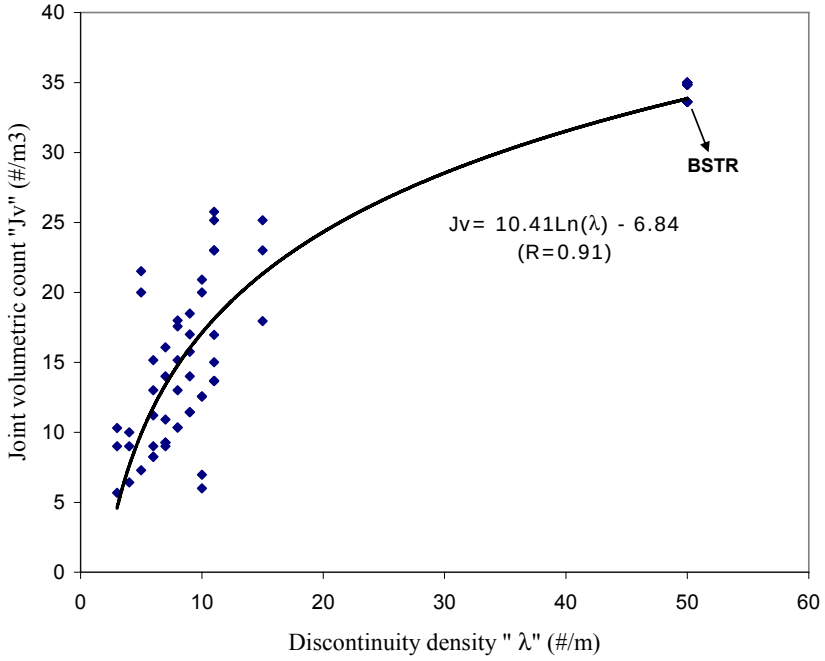

Figure 3-9 The variation of volumetric joint count with the joint density

In order to better correlate between volumetric joint count J_v and joint frequency λ_d for poor and very poor rock mass, it was recognized that the statistically proposed correlation gives more reliable results. Contrary to Equations 3-11 and 3-12, which are in insensitive when the rock mass being highly jointed or disintegrated (where rock mass is crushed or sheared, e.g. rock mass is categorized as the BSTR), Equation 3-13 provide the results considerably sensitive to degree of high jointing of the poor rock mass (see Figure 3-10).

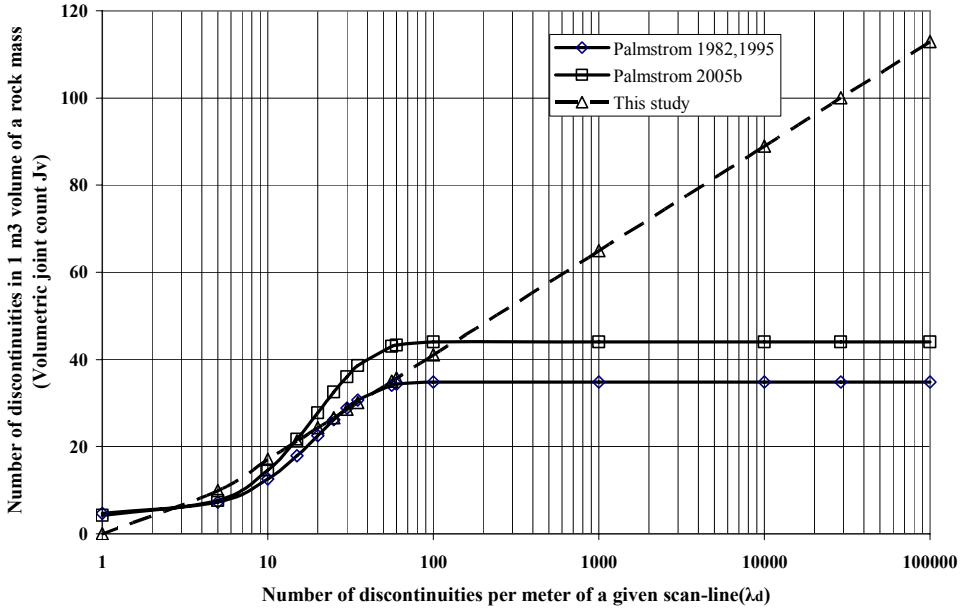

Figure 3-10 The correlation between average number of discontinuities per meter of a scan-line survey (λ_d) and volumetric joint count (Jv) with different approaches.

It is worthwhile to note that for low and medium degree of jointing; all three correlation produce more or less very closed results as indicated at Figure 3-10.

3.5.1.6 Determination of the Structure Rating (SR)

In the original GSI chart introduced by Hoek (1994), Hoek *et al.* (1995), Hoek & Brown (1997), the structure of the rock mass was qualitatively defined in terms of interlocking or blockiness of the rock pieces. This definition gives no quantitative information of the rock mass structure.

An effort has been made by Sönmez & Ulusay (2002) to let the rock mass structure be quantitatively defined. For this purpose a term called Structure Rating (SR) was suggested. In fact, the definition of the Structure Rating (SR) is mainly on the basis of the block size (volume), which signifies the rock mass geometry. Based on the intervals of J_v and corresponding descriptions for the blockiness ratings of GSI charts, structure rating (SR) was assigned to each defined category of rock mass; namely, massive or intact, blocky, very blocky, blocky/ disturbed/seamy, disintegrated/ decomposed, and extremely crushed / sheared. In the existing GSI charts, for example Sönmez & Ulusay (2002), the intervals between the structural categories were equally divided and selected as 100, 80, 60, 40, 20, and 0.

It is felt necessary here to adjust the previous SR intervals in order to include the poor and very poor rock mass categories or BSTR types. Therefore, the SR intervals are modified between 100, 80, 60, 40, 20, 10, and 0 to adopt also the BSTR types. Also, the corresponding values of the J_v (0.1, 0.3, 1, 3, 10, 30, 60, 100) are taken into account in accordance with its definition by ISRM (1981) and

Sönmez & Ulusay (1999). By doing this, a plausible way to quantitatively define the BSTR types is attained as illustrated in Figure 3-11.

The colleration between SR limits and corresponding J_v values, encompassing the wide range of the rock mass quality is suggested as follows:

$$SR = -15.58 \ln (J_v) + 74.62 \quad (3\text{-}14)$$

The BSTR values assigned for the poor and very poor rock mass lie between 0 and 20 as presented in Figure 3-11. A very helpful distinction to notice is that the broken structural domains (BSTR) can be categorized in range of the volumetric count joint (J_v) between 30 and 100; i.e. in the regions of disintegrated-decomposed and extremely crushed / sheared rock mass to calibrate the Modified-GSI chart.

3.5.2 Poor and very poor rock mass joint condition indicators

Joint condition plays a significant role in characterizing jointed rock masses. Almost in all of the existing classification systems, the ratings of joint condition account for a large percentage of total ratings. In Bieniawski's RMR system, for instance, joint condition rating account for 30 % of the total ratings; in the same way, of six input parameters of Barton's Q-system, two of which are directly in conjunction with joint condition.

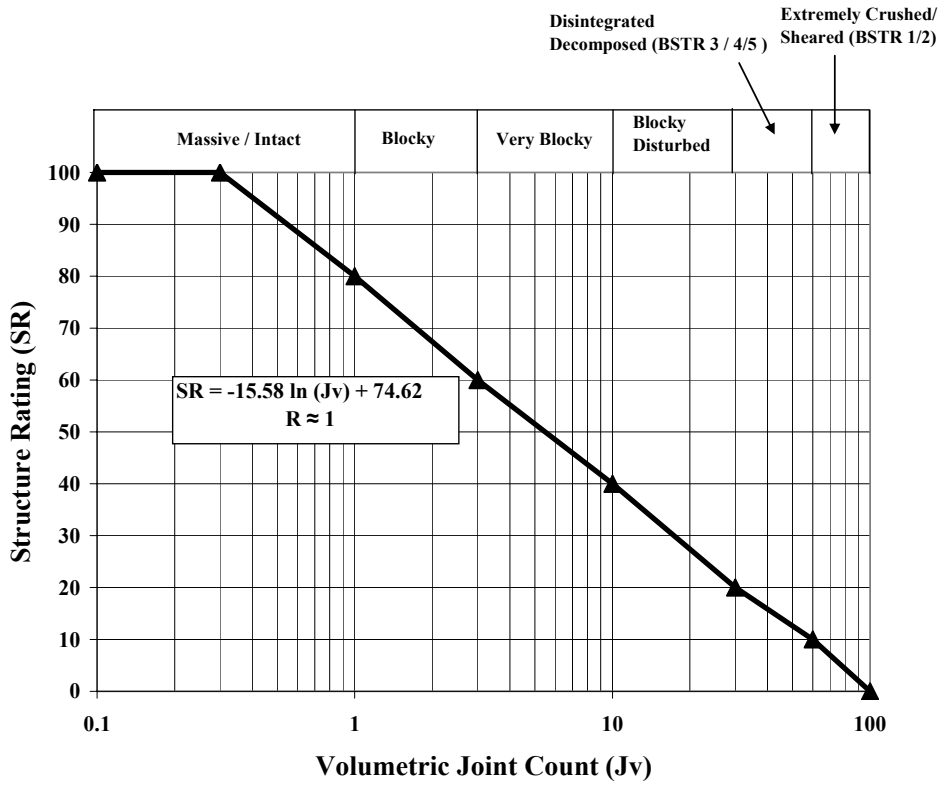

Figure 3-11 The relationship between structure rating (SR) and the Volumetric Joint Count (Jv), suggested in this study.

In the present study, the joint condition ratings for Modified-GSI for very poor rock masses are adopted from Modified–RMR system developed by Özkan (1995) and Ünal (1996). The M-RMR classification system has been recognized to better characterize the weak, stratified, anisotropic and clay-bearing jointed rock masses.

In order to determine the joint condition index (I_{jc}) used in Modified-GSI chart, BSTR type, Intact Core Recovery (ICR) values, filling condition, and weathering conditions should be known as shown in Table 3-3.

ICR is defined as the total length of the cylindrical core pieces greater than 2 cm divided by the total length of the structural region or drill-run. The ICR for poor and very poor rock masses (Disintegrated / Decomposed or BSTR 3/ 4/ 5, and Extremely Crushed/ Sheared or BSTR 1/ 2) is assumed to be less than 25 to satisfy the Modified-GSI requirements.

For joint condition rating, the upper part of Modified-GSI chart (Figure 3-3) is divided into 2 categories; namely, poor and very poor. For ICR < 25 %, the total rating of joint condition index varies between 0 and 16. A simple way of determining joint condition index (I_{jc}) is clearly described in Table 3-3.

Table 3-3 Joint condition index (Ijc) ratings for using in Modified-GSI

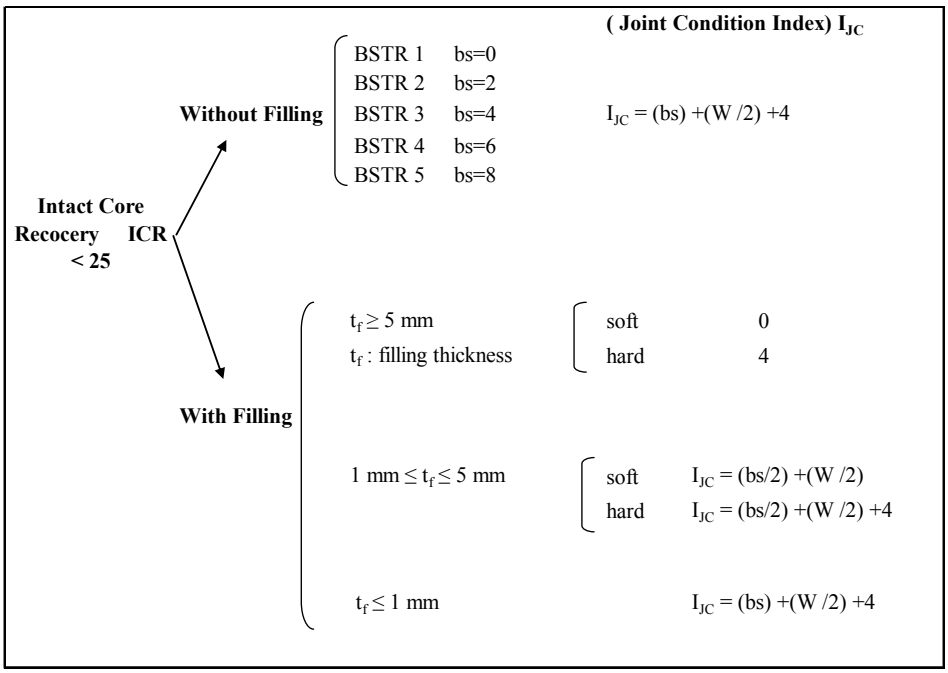

Condition					Rating
	Unal 1996	*ISRM 1981*	*Class*	*Wc*	
Weathering "W"	Unweathered	Fresh	1	<1,1	8
	Slightly Weathered	Slightly Weathered	2	1,1-1,5	7
	Moderately Weathered	Moderately Weathered	3	1,5-2,0	6
	Highly Weathered	Highly Weathered	4	>2,0	4
	Very Highly Weathered	Completely Weathered	5		2
	Decomposed	Residual Soil	6		0

$W_c = R_f / R_w$ *where R_f is the rebound number obtained from fresh rock surface and Rw is the rebound number gained from the weathered rock surface in Schmidt hammer test*

If Wc is known, Rating = 10,7-2,7 Wc ***(Gokceoğlu & Aksoy 2000)***

3.6 Poor and very poor rock mass strength envelope

In this section, the strength envelopes for various poor rock mass classes are presented. Hoek-Brown failure criterion is used to relate the major and minor principal stresses in a wide range of rock mass quality. This failure criterion will be considered as the yield criterion for the proposed elasto-plastic solution in Chapter 5.

3.6.1 Hoek - Brown failure criterion

The Hoek-Brown failure criterion was introduced in the early eighties to describe the shear strength of intact rock as measured in triaxial tests (Hoek & Brown 1980a, b). The failure criterion for intact rock defines the combination of major and minor principal stresses (σ_1 and σ_3) at failure to be:

$$\sigma_1' = \sigma_3' + \sigma_{ci}\left(m_i \frac{\sigma_3'}{\sigma_{ci}} + 1 \right)^{\frac{1}{2}} \tag{3-15}$$

In the equation above, σ_{ci} is the unconfined compressive strength of the rock and the coefficient m_i is a parameter that depends on the type of rock (normally $5 \leq m_i \leq 40$). Both parameters, σ_{ci} and m_i , can be determined from regression analysis of triaxial test results (Hoek & Brown 1980a, b; Hoek *et al*. 1995). The Hoek-Brown failure criterion was later extended to define the shear strength of rock masses. This form of the failure criterion, which is normally referred to as the generalized Hoek-Brown failure criterion, is:

$$\sigma_1' = \sigma_3' + \sigma_{ci}\left(m_b \frac{\sigma_3'}{\sigma_{ci}} + s \right)^{a} \tag{3-16}$$

The coefficients m_b, s and a in Equation 3-16 are semi-empirical parameters that characterize the rock mass. In practice, these parameters are associated with rock mass rating RMR and more recently the Geological Strength Index or GSI (Hoek, 1994; Hoek & Brown, 1997). This index lies in range 5-85 and can be quantified from charts based on the quality of the rock structure and the condition of the rock surfaces (Hoek & Brown 1997; Hoek *et al.*1998; Marinos & Hoek 2000). In the latest update of the Hoek-Brown failure criterion, the relationship between the coefficients m_b, s and a in Equation 3-16 and the GSI is as follows (Hoek *et al.* 2002):

$$m_b = m_i \exp\left(\frac{GSI - 100}{28 - 14D} \right) \tag{3-17}$$

$$s = \exp\left(\frac{GSI - 100}{9 - 3D} \right) \tag{3-18}$$

$$a = \frac{1}{2} + \frac{1}{6}\left(e^{-GSI/15} - e^{-20/3} \right) \tag{3-19}$$

In Equations 3-17 and 3-19, *D* is a factor that depends on the degree of disturbance to which the rock has been subjected to blast damage and stress relaxation. This factor varies between 0 and 1. It is worth noting that the failure criterion for intact rock (Equation 3-16) can be recovered from the failure criterion for rock masses (Equation 3-16) by making $m_b = m_i$, $s = 1$ and $a = 0.5$. The normalized form of Hoek-Brown failure criterion can be written as:

$$\sigma'_{1n} = \sigma'_{3n} + \left(m_b \sigma'_{3n} + s\right)^a \tag{3-20}$$

where σ'_{1n} and σ'_{3n} are the normalized principal stresses (σ'_1/σ_{ci}) and (σ'_3/σ_{ci}), σ_{ci} being the uniaxial compressive strength of the intact rock pieces in the rock mass.

Likewise, the generalized Hoek & Brown yield criterion in terms of the residual strength can be defined as follow:

$$\sigma_1 = \sigma_3 + \sigma'_{ci}\left(m_b' \frac{\sigma_3}{\sigma_{ci}'} + s'\right)^{a'} \tag{3-21}$$

The primed constants stand for the residual values of the rock mass.

Table 3-4 gives a set of approximate equations defining the relationships between principal stresses for poor and very poor rock masses in conformity with the latest version of the Hoek-Brown failure criterion (Hoek *et al*. 2002). The principal stresses are defined as the normalized stresses (stress / intact rock strength). In order to use Table 3-4 for the approximate analysis of poor and very poor rock mass failure, estimate either the value of the Modified- GSI or the type of BSTR and use the indicated equations to calculate the normalized major principal stress as required.

It should be noted that the uniaxial compressive strength of the intact rock used in Modified-GSI might be estimated by indirect tests such as the point load test (Bieniawski, 1975), or Block Punch Index (Ulusay & Gokçeoğlu, 1999; Sülükçü & Ulusay, 2001; Ulusay *et al.* 2001) or guideline given by ISRM (1981). This is due to the fact that in poor rocks, the indentation of the loading points may cause plastic deformation rather than fracture of the specimen. In such cases the point load test does not give reasonable results. This can be attributed to the fact that for small rock core discs, obtained from very poor rock mass, the core length may be too short to allow preparation of the specimens long enough even for the point load strength index test (Ulusay *et al.* 2001). Besides, in poor rock mass, the coring process often breaks up the weaker core pieces, and they are too small to be used in either uniaxial compressive or point load tests (Sülükçü & Ulusay, 2001). Therefore, another alternative is to use the Block Punch Index test, which requires only small, flat disc specimens. Where it is not possible to obtain samples for both point load and block punch index tests, the only remaining alternative is to turn to a

qualitative description of the rock material in order to estimate the uniaxial compressive strength of the intact rock. A guideline listing such descriptions is given elsewhere (Hoek & Brown, 1997).

Table 3-4 Approximate equations for normalized principal stress relationships of Hoek Brown failure criterion used for poor and very poor rock masses. Key: $\sigma_{1n} = \sigma_1/\sigma_{ci}$, $\sigma_{3n} = \sigma_3/\sigma_{ci}$, and σ_{ci} is the uniaxial compressive strength of the intact rock

ROCK CLASS	Failure Criterion Envelope Equations ($\sigma 1$ vs $\sigma 3$ and τ vs σ spaces)	Broken Structural Domain Type
Modified-GSI=6	$\sigma_{1n} = \sigma_{3n} + (0.209\ \sigma_{3n} + 0.0000291\ )^{0.612}$	BSTR 1
Modified-GSI=10	$\sigma_{1n} = \sigma_{3n} + (0.321\sigma_{3n} + 0.0000454\ )^{0.585}$	BSTR 2
Modified-GSI=15	$\sigma_{1n} = \sigma_{3n} + (0.432\sigma_{3n} + 0.0000791\ )^{0.561}$	BSTR 2
Modified-GSI=20	$\sigma_{1n} = \sigma_{3n} + (0.574\sigma_{3n} + 0.0001379\ )^{0.544}$	BSTR 3
Modified-GSI=24	$\sigma_{1n} = \sigma_{3n} + (0.663\sigma_{3n} + 0.0002\ )^{0.533}$	BSTR 4
Modified-GSI=27	$\sigma_{1n} = \sigma_{3n} + (0.737\sigma_{3n} + 0.0003\ )^{0.527}$	BSTR 5
Assumptions: The uniaxial compressive strength of intact rock (σci) varies between 0.25 MPa and 10 MPa in accordance with Modified-GSI value. The mi value for different values of Modified-GSI is assumed to be varied between 6 and 10.		

CHAPTER 4

SUPPORT PRESSURE (ROCK LOAD) ESTIMATION FOR TUNNELS IN POOR AND VERY POOR ROCK MASSES

4.1 Introduction

Reliable prediction of tunnel support pressure (rock load) is a difficult task in the area of rock engineering and has been highly subjective to argument. The term support pressure (rock load, rock pressure, and support load density) in this chapter is referred to the load, which acts on the support systems in a tunnel. Starting with Terzaghi's rock load concept (Terzaghi, 1946), several empirical approaches using rock mass classification systems (empirical design approaches) have been developed to, either explicitly or implicitly, estimate support pressure in tunnels (Protodyakonov, 1964; Deere & Deere, 1988; Wickham *et al*.1972; Bieniawski, 1989; Barton *et al.* 1974; Ünal, 1983, 1992, 1996; Venkateswarlu, 1986; Ghose & Ghosh, 1992; Verman, 1993; Singh *et al*.1992; Palmström 1995, 1996, 2000; Goel *et al.* 1996; Grimstad & Barton, 1993; Bhasin & Grimstad, 1996, and Barton, 2002). Most of these approaches classify tunnelling conditions into several distinctly different groups and correlate these groups with stable support capacities. The different empirical approaches for support pressure estimation are presented in Table 4-1.

However, there have been found in literature some analytical approaches based on elasto-plastic closed-form solutions for support pressure estimation (Talobre, 1957; Kastner, 1962; Rabcewicz, 1964, 1965; Daemen, 1975; Hoek & Brown, 1980b; Brown *et al*.1983; Sheorey, 1985; Carranza-Torres, 2004). Only a few efforts based on partial numerical studies (Voegele & Fairhurst, 1982) and physical modelling (Whittaker *et al*., 1992) have, up to date, been made in estimating support pressure (rock lod, rock pressure).

Although a good many approaches have been developed to estimate support pressure (rock load), three influential parameters on support pressure; namely, the effect of opening size, the effect of the overstressed rock (squeezing ground condition especially in weak rock mass), and the effect of anisotropy in field stress have not been, due to the lack of the numerical studies, comprehended. Nonetheless, those empirical design approaches based on rock mass classification have been realized to be more helpful in the early stage of design procedure.

In this part, an empirical approach (rock mass classification) in tandem with the numerical methods presents a comparable expression in such a way as to take all notably geotechnical parameters into consideration as presented in the flowchart of Figure 4-1.

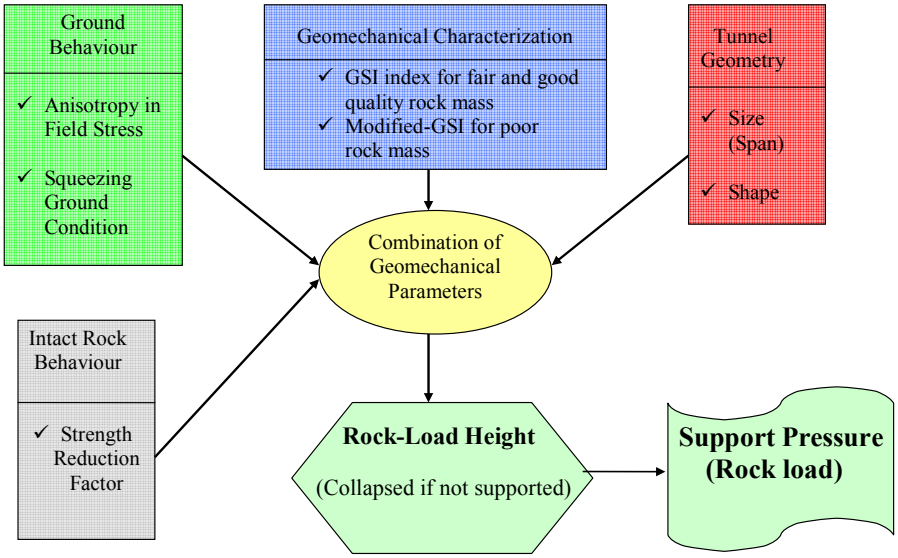

Figure 4-1 New concept for estimation of support pressure in rock tunnels

4.2 Squeezing-prone ground condition

There has been a recent interest in tunnels which have undergone large deformation. The cause of great deformation of tunnels is acknowledged to be due to the yielding of intact rock under a redistribution of state of stress following excavation which exceeds the rock's strength. If this deformation takes place gradually it is termed as squeezing (Aydan *et al*., 1993, 1996).

Incompetent or poor rock masses undergo plastic failure when overstressed. Such a rock mass around a tunnel fails when the tangential stress exceeds its strength. The failure of rock mass is associated with volumetric expansion, which is manifested in the form of radial inward displacement of the tunnel periphery. These deformations are called tunnel closure (convergence). The tunnel closures can be very large (measured closures have been as large as 17% of the tunnel diameter). This phenomenon is called "squeezing" of the rock mass (Aydan *et al*., 1993, 1996).

Squeezing of rock is the time dependent large deformation, which occurs around the tunnel, and is essentially associated with creep caused by exceeding the

ultimate rock mass strength. Deformation may terminate during construction or continue over a long time period (ISRM, 1981). Squeezing can occur in both rock and soil as long as the particular combination of induced stress and material properties pushes some zones around the tunnel beyond the ultimate strength of rock mass at which creep starts.

Table 4-1 Summary of various empirical approaches for support pressure estimation

Investigators	Support pressure estimation approaches	Remarks
Terzaghi (1946)	$P = H_P \cdot \gamma \cdot Z \qquad H_p \approx f(H_t, B)$ $P = \frac{B_i(\gamma - 2C/B_i)}{2k \cdot \tan\phi} \cdot \left[1 - \exp\left(-\frac{2kZ \cdot \tan\phi}{B_i}\right)\right]$ $B_i = 2B + 2H_t \tan(45 + \frac{\phi}{2})$	Size dependent, qualitative approach H_P: rock-load height, H_t: tunnel height, Φ: internal friction angle of rock, k=lateral earth pressure coefficient, C: cohesion of rock
Prtodyakonov (1964)	$P = \frac{1}{3}\gamma\frac{b^2}{f} \qquad H_p = \frac{b}{2f}$ $b = B + 2Z \cdot \tan(45 - \frac{\phi}{2})$	Size dependent, qualitative approach f : coefficient of internal friction angle
Deere & Deere (1988)	Modified the Terzaghi's approach	Size dependent, RQD included,
Wickham & Tiedemann (1974)	$P = \frac{D}{302}\left[\left(\frac{8800}{RSR + 30}\right) - 80\right]$	Size dependent, quantitative approach, D (ft) and P (kips/ft^2)
Barton *et al*. (1974) and Barton (2002)	$P = \frac{0.2}{3} \cdot \frac{J_n^{\frac{1}{2}}}{J_r} Q^{-\frac{1}{3}} \qquad P = \frac{0.2}{J_r} Q^{-\frac{1}{3}}$	Size independent, quantitative approach, hard rock
Voegele & Fairhurst (1982)	$P = nB^2$ $n = 2 + 5A \qquad B = 4\frac{c_h \tan\phi}{\gamma}$	Size dependent, distinct element modelling of jointed rock mass
Ünal (1983, 1992)	$P = S\frac{100 - RMR}{100}\gamma \cdot B$	Size dependent, quantitative approach, U.S. coal mining
Venkateswarlu (1986)	$P = (1.7 - 0.037\,RMR + 0.0002\,RMR^2) \cdot B \cdot \gamma$	Size dependent, quantitative approach, Indian coal mining, the value of RMR used in equation should be modified based on CMRS (Central Mining Research Station) classification
Goel & Jethwa (1991)	$P = \frac{0.75B^{0.1}H^{0.5} - RMR}{2RMR}$	Size dependent, quantitative approach
Ghose & Ghosh (1992)	$P = 5B^{0.3}\gamma\left(\frac{100 - RMR}{100}\right)^2$	Size dependent, quantitative approach, Indian coal mining
Bhasin & Grimstad (1996)	$P = \frac{0.04B}{J_r} Q^{-\frac{1}{3}}$	Size dependent, quantitative approach, for Q < 4
Singh *et al*. (1992)	$P = \frac{0.2}{J_r} Q_i^{-\frac{1}{3}} \cdot f \cdot f' \cdot f'' \quad Q_i = 5Q$	Size independent, quantitative approach, for arched roof (tunnels and caverns), applicable to hard and weak rock mass
Goel *et al*. (1996)	$Non - squeezing \;, P = \frac{0.12H^{0.1} \cdot a^{0.1}}{Q'^{0.33}} - 0.038$ $Squeezing \;, P = \left(\frac{f(N)}{30}\right) \cdot 10^{\left(\frac{H^{0.6} \cdot a^{0.1}}{50 \cdot Q'^{0.33}}\right)}$	Considerably size dependent in squeezing ground condition and slightly size dependent in non-squeezing, quantitative approach, for arched roof (tunnels and caverns), applicable to hard and weak rock mass
B : Tunnel span, Ht : Rock-load height, γ:Unit weight of overburden, Z : depth of tunnel, f: coefficient, D: tunnel diameter, A: coefficient, a : coefficient, C: cohesion		

The magnitude of tunnel convergence associated with squeezing, the rate of deformation, and the extent of the yielding zone around the tunnel depend on the geological conditions, the in-situ stresses relative to rock mass strength, the ground water flow and pore pressure and the rock mass properties (Barla, 1995, 2001).

Non-squeezing ground conditions are common in the majority of tunnelling projects. Squeezing ground conditions, on the other hand, have generally been encountered where the rock masses are weak, highly jointed, faulted, folded and tectonically disturbed and the overburden is high. The combination of the weak rock mass and the high in-situ stress is responsible for squeezing. Tunnelling in squeezing ground has its individual problems.

4.2.1 Support pressure and squeezing ground condition

As a first attempt to quantify the squeezing potential of rocks in terms of loading of the initial support, Terzaghi (1946) developed a range of values for the rock load for rock mass class 7 and 8 which relate to squeezing grpund conditions as outlined in Table 4-2.

Table 4-2 Terzaghi's rock-load classifications for squeezing ground condition (Terzaghi, 1946)

"Rock Condition"	"Rock-load (H_p) in m of rock on roof of support for m of tunnel length"
Class 7: squeezing rock, moderate depth	(1.1 to 2.1) ($B + H_t$)
Class 8: squeezing rock, great depth	(2.1 to 4.5) ($B+ H_t$)

where B and H_t are the width and height of the tunnel at depth more than 1.5 ($B+ H_t$), respectively.

Following Terzaghi's concept, a number of approaches have been proposed by various researchers, based on practical experience and documented case histories, to identify squeezing rock conditions and potential tunnel squeezing problems.

Singh *et al.*(1992) criticized that support pressure predicted from existing approaches is unreliable; particularly, in the case of the squeezing ground condition. Based on the results obtained from many case studies, they concluded that predicted support pressures by others' correlations were not compatible with those gained from in-situ measurements. They discovered that tunnel depth, tunnel convergence, support system stiffness, and time of support installation might have been effective parameters to be included in support pressure estimation.

Goel (1994) presented two sets of empirical correlations for estimating support pressure for tunnel under non-squeezing and squeezing ground conditions in eight tunnelling projects located in the Himalaya and India (see Table 4-1). He compared the support pressure estimated from Barton's approach (Barton *et al.* 1974) with the actual measured values for various test-sections. He found out that the estimates were reasonable for tunnel section through non-squeezing ground conditions. He also pointed out that, in squeezing ground conditions, the estimated support pressure had never exceeded 0.7 MPa whereas the measured value had been as high as 1.2 MPa for larger tunnels. Therefore, it was thought that the Q-system might be unsafe for larger tunnels (diameter > 9 m) under highly squeezing ground conditions.

Bhasin and Grimstad (1996) developed an approach accounting for the effect of the tunnel span. Based on support pressure values obtained both from equations and in-situ measurements, they concluded that the inclusion of the dimension factor for squeezing rocks provided more realistic and reasonable results.

4.2.1.1 Empirical approaches

The empirical approaches to identify the squeezing rock conditions are essentially based on classification systems. The Terzaghi's classification was the first of a number of methods for identifying saqueezing behaviour in tunnels. However, the Q-system (Barton *et al*. 1974) was the first to apply numerical indices to classify the amount of squeezing.

Singh *et al.* (1992) also proposed an empirical approach as a squeezing criterion using Barton's rock mass quality Q and overburden H_q (m) as below:

$$H_q = 350Q^{\frac{1}{3}} \tag{4-1}$$

where H_q= tunnel depth in metres; Q = rock mass quality (Barton *et al*. 1974) (Q= $(RQD/J_n)\ (J_r/J_a)\ (J_w/SRF)$); RQD = rock quality designation ≥ 10 even if RQD = 0; J_n = joint set number; J_r = joint roughness number for critically oriented joints; J_a= joint alteration number for critically oriented joints; J_w = joint water reduction factor; and SRF = stress reduction factor.

Goel *et al.* (1995) refined the Singh's approach and developed a new correlation in terms of depth of the tunnel and rock mass number. Their relations are in a good consistent with Singh's approach as shown below:

$$H_q=(275\ N^{0.33})\ B^{-1} \tag{4-2}$$

where $N= (Q)_{SRF=1}$, and B (m) is span of the tunnel.

The squeezing degree has also been expressed in terms of tunnel convergence or closure (Singh *et al*.1992, 1997. Indraratna & Kaiser 1990b), strength factor (Bhasin & Grimstad, 1996, Hoek & Marinos, 2000), and critical strain concept

(Hoek & Marinos, 2000, Lunardi, 2000). Since the tunnel convergence is an important indicator of tunnel stability, the squeezing behaviour has been evaluated in terms of tunnel convergence in the current study. The total convergence can be predicted through the elasto-plastic solution which will be introduced in Chapter 5.

Singh *et al* (1992, 1997) defined the normalized tunnel closure as a rational measure of squeezing intensity as below:

$$SI = \frac{u_{ri}}{r_i} \tag{4-3}$$

where u_{ri} is radial unsupported-tunnel closure, r_i is the tunnel radius or approximate half of the span. Given percentage of the squeezing intensity (SI), ground can be classified as:

If SI= 1-3 %, mild squeezing.

If SI= 3-5 %, moderate squeezing.

If SI > 5%, high squeezing.

The degree of squeezing behaviour in terms of strength factor was also presented by Jethwa *et al.* (1981) as given in Table 4-3. The strength factor can be defined as:

$$\text{Strength Factor (SF)} = \frac{c_{cm}}{\gamma H} \tag{4-4}$$

where σ_{cm} is the unconfined compressive strength of rock mass, γ is the unit weight of rock mass, and H is the tunnel depth below surface.

Table 4-3 The degree of squeezing ground condition in terms of the strength factor (Jethwa *et al.*1981), key: σ_{cm} : rock mass strength

$\sigma_{cm} / \gamma H$	*Degree of squeezing*
< 0.4	Highly squeezing
0.4-0.8	Moderately squeezing
0.8-2.0	Mildly squeezing
>2.0	No squeezing

According to a survey including 21 Japanese's tunnels excavated in very weak rock masses, (Aydan *et al.,*1993, 1996), where the uniaxial compressive of intact rocks (σ_{ci}) were less than 20 MPa, the degree of squeezing rock mass has been

characterized in terms of strength factor by Palmström (1995, 1996, 2000) as given in Table 4-4.

Barla (1995) presented a criterion for identify the squeezing ground condition based on some tunnel cases in Italy. The definition of the squeezing ground condition by ISRM (1981) was incorporated to his criterion as given in Table 4-5. σ_θ is the induced tangential stress around the tunnel.

Table 4-4 The squeezing class of rock mass in terms of strength factor (SF) (Aydan *et al.*, 1993, 1996 and Palmström, 1995)

Squeezing class	Rock mass behavior Aydan et al. (1993,1996)
No squeezing SF > 1	The rock behaves elastically and the tunnel will be stable as the face effect ceases.
Light squeezing SF=0,7-1	The rock exhibits a strain-hardening behavior. As a result, the tunnel will be stable and the displacement will converge as the face effect ceases.
Moderate squeezing SF=0,5 - 0,7	The rock exhibits a strain-softening behavior, and the displacement will be larger. However, it will converege as the face effect ceases.
Heavy squeezing SF= 0,35-0,5	The rock exhibits a strain-softening behavior at much higher rate. Subsequently, displacement will be large and will not tend to coverege as the face effect ceases.
Very heavy squeezing SF < 0,35	The rock flows, which will result in the collapse of the medium and the displacement will be very large and it will be necessary to re-excavate the tunnel and install heavy support.

Table 4-5 The degree of squeezing ground condition in terms of the strength factor (ISRM, 1981 and Barla, 1995)

Degree of squeezing	$\sigma_\theta / \sigma_{cm}$ *(ISRM,1981)*	$\sigma_{cm} / \gamma H$ *(Barla, 1995)*
No squeezing	< 1.0	> 1.0
Mild squeezing	1.0-2.0	0.4-1.0
Moderate squeezing	2.0-4.0	0.2-0.4
High squeezing	>4.0	<0.2

The criterion for predicting the squeezing phenomenon suggested by Bhasin & Grimstad (1996) is outlined in Table 4-6.

Furthermore, Hoek (1999) published details of an analysis showing that the ratio of the uniaxial compressive strength of the rock mass σ_{cm} to the in-situ stress P_o can be used as an indicator of potential tunnel squeezing problems when the tunnel strain is known. Hoek & Marinos (2000) reported, based on a large number of data, a sudden increase in tunnel convergence occured for a strength / stress ratio of less

than about one third. The following relationship was given for fitting the case histories data (Hoek & Marinos, 2000):

$$\varepsilon = 0.2\left(\frac{\sigma_{cm}}{P_o}\right)^{-2} \tag{4-5}$$

where ε = strain (tunnel closure/ tunnel diameter), σ_{cm} = rock mass strength, and P_o = in-situ stress. Sakurai's critical strain of approximately 2 %, which represents the boundary between stable tunnels and unstable tunnels, might have been well incorporated with the Hoek's observations (Sakurai, 1983).

Table 4-6 The degree of squeezing ground condition (Bhasin & Grimstad 1996)

Degree of squeezing	$\sigma_\theta / \sigma_{cm}$
Non-squeezing	0-1
Mild to moderate squeezing	1-5
Heavy squeezing	5-8

To illustrate, if Equation 4-5 is solved for $\left(\frac{\sigma_{cm}}{P_o}\right) = 0.3$, the acquired strain satisfies the Sakurai's criterion (1983). Correspondingly, Hoek (2001) points out that if the ratio of the rock mass strength to in-situ stress falls below 0.2, squeezing of rock mass becomes a problem that can cause instability of the tunnel. The variation of the critical strain (tunnel closure/ tunnel diameter) with ratio of rock mass strength over in-situ stress (strength factor) is demonstrated in Figure 4-2. In order to compare the approach of Hoek & Marinos (2000) and that of Aydan *et al*.(1993, 1996), Table 4-7 outlines the range of tunnel strains expected in two cases.

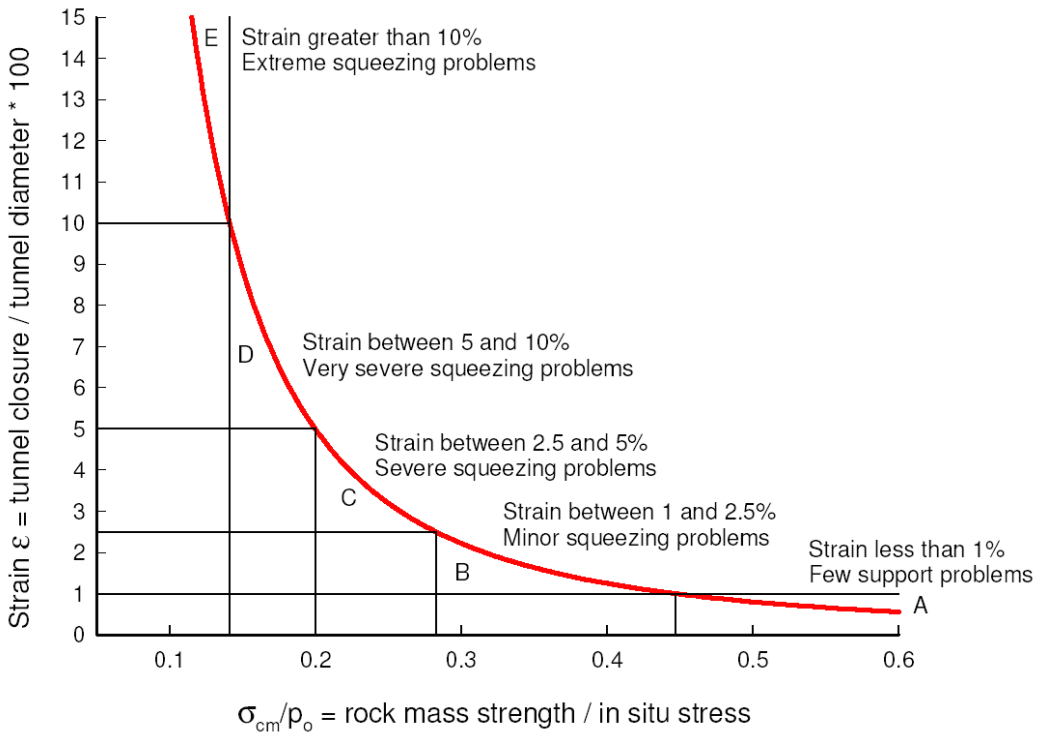

Figure 4-2 The relationship between the strain and strength factor to indicate the degree of squeezing ground condition (Hoek & Marinos, 2000)

Table 4-7 The squeezing ground classes in terms of critical strain concept

Approach	Aydan *et al.*(1993)		Hoek & Marinos (2000)	
Class No.	Squeezing Degree	Tunnel strain (%)	Squeezing Degree	Tunnel strain (%)
1	No squeezing	$\varepsilon \leq 1$	Few support problems	$\varepsilon \leq 1$
2	Light squeezing	$1 \leq \varepsilon \leq 2$	Minor squeezing	$1 \leq \varepsilon \leq 2.5$
3	Fair squeezing	$2 \leq \varepsilon \leq 3$	Severe squeezing	$2.5 \leq \varepsilon \leq 5$
4	Heavy squeezing	$3 \leq \varepsilon \leq 5$	Very severe squeezing	$5 \leq \varepsilon \leq 10$
5	Very heavy squeezing	$5 \leq \varepsilon$	Extreme squeezing	$10 \leq \varepsilon$

NATM (New Austrian Tunnelling Method) classes 5 and 6 are related to squeezing ground condition (Bieniawski, 1989; Palmström, 1995). The class 5 indicates that moderate squeezing, often caused by structural defect such as closely jointing, seams and shears. The rock support can sometimes be overloaded. Development of a deep zone with inward movement and slow decrease of the large deformation, ultimately culminating in overloaded rock support, fall in class 6 of NATM classes. The degree of squeezing ground condition in terms of competency factor corresponds to the NATM class as outlined in Table 4-8.

Table 4-8 The degree of squeezing ground condition in terms of strength factor or the competency factor (Palmström, 1995)

NATM class	Strength Factor (SF)
1. Stable	SF >2
2. Slightly ravelling	SF > 1
3. Ravelling	SF > 1
4. Strongly ravelling	SF = 0,7-2
5. Squeezing	SF =0,35 -0,7
6. Strongly squeezing	SF < 0,35

Owing to the fact that almost all of the tunnelling works in poor rock masses withstand squeezing ground condition, it is of paramount importance to take this effect into consideration in precisely estimating the support pressure. The guideline for squeezing correction factor used in the proposed empirical approach was adopted and modified from the results of Singh *et al*. (1992, 1997) and Hoek & Marinos (2000) as outlined in Table 4-9.

In proposed empirical equation, a rise in the value of correction factor (S_q) for tunnel closures beyond 5% is attributed to the increase in the loosening pressure which is reflected in a rising "ground reaction curve". Tunnel closures should normally not be allowed to exceed 5% of the tunnel size (Singh *et al*.1997).

Table 4-9 Suggested values for squeezing ground condition correction factors (S_q) used in empirical approach (adopted and modified from Hoek & Marinos, 2000 and Singh *et al.* 1997)

*Strains % (Tunnel closure or convergence/ tunnel diameter)*100*	*Rock mass strength / In-situ stress (σcm / Po)*	*Remarks*	*Suggested correction factor "S_q" for squeezing ground condition*
Less than 1% no squeezing	> 0.5	Few stability problems and very simple tunnel support design methods can be used. Tunnel support recommendations based upon rock mass classifications provide an adequate basis for design.	1
1- 2.5 % minor squeezing	0.3-0.5	Convergence confinement methods are used to predict the formation of a plastic zone in the rock mass surrounding a tunnel and of the interaction between the progressive development of this zone and different types of support.	1.5
2.5 -5 % severe squeezing	0.2-0.3	Two- dimensional finite element analysis, incorporating support elements and excavation sequence, is normally used for this type of problem. Face stability is generally not a major problem.	0.8
5- 10.0 % very severe squeezing	0.15-0.2	The design of the tunnel is dominated by face stability issues and , while two-dimensional finite analysis are generally carried out, some estimates of the effects of forepolling and face reinforcement are required.	1.6
More than 10 % extreme squeezing	< 0.15	Severe face instability as well as squeezing of the tunnel make this an extremely difficult three-dimensional problem for which no effective design methods are currently available. Most solutions are based on experience.	1.8

4.3 Newly proposed approach

4.3.1 Support pressure (rock-load) function

Not all the empirical approaches for support pressure estimation have been found to take into consideration all dominant geomechanical parameters. Most have limitations in their usage. Having realized the inadequacies of existing approaches, an attempt has been made to develop a more comparative approach to estimate the support pressure for tunnels (Osgoui & Ünal 2005b, Osgoui, 2006a). The proposed function was implicitly defined as:

$$P \approx f(GSI, D, c_{cr}, B, \gamma, C_s, S_q)$$

where GSI : Geological Strength Index defining the quality of rock mass, D: disturbance factor indicating the method of excavating, σ_{cr} : residual compressive strength of rock in broken zone around tunnel, B : span of tunnel, γ : unit weight of rock mass , C_s: correction factor for horizontal to vertical field stress ratio (k), S_q : correction factor for squeeze and non-squeeze ground condition.

As indicated by the foregoing support pressure function, nearly all influential parameters were taken into account. Similar to its previous counterpart developed by Ünal (1983, 1992, 1996), the newly proposed approach has its main advantage that the quality of rock mass is considered as the GSI. Due to its accepted applicability in a broad range of rock mass quality, the GSI was chosen to signify the rock mass quality in the proposed support pressure formula.

It makes it possible to estimate the support pressure (rock-load) for tunnels in various rock mass qualities provided that the GSI is determined. For very poor or poor rock masses where the GSI < 27, the Modified-GSI has to be used, instead of the GSI, for support pressure estimation (Osgoui & Ünal 2005b) as thoroughly explained in Chapter 3. It is, therefore, suggested that the new approach be applied to a wide spectrum of rock masses, the quality ranging from very good to very poor. The steps to be followed in defining the support pressure function were as below:

I. The original support pressure function previously developed by Ünal (1983, 1992) was considered to be main basis for the new equation because it uses Bieniawski's RMR system, which quantitavely evaluates the quality of rock mass.

II. The new support pressure function has been defined such that it does not have contradiction with Ünal's equation (1983, 1992), whose applicability have been widely accepted in the field of mining and tunnelling.

III. The importance of the two parameters (i.e. method of excavation and residual strength of rock), which are directly related to damage extention in rock mass around the tunnel, have been inspired from rock mass deformation equation introduced by Hoek *et al*. (2002).

IV. The definitions of squeezing ground condition and their correction factors have been adopted through descriptions originally introduced by Singh et al. (1992, 1997) and Hoek & Marinos (2000).

V. The effect of the unisotropy in field stress has been considered to follow its original definition given by Ünal (1992).

VI. The proposed support pressure function is valid only for cases where the horizontal stresses are equal in each direction.

VII. The proposed support pressure function applies for $\sigma_{ci} < 100$ MPa. The maximum value of σ_{ci} to be used in the proposed equation must be 100 MPa even if $\sigma_{ci} > 100$ MPa.

Therefore, the new equation for estimation of support pressure was proposed as follows:

$$P = \frac{100 - \left[(1 - \frac{D}{2}) \sqrt{\frac{\sigma_{cr}}{100}} GSI \right]}{100} C_s S_q \gamma B \qquad (4\text{-}6)$$

where $c_{cr} = S_r . c_{ci}$, $0 < S_r < 1$, S_r= post-peak strength reduction factor, characterizing the brittleness of the rock material as explained later on.

The most common form of the expression can be written when $S_r = 1$ as shown in Equation 4-7:

$$P = \frac{100 - \left[(1 - \frac{D}{2}) \sqrt{\frac{\sigma_{ci}}{100}} GSI \right]}{100} C_s S_q \gamma B = \gamma h_t \qquad (4\text{-}7)$$

Not considering the disturbance factor, uniaxial compressive strength of rock material, correction for both squeezing ground condition, and correction for field stress, the equation take a simple form as analogous to which that developed by Ünal (1983):

$$P = \frac{100 - RMR}{100} \gamma B \qquad (4\text{-}8)$$

where RMR is Bieniawski's Geomechanics Classification. The variation of the support pressure with rock mass quality and the opening span is demonstrated in Figure 4-3. As can be inferred, the support pressure increase as GSI value decreases. Further, the larger the span, the more considerably the rock load increases.

4.3.2 Rock- load height concept

This concept was primarily introduced by Terzaghi (1946) and a sophisticated definition of this idea was developed during a comprehensive study of roof strata in US coal mines by Ünal (1983, 1992, and 1996). The theory predicts the load on the support system purely based upon the rock quality (Bieniawski's RMR system) and tunnel span. Ünal's rock-load height concept states that above any underground opening excavated, a roof arch and a ground arch form. The existence of these two arches can be identified by examining the stress distribution in the roof strata. The support must withstand the weight of the roof arch and the portion of the ground arch load actively transferred on the roof arch. The major portion of the strata pressure (passive load), on the other hand, is transferred to the sides of the opening due to the existence of the roof arch preserved by the support system. Hence, the

total load that should be carried by support system is limited by the rock-load height, which is defined as the height of the potential instability zone, above the roof line and crown for rectangular, arch-roof, horse shoe openings, which will eventually fall if not properly supported (Ünal, 1992) (see Figure 4-4).

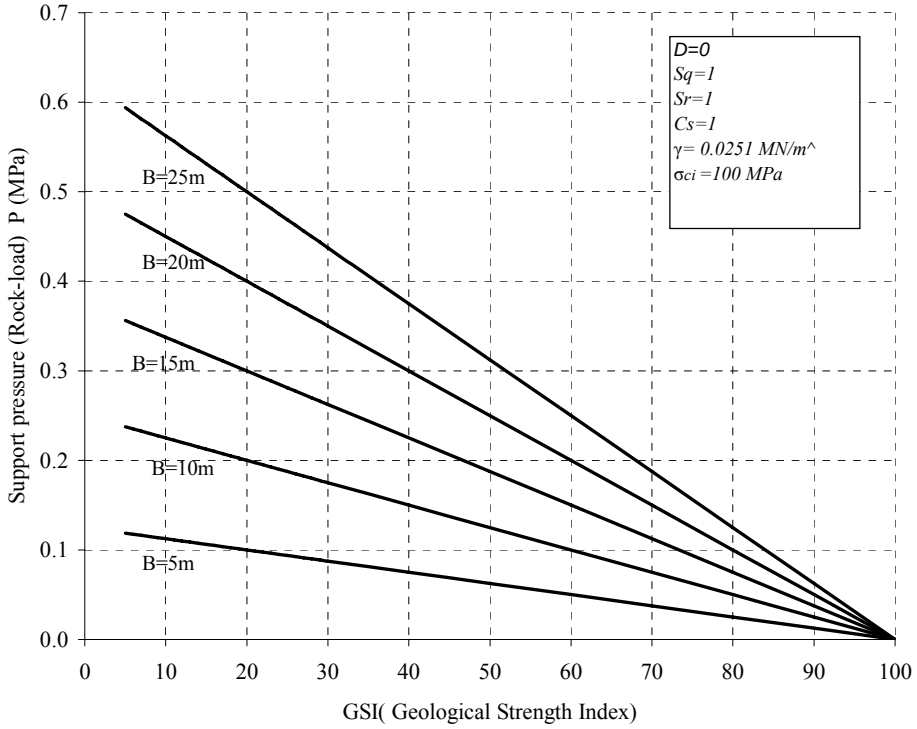

Figure 4-3 The variation of support pressure as a function of GSI for different roof spans

Given Ünal's rock-load height concept, the new proposed empirical function for support pressure estimation can be dependent on the parameters specified in previous expressions:

$$P \approx f(h_t\ , \gamma, C_s, S_q)$$

The rock-load height, on the other hand, can be expressed as shown in Equation 4-9:

$$h_t = \frac{100 - \left[\left(1 - \frac{D}{2}\right)\sqrt{\frac{\sigma_{cr}}{100}}GSI\right]}{100} C_s S_q B \qquad (4\text{-}9)$$

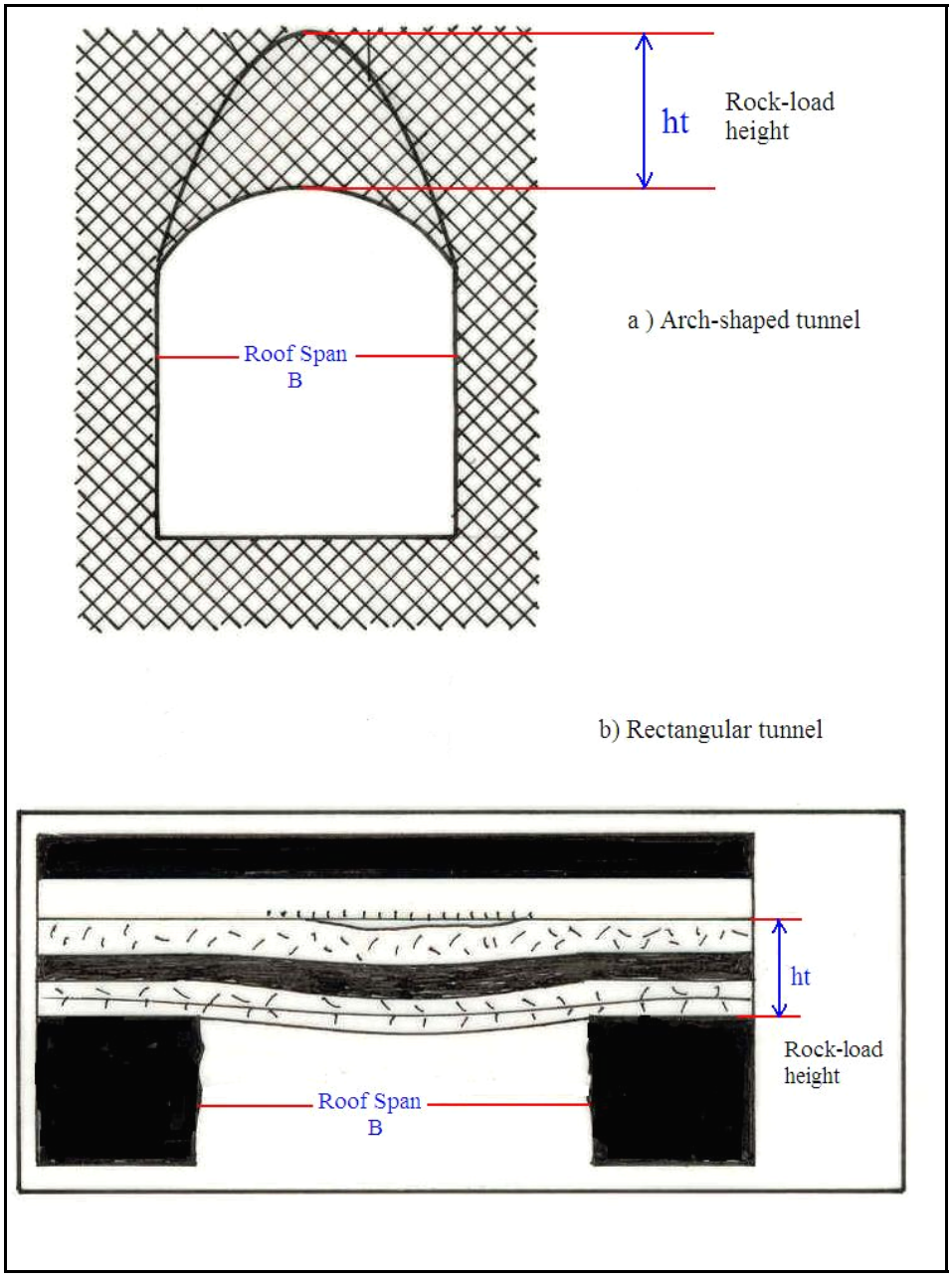

Figure 4-4 Rock-load height concept

4.3.3 Geomechanical parameters used in calculating support pressure

*4.3.3.1 Geological Strength Index (*GSI*) estimation*

In view of the fact that the Geological Strength Index (GSI) plays the most dominant role in determining the support pressure, it is of paramount importance that the GSI- index of rock mass be exactly estimated. GSI accounts for a large percentage of the support pressure value since it directly reflects the quality of the rock mass around the opening (see Figure 4-3).

As explained in Chapter 3, a distinction in estimating GSI for either fair to good quality rock mass or poor to very poor rock mass must be applied. The boundary which initiates the threshold of poor rock mass is defined at RMR=30. For fair to good quality rock mass if RMR > 30 then GSI= RMR. Consequently, the ways which have been developed so far by Hoek (1994), Hoek *et al.* (1995), and Hoek & Brown (1997) and extended by Hoek & Marinos (2000), Sönmez & Ulusay (1999, 2002), Cai *et al.* (2003, 2004), and Marinos *et al*. (2005) can be readily used. For poor rock mass where RMR < 30, on the other hand, as discussed in Part 3.3 , there are suggestions in estimating of the Modified-GSI.

4.3.3.2 The effect of the disturbance factor

The method of construction has a significant influence on support pressure. Conventional excavation methods (drill & blast) cause damage to the rock mass whereas controlled blasting and TBM tunnelling keep the rock mass undisturbed. Singh *et al*. (1992, 1997) declared that support pressure could be decreased up to 20% for cases such as those. In the empirical approach, this effective parameter was adopted and modified from that pointed out by Hoek *et al*. (2002).

In tunnels, the effects of heavy blast damage as well as stress relief (relaxation) as a result of the ground being unloaded cause a disturbance in the rock mass being defined by disturbance factor (*D*). This factor ranges from *D=0* for undisturbed rock masses, such as those excavated by a tunnel boring machine, to *D=1* for extremely disturbed rock masses such as driving tunnels or a large caverns that have been subjected to very heavy blasting. The factor also allows for the disruption of the interlocking of the individual rock pieces within rock masses as a result of the discontinuity pattern (Marinos *et al*., 2005).

Table 4-10 Modified guidline for estimating disturbance factor (D), which originally suggested by Hoek *et al.* (2002)

Description of rock mass	*Suggested value for D*
Excellent quality controlled blasting or excavation by Tunnel Boring Machine results in minimal disturbance to the confined rock mass surrounding a tunnel.	*D=0*
Mechanical or hand excavation in poor quality rock masses (no blasting) results in minimal disturbance to the surrounding rock mass	*D=0*
Usual blasting that causes local damages	*D= 0.5*
In mechanical excavation where squeezing problems result in significant floor heave unless a proper invert is placed	*D=0.5*
Very poor quality blasting in tunnel results in severe damages, extending 2 or 3 m, in the surrounding rock mass	*D=0.8*
Very poor quality blasting along with a intensive squeezing ground condition in tunnel - unexpectedly heavy blasting in caverns leading to significant cracks propagation on roof and walls	*D=1*

The results indicate that for the same properties of rock mass and opening, support pressure increases as the disturbance factor increases from 0 to 1 (See Figure 4-5). A guideline for choosing the disturbance factor is given in Table 4-10.

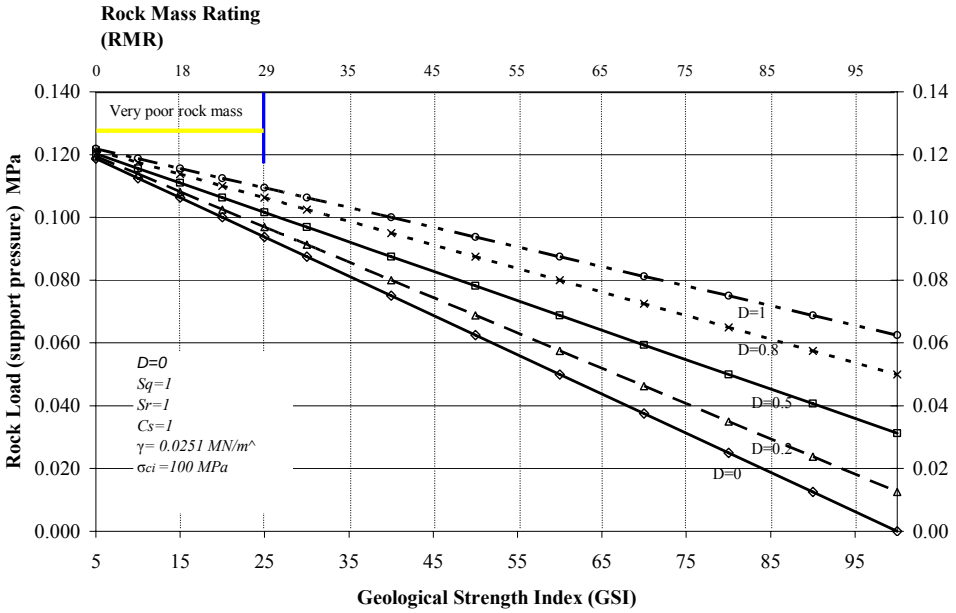

Figure 4-5 The variation of rock loads (support pressure) as a function of disturbance factor "*D*" for different rock mass classes

4.3.3.3 The effect of intact rock strength

Since the broken zone extension around an underground opening is dependent on the strength parameters of the rock, it is suggested that the compressive strength of rock material as an influential parameter in estimating the thickness of the broken zone (rock-load height) and support pressure be taken into account. In majority of sophisticated closed-form solutions for tunnels, the residual strength parameters are allowed for in calculations in accordance with the post failure behaviour of the rock. It is also substantiated that the extension of the broken zone relies on the residual value of the intact rock strength (Hoek & Brown, 1980b; Brown *et al*., 1983; Indraratna & Kaiser, 1990a; Carranza-Torres, 2004).

Hence, the effect of the compressive strength of rock material must be included in the form of the residual value because it loses its initial value due to stress relief or an increase in the strain. A stress reduction scale must, therefore, be considered as:

$$c_{cr} = S_r . c_{ci} \tag{4-10}$$

where S_r refers to the strength loss parameter quantifying the jump in strength from the intact condition to residual condition. The parameter S_r characterizes the brittleness of the rock material: ductile, softening, and brittle. By definition, *s* will fall within the range $0 < S_r < 1$. Where $S_r = 1$ implies no loss of strength and the rock material is ductile, or perfectly plastic. By contrast, if S_r tends to 0, the rock is brittle (elastic-brittle plastic) with the minimum possible value for the residual strength as highlighted in Figure 4-6.

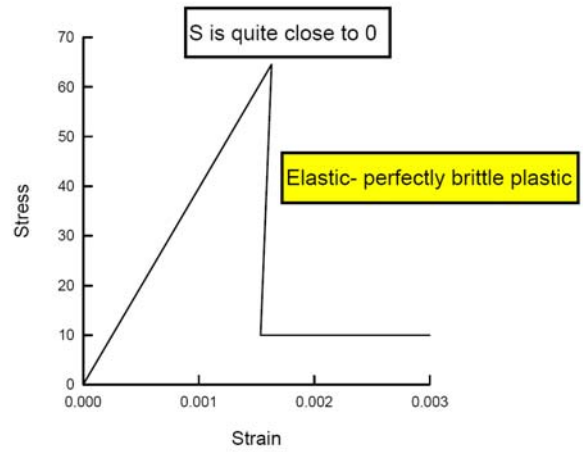

(a) Very good quality hard rock mass

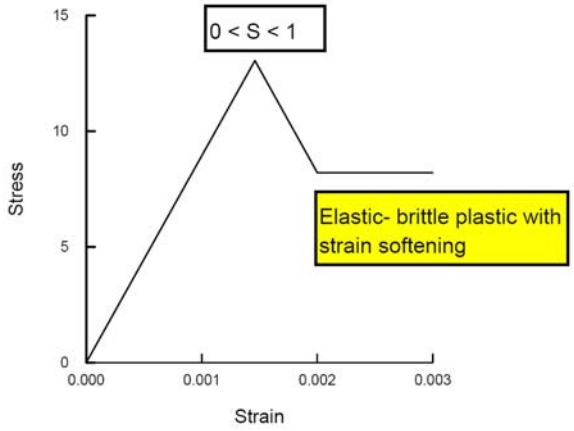

(b) Average quality rock mass

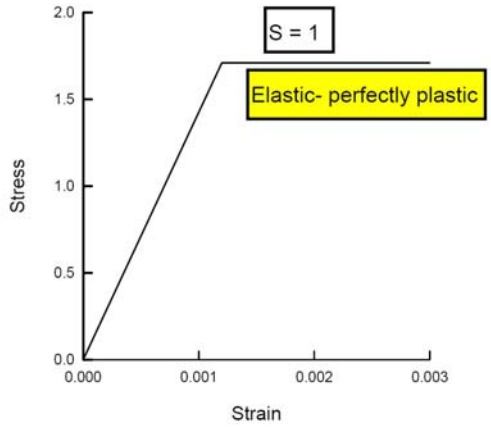

Figure 4-6 Suggested post- failure characteristics for different quality rock masses by Hoek & Brown (1997) and modified in terms of strength reduction factors in this study

4.4 Comparison of the support pressure with the estimates of Barton's Q-system

An empirical approach relating permanent support pressure and rock mass quality (Q-system), which fits available case records quite well, has been developed by Barton *et al*. (1974), in the following form:

$$P = \frac{0.2}{J_r} Q^{-\frac{1}{3}} \tag{4-11}$$

where P is the permanent roof-support pressure in MPa, J_r is the joint roughness number and Q is the rock mass Quality index. In cases where the number of joint sets is less than three, the following form of Equation 4-11 has been suggested:

$$P = \frac{2}{3} \cdot \frac{J_n^{\frac{1}{2}}}{J_r} Q^{\frac{-1}{3}} \tag{4-12}$$

where J_n is the joint set number. The estimates of the support pressure ranges, to be expected in practice, as a function of rock mass quality (Q) have also been presented by Barton *et al.* (1974) in the form of various plots.

In the current study, a comparison of the rock-load estimates between Q-system and proposed approach has been carried out as summarized in the following steps:

I. A number of Q values representing different rock classes are selected

II. For each Q value chosen, the corresponding RMR value is calculated using the well-known correlation proposed by Bieniawski (1979):

$$\text{RMR} = 9 \ln Q + 44 \tag{4-13}$$

III. For each RMR value selected, the associated value of GSI can be obtained as follows:

If RMR<30 then Modified- GSI $= 6 \exp(0.05\text{RMR})$

If RMR>30 then GSI = RMR

IV. For each Q value selected, the corresponding support pressure (rock-loads) ranges are estimated from the Braton equations suggested by Barton *et al.* (1974). It is worthwhile to note that support pressures were determined for upper, moderate, and lower value depending on *Jr* values.

V. The support pressure (rock-loads) is ultimately calculated using the empirically proposed equation based on GSI system.

Based on parametric studies, the summary of the support pressure and the rock loads as calculated respectively by Q-system and GSI- system are presented in the Table 4-11 and Figure 4-7.

The interpretation of support pressure obtained from Barton's equation (Barton *et al.* 1974; Barton, 2002) and proposed methods in terms of rock quality classes are explained as follows:

I. For very poor rock mass (RMR < 20): Irrespective of tunnel span, the constant support pressures suggested by Barton are significantly higher than those predicted by the proposed approach.

II. For poor rock mass (RMR: 21-40): Even though taken into account the effect of the tunnel span, the support pressures estimated by the proposed approach lay within the upper and lower limits of support pressures obtained by Barton's equation.

III. For fair quality rock mass (RMR: 41-60): If the J_r is considered as intermediate value .i.e. 2, the support pressures obtained by the proposed method are higher than those from Barton's equation irrespective of tunnel spans.

IV. For good quality of rock mass (RMR: 61-80): The predictions of the proposed method are in between the lower and the upper limits of the data of Barton's expression.

Table 4-11 A comparison between support pressure values of Q-system and proposed approach with the specified assumption.

Rock mass classes			Support pressure P (kPa) Barton *et al.* (1974) and Barton (2002)	Support pressure P (kPa) Barton *et al.* (1974) and Barton (2002)	Support pressure P (kPa) Barton *et al.* (1974) and Barton (2002)	Support pressure by proposed approach P (kPa)		
Q	**RMR**	**GSI**	**Jr=0,5 Upper limit**	**Jr=2 Moderate limit**	**Jr=4 Lower limit**	**B=5m**	**B=10m**	**B=15m**
0.001	N/A	5	4000.00	1000.00	500.00	124.38	248.75	373.13
0.01	3	7	1856.64	464.16	232.08	123.04	246.09	369.13
0.1	23	19	861.77	215.44	107.72	117.49	234.98	352.47
0.2	30	27	683.99	171.00	85.50	111.93	223.86	335.79
1	44	44	400.00	100.00	50.00	86.11	172.22	258.33
4	56	56	251.98	63.00	31.50	75.50	151.01	226.51
10	65	65	185.66	46.42	23.21	67.55	135.10	202.64
40	77	77	116.96	29.24	14.62	41.65	83.29	124.94
100	85	85	86.18	21.54	10.77	18.75	37.50	56.25
Jr	0.5		S	1		Slickensided, planar		
Jr	4		γ (MN/m3)	0.025		Discontinuous joint		
Jr	2		C	1		Undulating smooth		
B (m)	15		σci(MPa)	100				
			D	0				

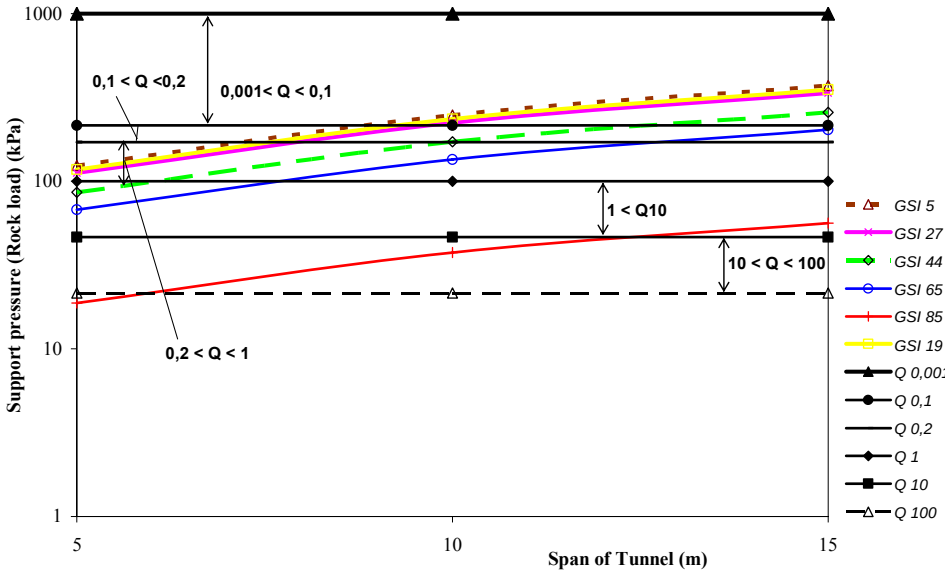

Figure 4-7 A comparison between support pressure values of Q-system and proposed approach

V. For very good quality rock mass (RMR: 81-100): The support pressures of Barton's method is much higher than those gained from the proposed approach if J_r=0.5. By contrast, the support pressure of proposed approach is higher than tha of Barton's equation in the case of J_r=2.

Note that in the foregoing comparison, for the proposed method, the machine excavation or controlled blasting method, isotropic field stress, non-squeezing ground condition, and constant strength factor are assumed.

It is worth noting that the support pressure obtained by Barton's method is independent of span of opening as indicated in Figure 4-7 and also from Equations 4-11 and 4-12. The validity of this concept has not been well revealed by Barton yet. Nevertheless, Bhasin and Grimstad (1996) modified the Barton's equation for very poor quality rock masses where the squeezing ground potential is bound to exist. They reported that for poor to very poor quality of rock masses, the support pressure directly increases with an increase in span. Also in the recent paper of Palmström and Broch (2006), they have not interpreted about the applicability and limitations of Barton's support pressure equation. Another uncertainties going to Barton's formula is that the effect of the joint roughness number (J_r) is taken into consideration twice in support pressure calculation. Firstly, in determining Q value itself and the secondly in the support pressure estimation with (J_r^{-1}). Therefore, it is recommended to apply the proposed approach especially for difficult ground condition (poor rock and possibility of the squeezing phenomenon) since it considerably contains more geomechanical factors.

Voegele & Fairhurst (1982) also compared the support pressures estimated by Barton's method to the rock loads calculated by Distinct Element Method (DEM).

Based on their analysis, it was concluded that the support load estimated by Q-system was considerably higher than that of DEM.

4.5 Analytical and numerical approaches for rock-load height estimates

A satisfactory cognizance of the rock load, which support system has to undergo, is a primary requirement in design of proper support system. In other words, the extent of the disturbed zone above excavation can be used to estimate the active load exerting on the support system and to design an appropriate support system accordingly.

The in-situ stress of rock mass remains in equilibrium before excavation of a tunnel. Following excavation, the stresses are re-distributed. If the new equilibrium stress state exceeds the yield limit or the strength of rock mass, the rock mass may develop cracks and reach a plastic state. In Chapter 5, it will be seen that as a consequence of decreasing the internal pressure below a critical value, a plastic region develops around the tunnel.

Another hypothetical concept is that when an opening is being excavated, the excavation removes the boundary stress around the circumference of the opening, and the process may be simulated by gradually reducing the internal support pressure. As the support pressure reduced, a plastic zone is formed when the material is overstressed. This region of the rock mass in the plastic state is called the plastic zone (broken zone, disturbed zone, yielding zone, and overstressed zone) which may propagate in the course of tunnel excavation (Pan & Chen, 1990). The configuration of the plastic zone around a tunnel may depend on a number of factors, such as the anisotropy in initial stress state, the tunnel's shape, and the rock mass properties and so on.

Note that from this point on, the failure zone above the tunnel span will be called "rock-load height" and "failure height" when estimated by the proposed empirical method and analytical or numerical methods, respectively.

The primary objectives of the analytical and numerical analyses carried out in this part are as follows:

I. To determine the extent of the failure zone (failure height) around various tunnel shapes (circular, arch-shaped, and rectangular).
II. To investigate the effect of rock mass quality (GSI), roof span (B), and anisotropy in field stress on failure zone.
III. To compare rock–load height (h_t), calculated by the proposed approach with failure height (h_f) determined by the analytical and numerical studies.
IV. To find the correction factor for horizontal to vertical stress ratio (k).

4.5.1 Comparison of the rock-load heights obtained from the proposed empirical approach with those determined by closed-form solutions for circular tunnels

An ealsto-plastic closed form solution of a tunnel makes it possible to determine the radius of the plastic zone or radius of elastic-plastic interface (radius of internal elastic zone) around the tunnel when the internal support pressure is lower than critical pressure (See Chapter 5). For the assumption of isotropy in field stress, circular shape of tunnel, homogeneity in rock mass, and axi-symmetrical plane strain condition, several approaches have been developed over the past 30 years.

A good many sophisticated elasto-plastic approaches have been developed to investigate the stresses, strains, and displacement regime around an opening (Ladanyi, 1974; Florence & Schwer, 1978; Hoek & Brown, 1980b; Brown *et al*. 1983; John *et al*. 1984; Ogawa & Lo, 1987; Detournay & John, 1988; Senseny *et al.* 1989; Indraratna & Kaiser, 1990 a, b; Pan & Chen, 1990; Panet, 1993; Duncan Fama, 1993; Wang, 1996 ; Carranza-Torres & Fairhurst, 1999; Cundall *et al*. 2003; Sharan, 2003, 2005; Carranza-Torres, 2004; Park & Kim, 2006 and the elasto-plastic solution proposed in this thesis). Some limitations, however, must be applied to simplify the solution. Among them, circular shape of tunnel, isotropy in field stresses, and homogeneity of the medium, elimination of the 3-dimensional face effect are the main constraints.

4.5.1.1 Plastic zone around a circular tunnel

Due to the axi-symmetrical condition of the existing analytical solutions for a circular tunnel, the resulted plastic zone around the tunnel remains uniform and axi-symmetrical. In other words, an axi-symmetrical plastic zone can exist only in the condition of a circular tunnel with initial hydrostatic stress sate. The real plastic zone and deformation distribution, however, contradictory to analytical solutions, often reveal non-uniform and non-axisymmetrical conditions resulting from anisotropic initial in-situ stress condition, a non-circular tunnel, or material heterogeneity and anisotropy.

For circular tunnel, an axi-symmetrical plastic zone, which looks like a circular ring, can exist only when the stress ratio (k) is equal to 1. As the stress ratio (k) departs from one, the plastic zone becomes more and more like an elliptical ring and the region of the plastic zone expands in the direction of the smaller initial stress component (Pan & Chen 1990).

For circular tunnels, in order to compare the analytically calculated failure height and empirically obtained rock-load height in an analogous and rational manner [i.e. the thickness of the plastic zone and rock load-height can be, to a large extent, comparable], the thickness of the plastic zone is called Equivalent Rock-load Height "ERH". Note that Equivalent Rock-load Height is only in the case of the axi-symmetrical condition of a circular tunnel.

In this section, the rock-load height of the proposed approach is compared with Equivalent Rock-load Height (ERH) gained from available foregoing elasto-plastic methods. Figure 4-8 exhibits the results of the comparison between the Equivalent Rock-load Heights of closed-form solutions and that of proposed empirical approach for poor rock mass where Modified-GSI < 30 for only a prescribed

geomechanical condition. As can be inferred, the rock-load heights obtained from the proposed approach can be comparable with the analytically obtained equivalent rock-load heights (thickness of plastic zone). It should be, at this point, noted that some approaches (indicated by indices R in Figure 4-8), result in higher values of equivalent rock-load height for the same quality of rock mass. It is due to effect of the residual strength parameters included in their analyses. In such analyses, the post-peak response of the rock mass around tunnel is taken into consideration, i.e. in the broken zone the rock mass constants are given the residual (ultimate) values.

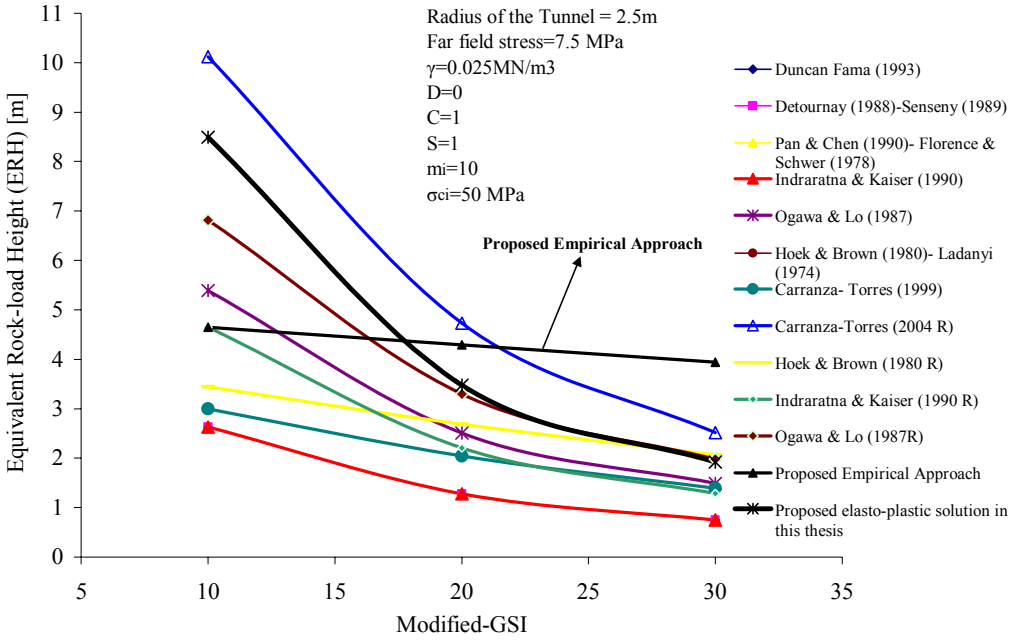

Figure 4-8 The relationship between Equivalent Rock-load Heights (ERH) and Modified-GSI. Note that the Index R indicates that in some solutions the residual strength parameters were taken into consideration. (Note that some elasto-plastic solutions are overlapped)

4.5.2 Comparison of the rock-load heights obtained from the proposed approach with those determined by numerical methods for arch-shaped and rectangular tunnels

Numerical methods are capable of modelling and analyzing the non-circular tunnels in an anisotropic field of stress. Provided that the input properties are sufficiently realistic, an elasto-plastic finite element or finite difference analysis of broken rock may perhaps lead to estimation of a reliable failure height. Therefore, a parametric study was, too, carried out using numerical analysis to investigate the influence of anisotropy in field stresses and the effect of the various shapes and sizes of tunnels on failure-height and support pressure in a variety quality of rock

masses. For this purpose, a Finite Difference Method (FLAC) (Itasca, 2000) and a Finite Element Analysis (FEA) program (PHASE2) (Rocscience, 2005b) were utilized in this study. In addition, the rock-load heights, estimated by the proposed approach were compared to the failure heights determined from the finite element analysis.

The most significant objective of the numerical analysis was to determine the stress correction factor used in the proposed empirical expression. Let the rock-load height of proposed expression be called h_t and the failure height of numerical analysis be h_f. Seeing that the effect of the stress ratio can only be taken into account in the numerical method, the ratio of h_f / h_t gives a ratio called as the stress correction factor (C_s), whose value can be then multiplied in the proposed formula to correct the stress effect and adjust the equation.

4.5.2.1 Configuration of the numerical models

The rock mass around the tunnel was considered to be isotropic and homogeneous without any remarkable discontinuity. A boundary condition of infinite medium was required to better simulate the model. Moreover, an elasto-plastic 2-D plane strain condition with a constant vertical stress of 10 MPa was applied.

To simulate the rock quality three sets of rock mass quality representing the poor, fair and good condition have been adopted using GSI (i.e. GSI= 20*,* 45*,* and 85). The arch-shaped and rectangular tunnels having widths of 5 m, 10 m, and 15 m have been imposed under an anisotropic field stress with ratio of 0.3, 0.5, 1.0, 1.5, and 2.5. In this parametric study, the side walls of tunnel are assumed to be 60 % of tunnel span for both rectangular and arch-shaped tunnel. Therfore, for the rectangular and for the arch-shaped tunnels the ratio of (W /H) are 1.7 and 1.0, respectively. A typical example of an arch-shaped tunnel modelled by Finite Difference Method (FDM) and Finite Element Method (FEM) are shown in Figure 4-9 and a summary of the fixed and variable input parameters used in the current study is also presented in Table 4-12.

In order to determine the effects of the variable parameters on the failure heights, a total of 180 FLAC and PHASE2 runs were performed and analyzed.

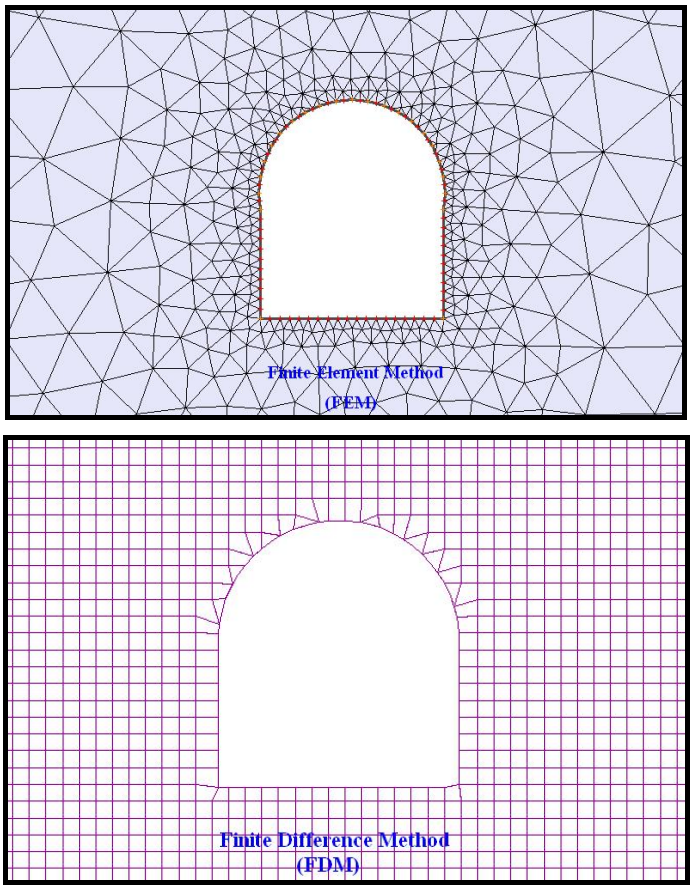

Figure 4-9 The meshes used for the arch-shaped tunnel by Finite Difference Method (FDM) (below) and Finite Element Method (FEM) (above) in an infinite Hoek- Brown medium.

Table 4-12 Fixed and variable parameters used in numerical parametric studies

<table>
<tr><th colspan="4">Fixed parameters</th></tr>
<tr><td colspan="2">Rock mass: isotropic, homogeneous. Boundary condition: infinite medium condition</td><td colspan="2">2-D plane strain condition</td></tr>
<tr><td colspan="2">Type of analysis: Elaso-plastic</td><td colspan="2">Failure Criterion: Hoek & Brown (2002)</td></tr>
<tr><td colspan="2">Field stress: constant
Vertical stress = 10 MPa</td><td colspan="2">Unit weight of rock mass: 0.025 MN/m^3</td></tr>
<tr><td colspan="4">Shape of tunnel :
Archd (horse-shoe) tunnel (W / H = 1)
Rectangular tunnel (W / H = 1.7)
(The side walls of tunnel are considered as 60 % of tunnel width)</td></tr>
<tr><th colspan="4">Variable parameters</th></tr>
<tr><th>Geological Strength Index (GSI)</th><th>Span (m)</th><th>Stress ratio k (σh/σv)</th><th>Rock mass properties</th></tr>
<tr><td rowspan="5">Poor quality rock mass 20</td><td></td><td>0.3</td><td rowspan="5">σci : 10 MPa , mi=10 , D=0 , mb=0,574
s=0.0001, a=0.544 , σcm = 0,812 MPa,
Em=562,34 MPa, ν = 0,27</td></tr>
<tr><td>5</td><td>0.5</td></tr>
<tr><td>10</td><td>1</td></tr>
<tr><td>15</td><td>1.5</td></tr>
<tr><td></td><td>2,5</td></tr>
<tr><td rowspan="5">Fair quality rock mass 45</td><td></td><td>0,3</td><td rowspan="5">σci : 50 MPa , mi=12 , D=0 , mb=1,683,
s=0.0022, a=0.508 , σcm = 8,536 MPa,
Em=5.3 GPa ν= 0,25</td></tr>
<tr><td>5</td><td>0.5</td></tr>
<tr><td>10</td><td>1</td></tr>
<tr><td>15</td><td>1.5</td></tr>
<tr><td></td><td>2.5</td></tr>
<tr><td rowspan="5">Good quality rock mass 85</td><td></td><td>0.3</td><td rowspan="5">σci : 100 MPa , mi=16 , D=0 , mb=9,346,
s=0.1889, a=0.5, σcm = 51,88 MPa, Em=75
GPa, ν=0,2</td></tr>
<tr><td>5</td><td>0.5</td></tr>
<tr><td>10</td><td>1</td></tr>
<tr><td>15</td><td>1.5</td></tr>
<tr><td></td><td>2.5</td></tr>
<tr><td colspan="4">The rock mass properties were obtained using Roclab program (Rocscience, 2005a).
Note that the values of σci, mi, D, and ν have been arbitrary assumed in this parametric study. All calculations are carried out based on the latest Hoek-Brown failure criterion published in 2002. (Hoek et al., 2002).

The values of rock mass deformation are obtained by the equations suggested by Hoek et al. (2002):
$$E_m = \left(1 - \frac{D}{2}\right)\sqrt{\frac{\sigma_{ci}}{100}}\,10^{\frac{GSI-10}{40}}$$
W = tunnel width , H = tunnel height</td></tr>
</table>

4.5.2.2 Analysis and interpretation of the results

The results of the numerical analysis are presented herein to investigate the effects of the variables parameters, B, GSI, k, and shape, on the extent of the failure zone (failure height) above the tunnel and to obtain a correction factor for stress ratio (k), which is used in empirical approach.

Stress ratio (k)

I. For both arch-shaped and rectangular tunnels, with a further increase in k, apart from the tension failure mode, the shear failure mode increases. Numerical analysis of broken zone around the tunnel implied that the extension of failure height above tunnels is predominantly dependent on the magnitude of the stress ratio (k). For both arch-shaped and rectangular tunnels, the extent of the failure zone decreases as the value of k changes from 0.3 to 0.5; conversely, the height of the failure zone starts to increase again as the value of k approaches 2.5 as shown in Figure 4-10 and Figure 4-11.

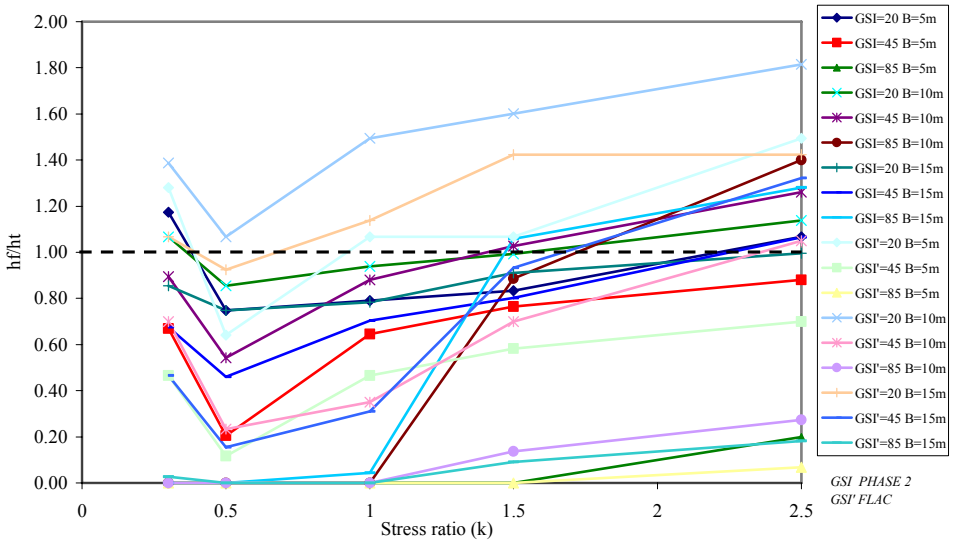

Figure 4-10 Representation of failure height to rock-load height ratio (hf/ht) with in-situ stress ratio (k) for various rock mass quality (GSI) and spans in arch-shaped tunnels

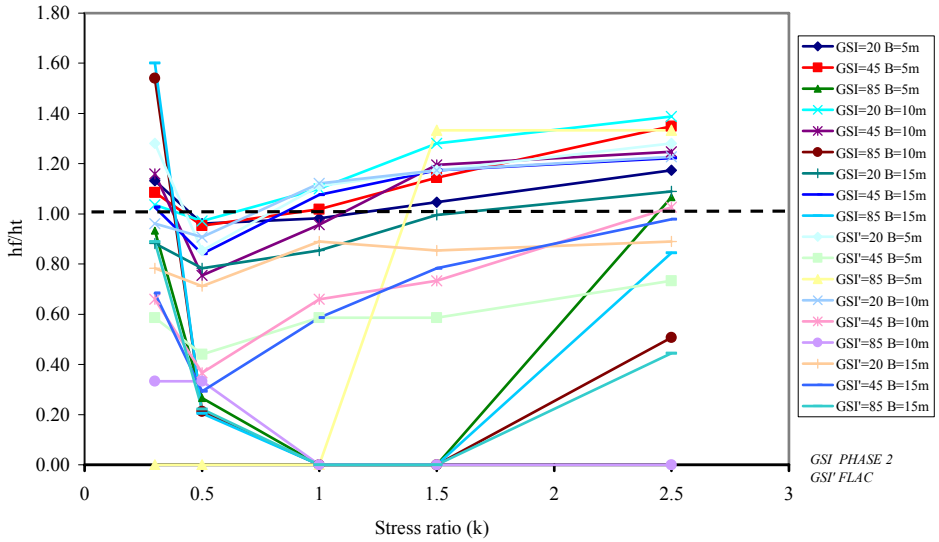

Figure 4-11 Representation of failure height to rock-load height ratio (hf/ht) with in-situ stress ratio (k) for various rock mass quality (GSI) and spans in rectangular tunnels

II. Generally speaking, for the same tunnels excavated through the similar quality rock masses, the failure height of those tunnels driving under the condition of the k > 1 would result in higher values. Examples of this founding for an arched-shaped and a rectangular tunnel are presented in Figure 4-12 and Figure 4-13, respectively.

III. Once the stress ratio k reaches to 2.5, both arch-shaped and rectangular tunnels exhibit the formation of larger failure zones in roof and floor of the tunnels. Shear failure plays a significant role in the formation of the broken zone with a wedge of failed material attempting to move laterally into the tunnel as also reported by Whittaker *et al*. (1992). The predominant fracture is that of lateral movement of the sidewalls into the tunnel which particularly generates floor instability.

Good quality rock mass

For different values of stress ratio (k) and tunnel size, the arch-shaped tunnel excavated in good quality rock mass (GSI=85) is self-supported as seen at Figure 4-14. However, in the case of highly horizontal stress (k >1.5) the roof is potentially unstable to a greater degree. In contrast, a rectangular tunnel, even if excavated in good quality rock mass, might withstand some problems. The reason behind these observations was also reported by Whittaker et al. (1992) during a physical modelling study. They observed that for an arched tunnel, the formed arch decreases, to some extent, the effect of the stress being imposed on the tunnel crown, whereas in the case flat roof, the separation or the sag of the roof strata due

to stress gives rise to an increase in the failure height. Simply put, the normal forces will be greater in the case of a rectangular opening with flat roof by virtue of the weight of detached blocks of rock that are free to fall. In contrast, the detached blocks in the case of an arch-shaped tunnel become interlocked on displacement because of the dilatant behaviour of rock masses.

Tunnel size

I. Numerical analysis puts forward a significant conclusion indicating that with increasing tunnel size, the failure height above the tunnel especially in poor rock masses (GSI=20) increases regardless of the tunnel shape. As can be proved in the plots shown in the Figure 4-16 to Figure 4-21 , the slope of failure height envelopes in poor rock mass, although not in all cases, is greater than that of fair to good quality rock masse under normal active loading (not k >1). For two same-sized tunnels whose widths are to be enlarged, a gradual increase in failure height takes place in the good quality rock mass whereas a sudden rise in failure height occurs in the weak rock mass. To put it more simply, the effect of the tunnel size on support pressure in weak rock mass is far more obvious than that in fair to good rock mass.

II. In strong rock mass (GSI=85), it is evident that the failure height and consequent rock load is independent of tunnel size in the normal loading condition (k=1). In other words, unlike the good rock masses, the support pressure is directly proportional to the size of the tunnel in the case of poor to fair rock masses undergoing squeezing ground condition. Ünal (1983) explored this phenomenon in coal mine studies.

III. These observations are found to be in contradiction with the results advocating that the support pressure is independent of roof span (Barton *et al.,*1974, Singh *et al*.1992, 1997).

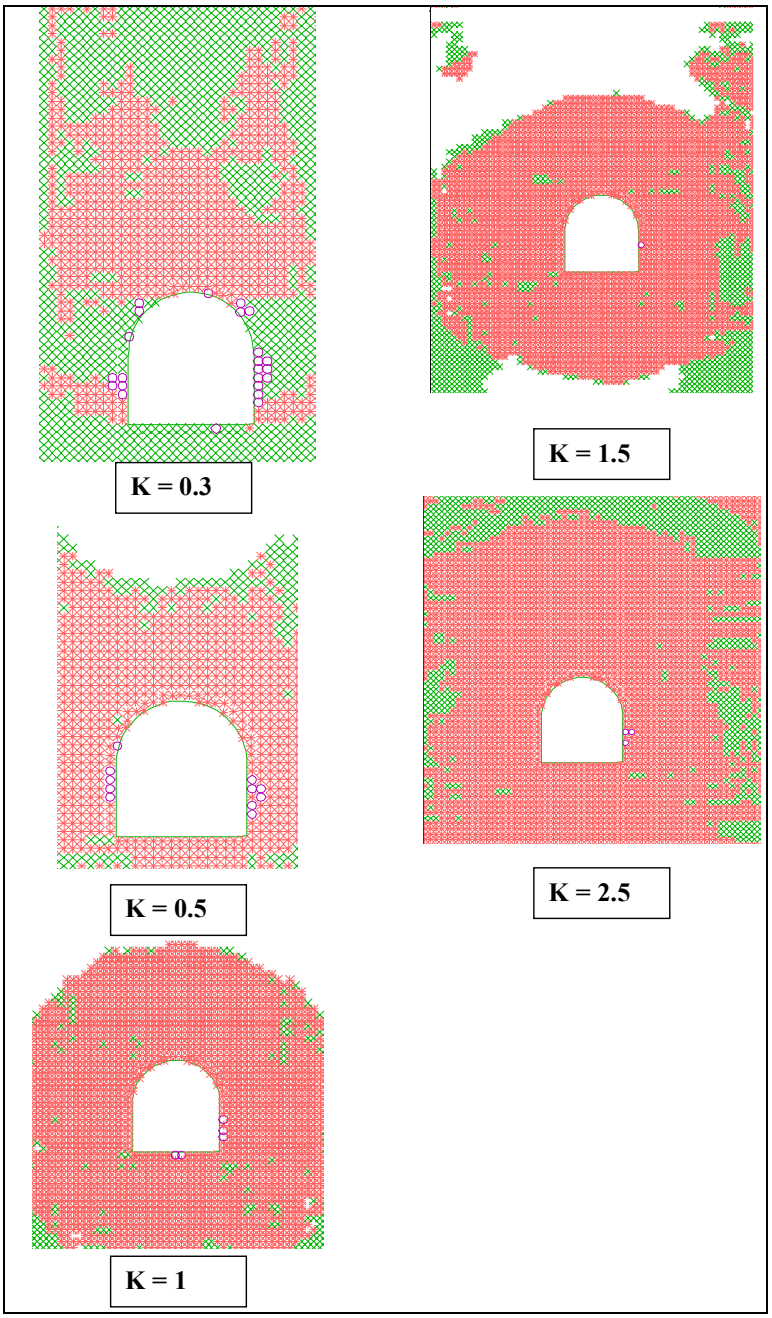

Figure 4-12 The variation of rock-load height with stress ratio (k) for an arch-shaped tunnel with width of 10m if GSI=20. As seen, the greater stress ratio (k), the bigger rock-load height expect for k=0.5.

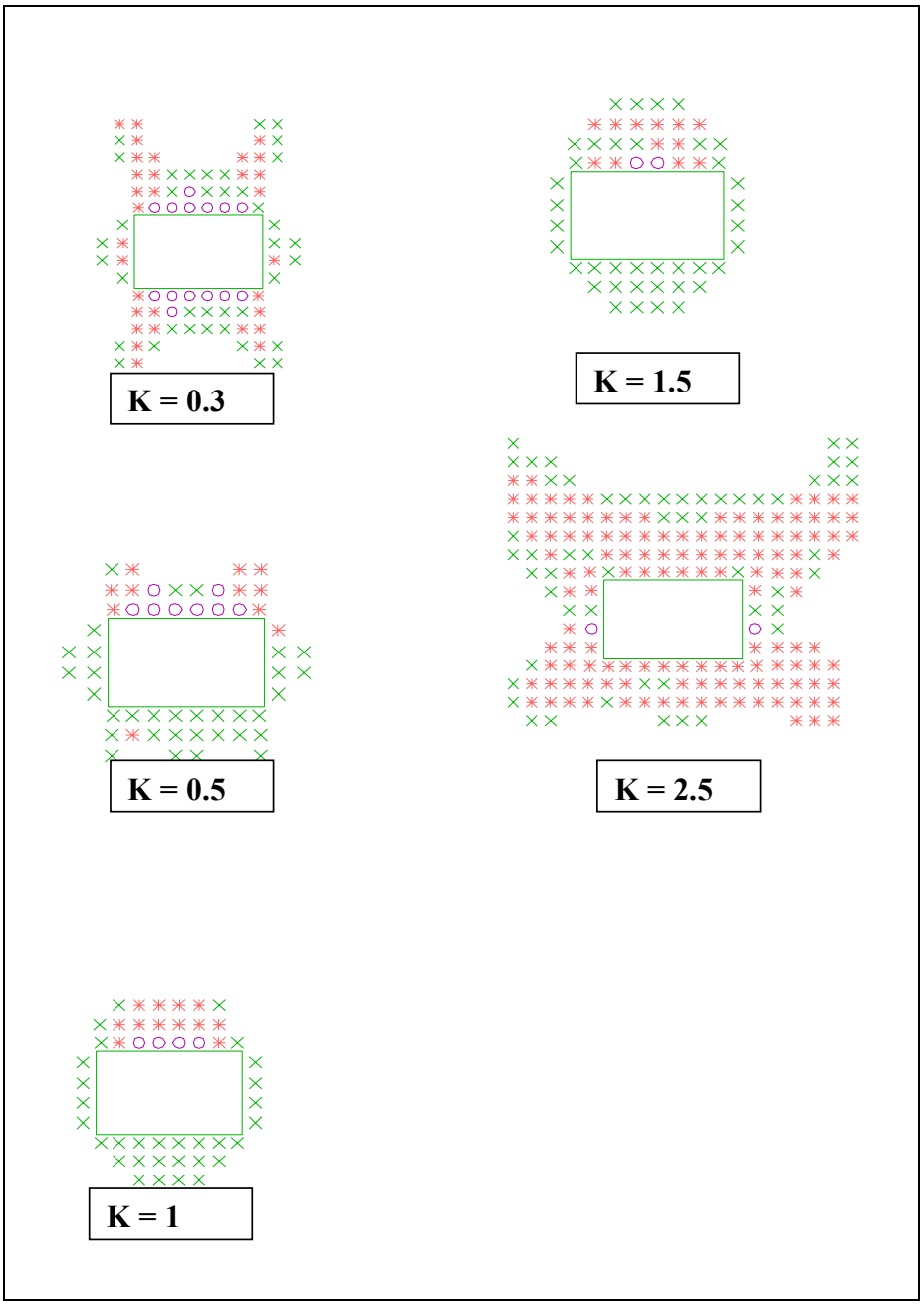

Figure 4-13 The variation of rock-load height with stress ratio (k) for a rectangular tunnel with width of 10m if GSI=45. As seen, the greater stress ratio (k), the bigger rock-load height expect for k=0.5.

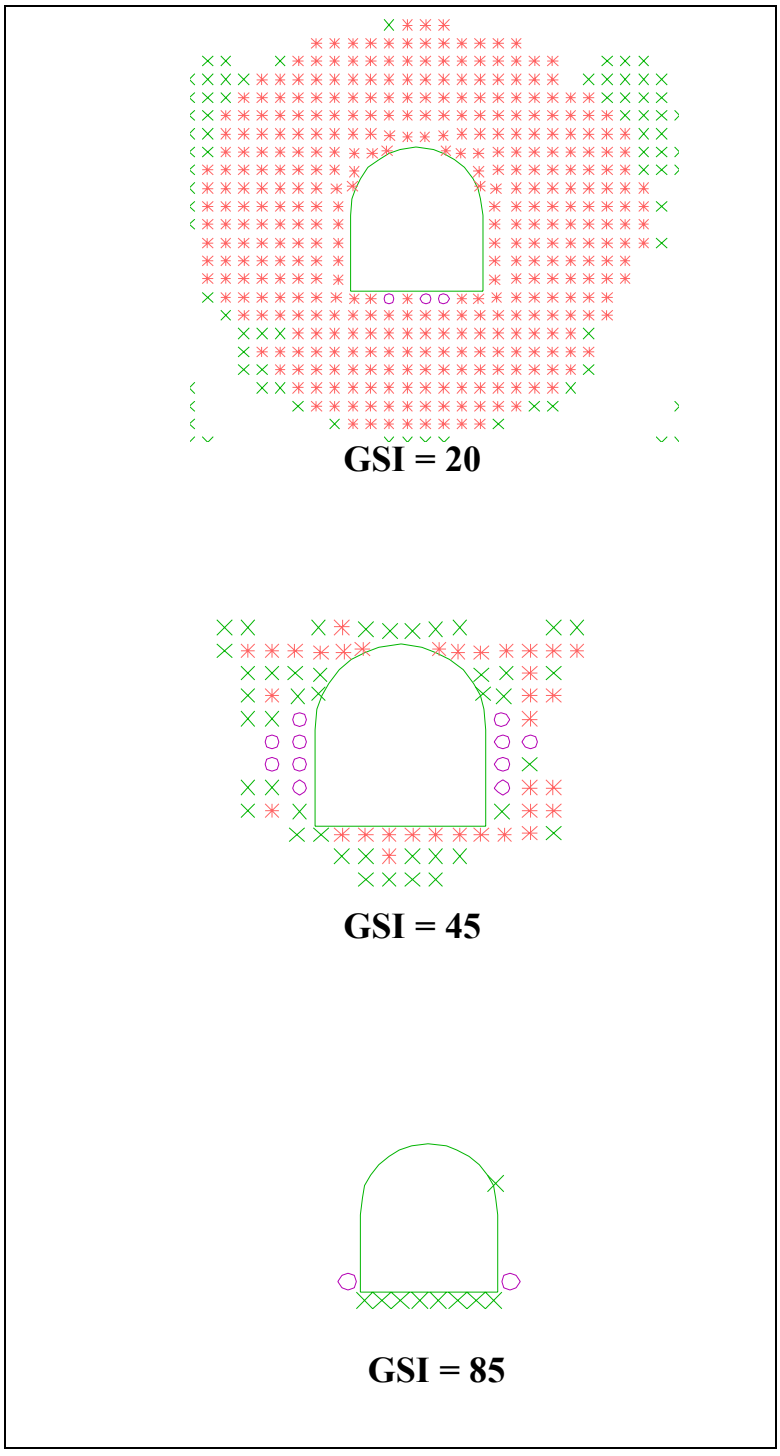

Figure 4-14 A representation showing the decreasing the failure height with improving rock mass quality for an arch-shaped tunnel of 5m wide excavated in a hydrostatic condition of in-situ stress.

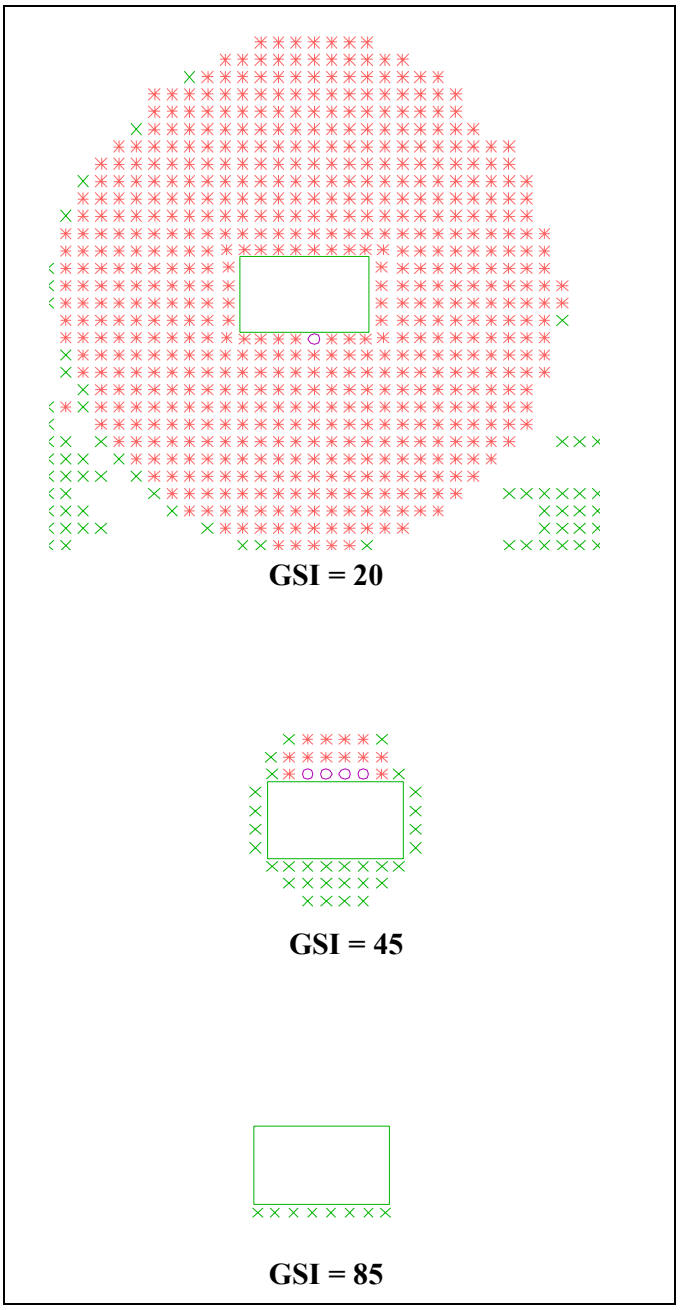

Figure 4-15 A representation showing the decreasing the failure height with improving rock mass quality for a rectangular tunnel of 5m wide excavated in a hydrostatic condition of in-situ stress.

Arch-shaped tunnel (W= H) versus rectangular tunnel (H= 60% W)

I. Numerical analysis on extension of the broken zone around tunnels, regardless of shape, reveals that with increasing the quality of rock mass the extent of broken zone decreases. Highlighted in Figure 4-14 and Figure 4-15 , the broken zone around the arch-shaped tunnel

having span of 5m is considerably decreased, provided that the quality of rock mass is improved.

II. For tunnels with corners, such as rectangular and horse-shoe shaped ones, relatively limited thin plastic zone may appear near the corners. This phenomenon was also reported by Pan & Chen (1990). The limited plastic zone near a corner may be explained by the fact that at corners where radius of curvature is small, the value of tangential stress is very high and its magnitude decreases rapidly with the distance from tunnel surface. That is why the yielding is limited to small distances at the sharp corners. On the other hand, at surface parts where radius of curvature is large, the tangential stress is not very high, but it decreases slowly with distance from the tunnel surface. That is why when yielding occurse at such points, the thickness of yielding zone is larger than those occurring at the corners. In the case of a horse-shoe shaped tunnel, it can also be observed that the plastic zone in the tunnel roof is relatively thinner than that in the tunnel sidewall and on the tunnel floor due to the arch effect.

III. For poor rock mass with GSI=20, the results of the empirical approach for both arch-shaped and rectangular tunnels lie in between the PHASE2 results (see Figure 4-16 and Figure 4-19). Conversely, the $FLAC^{2D}$ results constitute the upper limit of the failure height envelopes. These phenomena are attributed to two reasons. The first would be due to the fact that no effect of the rock mass disturbance and squeezing ground condition are taken into account in the parametric study of proposed approach. Considering the influences of the mentioned parameters in empirical proposed approach, the realistic and reliable results would, in turn, be obtained. The second one is that $FLAC^{2D}$ is far more potent than PHASE2 in modelling the poor rock masses as its usage ranges even for the soils.

IV. The analysis of results obtained form the numerical models indicates that the failure heights resulted from $FLAC^{2D}$ are significantly larger than those estimated by PHASE2 for poor rock masses (GSI=20). However, these differences are not considerable for rectangular tunnel having spans of 10 m and 15 m. In fair rock masses (GSI=45) the failure heights of $FLAC^{2D}$ are, in contrast, noticeably less than those of PHASE2 for both arched-shaped and rectangular tunnels regardless of tunnel shape (see Figure 4-17 and Figure 4-20). In addition, in good quality rock masses (GSI=85), the resulting failure heights determined by PHASE2 are more or less the same as those found out by $FLAC^{2D}$ as shown in Figure 4-18 and Figure 4-21.

V. It is worthwhile to note that irrespective of tunnel shape, the failure heights obtained from FLAC is a great deal grater that those gained from PHASES in the case of k >1,5 for a larger tunnel span (i.e.10m and 15m).

VI. In fair quality rock mass(GSI=45) for arch-shaped tunnels, the results of the empirical approach accounts for approximately the upper limit

of the failure height envelopes while for rectangular tunnels empirical results remain between the numerical results as shown in Figure 4-17. However, for the good quality rock mass where GSI =85, the proposed approach envelope stretches out between the envelopes of the numerical results (see Figure 4-18). In this case the furthermost limits are made of from the failure height envelope of high horizontal stress (k=2.5).

VII. In poor and fair rock masses (GSI varies between 20 and 45) withstanding squeezing ground condition, the failure height of rectangular tunnels is more than that of the arch-shaped tunnels with the same width.

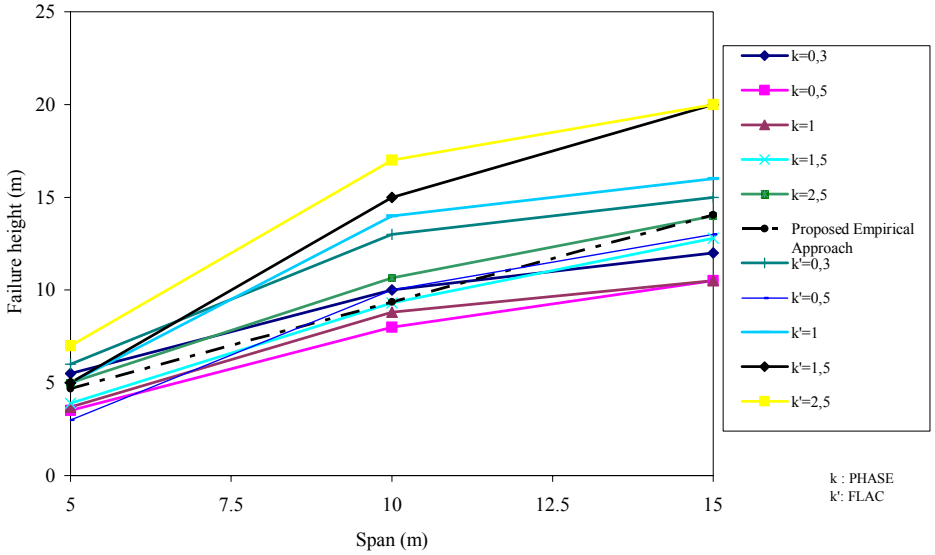

Figure 4-16 The variation of the failure height with roof span for different value of stress ratio (k) for poor rock mass GSI=20 in arch-shaped tunnel.

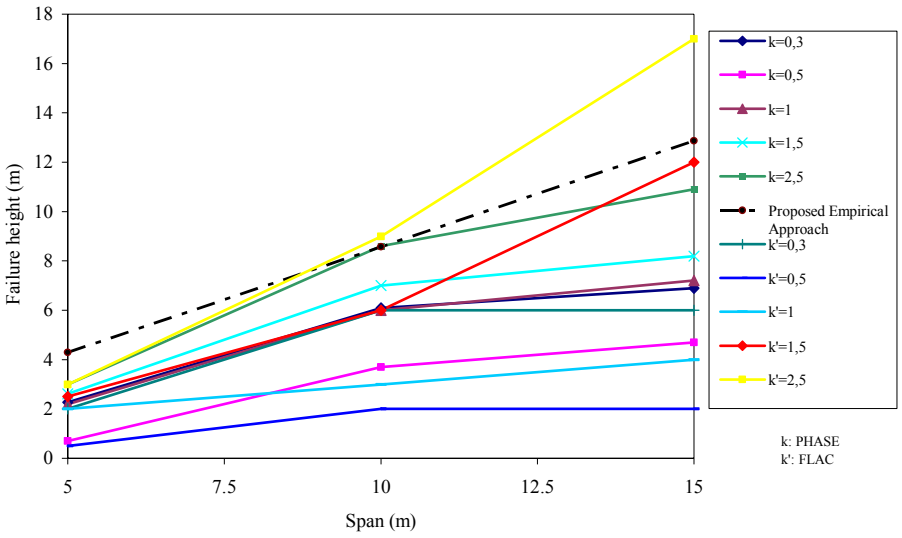

Figure 4-17 The variation of the failure height with roof span for different value of stress ratio (k) for fair rock mass GSI=45 in arched-shape tunnel.

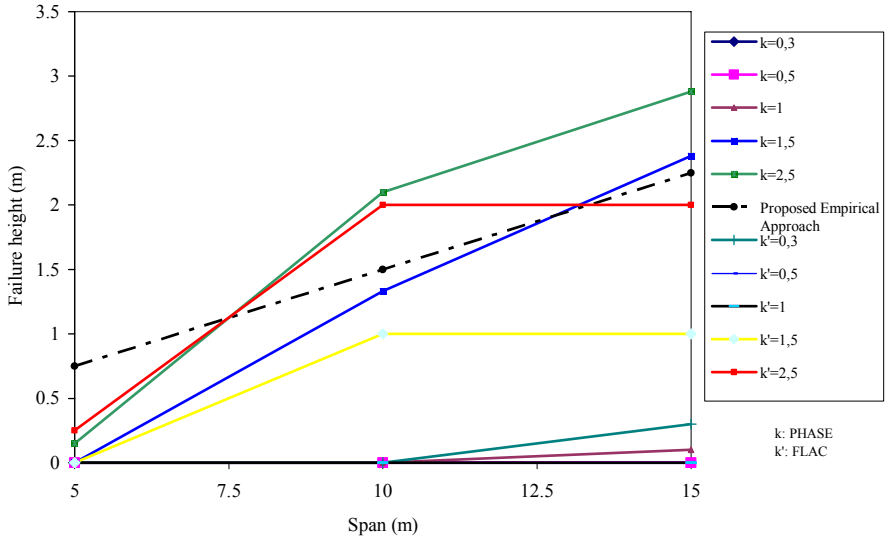

Figure 4-18 The variation of the failure height with roof span for different value of stress ratio (k) for good quality rock mass GSI=85 in arch-shaped tunnel.

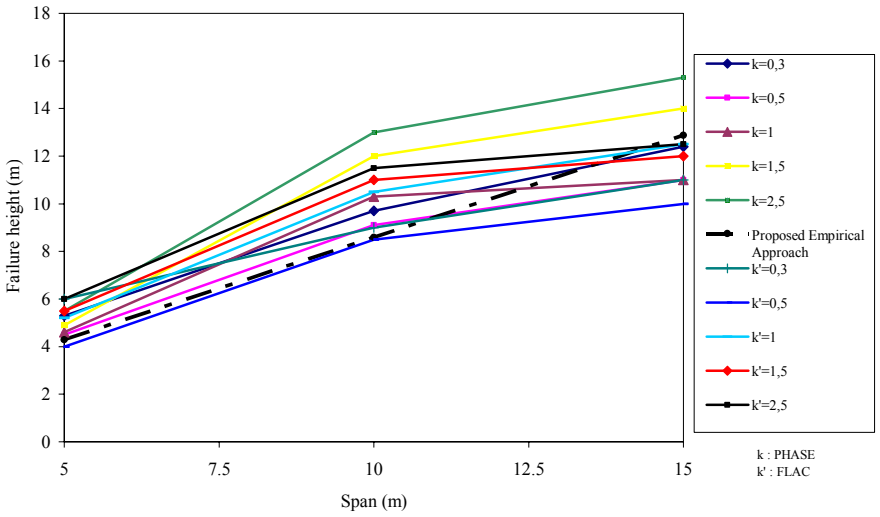

Figure 4-19 The variation of the failure height with roof span for different value of stress ratio (k) for poor rock mass GSI=20 in a rectangular-shaped tunnel.

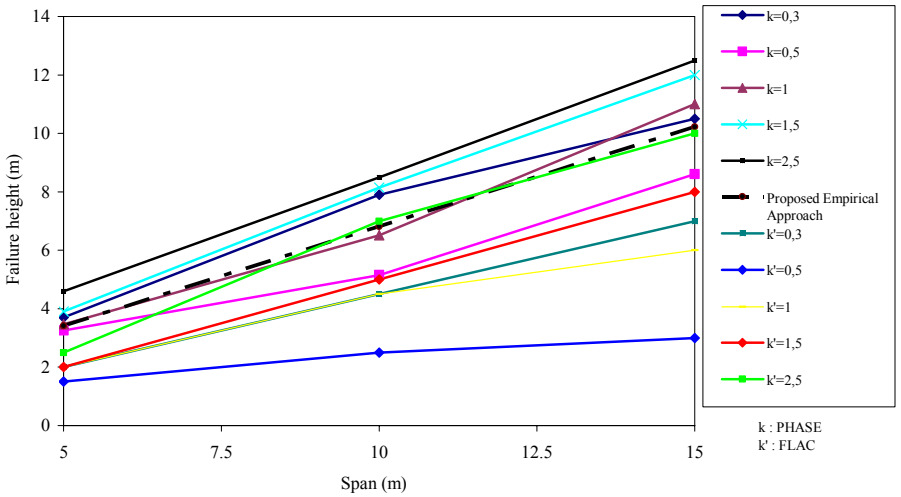

Figure 4-20 The variation of the failure height with roof span for different value of stress ratio (k) for fair rock mass GSI=45 in a rectangular shaped tunnel.

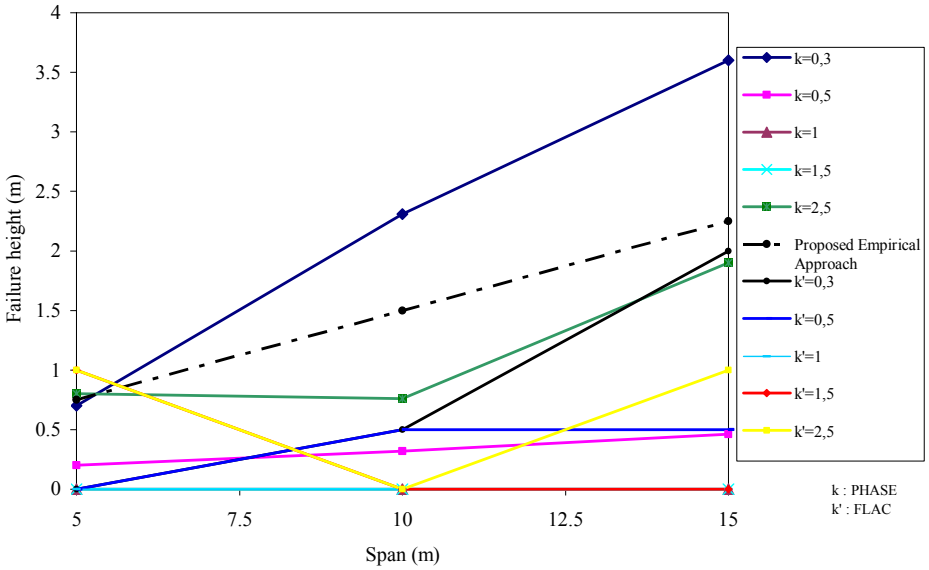

Figure 4-21 The variation of the failure height with roof span for different value of stress ratio (k) for good quality rock mass GSI=85.

4.5.2.3 Correction factor for horizontal to vertical stress ratio

Numerical analysis of broken zone around the tunnel implied that the extension of failure heights above tunnels is dependent upon the magnitude of the stress ratio (k). For arch-shaped and rectangular tunnels, the extent of the failure zone decreases as the value of k changes from 0.3 to 0.5; conversely, the height of the failure zone starts to increase again as the value of k approaches 2.5. Figure 4-10 and Figure 4-11 represent the effect of the stress ratio (k) on the failure heights for different values of the rock mass quality (GSI) in arch-shaped and rectangular tunnels, respectively.

The ratio of the failure height (obtained from numerical methods) to rock-load height (determined by the proposed formula) yields a value called the stress correction factor (C_s). This correction value has to be applied while using Equations 4-6 to 4-10. Therefore, a multiplier (C_s) is required to correct the stress ratio. For reliability, the minimum C_s for the proposed formula is always suggested as 1.0 for k=0.5. Figure 4-22 aims at choosing the stress correction factor.

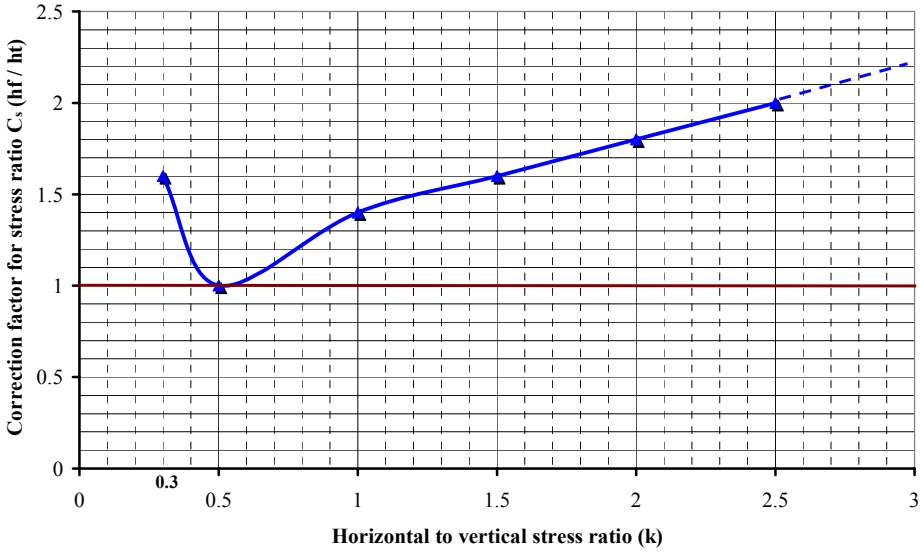

Figure 4-22 Suggested value for stress correction factor (C_s) used in proposed formula (h_f: failure height by numerical method, h_t; rock-load height by empirical approach).

CHAPTER 5

DEVELOPMENT OF A NEW ANALYTICAL ELASTO-PLASTIC SOLUTION FOR BOTH UNSUPPORTED AND REINFORCED TUNNEL

5.1 Introduction

Design of tunnels in soils and rocks entails the determination of stresses and displacements occurring around them. The assumptions of homogeneity, isotropy and linear elasticity before yielding occurs made to simplify the analysis. The elastic behaviour of an opening in an infinite medium is well documented in the literature. The application of Airy's stress functions and Hooke's law to determine the stress and strain fields constitutes the fundamentals of the elastic theory (Timoshenko & Goodier, 1970). Since tunnels are much longer than their diameter, it is reasonable to assume that the plane strain condition (longitudinal strain is neglected) prevails ultimately and horizontal stresses are equal in every direction.

The extent of yielding (plastic zone radius) is dependent on the material properties of the rock mass, the in-situ field stress and the tunnel radius (tunnel span). Yielding may be followed by rupture of the wall if uncontrollable deformations occur in weak ground. It is the objective of radial rock-bolting to minimize large displacements in order to maintain a coherent load bearing ring around the tunnel. The installation of bolts effectively improves the apparent material properties of the rock mass thereby reducing strains and displacements.

The analysis presented in this chapter is a rigorous elasto-plastic solution to assess the stresses and displacements of an unsupported tunnel and to investigate the influence of fully grouted rock-bolts on the rock mass behaviour around the tunnel. The following major assumptions, associated with the unsupported tunnel, have been made in this analysis:

I. Deep circular tunnel in a hydrostatic stress field (k=1)

II. Homogeneous, isotropic material with time-independent properties

III. Elastic-brittle-plastic strength model with non-linear Hoek & Brown yield criterion (version 2002, Hoek *et al*. 2002). Plastic deformations follow a flow rule with constant rate of dilation.

IV. Deformation pattern near the tunnel is properly described by plane strain condition. A section of tunnel far from the face is considered in order that the 3-D effects at tunnel face are vanished.

The following are the distinguishable steps of elasto-plastic analysis that will be taken into account in the proposed solution (Brown, 1986):

I. Constitutive model of rock behaviour
II. Lame's solution for determination of the stresses in the elastic zone
III. Stress in plastic (yielding, overstressed, broken, disturbed) zone
IV. Stress at the interface of plastic and elastic zones
V. Radius of plastic zone
VI. Strains and displacements in the elastic zone
VII. Strains and displacements in the plastic zone
VIII. Radial displacement or tunnel convergence (closure)

5.2 Definition of the problem

The problem is defined in Figure 5-1. Consider a circular tunnel being excavated in an infinite medium subjected to isotropic initial stress, P_o. The excavation removes the boundary stresses around the circumference of the opening, and the process may be simulated by gradually reducing the internal fictitious support pressure, P_i. As P_i is reduced, a plastic zone is formed when the material is overstressed, and the radial displacement, u_r, occurs. It is required to compute the stresses and displacements around the tunnel, when plane strain condition along the axis of the tunnel is reached.

5.3 Method of solution

For a solution of the elasto-plastic problem, the equation of equilibrium, compatibility condition, stress- elastic strain relationship, yield criteria, plastic potential, and a flow rule are required (Ogawa & Lo, 1987). The stresses and displacements in the elastic region may be readily determined by observing the continuity of radial stresses and displacements at the elastic-plastic interface. The solution within the plastic region will depend on the assumption of (a) the yield criterion, (b) the use of associated or non-associated flow rule, and (c) the dilatancy angle ψ.

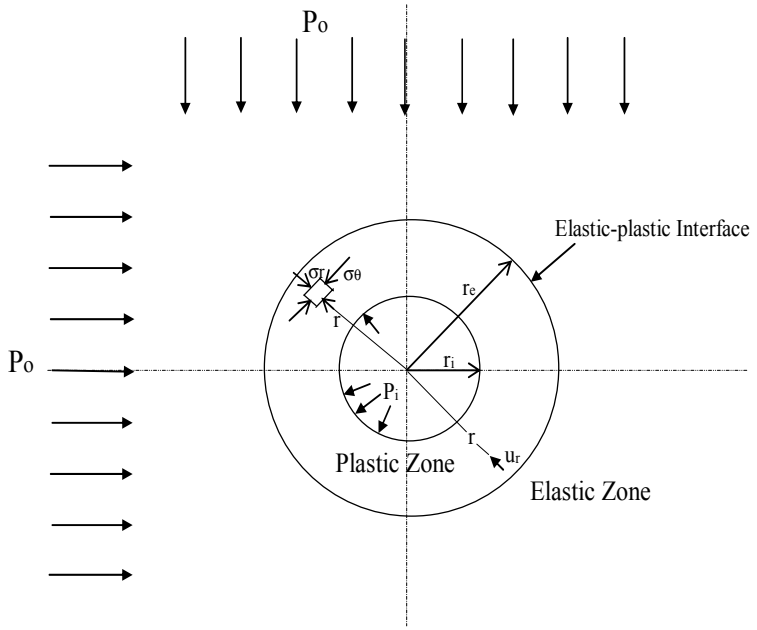

Figure 5-1 Definition of the model

Under the axi-symmetric plane strain condition, the strains and the displacements are expressed as:

$$u_r = u_r(r), u_\theta = 0, u_z = 0 \tag{5-1}$$

$$\varepsilon_r = \frac{\partial u_r}{\partial r}, \varepsilon_\theta = \frac{u_r}{r}, \varepsilon_z = 0 \tag{5-2}$$

where the subscripts *r, θ,* and *z* denote respectively radial, tangential, and longitudinal (axial) directions. The compatibility condition is given by:

$$\frac{\partial}{\partial r}(r\varepsilon_\theta) = \varepsilon_r \quad \text{or} \quad \frac{\partial \varepsilon_\theta}{\partial r} + \frac{\varepsilon_\theta - \varepsilon_r}{r} = 0 \tag{5-3}$$

or in differential equation form:

$$\frac{d\varepsilon_\theta^t}{dr} + \frac{\varepsilon_\theta^t - \varepsilon_r^t}{r} = 0$$

For small deformation and infinitesimal strains, the total strains are divided into the elastic and plastic components:

$$\varepsilon_{ij} = \varepsilon_{ij}^{e} + \varepsilon_{ij}^{p} \tag{5-4}$$

where the superscripts and *e* and *p* denote elastic and plastic components, respectively. Furthermore, the elastic strain component may be divided into the deviatoric and volumetric components (Timoshenko & Goodier, 1970) as:

$$\varepsilon_{ij}^{e} = D_{ij}^{e} + \Delta^{e}\delta_{ij} \tag{5-5}$$

where D_{ij}^{e} = elastic deviatoric strain component;

Δ^{e} = elastic volumetric component $(\frac{1}{3}\varepsilon_{kk}^{e})$ and

δ_{ij} =Kronecker's delta $\delta_{ij} = 1$ for $i = j$ and $\delta_{ij} = 0$ for $i \neq j$

where $i = 1,2,3$ or θ, r, z.

Similarly, the stress component c_{ij} is divided into the deviatoric and volumetric components:

$$c_{ij} = c'_{ij} + c_{o}\delta_{ij} \tag{5-6}$$

where c'_{ij} = deviatoric stress component, c_{o} = volumetric stress component $(\frac{1}{3}\sigma_{kk})$, and the summation convention is implied by the repeated dummy indices.

The constitutive equations relating the deviatoric and volumetric components of stresses and elastic strains are therefore given by:

$$D_{ij}^{e} = \frac{1+\nu}{E}\sigma'_{ij} \tag{5-7}$$

$$\Delta^{e} = \frac{1-2\nu}{E}\sigma_{o} \tag{5-8}$$

where *E* is Elasticity or Young's modulus and *v* is Poisson's ratio.

The flow rule of plasticity relating the plastic strain increment $\dot{\varepsilon}_{ij}^{p}$ and the plastic potential Q is given by:

$$\dot{\varepsilon}_{ij}^{p} = \lambda_f \frac{\partial Q}{\partial \sigma_{ij}} \tag{5-9}$$

The above elasto-plastic stress-strain and stress-strain increment relationships are generally used, and are listed for completeness. The choice of yield criteria and plastic potential will be discussed in the following parts.

5.4 Yield criterion

Yield initiation is assumed to occur following a non-linear Hoek-Brown failure criterion. In this elasto-plastic solution the latest version of the Hoek-Brown yield criterion introduced in 2002 has been chosen to be the main constitutive model for behaviour of the rock mass as given in Section 3.6.1.

Figure 5-2 depicts the Hoek-Brown yield criterion for different quality of rock masses (GSI= 100, 50, and 5) while Figure 5-3 represents the definition of both peak and residual values of Hoek & Brown constants. Post-peak (residual parameters) behaviour in the broken zone around the opening is characterized by the flow rule that governs the plastic deformations. In the perfectly plastic material model, there is no strength drop after peak; hence, yielding continues to occur at a constant peak stress level. However, a strain weakening behaviour is generally observed in most rocks where the post- failure behaviour is strain-dependent.

The elastic-brittle-plastic model is a simplification of the above described behaviour, and is characterized by an instantaneous strength drop at peak as shown in Figure 4-6. The Hoek-Brown failure criterion is still applicable although the post-peak strength is reduced.

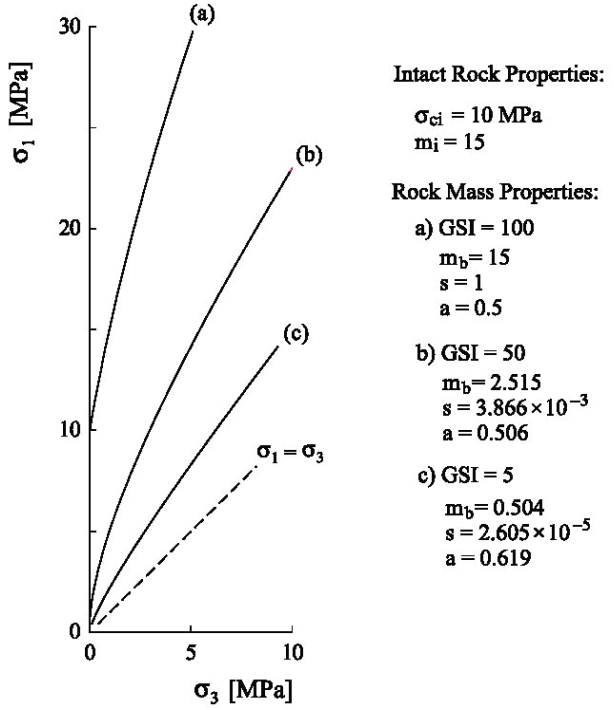

Figure 5-2 Hoek-Brown failure criterion for intact rock (curve a) and rock masses with decreasing values of GSI (curves b and c) (Carranza- Torres, 2004)

It has been substantiated that the extension of the broken zone relies on the residual value of the intact rock strength (Hoek & Brown, 1980b, Brown *et al*., 1983, Indraratna & Kaiser, 1990a, Carranza-Torres, 2004). Hence, the effect of the compressive strength of rock material must be included in the form of the residual value because it loses its initial value due to stress relief or an increase in the strain. A stress reduction scale must, therefore, be considered as:

$$\sigma'_{ci} = S_r . \sigma_{ci} \tag{4.10}$$

where S_r refers to the strength loss parameter quantifying the jump in strength from the intact condition to residual condition or a measure of the degree of strength loss occurring immediately after the peak strength is reached. The parameter S_r characterizes the brittleness of the rock material: ductile, softening, and brittle. By definition, S_r will fall within the range $0 < S_r < 1$. Where $S_r = 1$ implies no loss of strength and the rock material is ductile, or perfectly plastic. By contrast, if $S_r = 0$, the rock is brittle (elastic- perfectly brittle plastic) with the minimum possible value for the residual strength as highlighted in Figure 4-6.

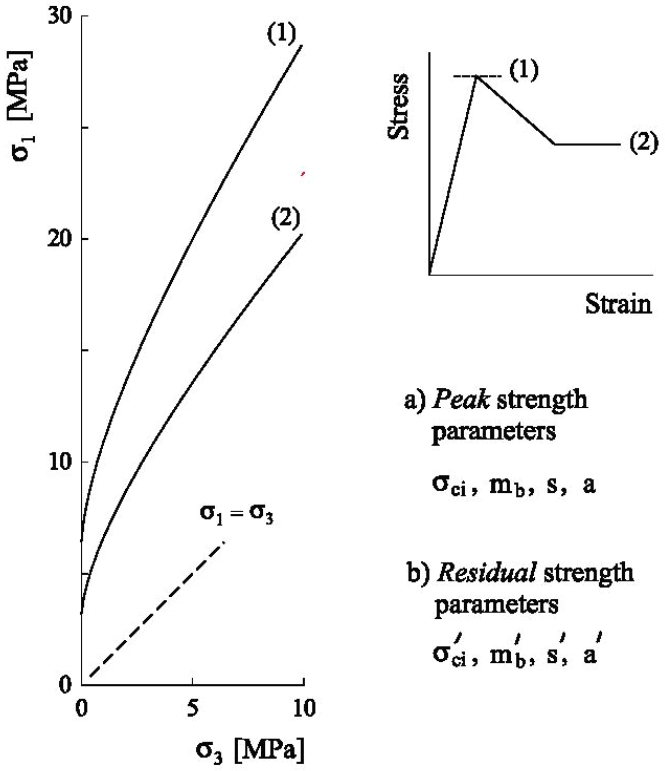

Figure 5-3 Peak and residual failure envelopes considered for the generalized Hoek-Brown failure criterion for the problem in Figure 5.1 (Carranza- Torres, 2004)

5.5 Flow rule of plasticity and the plastic potential

From the classical stress-strain curve standpoint, at the failure point and post –peak behaviour of a rock, it is important to understand the post-failure behaviour of rock due to its applicability in the analysis of the broken (yielded) zone as well as reinforced yielding zone around the opening. The theory of plasticity is recognized to be a tool, whereby the plastic strains and displacements of rock can be determined based on selected yield condition.

The flow rule of plasticity relating the plastic strain increment $\dot{\varepsilon}_{ij}^{p}$ and the plastic potential Q is, as shown before, given by (Hill, 1950, Brown, 1986):

$$\dot{\varepsilon}_{ij}^{p} = \lambda_f \frac{\partial Q}{\partial \sigma_{ij}} \tag{5-9}$$

where λ_f is a non-negative constant of proportionality which may vary throughout loading history and is therefore a scaler multiplier and not a fixed constant. It is

also necessary to be able to define the stress state at which yield will occur and plastic deformation will be initiated. For this purpose, a yield function $F(\sigma)$ is defined such that $F(\sigma) = 0$ at yield.

The concept of associated plastic flow was developed for perfectly plastic and strain-hardening materials using yield functions such as Tresca and Von Mises (Brown, 1986). Although associated flow rule has been firstly found to apply for some geological materials, it could not be assumed that it would be applied necessarily to rocks in which brittle fracture and dilatancy typically occur. Rocks often display strain-softening characteristics. However, modelling of strain-softening behaviour using plasticity theory presents a number of difficulties. There is limited evidence available to suggest that the dilation rate at peak stress in brittle rocks or tightly interlocked aggregates can be predicted closely using the associated flow rule. It is not clear, however, that the associated flow rule applies to heavily fractured and poorly interlocked rock masses (Brown *et al.,* 1983). Moreover, it has been found experimentally that an assumption of associated flow overestimates the amount of dilation occurring in yielding rocks (Michelis & Brown, 1986). These observations have lead to the development of a number of non-associated flow rules for rocks.

When an associated flow rule applies, the yield criterion and the plastic potential function are the same functions of the stress components $Q=F$. In other words, the flow rule is referred to as associated if the plastic potential and yield surface coincide. As a consequence, the plastic strain increment vector must be normal to the yield surface. If the yield surface is represented by a relation between principal stresses, σ_1 and σ_3, then the corresponding components of the strain increment vector are the increments of $\varepsilon_1^p$and ε_3^p. If the flow rule is non-associated, the yield criterion and the plastic potential function are not the same and the normality principles do not apply.

In terms of flow rule to consider for the Hoek-Brown material, most of the published analyses consider non-associated flow rule with a "constant dilation angle", derived from a "linear" potential. In the Hoek-Brown (H-B) failure criterion, the yield surface is a parabola, and then if the plastic potential is linear, the flow rule will be always non-associated. It should be noted that the situation is different as far as the Mohr-Coulomb (M-C) (i.e., linear) failure criterion is applied. if the plastic potential is linear and the dilation angle (ψ) is equal to the internal friction angle (ϕ), then both, yield surface and plastic potential are the same, therefore the flow rule is "associated" (on the other hand, if the dilation angle is different from the internal friction angle, then the flow rule will be non-associated).

Depending on the linearity or non-linearity of both the yield function and plastic potential, the following description given in Table 5-1 can be defined. The first one is to take a potential that has the same form as the yield surface, and this will be the associated flow rule. This case will show the maximum volumetric change possible, also maximum value justifiable in mechanical terms for the plastic state. The second, on the other hand, is to take a linear potential "$Q(\sigma_1,\sigma_3)=0$" with zero dilation angle, and this will be non-associated flow rule. This will show no volumetric change in the plastic state. In general, the most probable situation will

be one between both extreme types of volumetric behaviour in the failure state (associated flow rule and non-dilatant, non-associated).

For poor rock masses (GSI < 27) which is mostly related to the subject of the thesis, Hoek & Brown (1997) suggest taking zero dilation, so for poor rock masses, the second alternative defined above is therefore which that is used in proposed elasto-plastic solution.

Table 5-1 Yield and potential functions used in the various tunnel elasto-plastic models. Key : ψ = dilation angle, ϕ = internal friction angle

Yield and potential functions	
Linear Function	**Non-linear Function**
M-C	**H-B**
F(potential)=F(yield)	**F(potential)=F(yield)**
Linear potential function	Normality and associated flow rule
$\psi=\phi$ Associated flow rule	**F(potential)≠F(yield)**
$\psi\neq\phi$ Non-associated flow rule	Linear potential function
	Non-linear yield function
	Non-associated flow rule
	Constant dilation angle

Figure 5-4 presents the linearized plastic potential in the principal stress and plastic strain increment space. For an isotropic material, the principal axes of stress and strain increment coincide, and therefore a plastic strain increment vector AA' ($\dot{\varepsilon}_3, \dot{\varepsilon}_1$) may be plotted. Under plane strain condition, the ratio of plastic strain increment is given by (Ogawa & Lo, 1987):

$$\frac{d\varepsilon_3^p}{d\varepsilon_1^p} = -N_\psi \tag{5-10}$$

where $N_\psi = \frac{1+\sin\psi}{1-\sin\psi} = \tan^2(45^\circ + \frac{\psi}{2})$, which may be easily derived from the principal strain space in Figure 5-4 as described below. The parameter N_ψ controls

the inclination of the plastic-strain rate vector represented. The vector AA' is normal to the plastic potential, Q, then Q forms an angle $\tan^{-1}N_\psi$ with the ε_3-axis.

The linear plastic potential using Mohr-Coulomb function is defined as:

$$Q = (\sigma_1 - \sigma_3) - (\sigma_1 + \sigma_3)\sin\psi - 2c\cos\psi = 0 \tag{5-11}$$

or

$$Q = \sigma_1 - \sigma_3 N_\psi - 2c\sqrt{N_\psi} = 0$$

Using the flow rule (Equaion 5-9), then

$$\begin{aligned} \varepsilon_1^p &= \lambda(1-\sin\psi) \\ \varepsilon_3^p &= -\lambda(1+\sin\psi) \\ \frac{\varepsilon_3^p}{\varepsilon_1^p} &= -\left(\frac{1+\sin\psi}{1-\sin\psi}\right) \end{aligned} \tag{5-12}$$

then the equation 5-10 can be rewritten as

$$\frac{d\sigma_1}{d\sigma_3} = \frac{d\varepsilon_3^p}{d\varepsilon_1^p} = -N_\psi \tag{5-10}$$

or

$$d\varepsilon_3{}^p + N_\psi d\varepsilon_1{}^p = 0$$

In the polar coordinates ($\varepsilon_3^p = \varepsilon_r^p$ and $\varepsilon_1^p = \varepsilon_\theta^p$):

$$d\varepsilon_r{}^p + N_\psi d\varepsilon_\theta{}^p = 0 \tag{5-13}$$

Given the plastic part of the typical stress-strain curve of rock (see

Figure 5-5) the slope of the plastic part of the axial and lateral strains in plastic region is:

$$f = -\frac{d\varepsilon_3^p}{d\varepsilon_1^p} \tag{5-14}$$

Besides, the slope of volumetric strain versus axial strain in the plastic region can be obtained

$$F = f - 1 \tag{5-15}$$

Therefore

$$f = 1 + F = N_{\psi} \tag{5-16}$$

The parameter N_{ψ} is the dilation coefficient that characterizes the volume change in the plastic zone. Zero volumetric strain (no volume change) is represented by N_{ψ} =1, i.e. if ψ=0° (non-associated). However, if $N_{\psi} = \frac{1+\sin\psi}{1-\sin\psi}$, ψ=ϕ the associated flow rule is obtained. For a material with a friction angle of 30°, a value of N_{ψ} =3 is an upper bound for dilation.

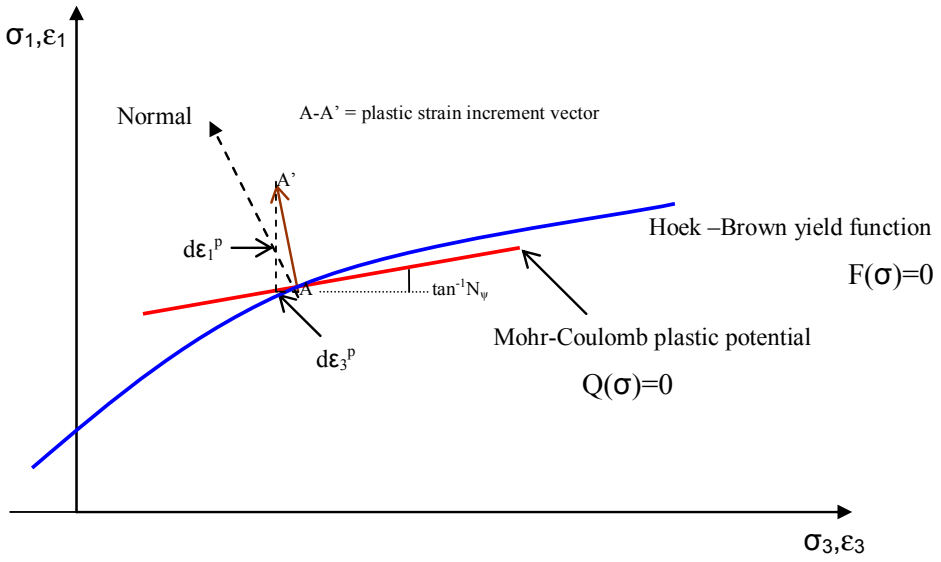

Figure 5-4 Hoek-Brown yield function, Mohr-Coulomb plastic potential, and plastic strain increment relationship in this study (Ogawa & Lo, 1987).

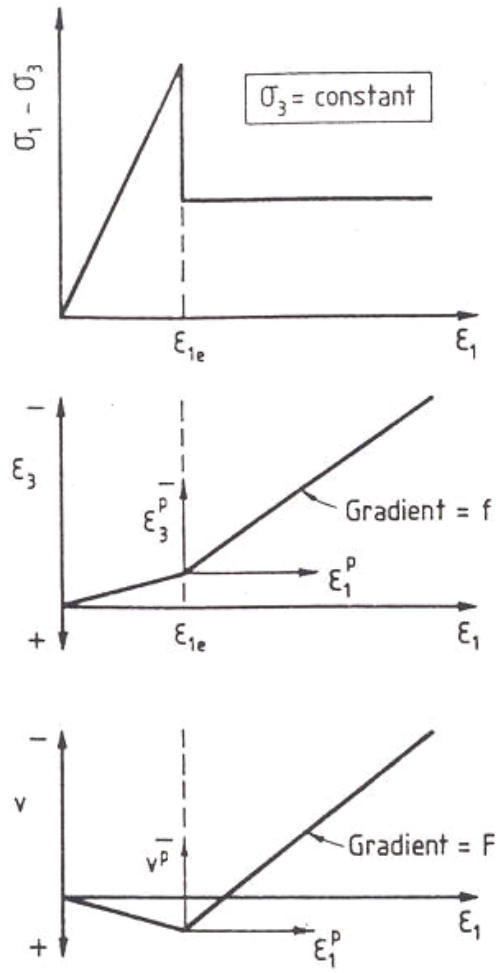

Figure 5-5 Stress-strain regime for a rock obeying elastic-britlle-plastic behaviour (Brown *et al*. 1983)

5.6 Stresses in the plastic zone

The combination of the stress equilibrium equation and residual Hoek-Brown failure criterion results in the ordinary differential equation in order to find the stress in the plastic (broken) zone around the opening (see Figure 5-1):

$$\frac{d\sigma_r}{dr} + \frac{c_r - c_\theta}{r} = 0 \tag{5-17}$$

Since $\tau_{r\theta} = 0$ for the axi-symmetrical problem, the residual strength envelope for the Hoek-Brown yield criterion becomes

$$\sigma_\theta = \sigma_r + \sigma'_{ci}\left(m_b' \frac{\sigma_r}{\sigma'_{ci}} + s' \right)^{a'} \tag{5-18}$$

When one substitutes Equation 5-18 into Equation 5-17, the following is obtained:

$$\frac{d\sigma_r}{dr} - \frac{\sigma'_{ci}(m_b' \frac{c_r}{\sigma'_{ci}} + s')^{a'}}{r} = 0 \tag{5-19}$$

For an unsupported opening, taking into account the boundary condition at $r=r_i$ ($\sigma_r = 0$), the solution of non-linear Equation 5-19 is given below. The details of derivations are given in the Appendix A.

$$\sigma_r = \frac{\Gamma - s'}{\frac{m_b'}{\sigma'_{ci}}} \tag{5-20}$$

$$\Gamma = \left[s'^{1-a'} - m_b'(a'-1)\ln\left(\frac{r}{r_i}\right) \right]^{\frac{1}{1-a'}} \tag{5-21}$$

In literature, some analytical solutions, mostly based on the convergence-confinement method, used the fictitious internal pressure (P_i) as the effect of the support pressure that imposes of the tunnel boundary. In such a case, in order to draw the ground reaction curve the support pressure must decrease gradually as the convergence increases. For this case, the solution of non-linear Equation 5-19 is obtained by taking into consideration the boundary condition at $r=r_i$, $\sigma_r = P_i$. Hence the radial stress in the plastic zone will be as below. The details of these derivations are also presented in the Appendix A.

$$\sigma_r = \frac{\frac{\Omega}{\sigma'_{ci}} - s'}{\frac{m_b'}{\sigma'_{ci}}} \tag{5-22}$$

$$\Omega = \left[(m_b' P_i + \sigma'_{ci} s')^{1-a'} - m_b'(a'-1)\sigma'^{\,1-a'}_{ci} \ln\left(\frac{r}{r_i}\right) \right]^{\frac{1}{1-a'}} \tag{5-23}$$

5.7 Stresses in the outer elastic zone

In the elastic zone, the stress distributions are given by classical Lame's solution as follows (Tutluoglu, 2002):

$$\sigma_\theta = P_o + (P_o - \sigma_{re})\left(\frac{r_e}{r}\right)^2 \text{ or } \sigma_\theta = P_o\left[1+\left(\frac{r_e}{r}\right)^2\right] - \sigma_{re}\left(\frac{r_e}{r}\right)^2 \tag{5-24}$$

$$\sigma_r = P_o - (P_o - \sigma_{re})\left(\frac{r_e}{r}\right)^2 \text{ or } \sigma_r = P_o\left[1-\left(\frac{r_e}{r}\right)^2\right] + \sigma_{re}\left(\frac{r_e}{r}\right)^2 \tag{5-25}$$

where σ_{re} is the radial stress at the elastic-plastic interface (see Figure 5-1).

The stress distribution in the elastic zone is equivalent to that of a larger opening of radius r_e, supported by a uniform internal stress σ_{re} under the same external field stress. r_e is the radial distance to the outer limit of the yielding zone surrounding the opening.

At the elastic-plastic boundary ($r=r_e$), the internal stresses are given by from plastic part:

$$\sigma_{re} = \frac{\Delta - s'}{\frac{m_b'}{\sigma_{ci}}} \tag{5-26}$$

$$\Delta = \left[s'^{1-a'} - m_b'(a'-1)\ln\left(\frac{r_e}{r_i}\right)\right]^{\frac{1}{1-a'}} \tag{5-27}$$

From elastic part at $r=r_e$ the Equations 5-24 and 5-25 can be arranged as:

$$\sigma_{\theta e} - \sigma_{re} = 2(P_o - \sigma_{re}) \tag{5-28}$$

$$\sigma_{\theta e} + \sigma_{re} = 2P_o \tag{5-29}$$

Using the peak strength criteria for elastic-plastic boundary:

$$\sigma_{\theta e} - \sigma_{re} = \sigma_{ci}\left(m_b\frac{\sigma_{re}}{\sigma_{ci}} + s\right)^a \tag{5-30}$$

Equating 5-28 and 5-30 yields the following non-homogeneous equation:

$$2(P_o - \sigma_{re}) = \sigma_{ci}\left(m_b \frac{\sigma_{re}}{\sigma_{ci}} + s \right)^a \tag{5-31}$$

An exact solution is only possible when $a = 0.5$. However, numerical methods (approximate solution), like the Newton-Raphson method, can be applied to approximate the exact solution to Equation 5-31 (Press *et al*., 1994). Subsequently, the Equation 5-31 is independently solved when $a = 0.5$:

$$\sigma_{re} = P_o + \frac{m_b c_{ci}}{8} \pm \frac{1}{8}\sqrt{16 P_o m_b \sigma_{ci} + m_b{}^2 \sigma_{ci}{}^2 + 16\sigma_{ci}{}^2 s} \tag{5-32}$$

Negative sign of the above equation is acceptable and after abbreviating:

$$c_{re} = P_o - M c_{ci} \tag{5-33}$$

where

$$M = \frac{1}{2}\left[\left(\frac{m_b}{4} \right)^2 + m_b \frac{P_o}{\sigma_{ci}} + s \right]^{\frac{1}{2}} - \frac{m_b}{8} \tag{5-34}$$

5.8 Radius of the plastic zone

The plastic zone radius r_e can be determined by assuming continuity of radial stress at the elastic-plastic boundary. It is also assumed that the field boundaries are far enough from the opening, such that their influence on the solution on the solution for r_e is negligible.

Equating the expressions 5-26 and 5-32 (for σ_{re} at $r = r_e$), the normalized plastic zone radius (r_e/r_i) can be derived as follows:

$$\frac{r_e}{r_i} = e^X \tag{5-35}$$

$$X = \frac{s'^{1-a'} - \left\{ s' + \frac{P_o m_b'}{\sigma_{ci}'} + \frac{m_b m_b' \sigma_{ci}}{8\sigma_{ci}'} - \frac{m_b'}{8\sigma_{ci}'}\left(16 P_o m_b \sigma_{ci} + m_b{}^2 \sigma_{ci}{}^2 + 16\sigma_{ci}{}^2 s\right)^{\frac{1}{2}} \right\}^{1-a'}}{m_b'(a'-1)}$$

5.9 Strains and displacement analysis

5.9.1 Strains in elastic zone

Hooke's law can be applied to determine the radial and tangential strains in the elastic region surrounding the plastic zone (Timoshenko & Goodier, 1970; Tutluoglu, 2002):

$$\varepsilon_r = \frac{1-\nu^2}{E}\left[\sigma_r - \left(\frac{\nu}{1-\nu}\right)\sigma_\theta\right] \tag{5-36}$$

$$\varepsilon_\theta = \frac{1-\nu^2}{E}\left[\sigma_\theta - \left(\frac{\nu}{1-\nu}\right)\sigma_r\right] \tag{5-37}$$

$$\gamma_{r\theta} = \frac{1}{G}\tau_{r\theta} \tag{5-38}$$

Under axi-symmetrical plane-strain condition

$$\varepsilon_z = 0\,,\ \gamma_{zr} = \gamma_{z\theta} = 0\,,\ \tau_{zr} = \tau_{z\theta} = 0\,, \gamma_{r\theta} = 0\,, \text{and } \tau_{r\theta} = 0$$

Recalling stresses in elastic zone (Equations 5-24 and 5-25) and substituting into Equations 5-36 and 5-37 provide the strain field for under plane strain condition:

$$\varepsilon_r = \frac{(1-2\nu)}{2G}P_o + \frac{(\sigma_{re} - P_o)}{2G}\left(\frac{r_e}{r}\right)^2 = \frac{(1-2\nu)}{2G}P_o - \frac{M\sigma_{ci}}{2G}\left(\frac{r_e}{r}\right)^2 \tag{5-39}$$

$$\varepsilon_\theta = \underbrace{\frac{(1-2\nu)}{2G}P_o}_{\text{Elastic deformation}} \underbrace{- \frac{(\sigma_{re} - P_o)}{2G}\left(\frac{r_e}{r}\right)^2}_{\text{Deformation due to excavation}} = \frac{(1-2\nu)}{2G}P_o + \frac{M\sigma_{ci}}{2G}\left(\frac{r_e}{r}\right)^2 \tag{5-40}$$

5.9.2 Strains in the plastic zone

The total strains in the plastic zone are made up of both elastic and plastic strains as given by the Equation 5-4. Hooke's law and flow rule have been applied to calculate the elastic and plastic strains, respectively. Expanding Equation 5-4 under plane strain condition yields:

$$\varepsilon_\theta^t = \varepsilon_\theta^e + \varepsilon_\theta^p$$
$$\varepsilon_r^t = \varepsilon_r^e + \varepsilon_r^p \tag{5-41}$$

It should be, at this point, noted that the elastic strains are very small compared to the plastic strains ($\varepsilon_{ij}^e << \varepsilon_{ij}^p$).

5.9.2.1 Determination of the elastic strains in the plastic zone

Using generalized Hook's law (Equations 5-36 and 5-37) and substituting stresses in the plastic zone (Equations 5-18 and 5-20):

$$\varepsilon_r^e = \frac{1}{2G}\left[(1-2\nu)\left(\frac{\Gamma - s'}{\frac{m_b}{\sigma_{ci}}'}\right) - \nu\sigma_{ci}{}'\Gamma^{a'}\right] \tag{5-42}$$

$$\varepsilon_\theta^e = \frac{1}{2G}\left[(1-2\nu)\left(\frac{\Gamma - s'}{\frac{m_b}{\sigma_{ci}}'}\right) + (1-\nu)\sigma_{ci}{}'\Gamma^{a'}\right] \tag{5-43}$$

Then

$$\varepsilon_\theta^e - \varepsilon_r^e = \frac{1}{2G}\sigma_{ci}{}'\Gamma^{a'} \tag{5-44}$$

5.9.2.2 Determination of the plastic strains in the plastic zone

Substituting the Equations 5-42 and 5-43 in the strain compatibility (Equation 5-3) and taking account of the flow rule (Equation 5-12) provide the following non-linear differential equation

$$\frac{d\varepsilon_\theta^p}{dr} + \frac{\sigma_{ci}{}'}{2Gr}\left[s'^{1-a'} - m_b{}'(a'-1)\ln\left(\frac{r}{r_i}\right)\right]^{\frac{a'}{1-a'}}\left[(1-2\nu) + a'm_b{}'(1-\nu)\right] +$$
$$\frac{1}{r}\left[\varepsilon_\theta^p(1+N_\psi) + \frac{\sigma_{ci}{}'}{2G}\left[s'^{1-a'} - m_b{}'(a'-1)\ln\left(\frac{r}{r_i}\right)\right]^{\frac{a'}{1-a'}}\right] = 0 \tag{5-45}$$

The boundary condition used in solving Equation 5-45 can be written as (Brown *et al*. 1983):

$$\varepsilon_\theta^p = \frac{Mc_{ci}}{2G} \text{ at } r = r_e$$

Even though it is first order, the non-liner Equation 5-45 can be solely solved by the numerical methods provided by some packages such as MATEMATICA (Mathematica V 5.1., 2004) or MAPLE (Maple V 9, 2003). The solution of the Equation 5-45, considering the prescribed boundary condition, will be as below:

$$\varepsilon_\theta^p = \frac{1}{r^{1+N_\psi}}\left[\frac{M\sigma_{ci}}{2G} r_e^{1+N_\psi} + \left(\frac{\sigma_{ci}'}{2G}(1-\nu)(2+a'm_b')\right)\int_r^{r_e} r^{N_\psi-1}\left[s'^{1-a'} + m_b'(1-a')\ln\left(\frac{r}{r_i}\right)\right]^{\frac{a'}{1-a'}} dr\right]$$

(5-46)

As can be seen from Equation 5-46, an integral function has been introduced in the result of the differential equation. The complete solution can be obtained provided that the integral on the right side of the Equation 5-46 is evaluated numerically as represented in the Appendix A.

5.9.2.3 Radial displacement field

The displacement field can be obtained directly by the following strain-displacement relationships which satisfy the compatibility conditions:

$$\varepsilon_\theta = \frac{u_r}{r} + \frac{1}{r}\cdot\frac{\partial u_\theta}{\partial \theta}$$

$$\varepsilon_r = \frac{\partial u_r}{\partial r} \qquad (5\text{-}2)$$

The conditions of plane strain under axi-symmetric deformation ($\gamma_{r\theta}$) imply that the total strains are independent of the tangential strain components. Therefore, the radial displacement field can be readily evaluated from any of the following expressions:

$$\frac{u_r}{r} = \varepsilon_\theta^t \quad \text{or} \quad u_r = \int \varepsilon_r^t dr \qquad (5\text{-}47)$$

The displacement field is then given by:

$$\frac{u_r}{r}=\frac{1}{2G}\left[\begin{array}{l}(1-2\nu)(\dfrac{\Gamma-s'}{\dfrac{m_b'}{\sigma_{ci}'}})+(1-\nu)\sigma_{ci}'\Gamma^{a'}+\dfrac{M\sigma_{ci}}{r^{1+N\psi}}r_e^{(1+N\psi)}+\\ \\ \dfrac{1}{r^{(1+N\psi)}}\sigma_{ci}'(1-\nu)(2+a'm_b')\displaystyle\int_r^{r_e}r^{N_\psi-1}\Gamma^{a'}dr\end{array}\right] \tag{5-48}$$

where Γ can be obtained from Equation 5-21 as below

$$\Gamma=\left[s'^{1-a'}-m_b'(a'-1)\ln\left(\frac{r}{r_i}\right)\right]^{\frac{1}{1-a'}} \tag{5-21}$$

Subsequently, elasto-plastic tunnel surface convergence can be subsequently determined by substituting $r=r_i$ in the above expressions.

$$\frac{u_r}{r_i}=\frac{1}{2G}\left[\begin{array}{l}(1-\nu)\sigma_{ci}'s'^{a'}+\dfrac{M\sigma_{ci}}{r_i^{1+N\psi}}r_e^{(1+N\psi)}+\\ \\ \dfrac{1}{r_i^{(1+N\psi)}}\sigma_{ci}'(1-\nu)(2+a'm_b')\displaystyle\int_{r_i}^{r_e}r^{N_\psi-1}\Gamma^{a'}dr\end{array}\right] \tag{5-49}$$

Neglecting elastic strain due to its very small magnitude in comparison with plastic strain, the above equation will be simplified as:

$$\frac{u_r}{r_i}=\frac{1}{2G}\left[\begin{array}{l}\dfrac{M\sigma_{ci}}{r_i^{1+N\psi}}r_e^{(1+N\psi)}+\\ \\ \dfrac{1}{r_i^{(1+N\psi)}}\sigma_{ci}'(1-\nu)(2+a'm_b')\displaystyle\int_{r_i}^{r_e}r^{N_\psi-1}\Gamma^{a'}dr\end{array}\right] \tag{5-50}$$

Appendix C presents the spreadsheet form of a practical solution that has been solved by this elastic-plastic solution.

5.10 Stress distribution along fully grouted bolts

In what follows, the same elasto-plastic problem will be investigated when the tunnel is reinforced by radial passive grouted bolts. The following major assumptions have been made in this analysis:

I. Shear stress distribution along the fully grouted bolts is assumed by the model illustrated in Figure 5-6. The influence of the relatively thin grout annulus on rock mass deformation has been ignored.
II. Axi-symmetric bolt pattern around the tunnel consists of identical bolts with equal spacing along the tunnel axis and around the circumference. The tangential bolt spacing around the opening is defined by the product of the tunnel radius and the angle between two adjacent bolts (i.e. $S_T = r_i \cdot \theta$) as shown in Figure 5-7.
III. The increase of the elastic modulus (E) and change in Poisson's ratio (ν) of the rock mass due to the presence of steel bolts around the tunnel is not modelled by the proposed analytical solution.
IV. The change in the rock mass strength parameters, as a result of the bolts, outside the plastic zone is not taken into account in this solution.

The shear stress distribution (τ_z) along a grouted bolt can be represented by (Xueyi, 1983; Indraratna & Kaiser, 1990a):

$$- dQ_s = \pi d \tau_s ds \tag{5-51}$$

$$\tau_s = -\frac{1}{\pi d} \cdot \frac{dQ_s}{ds} = -\frac{r_b}{2} \cdot \frac{dc_s}{d_s}$$

where bolt diameter d=2 × bolt radius (r_b), Q_s is the axial load distribution and σ_s is the axial stress distribution along the bolt.

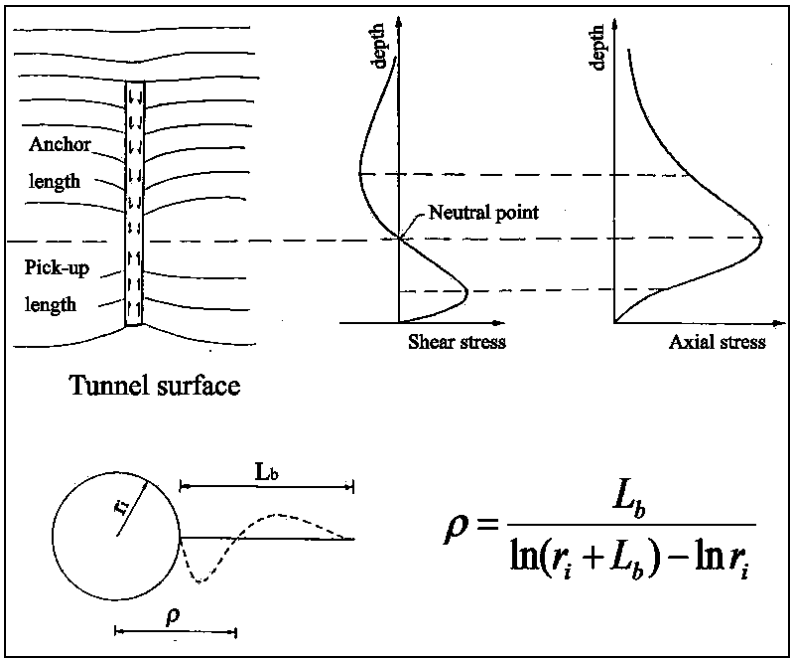

Figure 5-6 Stress distribution model for grouted bolts (Xueyi, 1983; Indraratna & Kaiser, 1990a)

Because the shear stress is related to the first derivative of the axial stress, a zero value of τ_s can be defined as the neutral point where the axial stress reaches a maximum. The model for stress distribution associated with grouted bolts has been proposed firstly by Freeman (1978) based on field measurements from the Kielder experimental tunnel (Ward *et al.* 1983) and later by Xueyi (1983), also based on field observations. This model incorporates with the proposed elasto-plastic solution to account for the effect of the grouted bolts. The model, illustrated diagrammatically in Figure 5-6, demonstrates the occurrence of the neutral point at the location of the maximum axial stress. It further presents points of inflection on the axial stress distribution associated with the maximum and minimum shear stress distribution, where:

$$\frac{d\tau_s}{ds} = \frac{d^2\sigma_s}{ds^2} = 0 \qquad (5\text{-}52)$$

The shear stress distribution can be defined by the division of the bolt into a pick-up length and an anchor length as shown in Figure 5-6. This is justified mathematically by considering the equilibrium of the grouted bolt relative to the surrounding rock. The pick-up length restrains the ground displacements towards the opening whereas the anchor length is restrained by the rock. The equilibrium of the bolt relative to the rock is thereby ensured as a result of the shear stresses acting in opposite directions along the pick-up length and anchor length, respectively (Indraratna & Kaiser, 1990a). Where the direction of shear stress is changed called neutral point and the relative displacement at the neutral point is zero. Yu & Xian

(1983) investigated the interaction mechanisms of the fully grouted bolts and provided additional theoretical justifications for this model. The location of the neutral point along the bolt suggested by Xueyi (1983) is:

$$\rho = \frac{L_b}{\ln\left[1+(\frac{L_b}{r_i})\right]} \tag{5-53}$$

where L_b is bolt length and r_i is opening radius. According to observations carried out by Xueyi (1983), it was seen that $\rho \approx 0.45 L_b + r_i$.

In an axi-symmetrical problem and taking into consideration the same bolts with equal spacings along the tunnel axis and around the circumference, the tangential bolt spacing around the tunnel is defined by the product of the tunnel radius and the angle between two adjacent bolts (i.e. $S_T = r_i \theta$) as represented in Figure 5-7.

5.11 Influence of bolting on strength parameters and bolt density parameter

It has already observed that the combination of equilibrium equation (Equation 5-17) and Hoek-Brown failure criterion (Equation 5-18) gave rise to the following , referred to as the unsupported tunnel (see Figure 5-7).

$$\frac{d\sigma_r}{dr} - \frac{\sigma'_{ci}(m_b' \frac{\sigma_r}{\sigma'_{ci}} + s')^{a'}}{r} = 0 \tag{5-19}$$

In a bolted element (Figure 5-7d), the additional radial force due to shear stresses along the bolt is assumed to be given by the following expression (Indraratna, 1987):

$$\Delta\tau = \pi \cdot d \cdot \sigma_\theta \cdot \lambda \cdot dr \tag{5-54}$$

Hence, the equilibrium condition for the bolted element can be represented by :

$$\frac{d\sigma_r}{dr} - \frac{1}{r}\sigma'_{ci}(1+\beta)\left[m'_b(1+\beta)\frac{\sigma_r}{\sigma'_{ci}(1+\beta)} + s'(1+\beta)\right]^a = 0 \tag{5-55}$$

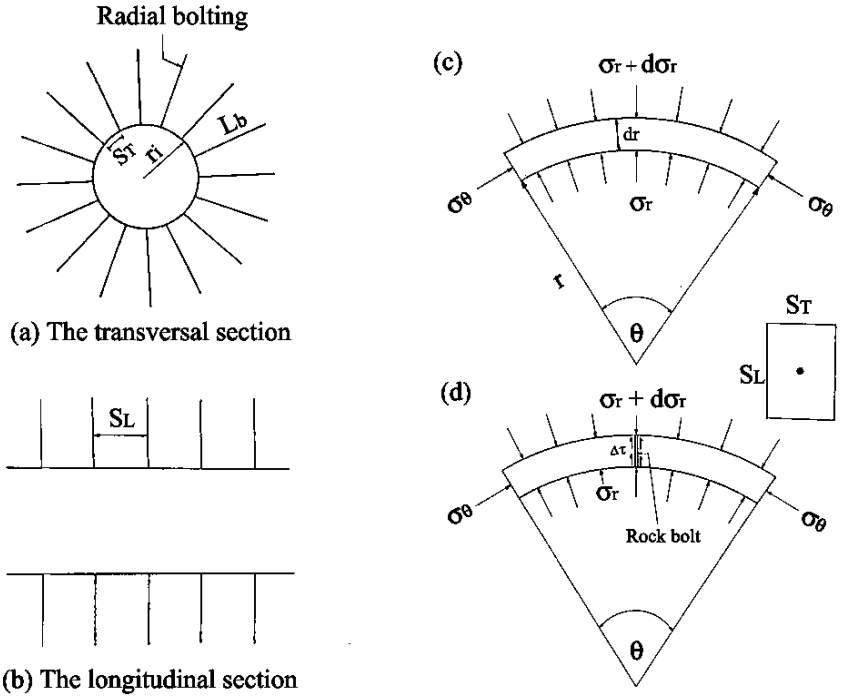

Figure 5-7 Fully reinforced circular excavation and equilibrium considerations for bolt-ground interaction (Indraratna & Kaiser, 1990a)

where the bolt density parameter can be defined as (Indraratna & Kaiser, 1990a):

$$\beta = \frac{\pi d\lambda}{S_L \theta} = \frac{\pi d\lambda r_i}{S_L S_T} \tag{5-56}$$

Aparently, the bolt density parameter (β) is dimensionless. It reflects the relative density of bolts with respect to the opening perimeter and takes into consideration the shear stresses on the bolt surface, which oppose the rock mass displacements near the opening wall. The magnitude of β can be increased by as stated by Indraratna & Kaiser (1990a, b):

I. Decreasing the bolt spacing,

II. Increasing the bolt surface area, or

III. Increasing the roughness of bolt surface.

The value of β varies between 0.05 and 0.20 for most cases. For tunnels excavated in very poor rock mass such at the Enasan tunnel, analyzed by Indraratna & Kaiser

(1990b) very high values for β (in excess of 0.4) were reached by very intensive bolting patterns.

The friction factor, λ, is analogous to the coefficient of friction. It relates the mean mobilized shear stress to the stress applied normal to the bolt surface. Indraratna & Kaiser (1990a) suggested that the magnitude of λ for smooth rebars falls in the range $tan\ (\varphi_g / 2) < \lambda < tan\ (2\varphi_g /3)$ and for shaped rebars approaches $\tan\varphi_g$, depending on the degree of adhesion (bond strength) at the bolt-grout interface.

5.12 Concept of equivalent material approach (equivalent strength parameters)

By embedding the grouted rock-bolts inside the plastic zone (yielded zone) around the tunnel, already characterized in terms of residual (post-peak) strength parameters, the strength parameters (Hoek-Brown constants) of the yielded rock mass will then be improved. In other words, grouted rock-bolts create a zone of improved, reinforced rock in the region defined by the pick-up length of the bolts. Within this zone, the strength parameters of yielded rock mass are increased as schematically shown in the Figure 5-8.

Introducing the bolt density parameter (β), the equivalent strength parameters can be hypothesized as:

$$\begin{aligned} m_b^* &= (1+\beta)\cdot m_b' \\ s^* &= (1+\beta)\cdot s' \\ \sigma_{ci}^* &= (1+\beta)\cdot \sigma_{ci}' \end{aligned} \qquad (5\text{-}57)$$

The definition of above equations is graphically illustrated in Figure 5-9 to Figure 5-11. The Equation 5-55 for bolted structure can be simplified as follows:

$$\frac{d\sigma_r}{dr} - \frac{\sigma_{ci}^* (m_b^* \frac{c_r}{\sigma_{ci}^*} + s^*)^a}{r} = 0 \qquad (5\text{-}58)$$

Comparison of this equation with Equation 5-19 for the unsupported case indicates that both equations have the same algebraic arrangement.

It is worth noting that the coefficient a (Hoek-Brown constant) for the reinforced tunnel is assumed not to be affected by the (β), rather it keeps its original value (i.e. $a^* = a$). In addition, it should be clarified that the extent of the plastic zone around the tunnel is dependent on residual compressive strength of intact rock as also taken into account in some solutions such as Kaiser *et al.* (1985), Indraratna & Kaiser (1990a), Cundall *et al.* (2003), and Carranza-Torres (2004). However, in

some solutions such as Brwon *et al.* (1983) and Sharan (2003, 2005), the magnitude of the intact rock strength does not vary for the yielded rock. Since in the proposed elastic-plastic solution, the residual value is given to the intact rock strength after it yields (i.e. σ'_{ci}), it is suggested that the yielded intact rock strength be increased as a result of bolting effect (i.e. σ_{ci}^{*}). If the value of bolt density (β) is assumed to be zero in $\sigma_{ci}^{*} = (1+\beta)\cdot\sigma'_{ci}$, it means that the yielded intact rock strength does not affected by bolts.

5.13 Rock stabilization through effective material strength parameters

As mentioned before, the strength parameters of rock mass (C_m and ϕ in the Mohr-Coulomb criterion and m_b, s, a, and σ_{ci} in the Hoek-Brown criterion) in yielding zone around the opening (or ahead of the face) may be assumed to be degraded from peak value to residual values identified with the primed superscript in the Figure 5-12.

Conversely, the Mohr envelope of the yielded material may be raised up by improving its strength parameters (C_m* and ϕ* in Mohr-Coulomb criterion and m*, s*, and σci* in Hoek-Brown criterion) by application of a radial, confining pressure through the use of grouted bolts.

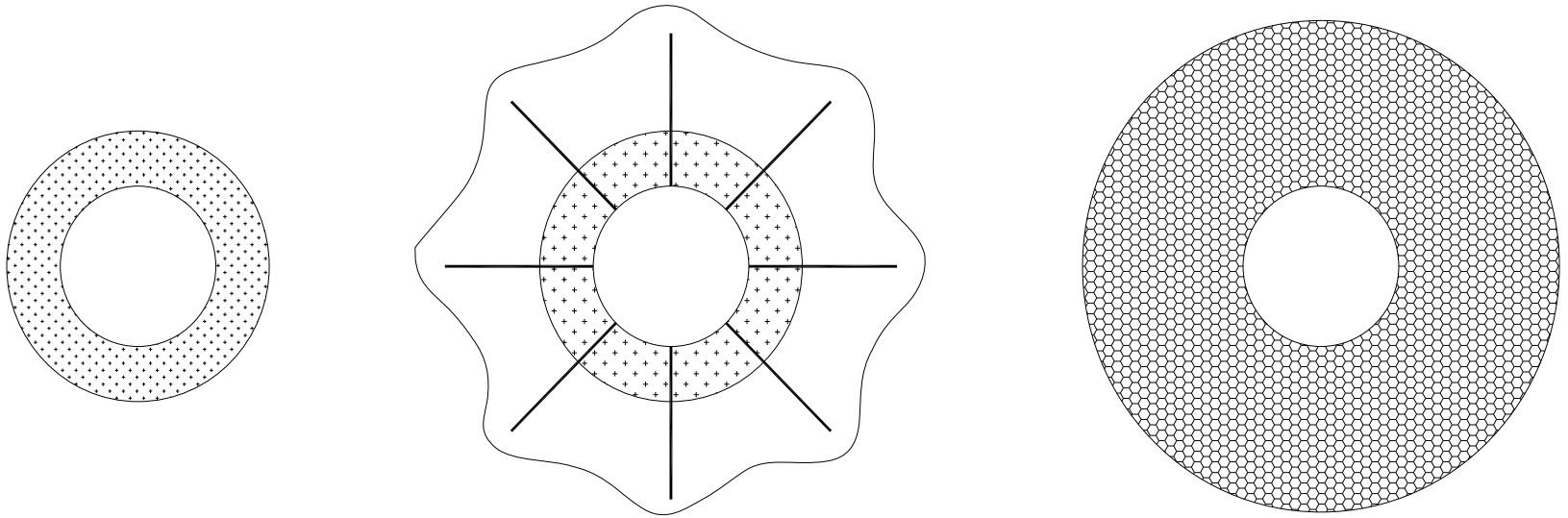

a) Plastic zone induced around the unsupported tunnel

Residual (Post-peak) strength parametes mb', s', σ_{ci}'

b) Grouted rock-bolts are installed in the already induced yielded zone around the tunnel

a) Induced plastic zone + grouted rock bolt can be considered as the Equivalent Plastic Zone

Equivalent strength parametes mb*, s*, σ_{ci}*

Figure 5-8 Creation of the Equivalent Plastic Zone around the circular tunnel reinforced by grouted bolts, considering equivalent material concept

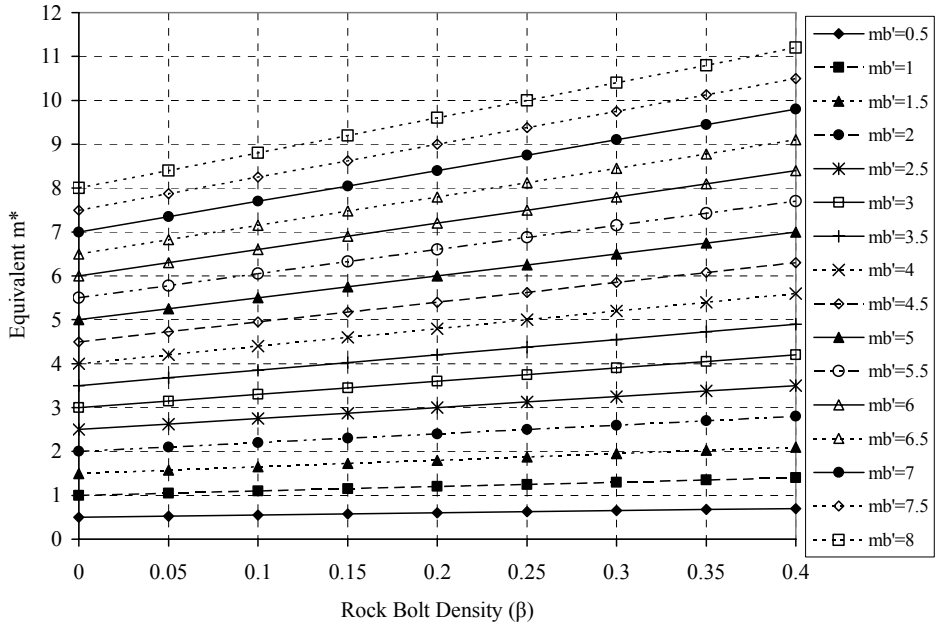

Figure 5-9 Variation of the equivalent strength parameter (m*) of Hoek-Brown failure criterion with β

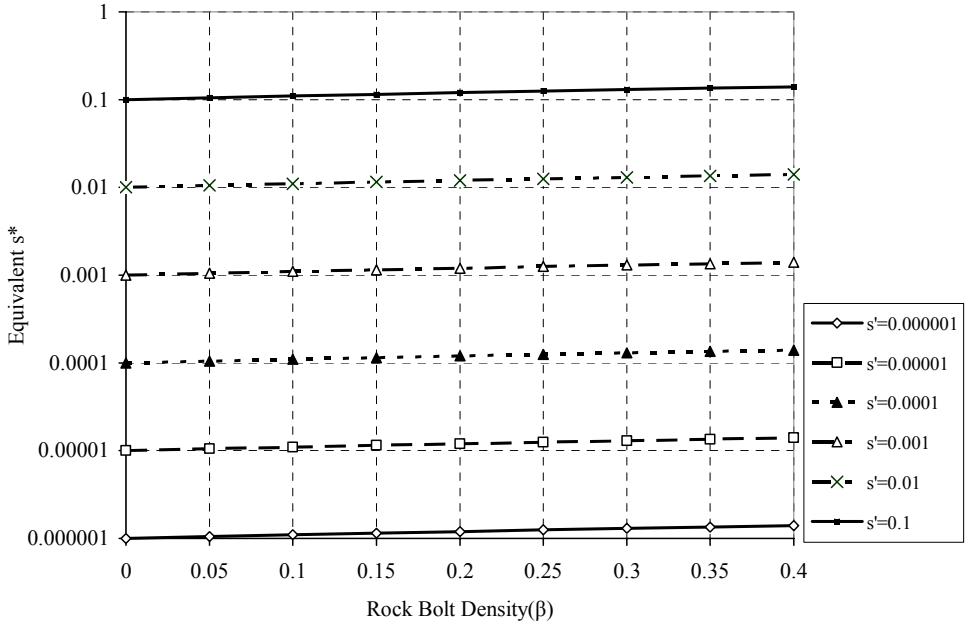

Figure 5-10 Variation of the equivalent strength parameter (s*) of Hoek-Brown failure criterion with β

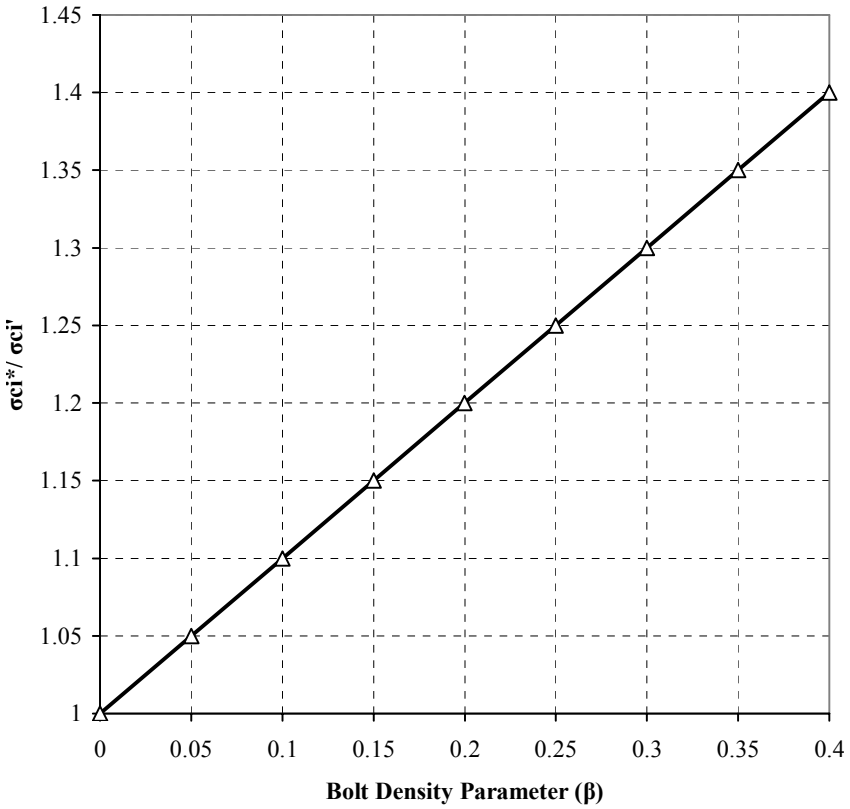

Figure 5-11 Variation of the equivalent compressive strength (σ_{ci}*) with β

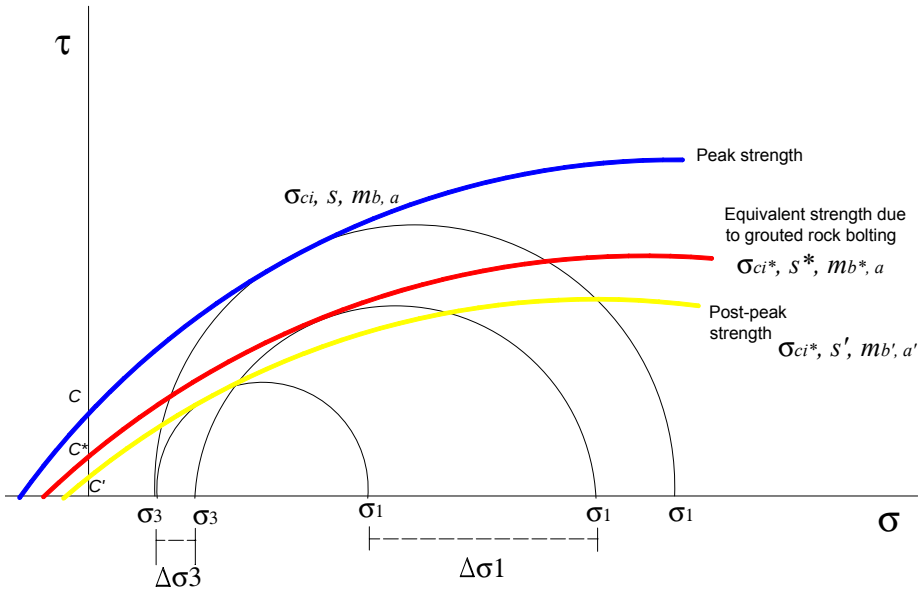

Figure 5-12 Increase of strength parameters by reinforcing the rock using grouted bolts, considering the equivalent material concept. Key: $\Delta\sigma_3$: confining action of grouted rock bolts in the plastic (post- peak) zone.

The development of load on a grouted bolt has the effect of providing additional confinement (increased radial stress) in the yielded zone. As a result, the tangential stress at the same point is increased more than proportionately. The original failure envelope is thereby shifted upwards, indicating an improvement of the strength parameters as represented by the Mohr diagram in Figure 5-12. This enables the rock mass to behave as a more strong material, leading to a corresponding reduction in opening convergence at a given field stress.

The following expression has been introduced in the literature to show the effect of the rock bolting on improving of the yielding zone around the tunnel in terms of effective cohesion (Grasso *et al*., 1989a, b and Pelizza *et al*., 2006).

$$C_m^{*} = C_m + \frac{1+\sin\phi}{2\cos\phi}\cdot\Delta\sigma_3 \tag{5-59}$$

where Δc_3 is the confinement produced by the action of the grouted bolts:

$$\Delta\sigma_3 = \frac{T_m}{S_T \cdot S_L} \tag{5-60}$$

where T_m is the mean force along each bolt, S_T and S_L are transversal and longitudinal spacing of the bolting pattern.

Grouted bolts themselves are not considered to establish any radial support pressure, P_i, on the rock surface, so equilibrium for the ground reaction curve is reached as for unsupported rock when P_i=0. The principal effect of grouted bolts, compared to the unsupported rock mass, is that the stability of rock mass is improved as the bolts through tension load influence the strength of the rock mass. Consequently, owing to the fact that fully grouted bolts effectively improve the apparent strength of the rock mass, the behaviour of the reinforced tunnel can be ideally represented by a shift of the ground convergence curve (Indraratna & Kaiser, 1990a; Stille *et al*., 1989; Oreste, 2003). The vertical axis of the ground convergence curve (Figure 5-13) represents the fictitious support pressure (radial stress) (P_i) required at the opening boundary to prevent further convergence. The horizontal axis represents the opening convergence at the opening wall (u_{ri}). The ground convergence curves are identical at every point along the opening boundary for the condition of axi-symmetric yielding under hydrostatic field stress.

The response of an unsupported tunnel in yielding rock is given by curve A. Curve B represents an imaginary ground convergence curve of the tunnel, where bolts would have been installed before any displacements could have occurred. In reality, an initial displacement (u_o) of the tunnel wall occurs prior to the installation and subsequent activation of the grouted bolts. The magnitude of the initial displacements is dependent on the percentage of fictitious support pressure (radial stress) which has already relieved. Normally, it can happen at 60 % of applied

fictitious support pressure. The magnitude of convergence after bolting is dependent on the apparent stiffness of the bolt- ground, and is reflected by a shift of the ground convergence curve from curve A to curve C, as a result of the reduced yield zone. An example of ground reaction curve of a reinforced tunnel will be presented in the following sections. In contrast to fully grouted bolts, pre-tensioned mechanical bolts provide direct radial pressure (active support) against the opening wall, but do not become an integral part of the deforming rock mass. Consequently, their performance is best represented by a support confinement curve with a specific stiffness and its interaction with the original ground convergence curve as those presented by Hoek & Brown (1980b), Carranza-Torres & Fairhurst (1999), Oreste (2003).

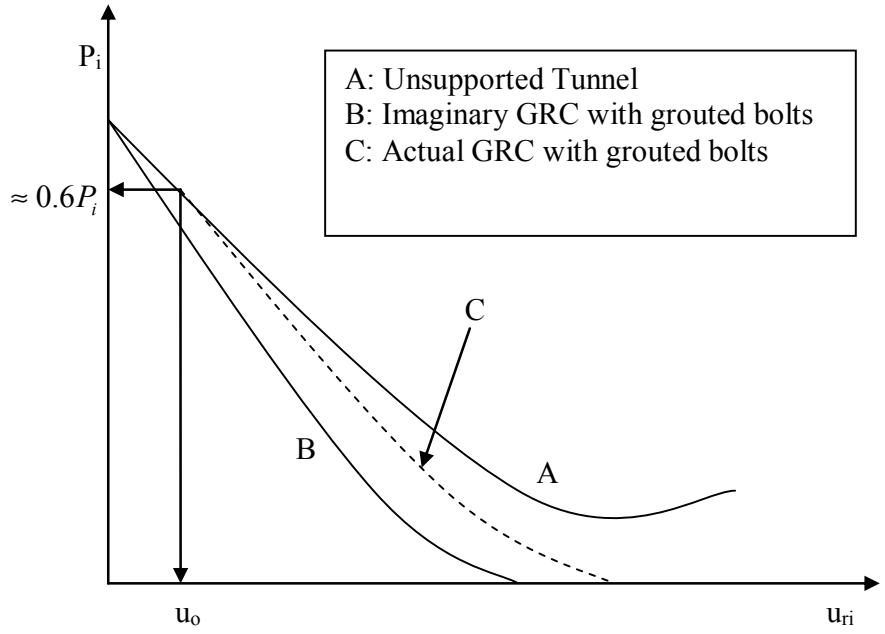

Figure 5-13 The effect of grouted bolts on the Ground Reaction Curve (GRC) (Indraratna & Kaiser, 1990a ; Oreste, 2003)

5.14 Influence of bolt length on tunnel wall stability

Bolt length, another important parameter for controlling displacement, is not included in the bolt density parameter because the effect of a bolt depends on its length relative to the radius of the yield zone. The shear stress distribution and, hence, the location of the neutral point are directly related to the bolt length, the extent of the plastic zone and the strength reduction in this zone. As it will be shown later, the extent of the yield zone and the tunnel wall displacement (convergence) can be effectively reduced by increasing the bolt length.

5.15 Concept of equivalent plastic zone

This concept was firstly defined by Indraratna & Kaiser (1990a, b). Grouted bolting is capable of improving plastic zone by increasing its strength in terms of Hoek- Brown constants (m_b, s, a, and σ_{ci}) as schematically represented in Figure 5-8. The extent of the plastic zone is directly related to this rock mass properties and any improvement of the rock strength must reduce the extent of the zone of overstressed rock, if the bolts are installed soon after excavation close to the face. Consequently, the plastic zone of a bolted opening is smaller than that of an unsupported opening in the same ground. This zone is called "Equivalent Plastic Zone" because it is the yield zone in a material of improved properties simulating a behaviour equivalent to the bolted rock mass. In other words, EPZ consists of a material with improved strength properties, representing the yielded, reinforced rock mass. A reduction of the apparent plastic zone, in turn, curtails opening wall displacement. The extent of the plastic zone is influenced by the strength parameters of yielded rock mass (Hoek- Brown constants). The following factors directly affect the radius r_e^* of the equivalent plastic zone (Indraratna & Kaiser, 1990a, b):

I. Bolt density parameter (β)
II. Bolt length (L_b)
III. Radius of the neutral point of the bolt (ρ)
IV. Opening radius (r_i)
V. Field stress (P_o)

The determination of the equivalent plastic zone EPZ radius, r_e^*, must be divided into three categories depending on the location of the interface between the elastic rock and the equivalent plastic zone relative to the neutral point and the bolt length as suggested by Indraratna & Kaiser (1987, 1990a, b). These three categories are diagrammatically illustrated in Figure 5-14:

I. $r_e^* < \rho < (r_i + L)$ minimal yielding
II. $\rho < r_e^* < (r_i + L)$ major yielding
III. $r_e^* > (r_i + L)$ excessive yielding

5.15.1 Determination of the Equivalent Plastic Zone Category I

The condition of minimal yielding "$r_e^* < \rho < (r_i + L_b)$" occurs either at relatively small field stresses or when the bolts are excessively long. In this case, the extent of the plastic zone is confined within the pick-up length of the bolt. In addition, four distinct zones can be identified by the location of the plastic zone corresponding to the neutral point and the bolt ends.

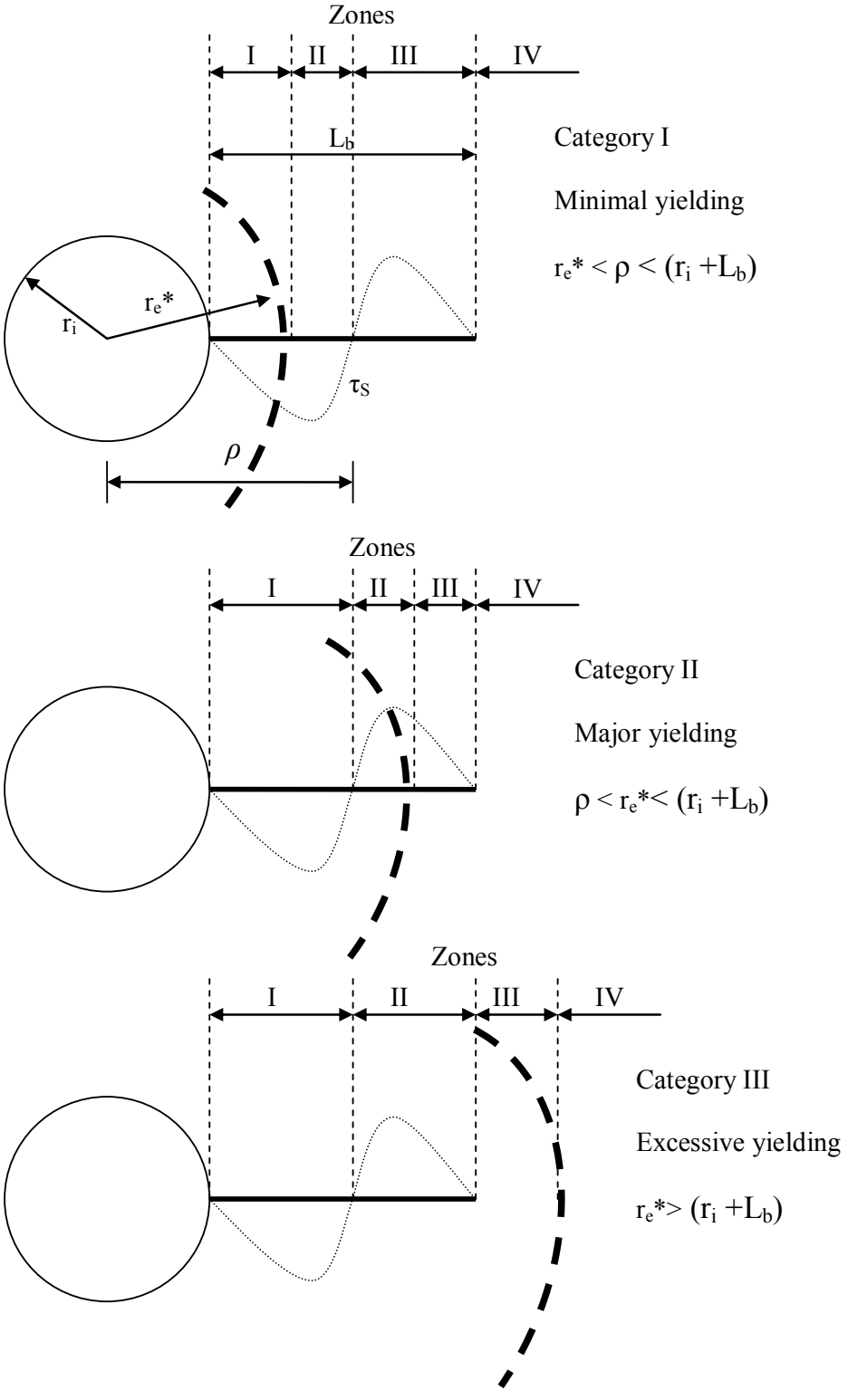

Figure 5-14 Categorization of the extent of the yielding (plastic zone) (Indraratna & Kaiser, 1990a, b)

5.15.1.1 Zone 1 : $r_i < r < r_e^*$

In this region of the pick-up length, the ground displacements toward the opening are resisted by positive shear stress. The equivalent stress field in this zone is represented by:

$$\sigma_r = \frac{\Gamma^* - s^*}{\frac{m_b^*}{\sigma_{ci}^*}} \tag{5-61}$$

$$\Gamma^* = \left[s^{*1-a} - m_b^*(a-1)\ln\left(\frac{r}{r_i}\right)\right]^{\frac{1}{1-a}} \tag{5-62}$$

$$\sigma_\theta = \sigma_r + \sigma_{ci}^*\left(m_b^* \frac{\sigma_r}{\sigma_{ci}^*} + s^* \right)^a \tag{5-63}$$

where: $m_b^* = (1+\beta)m_b'$, $s^* = (1+\beta)s'$, $\sigma_{ci}^* = (1+\beta)\sigma_{ci}'$, $c'_{ci} = S_r.c_{ci}$

5.15.1.2 Zone 2 : $r_e^* < r < \rho$

This part of the elastic zone is confined to the pick-up length of the bolt. The elastic stress fields in this zone are given by:

$$\sigma_r = P_o\left[1 - \left(\frac{r_e^*}{r}\right)^2\right] + \sigma_{re}\left(\frac{r_e^*}{r}\right)^2 \tag{5-64}$$

$$\sigma_\theta = P_o\left[1 + \left(\frac{r_e^*}{r}\right)^2\right] - \sigma_{re}\left(\frac{r_e^*}{r}\right)^2 \tag{5-65}$$

The peak tangential stress at the elasto-plastic interface for $S_r=1$ is given by the following condition:

$$\sigma_{\theta e} = \sigma_{re} + \sigma_{ci}^*\left(m_b^* \frac{\sigma_{re}}{\sigma_{ci}^*} + s^* \right)^a \tag{5-66}$$

The radial stress at the elasto-plastic boundary σ_{re} is, therefore, derived by:

$$\sigma_{re} = \frac{\Delta^* - s^*}{\frac{m_b^*}{\sigma_{ci}^*}} \tag{5-67}$$

$$\Delta^* = \left[s^{*1-a} - m_b^*(a-1)\ln\left(\frac{r_e^*}{r_i}\right)\right]^{\frac{1}{1-a}} \tag{5-68}$$

5.15.1.3 Zone 3 : $\rho < r < (r_i + L_b)$

This part of the elastic zone is contained within the anchor length of the bolt. The radial and tangential stress fields are given by:

$$\sigma_r = P_o\left[1-\left(\frac{\rho}{r}\right)^2\right] + \sigma_\rho\left(\frac{\rho}{r}\right)^2 \tag{5-69}$$

$$\sigma_\theta = P_o\left[1+\left(\frac{\rho}{r}\right)^2\right] - \sigma_\rho\left(\frac{\rho}{r}\right)^2 \tag{5-70}$$

where

$$\sigma_\rho = P_o\left[1-\left(\frac{r_e^*}{\rho}\right)^2\right] + \sigma_{re}\left(\frac{r_e^*}{\rho}\right)^2 \tag{5-71}$$

5.15.1.4 Zone 4 : $r > (r_i + L_b)$

This outermost elastic region, beyond the bolt, is in virgin rock and the elastic stresses are given by:

$$\sigma_r = P_o\left[1-\left(\frac{r_i+L_b}{r}\right)^2\right] + \sigma_{L_b}\left(\frac{r_i+L_b}{r}\right)^2 \tag{5-72}$$

$$\sigma_\theta = P_o\left[1+\left(\frac{r_i+L_b}{r}\right)^2\right] - \sigma_{L_b}\left(\frac{r_i+L_b}{r}\right)^2 \tag{5-73}$$

where

$$\sigma_{L_b} = P_o\left[1-\left(\frac{\rho}{r_i+L_b}\right)^2\right]+\sigma_\rho\left(\frac{\rho}{r_i+L_b}\right)^2 \tag{5-74}$$

The radial distance to the neutral point is given by Equation 5-51, as discussed earlier.

5.15.1.5 Equivalent Plastic Zone (EPZ)

At the elastic-plastic interface, the radial stress σ_{re} is obtained by Equations 5-67 and 5-68 through the assumption of continuity of radial stress. Equating Equations 5-30 and 5-67 and then solving provides the normalized radius of the equivalent plastic zone (EPZ):

$$\frac{r_e^*}{r_i} = e^Y \tag{5-75}$$

$$Y = \frac{s^{*1-a} - \left\{s^* + \frac{P_o m_b^*}{\sigma_{ci}^*} + \frac{m_b m_b^* \sigma_{ci}}{8\sigma_{ci}^*} - \frac{m_b^*}{8\sigma_{ci}^*}\left(16P_o m_b \sigma_{ci} + m_b{}^2\sigma_{ci}{}^2 + 16\sigma_{ci}{}^2 s\right)^{\frac{1}{2}}\right\}^{1-a}}{m_b^*(a-1)}$$

It is obvious that as β tends to zero, the parameters m_b^*, s^*, and σ_{ci}^* approach m_b, s ,and σ_{ci} . In other word, above equation becomes identical to that of unsupported case as Equation 5-33. Note that the equivalent value of a keeps its original value. Expressions for the Equivalent Plastic Zone radius can be derived for Categories (II) and (III) in the same manner (Appendix B). A summary is given below.

5.15.2 Determination of the Equivalent Plastic Zone Category II

The condition of major yielding, $\rho < r_i^* < (r_i+L_b)$, occurs when the extent of the plastic zone has propagated beyond the neutral point. In this situation, the plastic zone itself is divided by the neutral point into two zones. Consequently, only the plastic zone region that falls within the pick-up length of the bolt is effectively stabilized by the positive shear stresses. The Equivalent Plastic Zone radius is given by:

$$\frac{r_e^*}{r_i} = e^J \cdot e^h = e^{(J+h)} \tag{5-76}$$

where

$$J = \frac{(m_{b1}\sigma_\rho + \sigma_{ci1}s_1)^{1-a'} - \left[s_1\sigma_{ci1} + P_o m_{b1} + \frac{m_b m_{b1}\sigma_{ci}}{8} - \frac{m_{b1}}{8}(16P_o m_b\sigma_{ci} + m_b^2\sigma_{ci}^2 + 16\sigma_{ci}^2 s)^{\frac{1}{2}} \right]^{1-a'}}{m_{b1}(a'-1)\sigma_{ci1}{}^{(1-a')}}$$

$$h = \frac{s^{*\,1-a} - \Gamma^{*1-a}}{m_b^*(a-1)}$$

$$\sigma_\rho = \frac{\Gamma^* - s^*}{\frac{m_b^*}{\sigma_{ci}^*}}$$

$$\Gamma^* = \left[s^{*1-a} - m_b^*(a-1)\ln\left(\frac{\rho}{r_i}\right) \right]^{\frac{1}{1-a}}$$

$$m_{b1} = m_b'(1-\beta) \quad s_1 = s'(1-\beta) \quad c_{ci1} = c_{ci}'(1-\beta)$$

The derivations for this category are given in Appendix B.

5.15.3 Determination of the Equivalent Plastic Zone Category III

The condition of excessive yielding, $r_e^* > (r_i + L_b)$, occurs either due to large *in-situ* stress in relatively poor rock or as a result of inadequate bolt length. In this situation, the bolt is completely embedded in the yielded rock and no anchorage is provided from the outer elastic zone. In this case the radius of the Equivalent Plastic Zone is obtained by:

$$\frac{r_e^*}{r_i} = e^q \cdot e^h \cdot e^t = e^{(q+h+t)} \tag{5-77}$$

$$q = \frac{(m_b'\sigma_L + \sigma_{ci}'s')^{1-a'} - \left[s'\sigma_{ci}' + P_o m_b' + \frac{m_b m_b'\sigma_{ci}}{8} - \frac{m_b'}{8}(16P_o m_b\sigma_{ci} + m_b^2\sigma_{ci}^2 + 16\sigma_{ci}^2 s)^{\frac{1}{2}} \right]^{1-a'}}{m_b'(a'-1)\sigma_{ci}'{}^{(1-a')}}$$

$$h = \frac{s^{*\,1-a} - \Gamma^{*1-a}}{m_b^*(a-1)}$$

$$t = \frac{(m_{b1}\sigma_\rho + s_1\sigma_{ci1})^{1-a'} - (m_{b1}\sigma_L + s_1\sigma_{ci1})^{1-a'}}{m_{b1}(a'-1)\sigma_{ci1}{}^{1-a'}}$$

$$\sigma_L = \frac{\frac{\xi}{\sigma_{ci1}} - s_1}{\frac{m_{b1}}{\sigma_{ci1}}}$$

$$\xi = \left[(m_{b1}\sigma_\rho + \sigma_{ci1}s_1)^{1-a'} - m_{b1}(a'-1)\sigma_{ci1}{}^{1-a'} \ln\left(\frac{r_i + L_b}{\rho}\right) \right]^{\frac{1}{1-a'}}$$

$$\sigma_\rho = \frac{\Gamma^* - s^*}{\frac{m_b^*}{\sigma_{ci}^*}}$$

$$\Gamma^* = \left[s^{*1-a} - m_b^*(a-1)\ln\left(\frac{\rho}{r_i}\right) \right]^{\frac{1}{1-a}}$$

$$m_{b1} = m_b'(1 - \beta) \quad s_1 = s'(1 - \beta) \quad c_{ci1} = c_{ci}'(1 - \beta)$$

The derivation of equations of the category III is given in Appendix B.

Having determined the Equivalent Plastic Zone (EPZ) with respect to its category (categories I to III), the ultimate tunnel convergence can be obtained by:

$$\frac{u_{ri}^*}{r_i} = \frac{1}{2G}\left[M\sigma_{ci}\left(\frac{r_e^*}{r_i}\right)^{(1+N_\psi)} + \frac{1}{r_i^{(1+N\psi)}}\sigma_{ci}'(1-\nu)(2+a'm_b')\int_{r_i}^{r_e} r^{N_\psi - 1}\Gamma^{a'}dr \right] \quad (5\text{-}78)$$

$$\Gamma = \left[s'^{1-a'} - m_b{}'(a'-1)\ln\left(\frac{r}{r_i}\right) \right]^{\frac{1}{1-a'}}$$

$$M = \frac{1}{2}\left[\left(\frac{m_b}{4}\right)^2 + m_b\frac{P_o}{\sigma_{ci}} + s \right]^{\frac{1}{2}} - \frac{m_b}{8}$$

5.16 Practical application of the proposed elasto-plastic solution

The following examples, posed by Hoek & Brown (1980) and Carranza- Torres (2004), are intended to illustrate the practical application of the proposed approach and to compare the results of proposed model with those of Carranza-Torres's

solution.Two cases are considered, one for an unsupported tunnel, the other for a tunnel reinforced by grouted bolts, both for a rock mass of known properties outlined in the Table 5-2.

Calculated radial and tangential stresses are shown in Figure 5-15, indicating that the radius of plastic zone is 5.09 m. The maximum displacement of the tunnel surface is found to be 30.7 mm as illustrated in Figures 5-17 and 5-18. The Ground Reaction Curve, often being used in the rock-support interaction analysis, is depicted in Figure 5-18.

A comparion between the proposed elatso-plastic solution and that which developed by Carranza-Torres (2004), in terms of stresses and displacements around the tunnel, has been made here as highlighted in Figures 5-16 and 5-17. The plastic zone radius and radial surface displacement obtained by Carranza-Torres' solution are slightly higher that those calculated from proposed elasto-plastic model. The radius of plastiz zone and the tunnel surface displacement are obtained as 5.2 m and 34.5 mm respectively by Carranza-Torres' solution.

The effect of the grouted bolts can be best described with reference to Figure 5-19, Figure 5-20, and Figure 5-21. As can be seen from Figure 5-19, the additional radial stress can be attributed as previously presented in Figure 5-12. Also it can be observed that the radius of the plastic zone decreases from 5.09 m to 4.6 m while a convergence reduction by 20 % is recorded as referred to Figure 5-20.

Table 5-2 Input parameters used in the practical example

Rock mass properties		Grouted bolt specifications	
r_i (m)	2	λ	0.6
P_o (MPa)	15	d (mm)	32
E (GPa)	5.7	C_b (kN)	280
ν	0.3	S_T (m)	1.0
σ_{ci} (MPa)	30	S_L (m)	1.0
ψ	0	L_b (m)	3.0
m_b	1.7	ρ (m)	3.27
s	3.9e-3	β	0.121
m_b'	0.85	m_b*	0.953
s'	1.9e-3	σ_{ci}*	30.257
a	*0.5*	s*	2.129e-3
S	1		
σ_{ci}' (MPa)	27		
a'	*0.5*		
N_ψ	1		

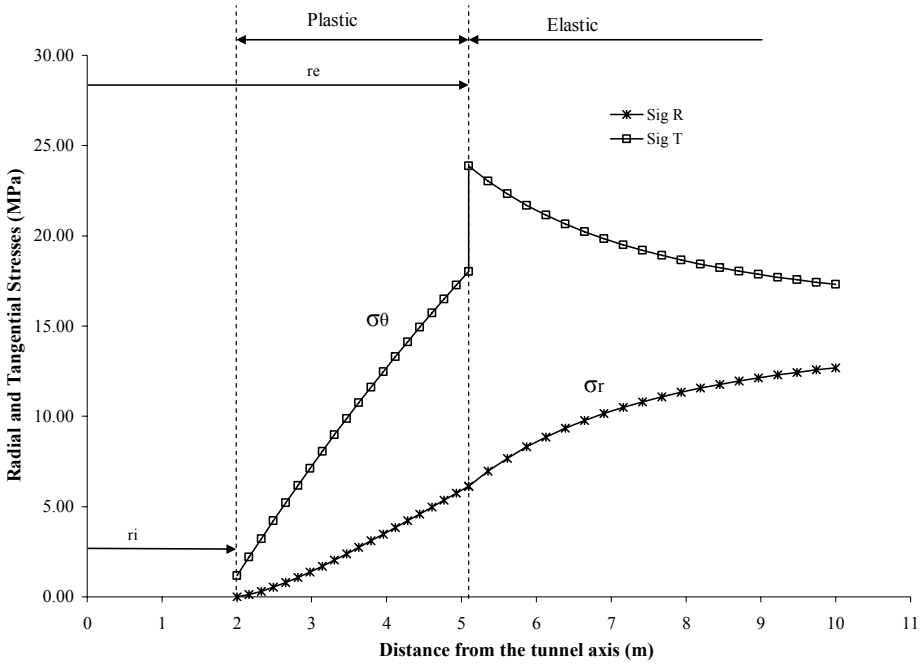

Figure 5-15 Stress field around the unsupported tunnel surface

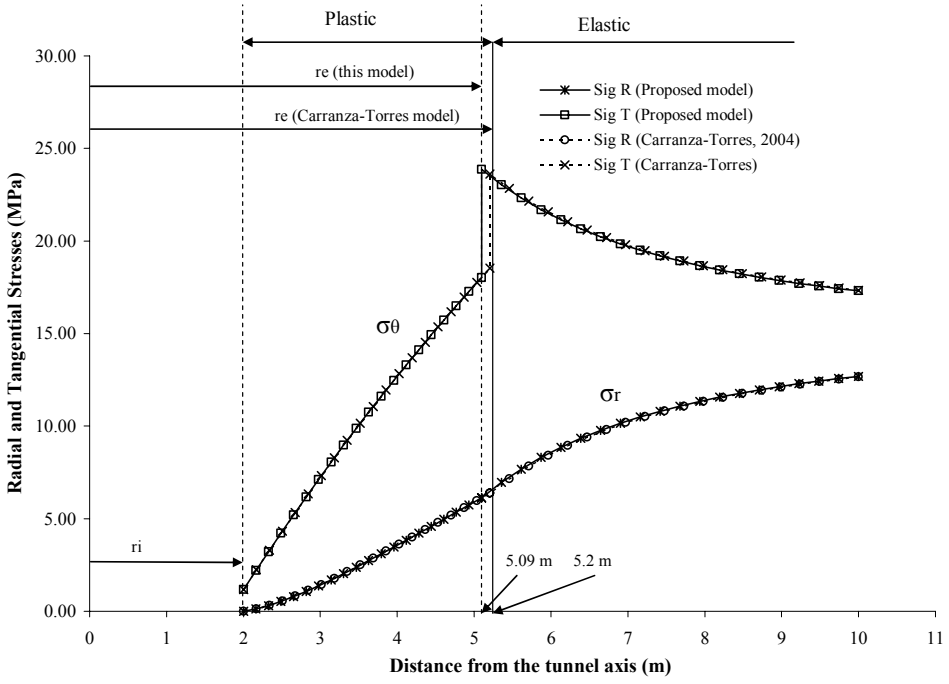

Figure 5-16 Distribution of the tangential and radial stresses obtained from the proposed elasto-plastic model and Carranza-Torres' solution (2004)

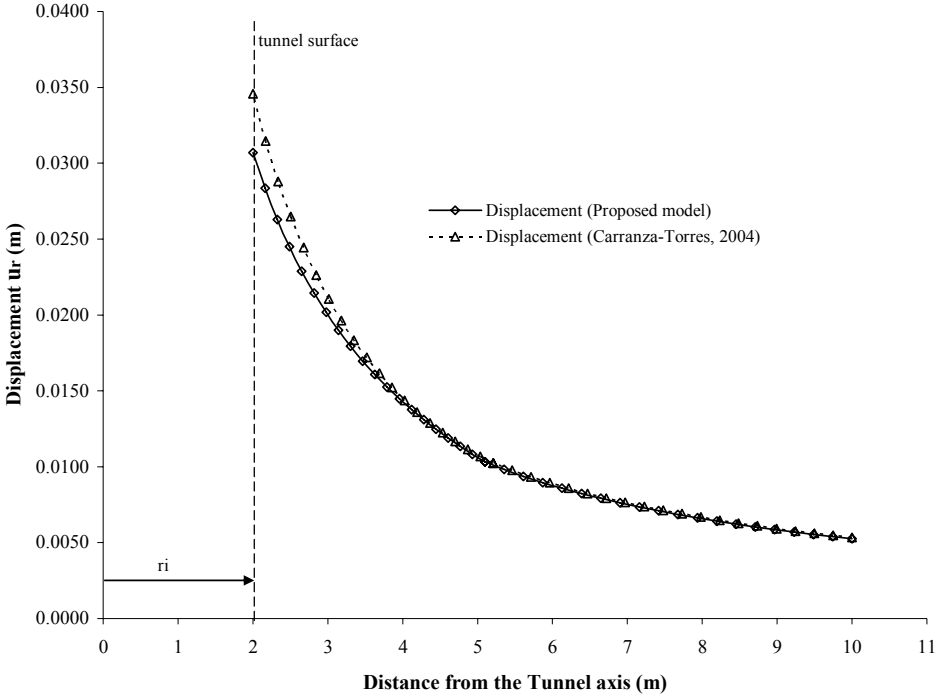

Figure 5-17 Displacement field obtained from the proposed elasto-plastic model and Carranza-Torres' solution (2004)

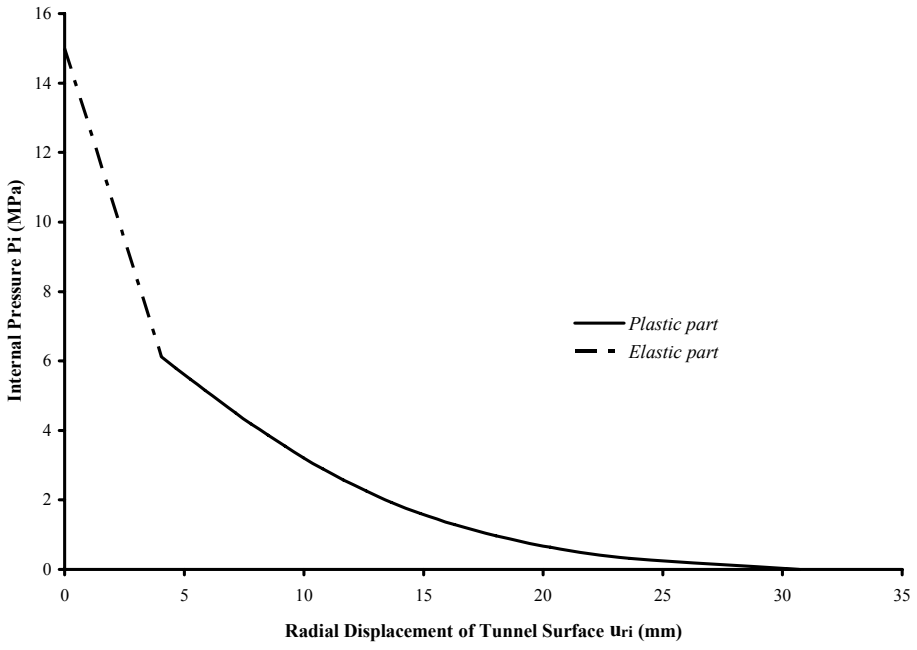

Figure 5-18 Ground Reaction Curve (GRC) of unsupported tunnel (natural ground) based on proposed elastic- plastic model

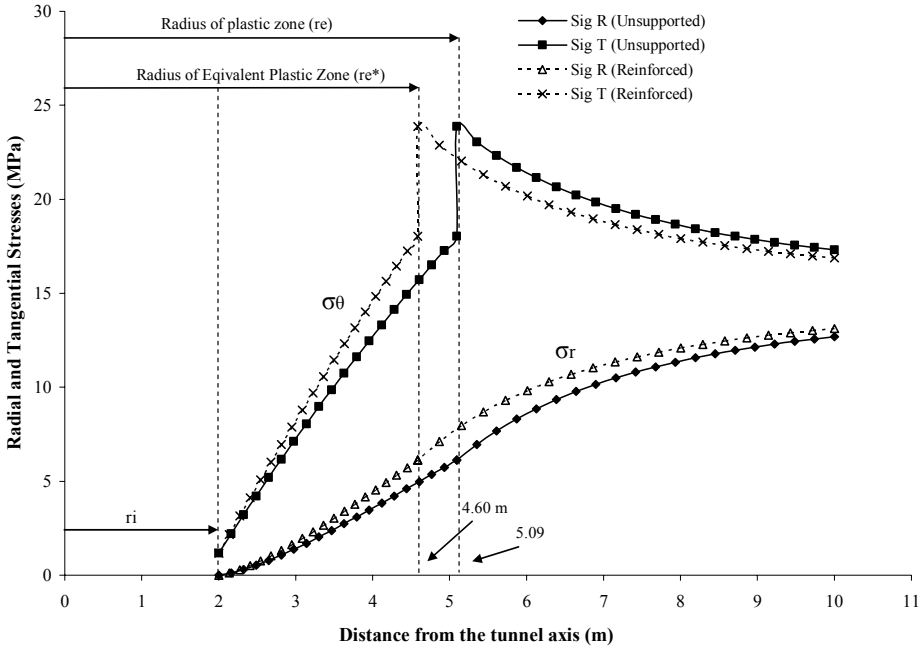

Figure 5-19 Radial and tangential stresses distribution near the reinforced tunnel

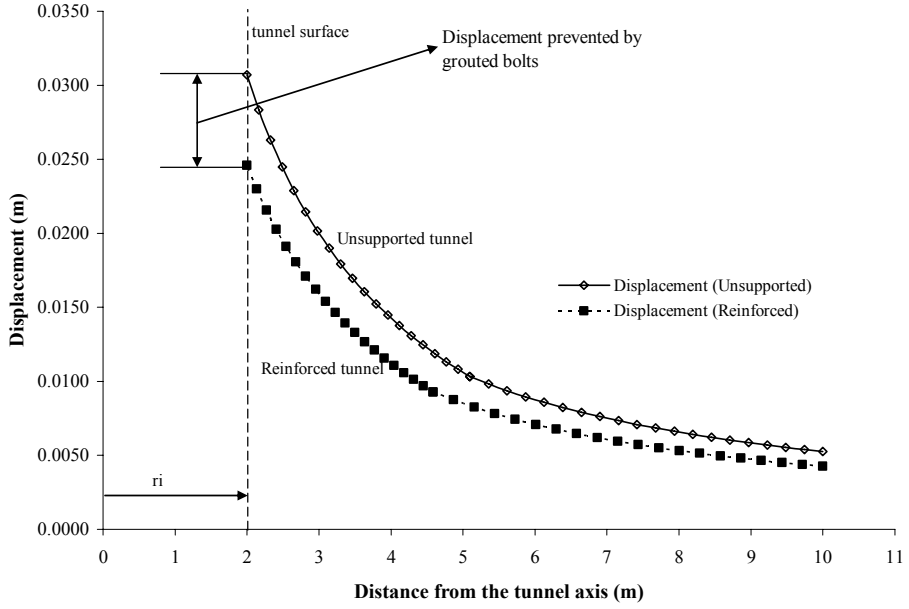

Figure 5-20 Comparison of the tunnel surface displacement for both unsupported and reinforced tunnel cases

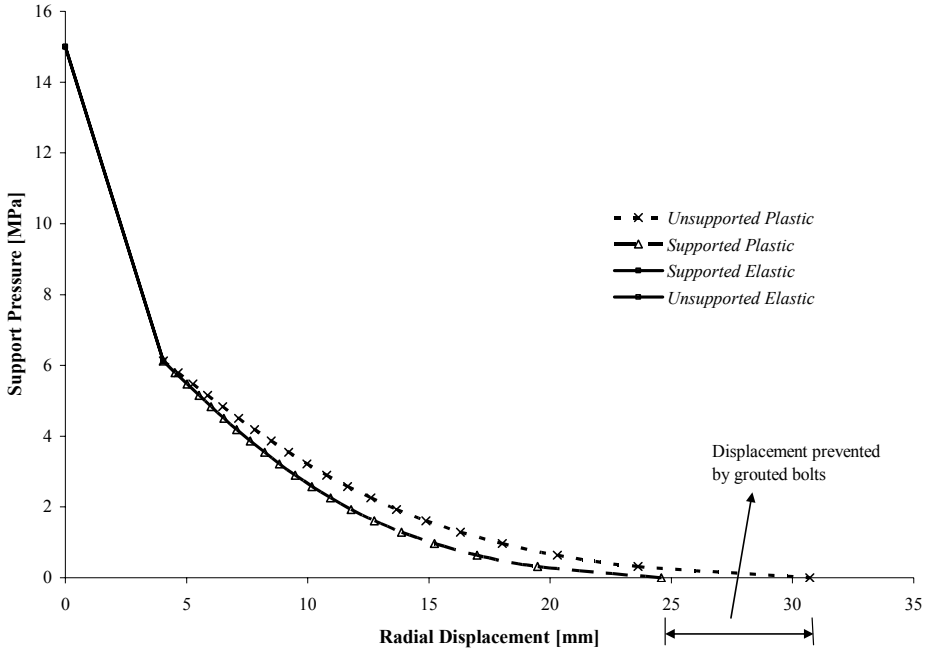

Figure 5-21 Ground Reaction Curve (GRC) with and without grouted bolts based on proposed elasto-plastic model

A helpful distinction to notice is that unlike the mechanical rock bolts which can be modelled through the Support Reaction Curve, the grouted bolts effect can be best investigated by reinforced ground reaction curve. This is due to the fact that in contrast to fully grouted bolts, mechanical bolts provide direct radial pressure against the tunnel wall, but do not become an integral part of the deformed rock mass. Consequently, their performance is appropriately represented by a support confinement curve with specific stiffness and its interaction with the original ground reaction curve. In brief, the effect of grouted bolts on ground improvement in terms of its elasto-plastic response is represented by GRC as shown in Figure 5-21 for this example.

5.17 Influence of grouted bolts on tunnel stability

The radial displacements at the tunnel wall are the most fundamental quantities required to evaluate the stability of a tunnel. In the field they are not only feasible to measure but are also generally reliable. The radial convergence of the reinforced opening wall can be predicted from Equation 5-78 provided that the magnitude of r_e^* has been determined for the respective categories I to III as specified in the section 5.15.

Figure 5-22 represents the variation of the predicted convergence of a case example for different bolt patterns obtained by the proposed analytical model.

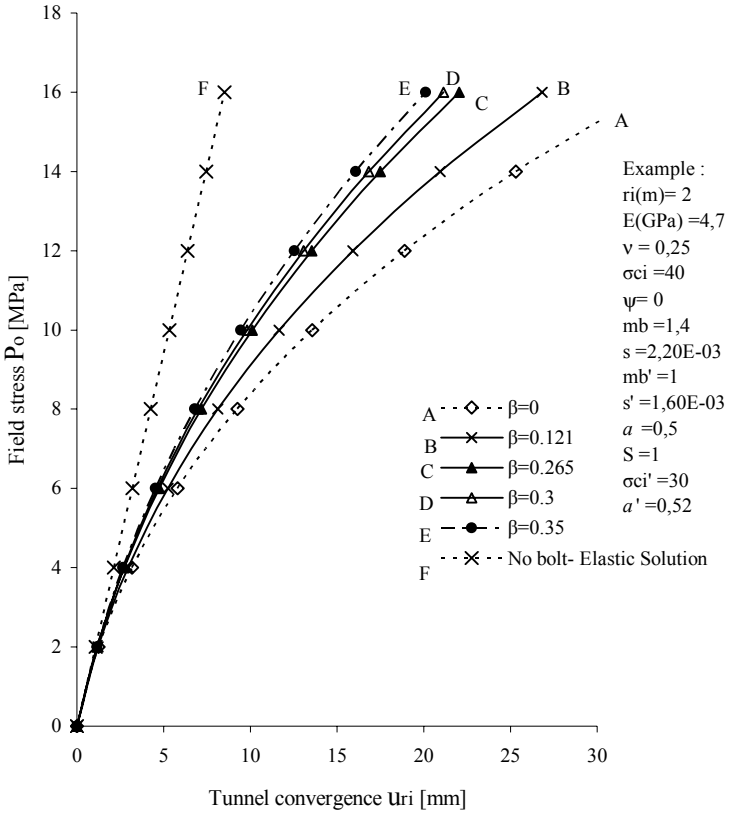

Figure 5-22 Influence of field stress on tunnel convergence for different magnitude of the bolt density parameter

The applied field stress ranges between 0 and 16 MPa. As the bolt density increases (i.e., increase in bolts diameter, decrease in bolts spacings or increase in friction factor between bolt and grout), the displacement of the reinforced tunnel surface (u_{ri}*) decreases and varies between the upper and lower bounds of the unsupported tunnel displacement (u_{ri}: dashed line A) and the response of tunnel in linear elastic rock (u_e: dashed line F). For reinforced tunnel, a sudden increase in convergence (shift to the right as shown in Figure 5-22) occurs for β =0.35-0.121 at Po > 12 MPa. This shift occurs when all bolts become completely embedded in the plastic zone, when Category III: $r_e^* > (r_i + L)$ happens. The same results have also been reported by Indraratna & Kaiser (1990b).

5.18 The effect of the bolt density on stresses and displacement field

The following example will depicts the influence of the bolt density on stresses and displacements field around a reinforced tunnel by grouted bolts. The input parameters of the example are given in the Table 5-3.

The predicted stress and displacement fields for this tunnel, reinforced with 32 mm grouted bolts and subjected to a far field stress of 15 MPa are presented in Figure 5-23 and Figure 5-24, respectively. Different bolt patterns ($\beta=0$ to $\beta=0.3$) are taken into account for comparison. The bolt density parameter can be increased as a consequence of an increase in bolts diameter, or a decrease in bolts spacings or an increase in friction factor between bolt and grout.

It can be seen from Figure 5-23 that as the bolt density parameter β increases, the radial and tangential stress fields approach those predicted for non-yielding, elastic rock, and the radius of equivalent plastic zone (r_e^*) approaches the tunnel radius. Further away from the tunnel, the stresses field approaches the far field stress.

Table 5-3 Input parameters used in this example

r_i(m)	2
Po (MPa)	15
E(GPa)	5.7
ν	0.3
σ_{ci} (MPa)	30
ψ	0
m_b	1.7
s	3.90E-03
m_b'	0.85
s'	1.90E-03
a	0.6
S_r	1
σci' (MPa)	25
a'	0.6
Nψ	1

For displacement field as shown in the Figure 5-24, as β increases, the displacement approaches the elastic solution. As distance from the tunnel surface increases, the effect of bolting diminishes rapidly and the far field conditions are

obtained. It is evident that the maximum decrease in strains and radial displacements occurs at the tunnel surface. Hence, the tunnel convergence can be well-considered as the most appropriate parameter for a displacement control design approach.

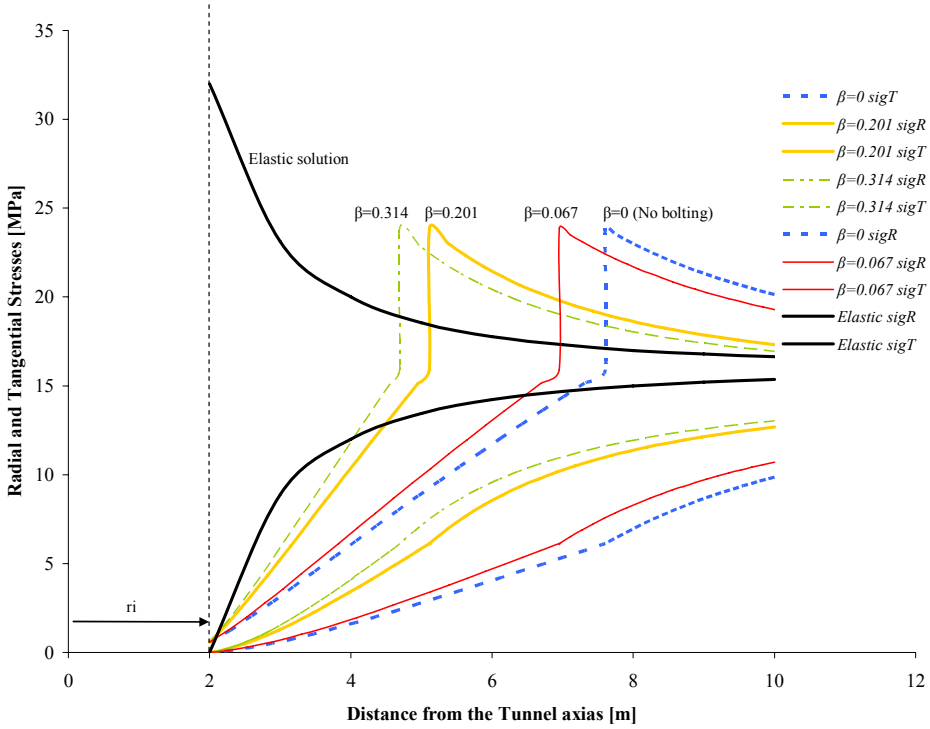

Figure 5-23 Stress field near the tunnel for different value of the bolt density parameter β

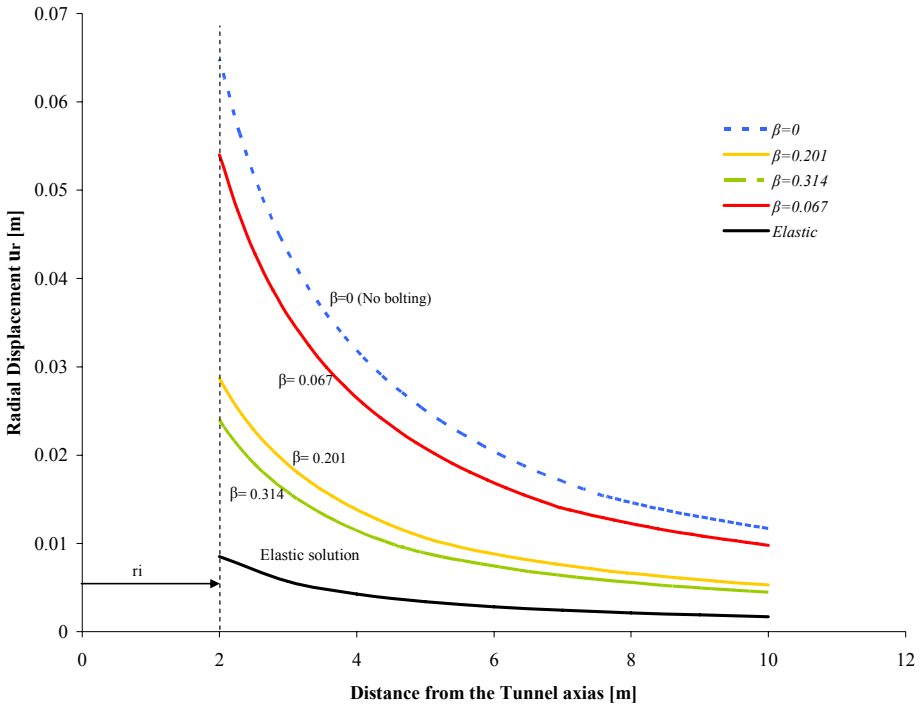

Figure 5-24 Displacement field near the tunnel for different value of the bolt density parameter β

5.19 Normalized convergence ratio

The total displacement (convergence) of a reinforced tunnel u_{ri}^* is a function of the rock mass properties, the field stress level and the reinforcement configuration. The convergence of a reinforced tunnel can be best evaluated by definition a dimensionless ratio u_{ri}^*/u_{ri} , where u_{ri}^* and u_{ri} are the total convergence of the reinforced and unsupported tunnel respectively at the same stress level. The total tunnel convergence includes both the elastic and plastic displacements. For a given field stress, u_{ri}^* is less than u_{ri} but it approaches u_{ri} when the bolt density (β) or the bolt length (L_b) tends to zero.

The normalized convergence ratio decreases as the bolt density increases. It obtains a minimum value when u_{ri}^* tends to u_e, the elastic portion of the total convergence. The latter condition may be approached at every intensive bolt densities such as $\beta > 0.30$, which is not only rare in practice but also is uneconomical. The normalized convergence ratio can be regarded as the main tool in design of the grouted bolts, since it is a sign of the reduction in convergence that can be achieved by a given bolting pattern.

An important characteristic of the convergence ratio is that it is insensitive to moderate changes of the deformation and strength parameters (Indraratna & Kaiser, 1990b). For instance, a change in Young's modulus affects both u_{ri}^* and u_{ri} equally,

hence the ratio u_{ri}^{*}/u_{ri} remains unchanged. For this reason, the normalized convergence ratio makes its use in design even more reliable, since the variation of in-situ geotechnical parameters can be tolerated without any significant error.

5.19.1 Normalized convergence ratio as a design tool

The normalized convergence ratio u_{ri}^{*}/u_{ri} is relatively insensitive to moderate change of the fundamental similitude parameters (m_b, s, σci, E, ν) for a given reinforcement configuration (β, L_b).

Figure 5-25 depicts the predicted results of analytical model for an example with various bolt pattern where $L_b / r_i = 1$ at applied field stress levels between 2 MPa and 16 MPa. The obtained normalized convergence ratio u_{ri}^{*}/u_{ri} is plotted for these stress levels and five bolt density parameters (β). u_{ri}^{*} and u_{ri} are the total convergence of the reinforced and unsupported tunnel, respectively. It is, therefore, believed that the relationship illustrated in Figure 5-25 for a given bolt length may be used for design purposes.

For instance, if a tunnel of 4 m diameter is excavated in a field stress of 10 MPa (i.e., 400 to 450 m deep) and reinforced with 2 m long grouted bolts ($Lb / r_i = 1$), the tunnel convergence (wall displacements) would be reduced by 33 % for a bolt density β of 0.265. This could be achieved by installing 45 mm shaped rebars (like self drilling anchors MAI-bolts $\lambda = 0.6$) with a spacing of 0.8m x 0.8m.

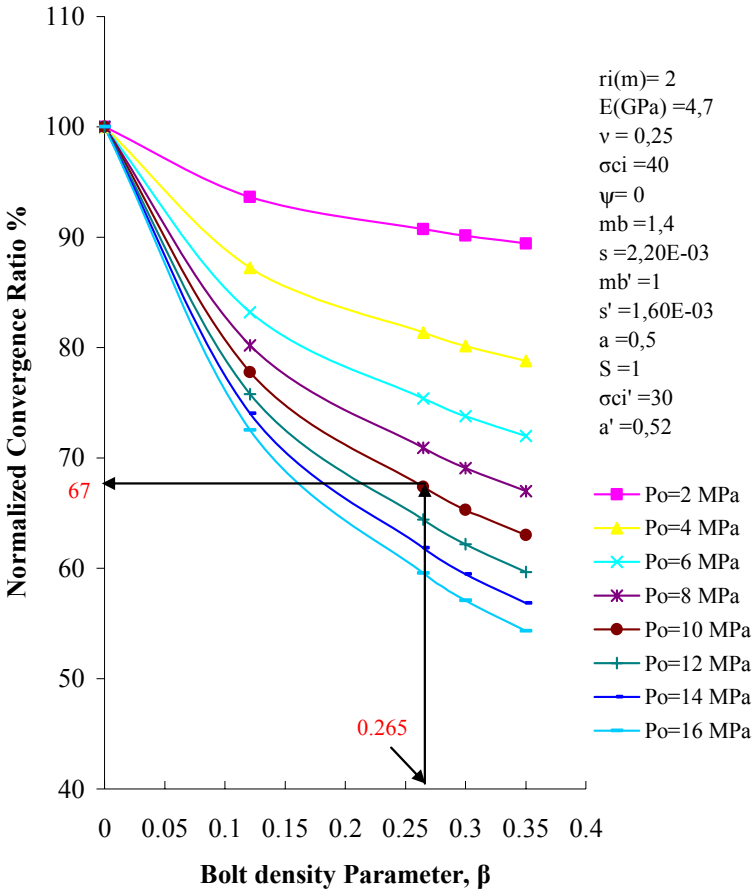

Figure 5-25 Variation of tunnel convergence with bolt density parameter for 2 m long grouted bolt

5.20 Influence of bolt length on tunnel convergence

In order to investigate the influence of the bolt length on tunnel convergence, a parametric study on two identical tunnels with similar diameter of 2 m, excavated in fair (GSI= 50) and poor rock mass (GSI=35), are considered.

The tunnel in fair rock mass (Case A) is to be investigated for two bolts configurations of 1.5 m (L_b / r_i =0.75) and 3 m (L_b / r_i =1.5) while the tunnel in poor rock mass (Case B) is assessed for bolts of 1.8 m (L_b / r_i =0.9) and 4 m (L_b / r_i =2). The rock mass properties, used in this parametric study, are outlined in the Table 5-4. Technically, the installation of the long bolts in a small diameter opening can be practical using bolt couplings, which join several short bolts together so that the required bolt length is achived.

Five different configurations of bolting have been examined for both Case A and Case B as below:

For Case A: β = 0.054, β = 0.121, β =0.20, β =0.265, β =0.35

For Case B: β = 0.121, β = 0.20, β =0.22, β =0.283, β =0.35

In Case A, the results of elasto-plastic analytical solution indicate that the formation of excessive yielding is impossible regardless of the intensity of the field stress. For bolts of 1.5 m ($L_b / r_i = 0.75$), the minimum and major yielding occurs at the field stresses of 2 to 10 MPa and 12 to 14 MPa respectively whereas employing bolts of 3 m ($L_b / r_i = 1.5$) prevents the formation of the major and excessive yielding irrespective of the field stress magnitude.

Table 5-4 Rock mass properties used in the parametric study on influence of grouted bolt length on tunnel convergence, key : ψ=0°

	Fair rock mass Case A	*Poor rock mass Case B*
GSI	50	35
ri(m)	2	2
Po (MPa)	14	8
E(Gpa)	7	2.1
v	0.25	0.25
σ_{ci}	50	25
ψ	0	0
m_b	2.515	1
s	3.86E-03	7.30E-03
m_b'	1.886	1
s'	2.89E-03	7.30E-03
a	0.5	0.52
S_r	1	1
σ_{ci}'	37.5	25
a'	0.52	0.52
$N\psi$	1.0	1.0

The normalized convergence ratio against bolt density parameter for 1.5 m and 3 m long bolts in a stress field ranging between 2 and 14 MPa for Case A is depicted in the Figure 5-26. As can be seen, it can be observed that the differences between convergence reductions attained by both 1.5 m and 3 m bolts are more or less negligible. In this condition, the bolt length does not have a considerable effect on convergence; rather the bolt density dominantly decreases the convergence. It can be ascribed to the fact that the bolt lengths are sufficient in this condition. It can also be inferred from Figure 5-26 that the shorter bolts (1.5 m) reduce the

convergence between a minimum of 3 to a maximum of 26 % whereas a convergence reduction of 3 to 29 % is achieved for longer bolts (3 m).

The reduction in total convergences attained is quite similar for both short and long bolts, because the plastic zone is enclosed within the reinforced zone ($r_e^* < r_i + L_b$).

In Case B, the results of elasto-plastic solution reveals that for bolts of 1.8 m ($L_b / r_i = 0.9$), the minimum yielding occurs at the stress field between 2 to 4 MPa whereas the major and excessive yielding take place at the field stress of 6-8 MPa and 10-14 MPa, respectively. On the other hand, in the case of use of bolts of 4 m long ($L_b / r_i = 2$) the minimum and major yielding have happened at the stress field of 2-10 and 12-14 MPa, respectively. It can be understood that using longer bolts in a given identical rock mass properties can prevent the excessive yielding.

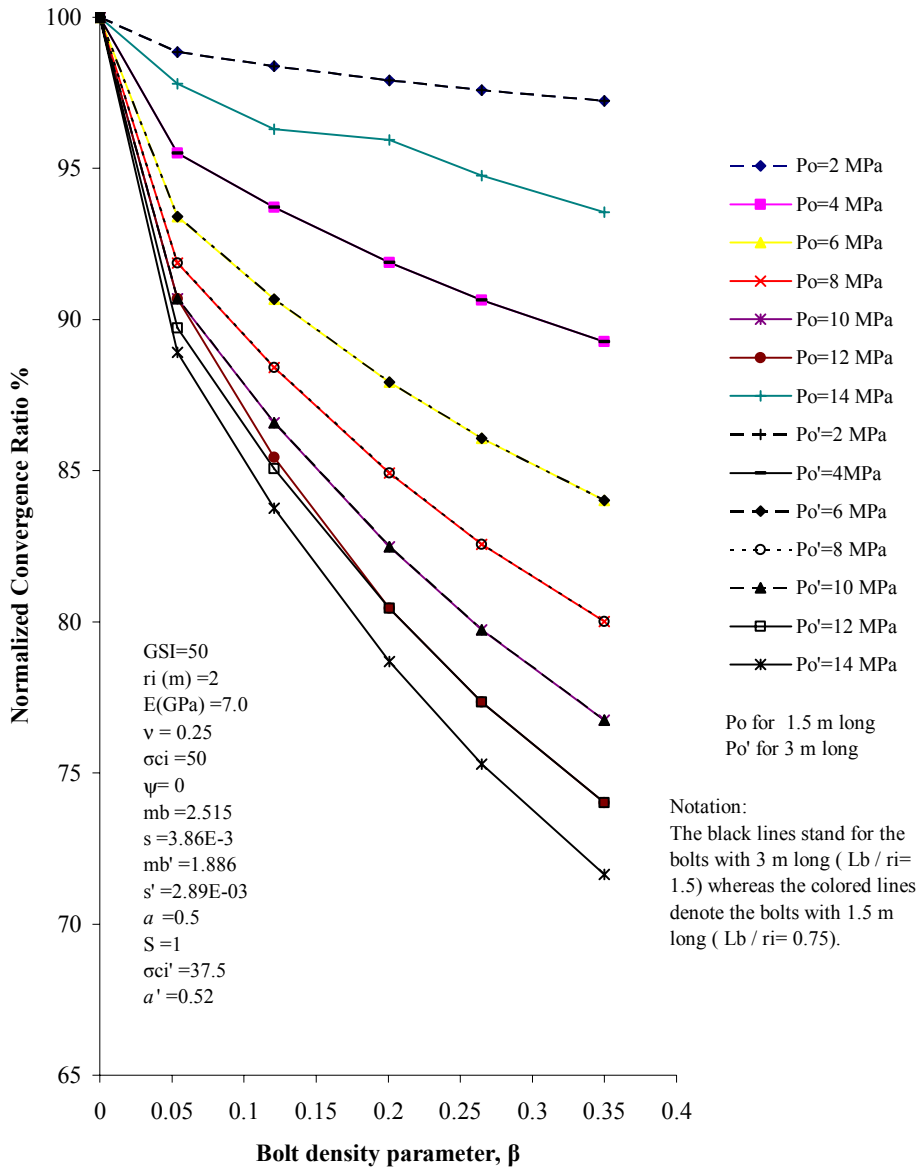

Figure 5-26 Variation of the tunnel convergence with bolt density parameter for grouted bolts of 1.5 and 3m (Case A)

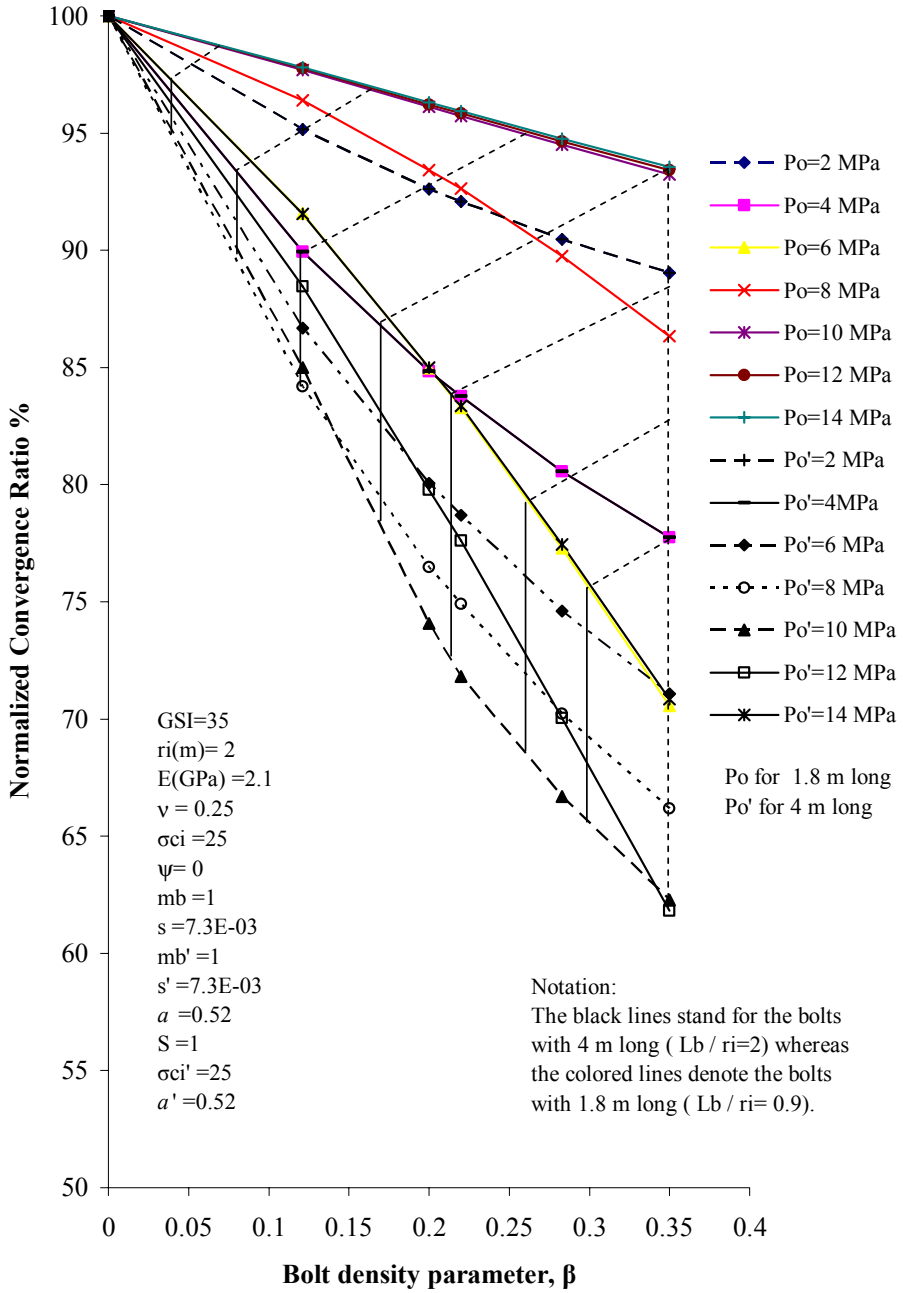

Figure 5-27 Variation of the tunnel convergence with bolt density parameter for grouted bolts of 1.8 and 4m (Case B)

Figure 5-27 summarizes the normalized convergence ratio against bolt density parameter for 1.8 m and 4 m long bolts in a stress field ranging between 2 and 14 MPa for Case B. With reference to Figure 5-27, the convergence reductions attained by bolts of 4 m long ($L_b / r_i = 2$) are considerably more than those achieved by bolts of 1.8 m long ($L_b / r_i = 0.9$), particularly at high bolt densities. The convergence reduction region of the shorter bolts is enclosed between the

diagonally shaded lines and the additional convergence reduction achieved by longer bolts is identified by vertically shaded lines in Figure 5-27. It can also be understood that the shorter bolts (1.8 m) reduce the convergence between a minimum of 7 to a maximum of 30 % whereas a convergence reduction of 10 to 38 % is achieved for longer bolts (4 m).

At relatively low bolt densities ($\beta < 0.15$), the reduction in total convergence is less pronounced for any given bolt length, because the magnitude of equivalent strength parameters decrease rapidly with reduction of bolt density parameter β. For instance, at β= 0.10, a convergence reduction of 2 % to 7 % is predicted for 1.8 m bolts whereas the installation of 4 m bolts curtails tunnel displacements of 3 to 12 %. Hence, the virtue of increasing the bolt length is less significant at low bolt densities where yielding is considerable.

In view of the fact that the higher bolt densities of 0.5 to 0.6 are both impractical and uneconomical to apply, where high bolt densities (β =0.25 to 0.30) are required (poor to very poor rock mass), the effective convergence reductions can only be attained by increasing the bolt lengths apart from application of high bolt denisty.

The reduction in total convergence attained is less pronounced for short bolts, because the excessive yielding condition becomes increasingly predominant as the bolt length decreases, particularly at relatively high field stresses. In other words, the effect of bolt length increase on the tunnel convergence is particularly emphasized if the extent of the plastic zone becomes enclosed within the reinforced zone ($r_e^* < r_i + L_b$). For example, at β = 0.35 and at P_o= 12 MPa, a decease in convergence from 52 mm to 32 mm (36 % reduction) can be achieved by bolts of 4 m long, because the plastic zone has not propagated beyond the reinforced zone at this stress level. However, if 1.8 m bolts are installed at the same field stress of 12 MPa, the plastic zone extends beyond the reinforced zone generating a much higher tunnel convergence of 49 mm (i.e., only 5.8 % convergence reduction).

The influence of bolt length on tunnel convergence decreases significantly if the plastic zone has propagated much beyond the reinforced zone ($r_e^* > r_i + L_b$). To illustrate, for β = 0.121 and at a field stress of 14 MPa, the convergence reductions associated with 4 m and 1.8 m bolts are 8.5 % and 2 % respectively, indicating a less effect of increasing the bolt length. In such situations, increasing the bolt density together with bolt length is more effective.

5.21 Use of displacement control (convergence reduction) approach for design

The following example enlightens the use of the displacement control (convergence reduction) approach for design of grouted bolts. Consider a tunnel of 3 m radius excavated at a depth of 150 m in a relatively weak sedimentary rock mass with the representative material properties outlined in the Table 5-5.

Using proposed elasto-plastic solution, the predicted convergence of the unsupported tunnel is determined as 40.7 mm with a plastic zone radius of 8.9 m. Following installation of grouted bolts of 6 m long (λ = 0.6 and diameter 32 mm)

with bolt density β = 0.08, a 20 % reduction in extent of plastic zone and an approximate 25.3 % reduction in tunnel convergence can be achieved. However, the application of a greater bolt density (β = 0.181) results in the reduction of plastic zone extension by 26 % and the tunnel convergence as much as 32 %.

Table 5-5 Rock mass properties used in example corresponding to displacement control approach

E(GPa)	2
v	0,25
σ_{ci}	25
ψ	0
mb	0,55
s	2,00E-04
m_b'	0,4
s'	1,70E-04
a	0,531
S_r	1
σ_{ci}'	20
r(m)	3
a'	0,56
$N\psi$	1,0

Table 5-6 The influence of bolt density parameter β on tunnel convergence

L_b (m)	$S_T \cdot S_L$	S_T / L_b	S_L / L_b	β	% Reduction of convergence
		Unsupported		0	0
3	1,5 * 1,5	0,5	0,5	0,08	16
3	1,2 * 1,5	0,4	0,5	0,101	17
3	1,0 * 1,2	0,33	0,4	0,151	18
3	0,8 * 0,8	0,26	0,26	0,283	21
L_b (m)	$S_T \cdot S_L$	S_T / L_b	S_L / L_b	β	% Reduction of convergence
		Unsupported		0	0
6	1,5 * 1,5	0,25	0,25	0,08	25
6	1,2 * 1,5	0,2	0,25	0,101	27
6	1,0 * 1,2	0,16	0,2	0,151	30
6	0,8 * 0,8	0,13	0,13	0,283	40

With reference to Table 5-6, it can be implied that an increase only in either bolt density or bolt length will not always guarantee the appropriate amount of the convergence reduction. To illustrate, if the desired convergence reduction being 30 %, the increase of bolt density up to 0.28 will also be insufficient for short bolts (3 m long) whereas if the long bolts (6 m long) are applied the convergence of 30 % will be easily realized even in less bolt density of 0.151.

The differences between predictable convergence reductions (30 % - 40 %) for bolts of 6 m long is far more considerable than those (18 % - 21 %) from bolts of 3 m long for the same given bolt densities (0.15- 0.28). Therefore, it can be understood that in poor rock mass a proportionate increase in both bolt length and bolt density must be taken into account. Note that if in such rock mass the bolting design focuses only on bolt density rather than bolt length or vice versa, the final convergence reduction will not be satisfactory.

Similarly, Orate (2003) introduced the following criterion that prevents the plastic zone radius further than the anchor length of the bolt:

$$r_e^* < (r_i + a \cdot L_b) \text{ , where a =0.5 – 0.75}$$

It is worthwhile to note that the installation of long bolts in a small tunnel is achived by using bolt couplings. For example, in a tunnel with a diameter of of 5 m, the installation of bolts of 9 m long is possible and practical provided that the

total length of the bolt is divided into three distinct parts and then joined with 3 cuplings. The MAI-bolts introduced by Atlas Copco (2004) are the example of this type of bolts.

5.22 Comparison with empirical design methods

The geomechanical classification or RMR system of Bieniawski (1973, 1989) has been acknowledged to be applicable to fully grouted rock bolts in all type of rock masses. The design tables and recommendations proposed by Bieniawski are intended for tunnels in the order of 10 m width, excavated by the drill and blast method at depths of less than 1000 m and reinforced by 20 mm diameter grouted bolts. Supplemental support by shotcrete, wire mesh and steel sets are also suggested for poorer ground.

With the help of the results of the proposed elasto-plastic solution, it is possible to build an informative table, like that of Bieniawski (1973, 1989), for any rock mass condition and tunnel size, provided that the rock mass class is accurately defined and strength parameters of rock mass are estimated accurately. To illustrate, the recommended bolt configurations for an arbitrary tunnel of 5 m span which is excavated in the far filed stress of 15 MPa are represented in Table 5-7.

It should be noted that only a change in bolt length for displacement control in the poor rock mass does not agree with the findings from this study. For example, a bolt density parameter (β) more than doubles is needed as the spacing is decreased from 1.5 m to 1.0 m when the quality of rock mass diminishes from fair to poor. Hence, a further reduction of the bolt spacing for the poorest rock class would provide a sufficiently high magnitude for β to curtail displacements more effectively than by increasing the bolt length. This is supported by Laubscher (1977) who proposed a bolt spacing less than 0.75 m for poor ground at RMR < 30. This bolt spacing corresponds to a β values more than even 0.236 for $\lambda = 0.6$, $d = 32$ *mm*, and seems to be in good agreement with the densities proposed earlier for effective convergence reduction.

Table 5-7 Recommended grouted bolt densities for a reinforced tunnel of 2.5 m radius for different rock classes (field stress = 15 MPa, grouted bolt diameter = 32 mm), key: the use of bolt couplings for installation of long bolts in small diameter tunnel must be applied.

GSI	Definition	L_b (m)	S_T and S_L (m) squred pattern assumed	β / λ	β at λ= 0.6	Possible Yielding category
81-100	Very good	Generally no support required			0.000	No Yielding
61-80	Good	2 to 3	2.0-2.5	0.063-0.040	0.038-0.024	Minimal
41-60	Fair	3 to 5	1.5-2.0	0.112-0.063	0.067-0.038	Minimal-Major
31-40	Relatively Poor	5 to 6	1.0-1.25	0.251-0.112	0.151-0.067	Major
21-30	Poor	≥ 6	1.0	0.251	0.151	Major-Excessive
< 20	Very poor	≥ 6	0.8	0.393	0.236	Excessive

The influence of bolt- ground interaction as a very important design parameter is also ignored in the empirical design method. Having introduced the analytical elasto-plastic solution, it can be concluded that the RMR system may not provide a sufficiently sensitive guide to properly design the grouted bolts in relatively poor to very poor rock mass. For classes of rock mass RMR < 40, a rational design method for grouted bolts should be based on the proposed analytical approach, whish provides a sound basis for effective tunnel convergence control.

5.23 Correlation between Support pressure and rock-bolt density parameter

In order to relate the analytical method to empirical design approach and to obtain an optimum rock-bolting pattern for any shape of opening, the empirically estimated support pressure is incorporated with the elasto-plastic solution of grouted bolt design. Due to the fact that the elasto-plastic analytical solution is constrained only for a circular tunnel, the new expression makes it possible to delineate bolting configuration regardless of tunnel shape.

As previously discussed, the support pressure (rock-load) can be expressed as:

$$P = \frac{100 - \left[(1 - \frac{D}{2})\sqrt{\frac{\sigma_{cr}}{100}} GSI\right]}{100} CS\gamma B \qquad (4\text{-}7)$$

If the effective area of each bolt is defined as the area of longitudinal and transversal spacing (Figure 5-7), the following limiting equilibrium equation can therefore be written taking into consideration the bolt yield capacity:

$$C_b = P \cdot S_T \cdot S_L \tag{5-79}$$

Taking into account the factor of safety (FOS), which is defind as the resistant force to the imposing force:

$$FOS = \frac{C_b}{P \cdot S_t \cdot S_l} \tag{5-80}$$

Substituting Equation 5-79 into Equation 5-56, the relationship between rock bolt density (β) and support pressure (P) will be:

$$\beta = \frac{P\pi d\lambda r_i}{C_b} \quad \text{or} \quad \beta = \frac{P\pi d\lambda B}{2C_b} \tag{5-81}$$

where, P= support pressure, d= bolt diameter, λ=friction factor for bolt-ground interaction relates the mobilized shear stress acting on the grouted bolt to the stress acting normal to the bolt, B= tunnel span ~ $2r_i$, C_b= yield load capacity of bolt.

The main application of the Equation 5-81 is that of determining the bolt density parameter accounting of the support pressure. At the same time, the already determined β can be used as a the first estimate of bolt densities in the elasto-plastic analysis so as to determine the Equivalent Plastic Zone (EPZ) and the displacement of the reinforced tunnel with respect to appropriate yielding category (Section 5.15) in conjunction with Equation 5-78.

The most important usage of the equation 5-81 falls in the fact that the first approximate of β for a tunnel can be obtained through a real characterization of rock mass because two significant indicators of rock mass characterization have been incorporated, i.e. the support pressure function, to a large degree, relies on the rock mass quality (GSI). Note that in the poor and very poor rock mass application (GSI < *27*) the use of Modified-GSI, put forward in Chapter 3, is recommended.

For a square-shaped of bolting pattern the bolts spacing is then calculated by:

$$S_s = \sqrt{\frac{\pi d\lambda r_i}{\beta}} \tag{5-82}$$

The variation of the bolt density parameter with the support pressure for a tunnel with the span of 5 m reinforced with the different types of grouted rock-bolts (MAI- bolts, Atlas Copco 2004) is represented in the Figure 5-28, which indicates that with increasing support pressure, more severe bolt density is required to satisfy the minimum stability condition of opening. The specifications of different grouted bolts (MAI-bolts) used in this study is outlined in Table 5-8.

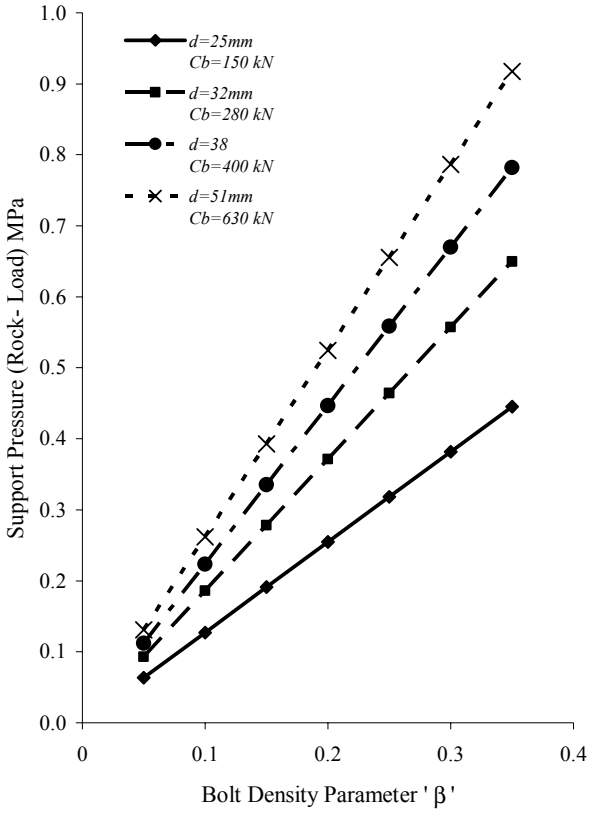

Figure 5-28 Variation of the bolt density parameter with support pressure (rock load) for different types of grouted bolts in terms of their yield capacity and diameter

Table 5-8 Engineering specifications of grouted bolts (MAI-bolts or Self Drilling Anchor) used in this study (after Atlas Copco, 2004)

Type	R25N	R32S	R38N	R51N
Outside diameter (mm)	25	32	38	51
Average internal diameter (mm)	14	15	19	33
Effective external diameter (mm)	22.5	29.1	35.7	47.8
Aver. eff. cross sectional area (mm2)	244	488	717	939
Ultimate load capacity (kN)	20	360	500	800
Yield load capacity (kN)	150	280	400	630
Average tensile strength Rm (N/mm2)	805	740	700	840
Weight (kg)	2.3	4.1	6	8.4
Steel grade	In accordance with EN 10083-1			

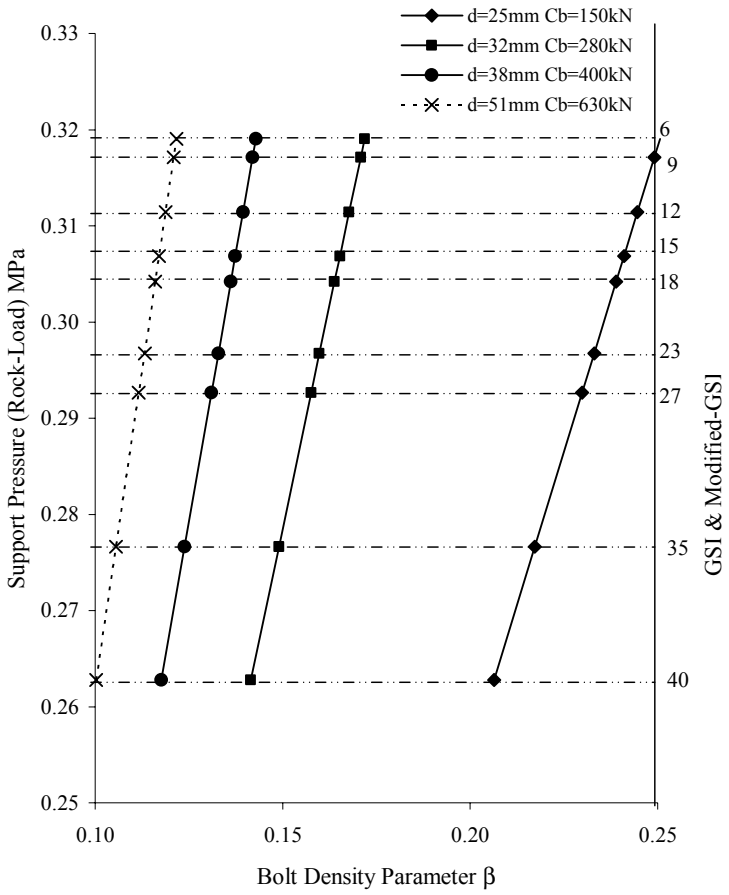

Figure 5-29 Correlation between the bolt density parameter and support pressure for a tunnel of 2.5 m radius excavated in relatively poor to very poor rock mass (GSI < 40) and undergoing a very high squeezing, $\frac{c_h}{\sigma_v} = 1.5$

Figure 5-29 illustrates the correlation of the bolt density parameter β and support pressure for a tunnel of 2.5m diameter which is excavated in relatively poor to very poor rock mass (GSI < 40). For the different ranges of support pressure provided at GSI < 40, the variations of bolt density β change between 0.10 and 0.25 depending on the types of applied grouted bolts.

With reference to Figure 5-29, it can be inferred that the appropriate choice of bolt density parameter in design, regardless of grouted bolt types, can lead to the same results for different support pressure magnitudes. To illustrate, for a support pressure of 0.296 MPa associated with Modified-GSI = 23, the primary stability of the tunnel can be achieved by installation of arbitrary pattern of grouted bolts of 25 mm, 32 mm, and 51 mm in diameters corresponding to bolt densities of 0.23, 0.16, and 0.11, respectively. It should be noted that the usage of the thicker and longer grouted bolts having higher yield capacity is preferably suggested in poor rock masses because the spacing of bolting less than 0.8 m is to a large degree impractical and uneconomical.

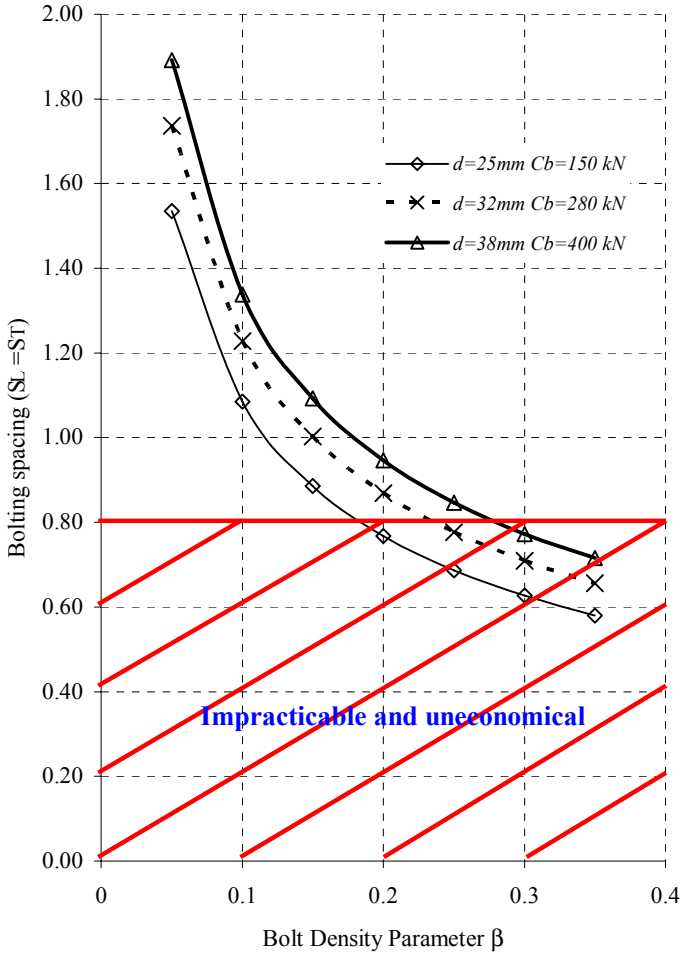

Figure 5-30 An informative sketch highlighting the variation of the bolt density parameter β with the square configuration of the bolting of a 2.5m width tunnel with respect to different bolt diameter. The hatched area denotes that the bolting pattern is not practical and economical.

The relationship between equal spacing pattern and rock-bolt density for a tunnel having diameter of 5m are illustrated in Figure 5-30. As can be seen, the more bolt density, the less spacing of bolting pattern. To illustrate, for bolt density of 0.18 mostly used for a tunnel in poor rock mass the stability of tunnel might be achieved by spacings of $1m \times 1m$ if the bolts having diameter of 38 mm are used whereas if the bolts with diameter of 25 mm are installed the spacing must be $80cm \times 80cm$. It should be kept in mind that minimum practical spacing is 0.8 m. The spacing less than 80 cm is, in turn, impracticable and uneconomical.

5.24 Summary of advantages of proposed elasto-plastic analytical model and its contribution to the grouted bolts design

The distinctions of the proposed elasto plastic model from others and backbone of the proposed model are presented herein. The followings are the specifications of developed elasto-plastic model:

Due to its simplicity, most elasto-plastic models, developed so far, used the Mohr – Coulomb or original Hoek-Brown failure criterion (Hoek & Brown, 1980a). The new elasto-plastic solution, on the other hand, satisfied the latest version of non-linear Hoek-Brown failure criterion (Hoek *et al*., 2002). Having been modified for several times, the new version of the Hoek-Brown failure criterion is applied in a wide range of rock mass quality from very poor to very good. Hence, the results of the proposed model are found to be more realistic.

Most of the existing elasto-plastic solutions for tunnel problems in Hoek-Brown media consider $a = 0.5$. This is not only due to historical reasons (the failure criterion was originally developed for intact rock), but also due to the mathematical difficulties of deriving neat, closed-form expressions for the general case in which $a \geq 0.5$. The proposed elasto-plastic solution for the axi-symmetrical problem of excavating a circular tunnel in generalized Hoek-Brown material supposes $a > 0.5$. In addition, this solution was based on the assumption that after the intact strength of the rock is exceeded, the material loses its strength, as dictated by a strength loss parameter (S_r).

Most of the elasto-plastic solutions developed until now turn out to be complicated in terms of mathematical formulations (For example: Carranza-Torres approach 1998, 2004). The proposed model, on the other hand, used the basic elasto-plasticity formulations. The applied method to obtain the expression for the radial displacements in the plastic zone was entirely different from that in some other models. Unlike the method used by Carranza-Torres (1998, 2004), the present method did not require any transformation technique. The differential equation of compatibility solved in this part was of the first order, whereas that in Carranza-Torres was of the second order. However, the resulting expressions for the radial displacements are also quite comparable.

A simple spreadsheet of proposed elasto-plastic model was prepared to assist the designer. The integral function revealed by results of solution of the plastic strain differential equation (compatibility equation) was calculated numerically and included in the spreadsheet to find the stresses and displacements point by point far away from opening surface.

The bolt density parameter could be related to support pressure to find the first estimation of the bolt density parameter. It made it possible to depict the bolting pattern for non-circular shape of openings. Since the magnitude of support pressure directly depended on rock mass quality, hence the obtained results were expected to be more realistic. Seeing that the Modified-GSI used for characterization of poor to very poor rock masses accounts for a main component of support pressure, therefore, it makes it possible to determine the magnitude of bolt density parameter

applicable to poor to very poor rock mass. In other words, the proposed elasto-plastic model would also be by far practical in such rock masses.

Not all of the elasto-plastic solutions used in rock bolt design have been validated by numerical modelling. Among them, for example, the elasto-plastic numerical solution of rock bolt design developed by Oreste (1995) was validated by numerical modelling. In the following chapter, the results of the proposed analytical solution will be compared with those of the numerical model ($FLAC^{2D}$).

The proposed elasto-plastic model was to some degree an improved model of Indraratna & Kaiser model (Indraratna & Kaiser 1990 a, b). Having been realized some limitations and constrains such as:

IV. Applicable to rock mass obeying the linear Mohr-Coulomb failure criterion
V. Residual strength parameters of rock mass is only applied for cohesion
VI. Erroneous calculation of plastic strain in elasto-plasticity formulations
VII. Lack of numerical validation
VIII. Deficiency in link between empirical design method (rock mass classification) and elasto-plastic analytical solution
IX. Limited application in circular tunnel

The proposed elasto-plastic model also overcame abovementioned deficiencies.

Unlike some other models which often solely focus on coupling effect of the rock bolt, grout and rock to model the rock- support interaction, in the developed elasto-plastic model, the use of equivalent material properties (equivalent strength parameters) was taken into consideration in such a manner that a reinforced zone, due to effect of grouted bolts, was created around the tunnel with improved Hoek-Brown strength parameters. Bolt density parameter and bolt- grout interface friction factor facilitate to know to what extent the Hoek-Brown strength parameters are increased and to define the force equilibrium equation for reinforced zone.

CHAPTER 6

NUMERICAL VERIFICATION OF THE PROPOSED ELASTO-PLASTIC SOLUTION

6.1 Introduction

There is advantage in being able to validate the results of analytical solution with those of numerical modelling. In this chapter, as a check on the analytical results and to ensure the validity of the proposed elasto-plastic analytical model, a series of numerical analyses are to be carried out using the Finite Difference Code (Fast Lagrangian of Continua "FLAC") and both results will be compared.

In order to verify the elastic-plastic analytical solutions for both unsupported and bolted tunnels, two series of numerical implementations are performed. The adopted geomechanical parameters used in the numerical analyses are the same of analytical solution outlined in Table 5-2.

6.2 Numerical model of unsupported tunnel

The validity of the proposed elasto-plastic model of Chapter 5 must be tested by numerical approach (FLAC codes). Therefore, it is appropriate that the stresses and displacements be determined for the case of a cylindrical tunnel in an infinite Hoek-Brown medium subjected to a hydrostatic field of in-situ stress.

The problem is based on the example used in Chapter 5 and the gemomechanical parameters of the rock mass are those given in the Table 5-2.The strength is assumed to reduce after failure initiates; this is simulated by assigning a different set of Hoek-Brown properties for material that has failed (broken material) versus material that has not failed (intact material).

This problem demonstrates the implementation of a FLAC constitutive model that has been modified with FISH. The Mohr-Coulomb failure surface is adjusted to approximate the Hoek-Brown failure surface. The FLAC codes of this example are, in details, given in the Appendix D.

A two-dimensional plane-strain FLAC model with the plane of analysis oriented normal to the axis of the opening is created for this problem. For this model, only a quarter of the problem needs to be analyzed because of the symmetry of the problem (quarter-symmetry). The model and boundary conditions are shown in

Figure 6-1. In FLAC analysis the area representing the problem is divided into finite-difference zones, as shown in Figure 6-2. A total of 14400 zones (120×120) are used in this grid. The model should be large enough to ignore the boundary effects. Therefore the boundaries are taken as 15 times of the tunnel radius from each side of the opening as shown in Figure 6-2. The in-situ stresses are applied to the top and right side boundaries.

To reach to an accurate final displacement of a predefined tunnel section with an enough distance from tunnel face (the 3-D effect of tunnel face can be vanished), an inner radial pressure equal to the in-situ stress is applied to the tunnel boundary surface and then gradually decreased step by step to simulate the tunnel face advancement from the related section. This gradual decrease in inner pressure is referred as the stress relaxation.

After nullifying the excavation area, nodal forces (fictitious inner pressure), which are equal to in-situ stress at the start of the modelling procedure, are applied. The nodal forces are decrease gradually until they reach zero. For this purpose, ten steps are chosen in the model. In the first step, the nodal forces are equivalent to the in-situ stresses and in the last step (the 10^{th} step) the nodal forces are zero. The zero nodal forces resemble the advancement state in which the tunnel face has advanced far enough from the pertinent tunnel section and therefore the tunnel face does not affect on the deformations at considered section. As nodal forces decrease at each step, more convergence and relaxation occur in the tunnel perimeter and this means that tunnel face is advancing.

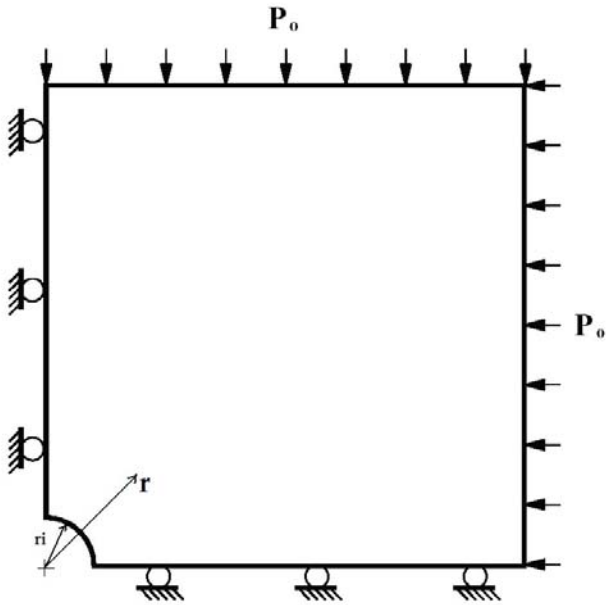

Figure 6-1 Model for FLAC analysis of a circular tunnel in an infinite Hoek- Brown medium (quarter symmetry model)

Figure 6-3 represents the radial and tangential stresses calculated by FLAC and analytical model for the quarter-symmetry model, thereby leading to reasonably comparable results. The displacement field of both analytical and numerical methods is demonstrated in Figure 6-4. It can be observed that there is a good agreement between the results of analytical and the FLAC models.

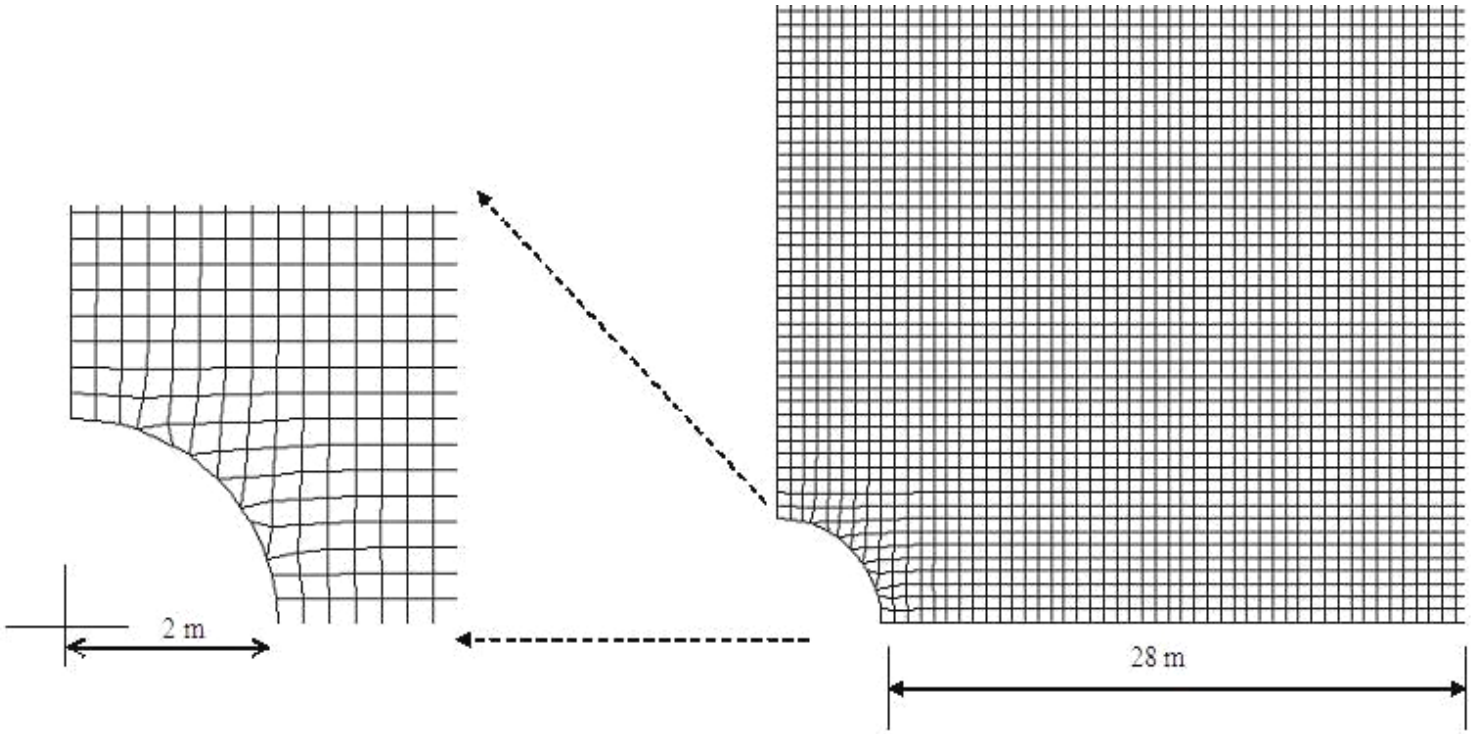

Figure 6-2 Quadratic Finite Difference Model adopted in the FLAC 2-D analysis with grid 120 * 120

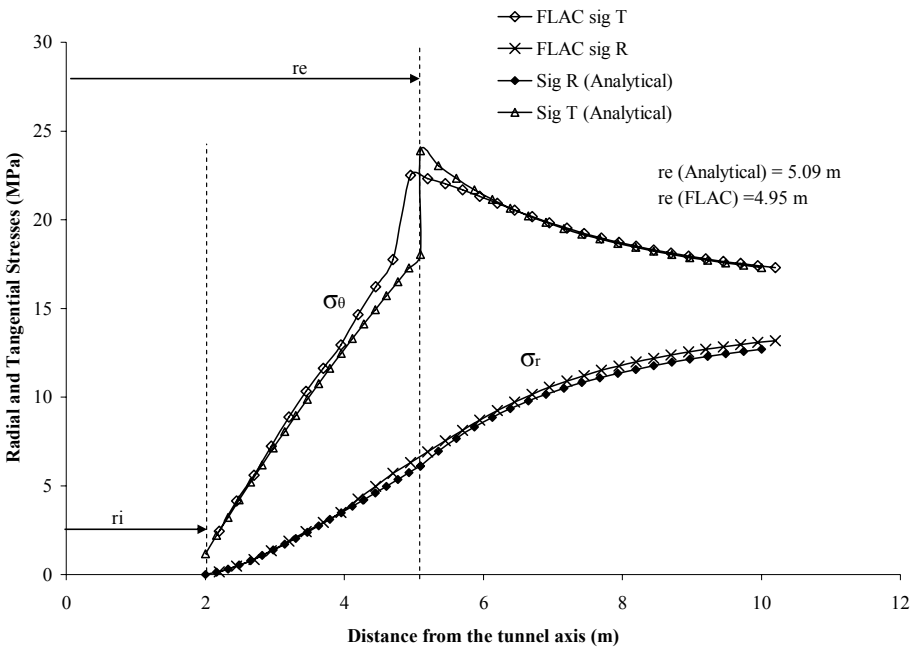

Figure 6-3 Tangential and radial stress filed result from the analytical and numerical methods

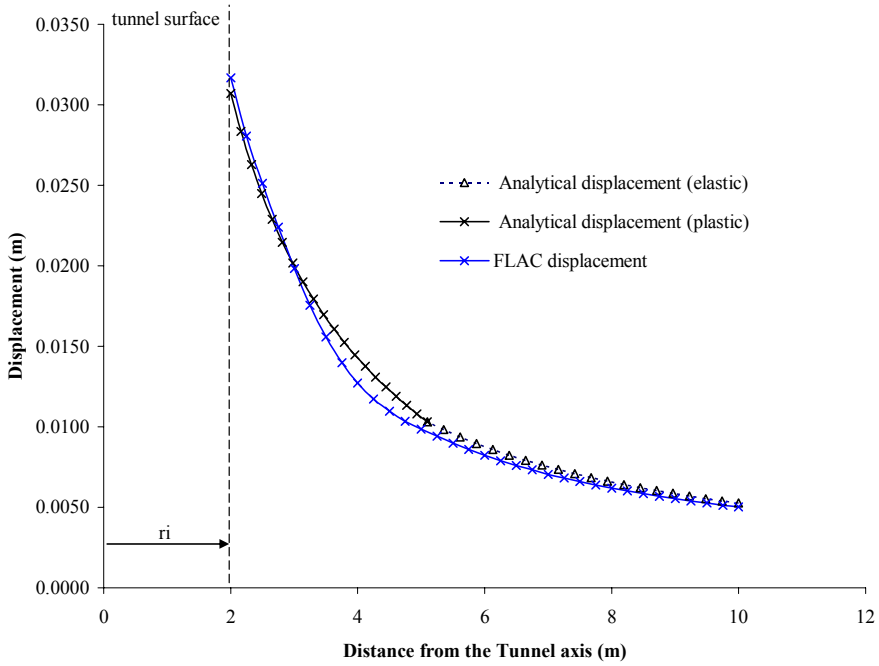

Figure 6-4 Displacement filed stems from the analytical and numerical methods

As can be seen from Figure 6-3, the tangential stress and the plastic zone radius of FLAC^{2D} model is slightly higher than those of proposed elasto-plastic model. This can be attributed to the fact that the FLAC^{2D} does not directly use the Hoek-Brown failure criterion. The FISH in FLAC^{2D} makes it possible to adapt the Mohr-Coulomb failure criterion to approximate the nonlinear failure surface for Hoek-Brown material as given in Appendix D. The same phenomenon can also be seen in the displacement distribution in plastic zone around the tunnel in Figure 6-4.

A significant result to be noted is that the displacements obtained from analytical solution vary considerably with the variation of the constant *'a'* of Hoek-Brown failure criterion. Unlike most of the existing elasto-plastic solutions for tunnel problems in Hoek-Brown media that consider $a = 0.5$, the proposed elasto-plastic solution adopts the value of (a) in accordance with rock mass quality (i.e., $a \geq 0.5$). The differences between the displacements filed near the tunnel are presented in the Figure 6-5. As the magnitude of (a) increases proportionally with decreasing rock mass quality, a drastic increases in tunnel wall displacement is evident.

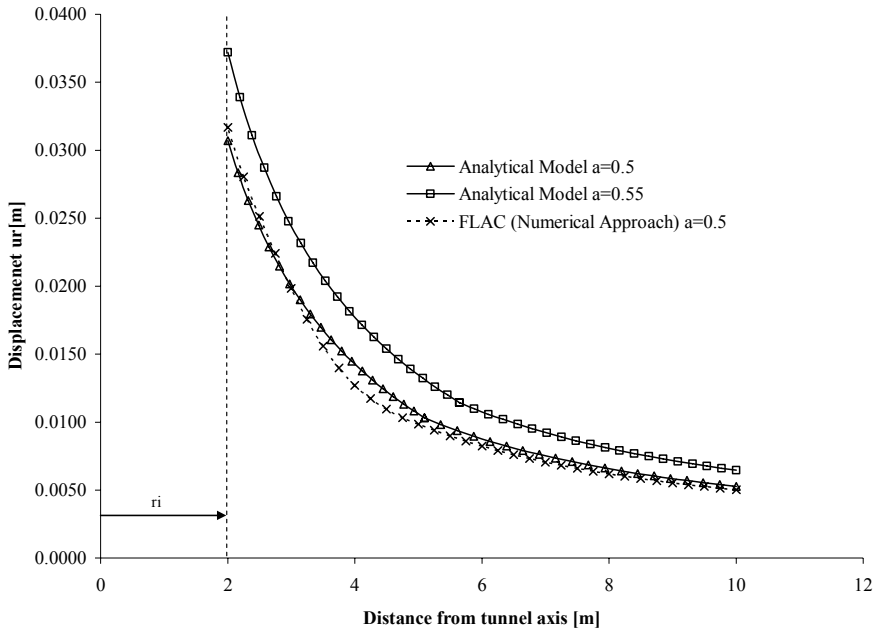

Figure 6-5 The variation of the displacements with different values of Hoek - Brown constant (a).

6.3 Grouted rock-bolt numerical simulation and numerical model of reinforced tunnel

In this part the numerical formulation of grouted rock-bolts which accounts for the shear behaviour of the grout annulus is firstly described. Secondly, the same problem previous section will be modelled for the tunnel reinforced by grouted bolts. For this purpose, the same quarter-symmetrical tunnel is reinforced with 3 m long of grouted bolts as demonstrated in Figure 6-6. The aim is again to compare the results of analytical elasto-plastic solution with those of numerical approach.

As previously explained, as nodal forces decrease at each tunnel advancement step, more convergence and relaxation occur in the tunnel perimeter and this means that tunnel face is advancing. At a reasonable relaxation, the temporary reinforcement (in this study, grouted bolts) must be installed and then the procedure is continued so that the tunnel convergence at each relaxation step is obtained. These progressing steps should be continued until the last nodal force approaches to zero. Generally, the temporary support system is installed when the inner radial pressure reaches to approximate 60 % of the in-situ stress. At the same time, the displacement at the tunnel face is supposed to be about 30 % of final tunnel displacement.

To model the grouted bolt, the cemented zone can be represented by surface or solid elements and the effects of the contrast in stiffness between the rock mass, the grout and the steel can be studied.

Not taking into account the bending effect, the rock bolts are solely modelled by a shearing resistance along their length, as provided by the shear resistance (bond) between the grout and the rock-bolt or the grout and the rock mass (Itasca, 2000). The rock-bolt is assumed to be divided into a number of segments of length, L, with nodal points located at each segment end. The mass of each segment is lumped at the nodal points, as in the continuum formulation of FLAC (Itasca, 2000).

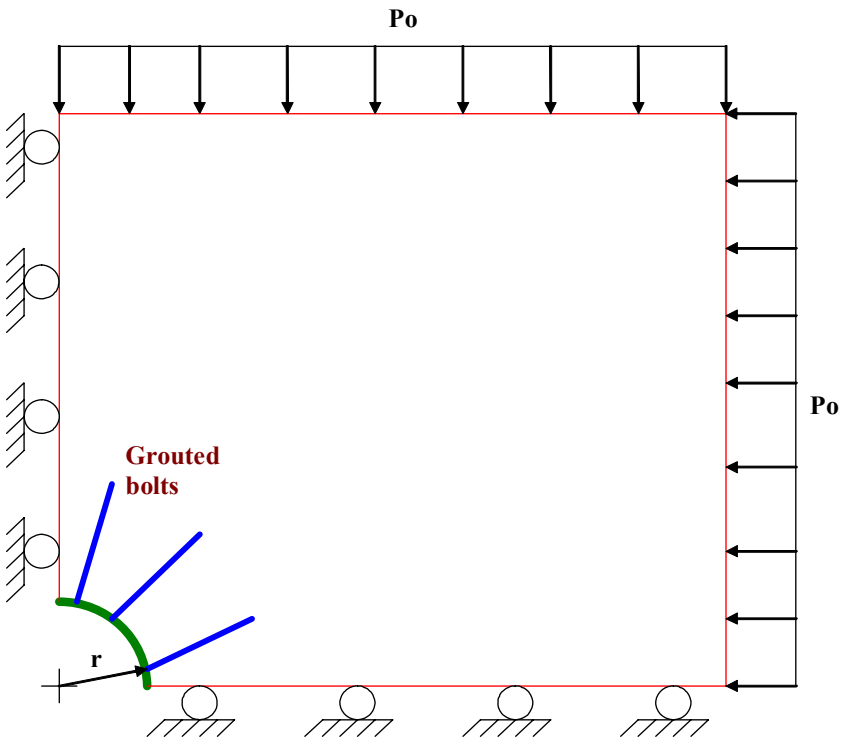

Figure 6-6 Numerical model of reinforced circular tunnel- quarter symmetrical model

6.3.1 Axial behaviour

The axial behaviour of conventional reinforcement systems may be assumed to be governed entirely by the reinforcing element itself. The reinforcing element is usually steel and may be either a bar or rock-bolt. Because rock bolt is slender, it provides little bending resistance, and is treated as a one-dimensional member with capacity to sustain uniaxial tension (Compression is also allowed) (Itasca, 2000). A one-dimensional model is adequate for describing the axial behaviour of the rock bolt. In the present formulation, the axial stiffness is described in terms of the reinforcement cross-sectional area (A) and Young's modulus (E).

The incremental axial force ΔF^s is calculated from the incremental axial displacement by (Itasca, 2000):

$$\Delta F^s = -\frac{EA}{L}\Delta u^t \qquad (6\text{-}1)$$

where

$$\Delta u^t = \Delta u_i t_i = \Delta u_1 t_1 + \Delta u_2 t_2 = (u_1^{[b]} - u_1^{[a]})t_1 + (u_2^{[b]} - u_2^{[a]})t_2$$

$u_1^{[a]}$, $u_1^{[b]}$, $u_2^{[a]}$ and $u_2^{[b]}$ are shown in Figure 6-7. The superscripts [a] and [b] refer to the nodes. The direction cosines t_1, t_2 refer to the tangential (axial) direction of the rock-bolt.

FLAC evaluates the axial forces, developed in the rock bolt, in such a way that the displacements are computed at nodal points along the axis of the reinforcement, as shown in Figure 6-8 (Itasca, 2000). Out-of-balance forces at each nodal point are computed from axial forces in the rock bolt as well as shear forces contributed through shear interaction along the grout annulus. Axial displacements are computed based on accelerations from integration of the laws of motion using the computed out-of-balance axial force and a mass lumped at each nodal point (Itasca, 2000).

6.3.2 The shear behaviour of the grout annulus

The shear behaviour of the grout annulus is represented as a spring-slider system located at the nodal points shown in Figure 6-8. The shear behaviour of the grout annulus, during relative displacement between the bolt- grout interface and the grout- host rock interface, is obtained as (Kbond in Figure 6-9(b)) (Itasca, 2000):

$$\frac{F_s}{L} = Kbond \cdot (u_b - u_m) \qquad (6\text{- }2)$$

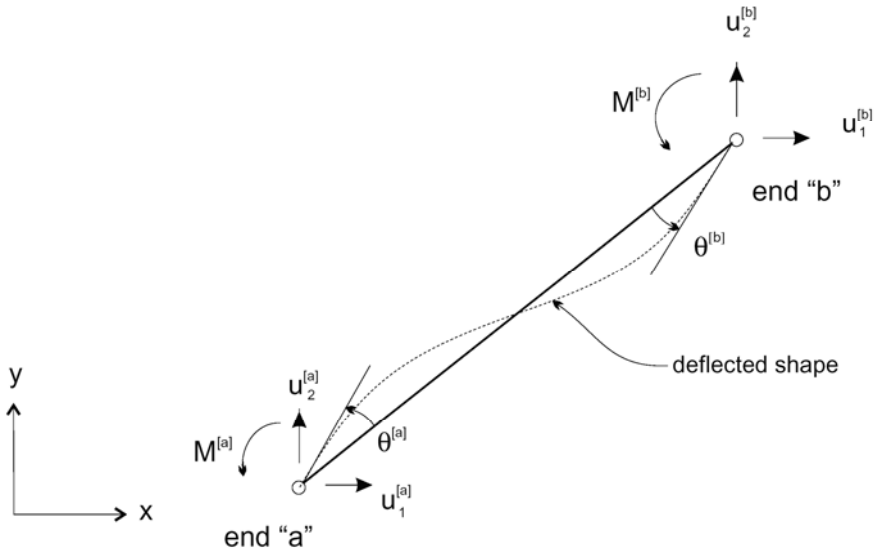

Figure 6-7 Nomenclature for beam elements (Itasca, 2000)

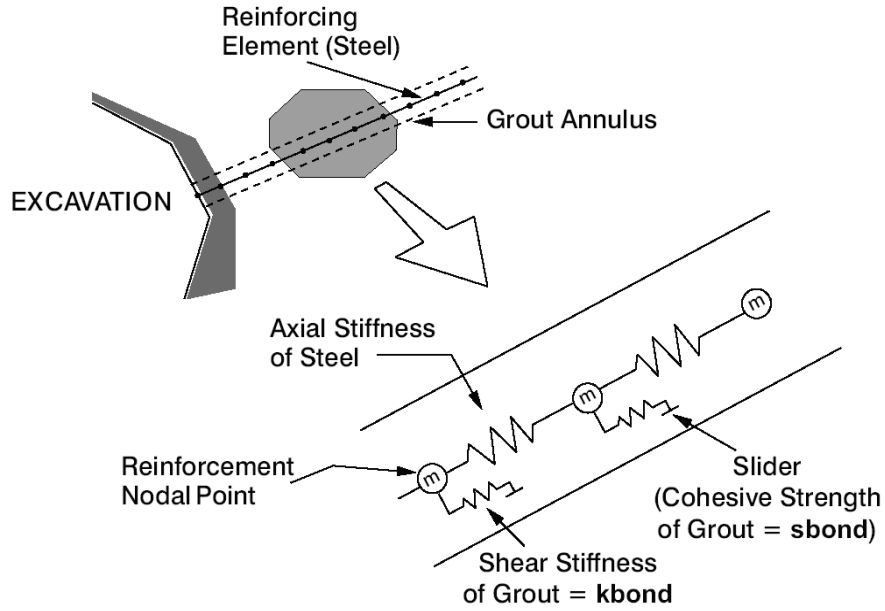

Figure 6-8 Conceptual mechanical representation of fully bonded reinforcement which accounts for shear behaviour of the grout annulus (Itasca, 2000)

where F_s = shear force that develops in the grout (i.e., along the interface between the rock-bolt and the grout); K*bond* = grout shear stiffness; u_b = axial displacement of the rock-bolt; u_m = axial displacement of the medium (soil or rock); and L = contributing bolt length.

Kbond can be also measured directly by pull-out tests. The magnitude of the Kbond can be determined from:

$$Kbond = \frac{\frac{T}{L}}{u_b} \qquad MN/m/m \tag{6- 3}$$

where T= tensile force (kN) ; L= rock bolt length (m); and u_b= induced displacement of the bolt (mm).

From the results of the several non-destructive pull-out tests on grouted rock bolts of 3 m in length, the parameters used in numerical parametric study are described in Table 6-1.

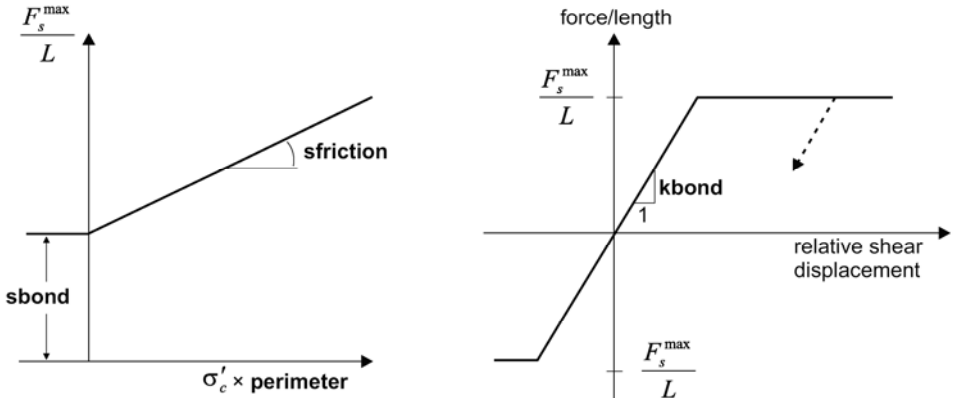

a) Grout shear strength criterion b) Grout shear force versus displacement

Figure 6-9 Grout material behaviour for grouted bolts (Itasca, 2000)

The maximum shear force that can be developed in the grout, per length of bolt, is a function of the cohesive strength of the grout and the stress-dependent frictional resistance of the grout. The bond cohesive strength and friction angle can be estimated from the results of pull-out tests conducted at different confining pressures or, should such results not be available, the maximum force per length may be approximated from the peak shear strength of grout (Itasca, 2000):

$$\tau_{peak} = \tau_{limit} \tag{6- 4}$$

where τ_{limit} is approximately one-half of the uniaxial compressive strength of the weaker of the rock and grout.

Another assumption which can be considered is the τ_{limit} is approximately equal to the inherent cohesion of the grout no matter whether failure occurs in the shank-grout or grout- rock interface. If the failure takes place inside the grout or bolt-grout interface under low confining pressure (this condition occurs more often in component rock mass), it can be proved that:

$$\tau_{limit} = C_g$$

where C_g is the bond cohesive strength and obtained easily from the Mohr-Coulomb failure criterion:

$$C_g = \frac{c_{cg}(1 - \sin\varphi_g)}{2\cos\varphi_g} \tag{6- 5}$$

where σ_{cg} = uniaxial compressive strength of the grout and φ_g = internal friction angle of the gout.

Generally for grout material the σg varies between the 12 MPa and 20 MPa and φ_g ranges between 30˚ and 36˚. Table 6-2 demonstrates the cohesive strength of the grout.

Table 6-1 The results of pull-out test in different rock mass quality used in the parametric study of FLAC analysis (TUSC, 2006).

FLAC MODEL	GSI	τ_{lim} (MPa)	δ (mm)	Kbond MN/m/m	Sbond MN/m
3	65	1	1.5	22.22	0.1885
2	45	0.6	3	11.11	0.1131
1	25	0.2	4.5	7.41	0.0377
4	Great value	3.06	1	33.33	0.5768
5	Great value	5.77	0.5	66.67	1.0876

Table 6-2 Cohesive strength of the grout used in the grouted rock bolts

σ_{cg} (MPa)	φ_g˚	C_g (MPa)
12	30	3.46
12	33	3.26
12	36	3.06
20	30	5.77
20	33	5.43
20	36	5.10

On the other hand, if the failure propagates at the grout- rock interface (this condition occurs often in the poor rock mass), the σ_{cg} and φ_g of the grout material should substitute for those values of host rock mass as follows:

$$C_m = \frac{c_{cm}(1 - \sin\varphi_m)}{2\cos\varphi_m} \qquad (6\text{-}6)$$

where σ_{cm} and φ_m are the uniaxial compressive strength and the internal friction angle of the surrounding rock mass, respectively. Therefore:

$$\tau_{limit} = C_m$$

Consequently, neglecting frictional confinement effects, Sbond might be obtained from:

$$Sbond = \pi(\phi_h)\tau_{limit} \quad MN/m \qquad (6\text{-}7)$$

where ϕ_h is the hole diameter i.e. $\phi_h = (d_b + 2t)$. d_b and t denote the bolt diameter and the grout annulus thickness, respectively.

The result of pull-out test provides sufficient information to obtain the value of the Kbond and Sbond as input parameters in FLAC model. The results of pull-out tests carried out for some cases in Italy have been used in the parametric analysis of FLAC. The results of a number of pull-out tests performed with 100 kN for grouted bolts of 32 mm in diameter and of 3 m in length in different rock mass quality are outlined in Table 6-1.

6.3.2.1 Correlation between bond cohesive strength "Sbond" of FLAC and λ of the bolt density parameter of the analytical model

The friction factor (λ) of rock bolt density parameter is analogous to the coefficient of friction. It relates the shear stress to the stress applied normal to the bolt surface. The corresponding shear stress at the pick-up length opposes the rock mass displacement near the tunnel surface.

Depending on the degree of adhesion (bond strength) at the bolt- grout interface the magnitude of λ for smooth rebar falls in the range of as suggested by Indraratna & Kaiser (1990a):

$$\tan(\varphi_g / 2) < \lambda < \tan(2\varphi_g / 3)$$

Hence, for smooth rebar the magnitude of the λ will, if the $\varphi_g = 30^\circ$, vary:

$0.26 < \lambda < 0.36$

If the $\varphi_g = 36^\circ$: $0.32 < \lambda < 0.44$

For shaped rebars approaches $\tan\varphi_g$ (Indraratna & Kaiser, 1990a):

$$\lambda = \tan\varphi_g$$

Then, for shaped rebar, the magnitude of the λ falls within:

$\lambda = 0.6$ if $\varphi_g = 31^\circ$, $\lambda = 0.72$ if $\varphi_g = 36^\circ$

Therefore, what can be concluded is that the λ of bolt density parameter is proportional to the bond strength Sbond of FLAC model. Both of them are dependent on frictional strength of the grout. In order to compare the results of analytical and numerical models, the value of the $\lambda = 0.6$ is considered to simulate the shaped-rebar in analytical model.

Besides, to find a justifiable link between λ and Sbond five FLAC models with different Kbond and Sbond whose magnitudes simulate the quality of rock mass have been chosen.

Those results of the numerical model with independently prescribed values of Kbond and Sbond which would be well-fitted with the results of analytical model with $\lambda = 0.6$ provide proper link between λ and Sbond. Hence, with references to the rock mass quality and the results of pull-out test, one is able to pick up the approximate estimates for Sbond and Kbond.

Considering the input parameters of Table 5-2, the stresses distribution of both analytical and numerical model around the tunnel is outlined in the Figure 6-10. As can be observed, with increasing the Kbond and Sbond of the reinforcement, a decrease in plastic zone extension would result. The results of numerical model 2 seem to be well-fitted with the analytical solution. Both provide more or less the same maximum tangential stress and plastic zone radius.

An interesting finding is that no significant change in the stress distribution and plastic zone extension take place with rising up the magnitude of the Sbond and Kbond from model 3 to model 5. The magnitude of $\lambda = 0.6$ makes then it possible to model the grouted rock-bolt with shaped rebar. Accordingly, the results of the numerical studies can be compared with those of analytical model only if $\lambda = 0.6$ is taken into consideration.

Figure 6-11 delineates the satisfactory agreement between the stresses distribution determined through both analytical and numerical analyses.

FLAC model 2 also provides well-fitted displacements values with the analytical model. The maximum expected displacement, occurring at the tunnel surface, of analytical model is less than that of numerical simulation. However, after a very small distance of tunnel surface the trend of displacements are quite alike. These findings are distinguished in Figure 6-12 and Figure 6-13.

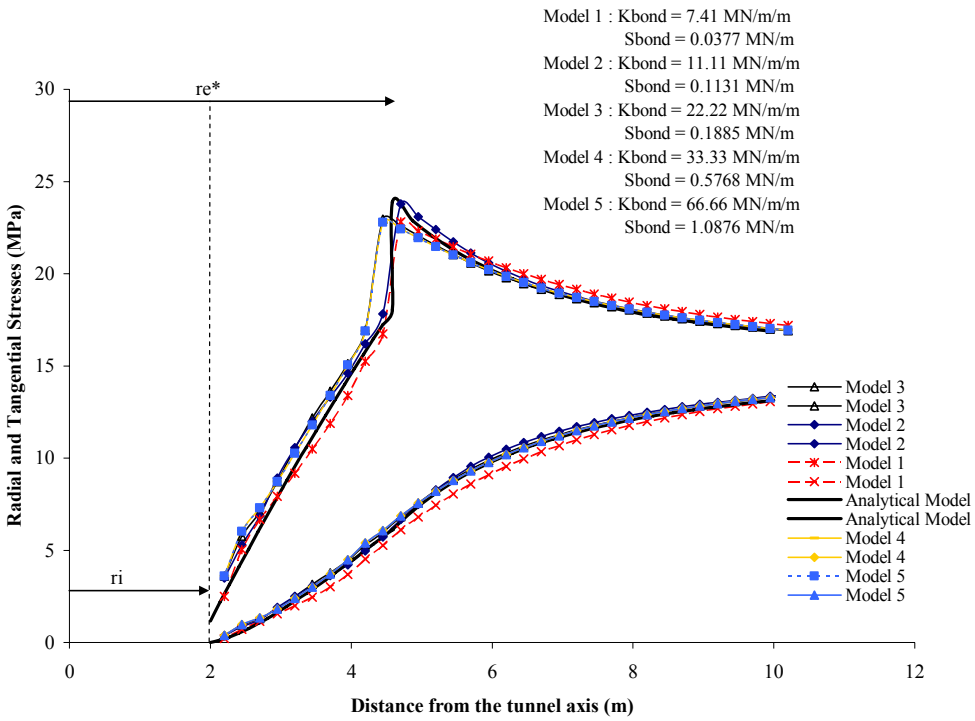

Figure 6-10 Analytically and numerically calculated tangential and radial stress around the bolted tunnel with different values of grout shear stiffness and bond strength. The stress field of model 2 and analytical solution are to a certain extent compatible.

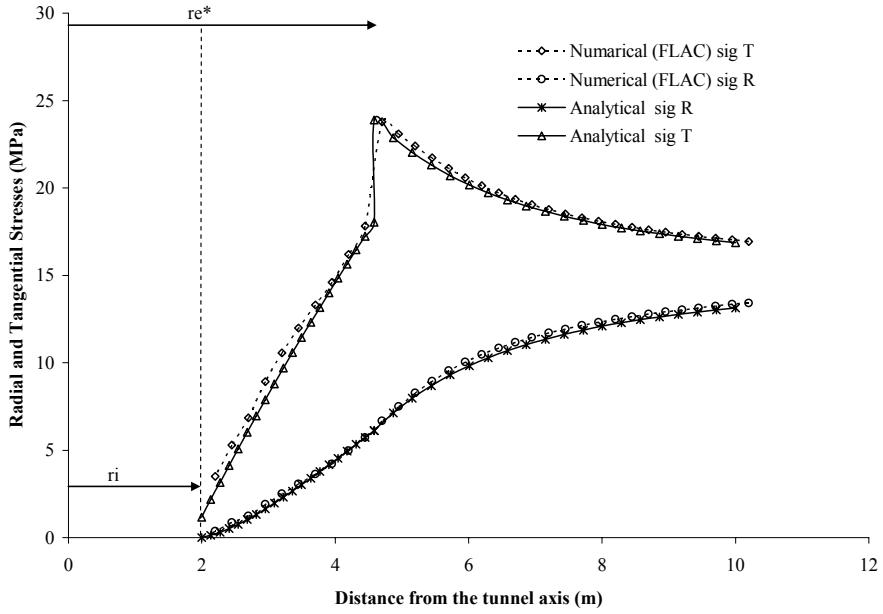

Figure 6-11 Stresses distribution around the bolted tunnel from both analytical and numerical methods

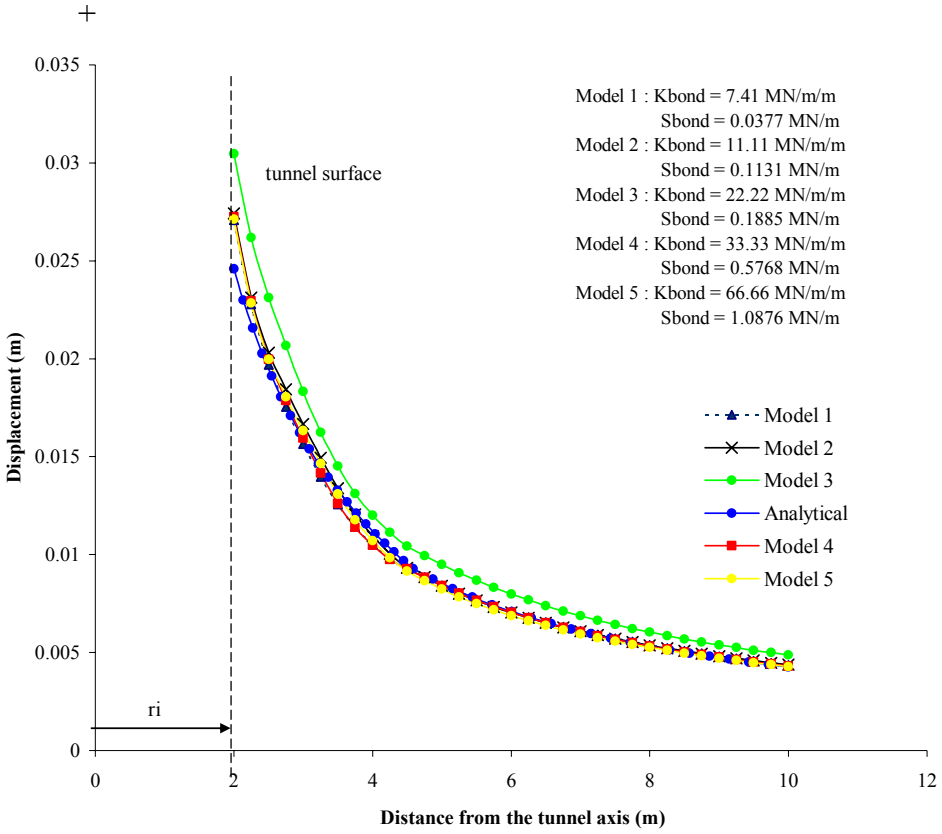

Figure 6-12 Analytically and numerically calculated displacement around the bolted tunnel with different values of grout shear stiffness and bond strength. The displacement field of model 2 and analytical solution are well-matched.

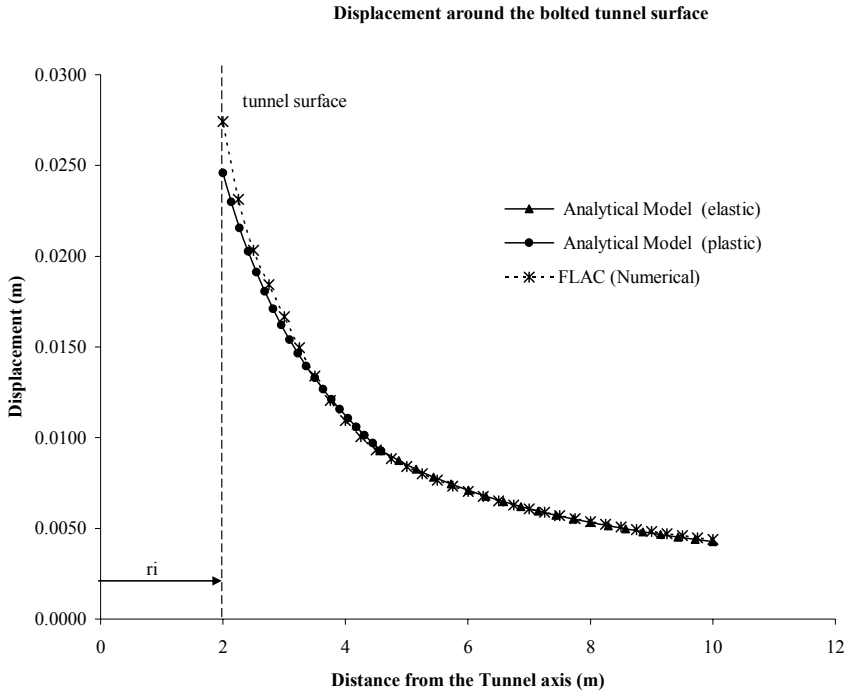

Figure 6-13 Displacements distribution around the bolted tunnel from both analytical and numerical methods

CHAPTER 7

CRITICAL DISCUSSIONS AND FIELD VERIFICATION OF THE DEVELOPED MODEL

7.1 Implication of the Modified-GSI

The use of RMR values less than 30 and Q values of less than 0.1 for characterization of very poor rock mass are not recommended because of the dominant role of RQD in these classification systems and the difficulty of determining its value for very poor quality rock masses. The method explained in Chapter 3 aimed at providing an alternative and practical approach to characterizing poor and very poor rock masses.

For this purpose, a quantitative and qualitative means based on the GSI was set up to be applicable to poor rock mass where the value of RMR < 30. The Modified-GSI takes the advantage of utilizing the parameters defining the degree of jointing (degree of blockiness) and joint conditions. The degree of jointing can be defined in terms of the volumetric joint count, and structural rating apart from field observations. Those indicators might be obtained from scanline mapping, borehole logging, window mapping, and overall field observations. In order to assist the Modified-GSI, the Broken Structure Domain (BSTR) and Intact Core Recovery (ICR) indicators were defined and embedded into Modified-GSI. The BSTR stands for the degree of blockiness and interlocking of the poor rock mass appropriately while the ICR helps to assess the joint condition of poor rock. The Modified-GSI obtained for a given poor rock mass can, in turn, contribute in developed rock bolt design model as demonstrated in Figure 7-1.

7.2 Implication of the support pressure function

A practical approach to estimate the support pressure has been developed. Not only does the proposed approach take into account the quality and quantity of the rock mass, but it also takes into account the squeezing ground condition and anisotropy in field stress.

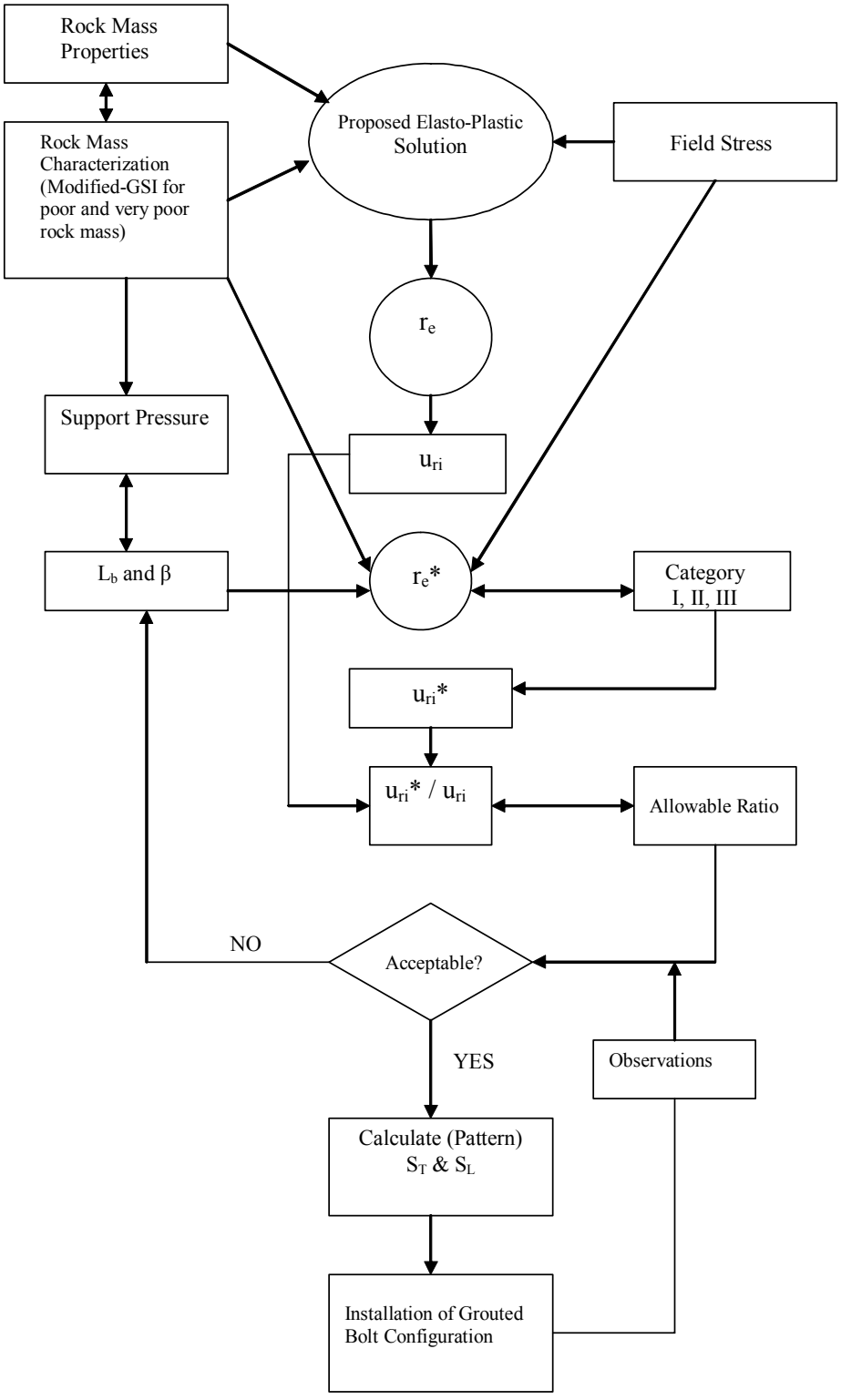

Figure 7-1 Computational steps of the developed model for design of grouted bolts in this thesis

Numerical studies have been carried out to study the effects of the anisotropy in field stress in order that a correction factor for stress ratio (k) should be included in the proposed empirical expression. The resulting stress correction factors (C_s) are limited to arch-shaped and rectangular tunnel sections, whose sides walls are 60 % of their total height. However, for both tunnel cases, the trend line of the stress correction factor against stress ratio is observed to be, to a large degree, identical. Therefore, it can be stated that the proposed approach would be applicable to other tunnel sections. It is worth noting that much more tunnel shapes are suggested to be modelled so as to be reach to more realistic stress correction factor (C_s). Evidence to validate the proposed approach has been obtained by numerical modelling. In most of cases, rock-load heights of proposed approach were in a good agreement with those of numerical studies.

A distinguished conclusion that can be extracted is that the proposed approach can be used safely in the fair to good quality rock mass. More care, however, has to be taken where tunnelling in poor rock masses is concerned. In such rock masses the use of Modified-GSI (explained in Chapter 3) is recommended.

The preliminary pattern of grouted bolting for any shape of tunnel opening can be acquired by means of Equation 5-81 that links the bolt density parameter (β) and support pressure as indicated in flowchart Figure 7-1. It means that with the help of a quite accurate rock mass characterization, a reasonable value for first approximate of rock bolt density would be obtained and the need for counter-measure or redesign of the reinforcement system will be disregarded. The subsequent design procedure will be outlined in next part.

In the end, the proposed support pressure approach cannot be advisable to be used for determination of rock support measure during construction. It can be helpful for engineers who deal with the planning stage of tunnel design.

7.3 Implication of the proposed elastic-plastic analytical model

The elasto-plastic theoretical analysis presented in this thesis was based on the convergence control approach for the design of fully grouted bolts. Therefore, the effectiveness of fully grouted bolts should be assessed on the basis of convergence reduction, which in turn may assist the designer in selecting the optimum bolting pattern. The numerical studies have verified the reliability of the elasto-plastic analytical solution in the convergence prediction of un-reinforced and reinforced deep tunnels.

The influence of the bolt density parameter (β) on the strength parameters of the rock mass profoundly reflects the importance of the bolt spacing and bolt-grout interaction (frictional) in design. In poor rock mass, the use of shaped rebars, relatively high bolt density, and appropriate length are recommended. The evaluation of the Equivalent Plastic Zone radius (r_e*) in terms of the bolt density parameter and bolt length, provides a fundamental basis for the determination of a reinforced tunnel convergence.

The normalized convergence ratio is the fundamental design aids in this analysis. The normalized convergence ratio is most appropriate in design, where the strength and frictional parameters are poorly defined.

It can be inferred from the results of analytical studies that the installation of a sound pattern of bolts immediately after excavation near the tunnel face contributes to a much greater degree of stabilization that the provision of supplemental bolting at a later stage. The initial bolting pattern is predominant in controlling the extent of plastic zone around the tunnel and the final tunnel convergence. Besides, the preliminary bolting immediately after excavation modifies the ground reaction curve in such a way that the final lining of tunnel will undergo less support pressure.

The mathematical treatment of the elasto-plastic analysis has been based on several simplifying assumptions in addition to numerical techniques. For instance, a circular opening reinforced with an axi-symmetric bolt pattern, excavated in an isotropic, homogeneous medium, subjected to a hydrostatic field stress has been taken into consideration. Some numerical techniques have been also adopted in order to solve the equilibrium and compatibility equations and relevant integrals. The Equivalent Plastic Zone, as a result, determined by the analytical solution is axi-symmetric or circular in shape. Therefore, the accuracy of the proposed elasto-plastic analytical solution becomes questionable as the complexity of the geomechanical conditions increases. Nevertheless, the bolt density parameter incorporated with support pressure relates the analytical to empirical design methods, thereby resulting in designing of a systematically rock-bolt pattern in non-circular tunnels and it acts as an integrated support design method.

Since the behaviour of the rock mass is modelled, in this study, by either elastic-perfectly plastic or elastic-brittle-plastic behaviour with a corresponding non-linear Hoek-Brown failure criterion, the rock materials obeying this behaviour are believed to be modelled more accurately and realistically that those analytical solutions based on linear Mohr-Coulomb failure criterion.

It is suggested to set up a guideline relating the rock mass class and bolting pattern for any given on-site geomechanical condition based on elasto-plastic model (for example Table 5-7) because every so often the empirical design approaches (RMR and Q-system) may not provide a sufficiently sensitive guide to properly design the grouted bolts in poor, yielding rock mass. By doing so, a sound basis for effective tunnel convergence control can be achieved.

It should be noted that the proposed analytical solution is valid only for isotropic and homogenous rock medium. Even so, it can also be used for fractured and heavily jointed rock mass dominated at least by four sets of discontinuities as also mentioned by (Hoek & Brown, 1980b). Therefore, for rock masses with presence of a considerable discontinuity (such as a major fault) or fewer than four discontinuities the proposed analytical solution cannot be used.

The influence of time-dependent material properties on ground convergence has not been investigated in this study. Time-dependent behaviour can be critical if a tunnel is kept unsupported for a considerable period of time. However, time dependent convergence of a tunnel opening can be minimized by installing

reinforcement at the face immediately after excavation. Therefore, it may be deduced that the theoretical convergence predictions are realistic, if fully grouted bolts are installed soon after excavation.

The developed approach for the design of fully grouted bolts for tunnels in this thesis clearly illustrates the capability of the fully grouted bolts in controlling rock mass displacements. Comparison with empirical method implies the superiority of the convergence control approach for poor to very poor rock masses.

The suggested methodology for reinforcement design is summarized in the flowchart presented in Figure 7-1 and the relevant computational steps are as follows:

Step 1: The rock mass in which the tunnel is to be excavated must be appropriately characterized so as to determine its geomechanical parameters and support pressure. For poor to very poor rock masses, the use of Modified-GSI is recommended.

Step 2: The support pressure must be determined through Equation 4-6. By using Equation 5-81, which relates the support pressure to bolt density parameter, the initial value (first approximate) of β can be estimated.

Step 3: For the unsupported tunnel ($\beta=0$, $L_b=0$), the plastic zone radius (r_e) and hence the associated radial displacement of the tunnel surface (u_{ri}) is determined from the proposed elasto-plastic solution (Equations 5-35 and 5-50), for the given rock mass properties and in situ field stress.

Step 4: The equivalent plastic zone (r_e*) and the displacement of the reinforced tunnel surface (u_{ri}*) are determined (Equation 5-78), for an initial combination of the bolt length (L_b) and density (β) obtained in the Step 2.

Step 5: The normalized convergence ratio (u_{ri}^*/u_{ri}) is computed and compared with the allowable (design) convergence ratio.

Step 6: If this value of u_{ri}^*/u_{ri} satisfies the required convergence reduction, then the initial combination of bolt length and density is appropriate and acceptable. Hence, the required bolt spacing (S_L and S_T) can then be calculated from Equation 5-82.

Step 7: The convergence of the reinforced tunnel after the installation of suggested bolt configuration is measured to verify the efficacy of the design. If either the predicted convergence ratio (u_{ri}^*/u_{ri}) or the observed displacements do not provide the desired or allowable convergence reduction, then the computation must be repeated from Step 4, for a different combination of L_b and β.

7.4 Implications of the advancing tunnel face

The proposed elasto-plastic analytical solution predicts the ultimate convergence (more than two tunnel diameter behind the face) where the 3-D effects close to the face have been neglected. Therefore, the convergence ratio introduced in this analysis is related to a 2-D solution. In reality, the observed convergence (u_r) is affected by the face effects. It is generally less than the predicted total convergence (u_t) and more than displacement of the face (u_i) (See Figure 7-2).

Panet & Guenot (1982) have presented numerical analyses of the advancing face effect for circular tunnels driven through elasto-plastic material under hydrostatic stress condition. In their solutions, the prediction of the convergence profile behind the face requires a preliminary assessment of the ultimate time-independent convergence and the final extent of the plastic zone. The final convergence of the numerical axi-symmetric model of a tunnel, whose properties outlined in Table 5-2, has been found to be equal to tunnel surface convergence of proposed analytical solution. As can be seen from Figure 7-2, the displacement at tunnel face is 30 % of final displacement. Alternatively, several in-situ convergence measurements behind the face may be utilized for the purpose of semi-empirical solution. Nevertheless, the ultimate tunnel convergence and the corresponding plastic zone radius for both unsupported and reinforced openings can be determined by the analytical solution proposed in this thesis.

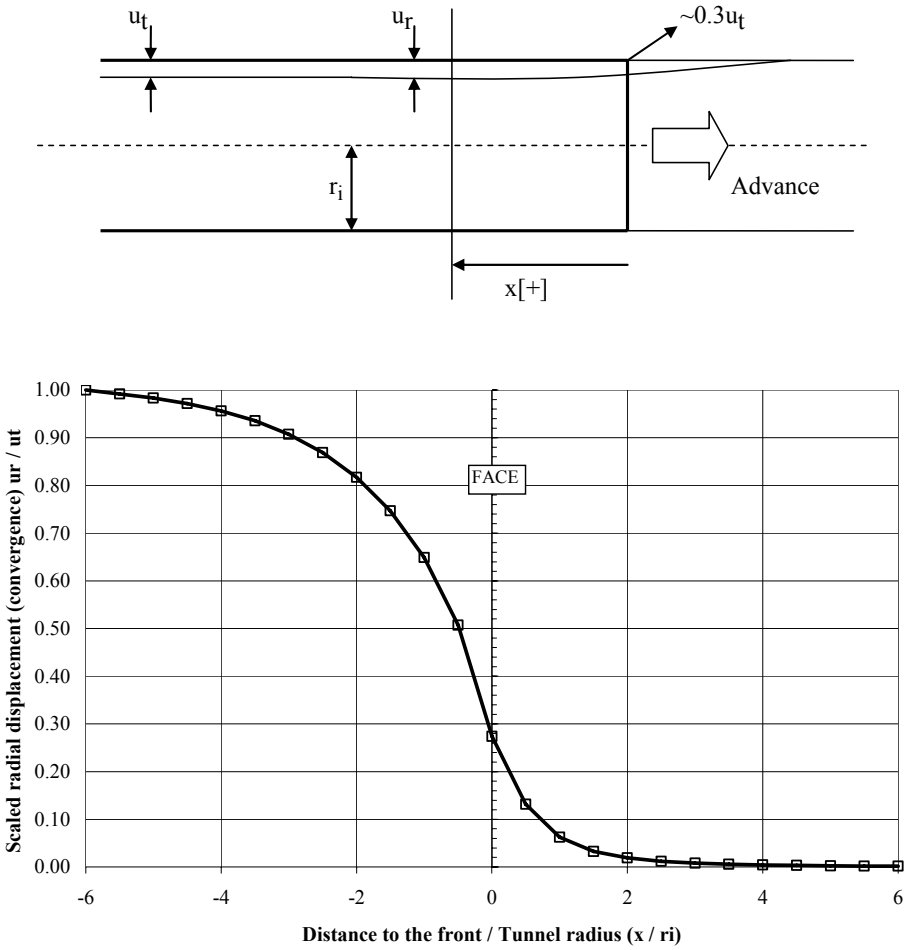

Figure 7-2 Profile of radial displacements u_r for an unsupported tunnel in the vicinity of the tunnel face (Osgoui, 2006b). This deformation profile was drawn based on input parameters given in Table 5-2. The upper figure was reproduced from Carranza- Torres & Fairhurst (2000).

7.5 Implication of numerical modelling

The validity of the proposed elasto-plastic model has been verified with numerical modelling (FLAC) for both unsupported and reinforced tunnels.

In case of unsupported tunnel, the numerical modelling has proved the predicted stresses, displacements, and plastic zone radius around the tunnel by proposed elasto plastic model. It is interesting to note that in analytical solution in addition to *m*, *s* of Hoek- Brown constants, the constant (*a*) also changes in accordance with the GSI variation; thereby leading to more realistic results.

The numerical modelling, in case of reinforced opening, has verified the analytical predictions such that the grouted bolts increase the apparent strength of the rock mass around the opening; thereby resulting in curtailing and controlling the convergence around the opening.

The numerical modelling of a bolted tunnel has revealed that the friction factor (λ) of bolt density parameter is directly proportional to the bond strength (Sbond) of FLAC model. Hence, to find a justifiable link between λ and Sbond five FLAC models with different Kbond and Sbond, whose magnitudes were obtained through pull-out tests in various quality of rock mass, were chosen. Those results of the numerical model with independently prescribed values of Kbond and Sbond which would be well-fitted with the results of analytical model with λ =0.6 provide proper link between λ and Sbond. Therefore, it was concluded that in analytical model the magnitude of λ must be 0.6 to accurately simulate the shaped-rebar. Accordingly, the results of the numerical studies can be compared with those of analytical model only if the λ=0.6 is taken into consideration.

7.6 Field verification of proposed empirical and elasto-plastic analytical approaches (A case study: the rock reinforcement design applied to No: 7 Malatya Railroad Tunnel in Turkey)

The application of the proposed elasto-plastic analytical solution for design of grouted bolts to the No: 7 Malatya Tunnel project in Turkey will be demonstrated here in order to present field verification of the proposed approach.

The No: 7 Malatya railroad tunnel, situated in the South-Eastern part of Turkey, was excavated in 1930 through a toe of a paleo-landslide material. This tunnel is 537 m long and its width and height are 5m and 6m, respectively. This sheared zone of rock-mass around the tunnel consists of metavolcanics, schist, fractured limestone blocks, antigorite and radyolite in patches. The matrix material consists of clay and schist having low swelling potential. Limestone blocks are heavily jointed and highly fractured. There are also voids within the rock mass (Osgoui & Ünal, 2005a, b).

Ever since 1930, this horseshoe shape tunnel has struggled with severe stability problems. These problems are associated with the existence of a very poor rock mass around the tunnel, underground water or seepage pressure, and considerable amount of convergence (squeezing phenomenon). A large amount of deformation developing through many years and leading to misalignment of the tunnel was

observed. This excessive deformation is mainly attributed to the squeezing ground condition in which the rock stress exceeds its strength in the passage of time.

As a consequence of the collective effect of weathering and severe tectonic stresses, an intensive weathered sheared zone without any identifiable joint pattern is assumed to have been formed. In view of this fact, the whole rock mass around the Malatya tunnel was regarded as the homogenous and isotropic medium.

As for squeezing ground condition, the *in-situ* stress was assumed to equal to product of the depth below surface and the unit weight of the rock mass. Considering that the vertical *in-situ* stress due to gravity loading was 1.54 MPa with the assumption that the unit weight of very poor rock mass was 0.025 MN/m^3 as well as the rock mass strength was 0.156 MPa, the rock mass strength to *in-situ* stress ratio would be 0.101. Hence, even from this point of view, a huge amount of convergence would have been anticipated as the maximum wall deformation of tunnel had been recorded about 170 cm (Osgoui & Ünal 2005a). In 2002, the rehabilitation of the tunnel (while retrieving the original span of the tunnel) brought about a huge collapse inside the tunnel where the rock mass had undergone remarkable amount of displacement. This phenomenon is ascribed, to a great extent, to the severe squeezing ground condition along with remarkable amount of uncontrolled convergence.

Figure 7-3 Huge collapse as a result of remarkable amount of convergence in squeezing ground condition in Malatya Railroad Tunnel

The test results of core specimens taken from 67 boreholes were used as the input parameters for the assessment of rock mass as typically shown in Figure 3-6. During rock mass classifying, it was difficult to obtain representative samples of the worst quality materials, especially when there are alternating weak materials. Consequently, due to difficulty in retrieving the intact rock pieces, the uniaxial compressive strength σ_{ci}, and the material constant m_i, for example, are determined from tables published elsewhere. Core logging indicated that the value of RQD for almost all cores were zero; accordingly, the RMR or M-RMR and Q-system were not been estimated soundly. For this reason, an alternative approach should have been taken into consideration to be more plausible. Modified-GSI was found to be a practical tool to characterize the poor rock mass of Malatya Tunnel.

7.6.1 Application of the proposed empirical approach to characterize the rock mass

In order to find the GSI for very poor quality rock mass the use of Modified-GSI chart is suggested (Figure 3-3):

BSTR = 2 the BSTR type 2 has been assumed to dominantly governed whole rock mass (i.e. foliated/laminated/ sheared type of poor rock mass with completely loss of blockiness) (Figures 3-5 and 3-6).

Joint Condition Index for completely weathered rock mass: ICR < 25%, bs=2, highly weathered W_c=2, without filling.

I_{jc} = 2+ (2/2) + 4 = 7 (Table 3-3)

Modified-GSI = 13 -15 (Figure 3-3)

Having determined the Modified-GSI, the expected rock-load height and support pressure are estimated using the proposed empirical approach as follows:

$$h_t = \frac{100 - \left[(1 - \frac{0}{2}) \sqrt{\frac{5}{100}} \times 14 \right]}{100} \times 1.8 \times 1.5 \times 5 = 13m$$

where:

D=0 (Table 4-10), S_q=1.8 (Table 4-9) due to extreme degree of squeezing

C_s=1.5 (Figure 4-22) $\frac{c_h}{\sigma_v} = 1.2$ is assumed due to shallow tunnel,

σ_{ci} =5 MPa

$P = \gamma \cdot h_t = 13 \times 0.025 = 0.325MPa$

where γ rock mass=0.025 MN/m^3

7.6.2 Application of the proposed elasto-plastic model to design of reinforcement

The primary support system prior to rehabilitation of the Malatya Tunnel was comprised of steel-arches, concrete lining, and final bricking. Since 1930 the support systems have withstood squeezing ground condition, ultimately resulting in failure in support system. In order to re-design the support system the use of grouted bolts were recommended following a convergence measurement program.

In order to understand the short term behaviour of the tunnel and to evaluate its stability before rock reinforcement applications, a series of convergence measurements were carried out. A total of 15 monitoring stations were set up inside the tunnel, 11 of which were installed in the deformed section and 4 of which were set up in the non-deformed part. The period of convergence monitoring of the tunnel was around 100 days. A maximum horizontal displacement of 8.78 mm was recorded in 3 stations inside the deformed part of the tunnel, indicating that there were still horizontal movements.

For poor rock mass surrounding the Malatya tunnel, MAI-bolts (Atlas Copco, 2004), which are self-driving full column cement-grouted bolts, were chosen to be the most suitable because drill holes usually close before the bolt has been installed, and the injection operation associated with rock-bolting make the ground improved in terms of engineering parameters. Therefore, it was hoped that with the use of systematically grouted bolts the extent of the yielding and convergence decreased. The MAI-bolts, like ordinary grouted bolts, develop load as the rock mass deforms. Relatively small displacements are normally sufficient to mobilize axial bolt tension by shear stress transmission from the rock to the bolt surface.

For rock reinforcement design, the section of the tunnel to be supported was divided into three parts namely; A1, A2, and B. A systematic rock bolting was performed at that section. Accordingly, 110 m long section of the tunnel was supported systematically by MAI-bolts having a diameter of 32 mm, length of 6 m or 9 m with transversal and longitudinal spacing of 1m and 0.8 m, respectively (Osgoui & Ünal, 2005a). The properties of MAI- bolts used in Malatya tunnel are given in Table 5-8. A total of 15 rock bolts were installed around the tunnel except for invert. Floor was supported by installing 5 grouted bolts with the length of 5 m. The rock reinforcement details of tunnel are shown in Figure 7-4.

To find the preliminary value of rock bolt density (β), the use of Equation 5-81 is advised as outlined in flowchart of Figure 7-1. Hence:

$$\beta = \frac{P\pi d\lambda B}{2C_b} = \frac{0.325e3 \times \pi \times 32e-3 \times 0.6 \times 5}{2 \times 280} = 0.175$$

It is interesting, at this point; to note that the calculated bolt density is quite close to real (measured) bolt density used for reinforcement design, i.e. Equation 5-56:

$$\beta = \frac{\pi d\lambda r_i}{S_L S_T} = \frac{\pi \times 32e-3 \times 0.6 \times 2.5}{1 \times 0.8} = 0.18$$

Referring to quite close values of the bolt density, it would be evident that magnitude of support pressure has been realistically estimated through Equation 5-81. Because Equation 5-81 is mainly function of rock mass quality, it can be concluded that the poor quality rock mass of Malatya tunnel has been best characterized by using Modified- GSI.

According to results of proposed elasto-plastic solution for unsupported tunnel, a total convergence and plastic zone radius have been found to be 166.8 mm and 15.0 m, respectively.

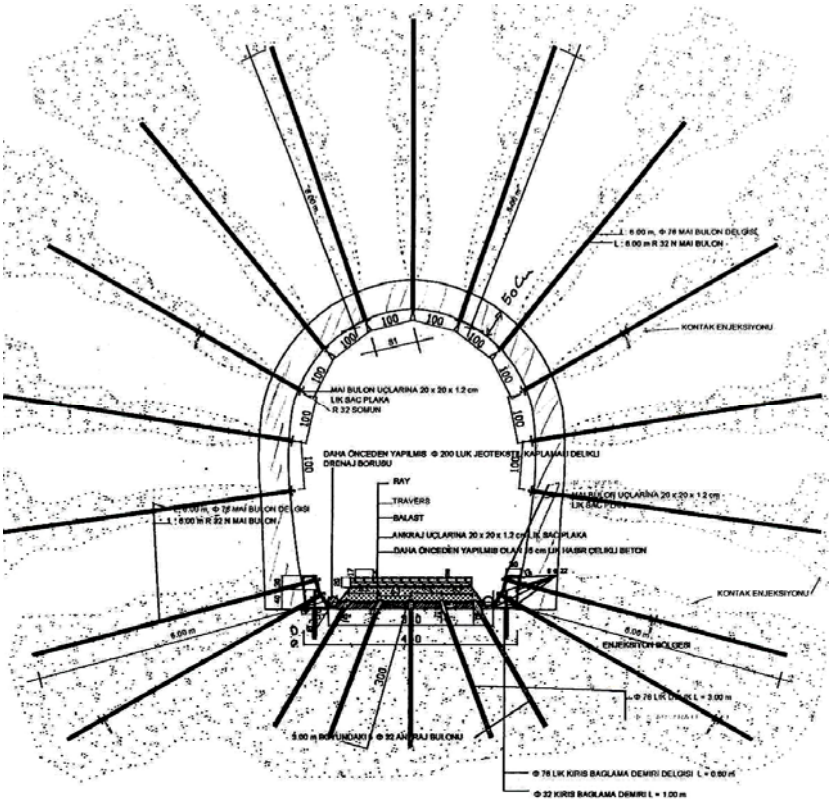

Figure 7-4 Grouted bolts configuration in Malatya Tunnel

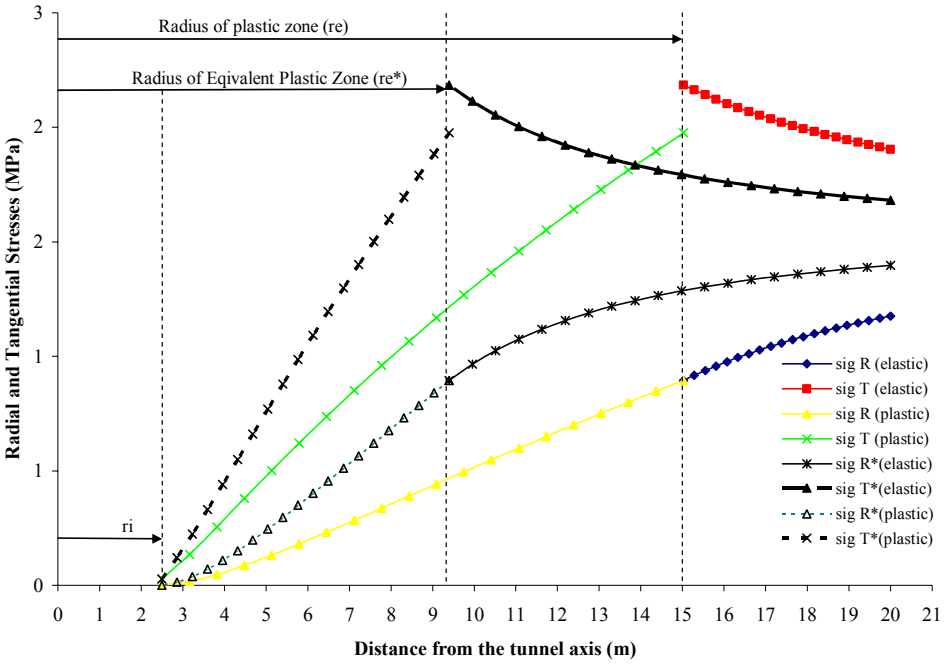

Figure 7-5 Predicted tangential and radial stresses around the Malatya Tunnel in both natural and reinforced cases. The radius of yielding for both unsupported and reinforced cases is indicated.

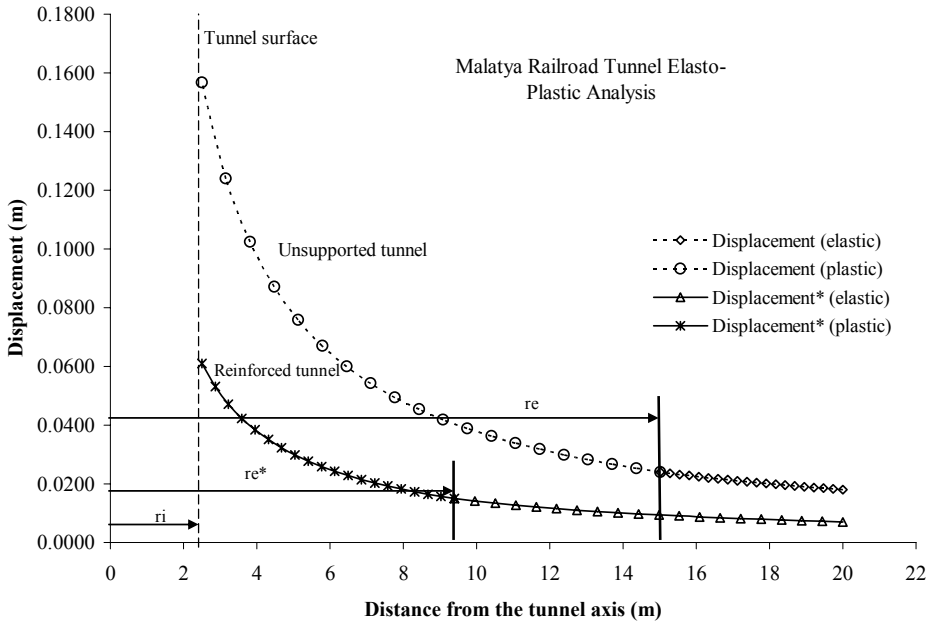

Figure 7-6 Predicted displacement (convergence) around the Malatya Tunnel in the absence and presence of grouted bolts

By using high rock bolt density (β= 0.18) in reinforcement design, a reduction in tunnel convergence of 61 % and a reduction of 37.4 % in plastic zone extension have been expected. The results of analytical solution have been based on major yielding (i.e. Category 2) of analytical model. Figure 7-5 and Figure 7-6 illustrate the predicted stresses and displacements around the tunnel for both natural and reinforced cases.

The reduction of as much as 61 % in tunnel convergence is reasonable value as discussed in Chapter 5. Therefore, the real bolt density and bolt length used in Malatya Tunnel has been found appropriate. Although the major yielding (Category II) of equivalent plastic zone has been reached $\rho < r_i^* < (r_i+L_b)$ as a result of application of shorter bolts (9 m bolt length in compared to 15 m of plastic zone extent), the use of high bolt density has successfully compensated this deficiency and has satisfied the convergence reduction.

CHAPTER 8

CONCLUSIONS AND RECOMMENDATIONS

An elasto-plastic analytical solution for the axi-symmetrical problem of unsupported and reinforced circular tunnel has been developed. In this analysis the rock mass obeys the latest Hoek & Brown yield criterion (version 2002). Although most of the existing elasto-plastic solutions for tunnel problems in Hoek & Brown media consider $a = 0.5$, the proposed approach supposes $a \geq 0.5$ for rock mass. In addition, this solution is based on the assumption that after the intact strength of the rock is exceeded, the material loses its strength, as dictated by a strength loss parameter (S_r). The solution allows a representation of the Ground Reaction Curve for tunnels, which is used mostly in convergence-confinement method. Illustrative applications of the derived elasto-plastic solutions are also described and the results are compared with those obtained with numerical modeling. The effectiveness of grouted bolts in stability of tunnel is evaluated by convergence control approach. The concept of an equivalent material approach (equivalent strength parameter) was introduced to describe the extent of yielding around a circular tunnel, reinforced with fully grouted bolts. The link between the analytical and empirical approaches (support pressure function) developed in this study makes it possible to design the bolting pattern even for non-circular tunnel. Characterizing poor rock masses using Modified-GSI allows the prposed model to be also applicable in such rock masses as verified in the Malatya railroad tunnel in Tuekey. The main conclusion and suggestions are summarized as follows:

1. In a nutshell, the proposed methodology provides a practical means to quickly evaluate the deformational behaviour of an opening and then to quickly design temporary rock reinforcement with a reasonable degree of safety and reliability.
2. Where the use of numerical solution is restricted for assessing the opening stability and reaching design conclusions, the use of proposed method would be an attractive alternative. A tunnel engineer can simply use the developed model with a programmable calculator or notebook (pocket PC) on job-site.
3. A significant contribution in better characterization of poor rock mass with GSI has been offered by the introduction of Modified-GSI and support pressure function.

4. An additional contribution in the elasto-plastic models of unsupported and reinforced tunnels has been introduced in such a manner that apart from its simplicity, it has overcome the deficiencies and complexities of other tunnel design approaches found in the literature.
5. The use of the proposed empirical approach in Malatya railway tunnel indicated that following a quite accurate rock mass characterization, a reasonable value for the first approximation of rock bolt density would be obtained, and the need for counter-measure or re-design of the reinforcement system will be eliminated.
6. The ability of the bolting system can be best evaluated by normalized convergence ratio which is the fundamental design aid in this analysis. The ratio indicates the amount of convergence reduction in the tunnel achieved by the reinforcement system designed, and thus leading to conclusions about to what degree the convergence of the tunnel can be reduced and whether a redesign and optimization is necessary.
7. It can be inferred from the results of this study that the installation of a sound pattern of bolts immediately after excavation near the tunnel face leads to a much greater degree of stabilization than the provision of supplemental bolting at a later stage. The initial bolting pattern is predominant in controlling the extent of plastic zone around the tunnel and the final tunnel convergence.
8. The link between empirical and analytical approaches makes it possible to design grouted bolts even for non-circular tunnels as has been proved in Malatya tunnel.
9. The flexibility of the proposed elasto-plastic solution makes it possible to simultaneously evaluate the effect of several bolting patterns (with respect to financial and technical availability) for a desired convergence reduction, and finalize the required pattern for such reduction.
10. As a result of elastic-plastic analysis developed here, a guideline relating the rock mass class and grouted bolt design including the pattern and bolt length can be presented for any given tunnel site, and it is recommended to use this guideline in the first stage of tunnel design for a particular site. This guideline will be especially useful in poor and excessively yielding rock masses where regular classification systems (RMR & Q-system) may not provide a sufficiently sensitive and detailed guide for the design.
11. The very poor quality rock masses having Broken Structural Domain (BSTR) types 1 and 2, may behave like cohesionless soil; these rock masses can be classified as extremely poor or completely disintegrated and the use of proposed approach here is not recommended for these ground types since the bolting type support system is not going to be the choice for such rock masses. It is recommended to develop a design approach especially for extremely poor rock mass in future studies.

REFERENCES

1. Adali, S. & Rosel, R. Preliminary assessment of effect of grouted bolts in mine tunnels.Trans. Instn Min. Metall. Vol 89. pp. 190-197.1980.

2. Atlas Copco Rock Drills AB. Numerical approach for evaluation of tunnelling supported by swellex rock bolt. Japan construction method and machinery research institute. 1998.

3. Atlas Copco. MAI, International GmbH, Werkstraße 17, A-9710 Feistritz/Drau.Austria. http://www.mai.co.at/ankere/anker_frame.htm.2004. Last accessed on March 2006.

4. Aydan, Ö., Ichikava, Y. and Kawamoto, T. load bearing capacity and stress distribution in/along rock-bolts with elastic behaviour of interfaces. 5th Int. Conf. Numerical Methods in Geomechanics. Nagoya. 1985.

5. Aydan, Ö. The stabilization of engineering structures by rock bolts. Ph.D Thesis. Nagoya University. Japan. 1989.

6. Aydan, Ö., Akagi, T. and Kawamoto, T. The squeezing potential of rocks around tunnels; theory and prediction. Rock Mech. Rock Eng. 26 (2): 137-163. 1993.

7. Aydan, Ö., Akagi, T. and Kawamoto, T. The squeezing potential of rock around tunnels: theory and prediction with examples taken from Japan. Rock Mech. Rock Eng. 29 (3): 125-143. 1996.

8. Barla, G. Squeezing Rocks in Tunnels, ISRM News Journal, Vol. 2, No. 3 & 4:44-49.1995.

9. Barla, G. Tunnelling under squeezing ground conditions. Euro Summer school on Tunnelling. Institute for Geotechnical and Tunnelling Engineering Technikerstrasse 13 A-6020 Innsbruck, Austria. 2001.

10. Barton, N., Lien. R.and Lunde, J. Engineering classification of rock masses for the design of tunnel support. Rock Mech. Rock Eng. 6 (4): 189-239. 1974.

11. Barton, N. Some new Q value correlations to assist in site characterization and tunnel design. Int J Rock Mech Min Sci. 39:185-216.2002.

12. Bhasin, R. & Grimstad, E. The use of stress-strength relationship in the assessment of tunnel stability. Proc. Recent Advances in Tunnelling Technology, New Delhi, India. 1996.

13. Bieniawski, Z.T. Engineering classification of jointed rock masses. Trans. S. Afr. Inst. Civ. Eng. 15, 335 344. 1973.

14. Bieniawski, Z. T. The point-load test in geotechnical practice. Engineering Geology. Vol 9. pp. 1-11.1975.

15. Bieniawski, Z. T. Rock mass classification of jointed rock masses. Exploration for Rock Engineering, (ed. Z. T. Bieniawski).97-106. Johannesburg. 1976.

16. Bieniawski, Z. T. The geomechanics classification in rock engineering applications. In Proc. 4th Int. Cong. Rock Mech. ISRM, Montreux, Vol. 2, 41-48.1979.

17. Bieniawski, Z.T. Engineering Rock Mass Classification. John Wiley & Sons. New York. 251 pp. 1989.

18. Brady, B.H.G. & Loring, L. Analysis of rock reinforcement using finite difference method. Computers and Geotechnics; 5: 123-149.1988.

19. Brown, E. T., Bray. J. W., Landanyi. B. and Hoek. E. Ground response curves for rock tunnels. J. Geothechnical Engng; 109: 15-39. 1983.

20. Brown, E. T. Analytical and computational methods in engineering rock mechanics. Allen- Unwin. London.1986.

21. Cai, M., Kaiser, P. K. and Minami, M. Characterization of jointed hard rock masses using the GSI system. 39th U.S. Rock Mechanics Symposium. Massachusetts Institute of Technology (MIT).683-690. 2003.

22. Cai, M., Kaiser P.K., Uno, H., Tasaka, Y. and Minami, M. Estimation of rock mass deformation modulus and strength of jointed hard rock masses using the GSI System. Int J Rock Mech Min Sci. 41(1):3–19.2004.

23. Cai, Y., Esaki, T. and Jiang, Y. A rock bolt and rock mass interaction model. Int J Rock Mech Min Sci. 41: 1055–1067. 2004a.

24. Cai, Y., Esaki, T. and Jiang, Y. An analytical model to predict axial load in grouted rock bolt for soft rock tunnelling. Tunnelling and Underground Space Technology; 18: 347-363. 2004b.

25. Cai, Y., Jiang, Y. and Esaki, T. A study of rock bolting design in soft rock. Int J Rock Mech Min Sci. 41. No 3. CD ROM. 2004c.

26. Carranza- Torres, C. Self-similarity amalysis of the elasto-plastic response of underground openings in rock and effects of practical variables. PhD Thesis. The University of Minnesota. 1998.

27. Carranza-Torres, C. & Fairhurst, C. The elasto-plastic response of underground excavations in rock masses that satisfy the Hoek-Brown failure criterion. Int J Rock Mech Min Sci. 36: 777-809.1999.

28. Carranza-Torres, C. & Fairhurst, C. Application of convergence-confinement method of tunnel design to rock masses that satisfy the Hoek-Brown failure criterion. Tunnelling and Underground Space Technology; 15: 187-213. 2000.

29. Carranza-Torres, C. Elasto-plastic solution of tunnel problems using the generalized form of the Hoek-Brown failure criterion. Int J Rock Mech Min Sci. 4: supplement 1, 629-639. 2004.

30. Coates, D. F. & Yu, Y. S. Three dimensional stress distribution around a cylindrical hole and anchor. Proc. 2nd Int. Cong. Rock Mechanics. Vol 2. 175-182. 1970.

31. Cundall, P., Carranza-Torres, C. and Hart, R. A new constitutive model based on the Hoek-Brown failure criterion. Proc. 3rd Int. FLAC Symposium. FLAC and numerical modelling in geomechanics, Sudbury, Canada. 2003.

32. Daemen, J. J. K. Tunnel Supprt Loading Caused by Rock Failure, Ph.D. Thesis, University of Minnesota, Minneapolis, 1975.

33. Deere, D. U. & Deere, D. W. The RQD index in practice. Rock Classification Systems for Engineering Purposes, L. Kirkaldie, ed. ASTM, 91-101. 1988.

34. Detournay, E & John, C. M. Design charts for a deep circular tunnel under non-uniform loading. Rock Mech. Rock Eng. 21: 119-137. 1988.

35. Duan, F. Numerical modelling of cable bolt support systems. Ph. D Theis. The University of Utah. Utah. 1991.

36. Ducan Fama, M. E. Numerical modelling of yield zones in weak rocks. In Comprehensive rock engineering, (ed. J. A. Hudson) Vol 2. 49-75. Oxford: Pergamon. 1993.

37. EN 10083-1. Standard of quenched and tempered steel. British Standard. 2006.

38. Edelbro, C. Rock mass strength: a review. Technical Report, Lulea University of Technology, 132 p. 2003.

39. Fahimifar, A. & Soroush, H. A theoretical approach for analysis of the interaction between grouted rockbolts and rock masses. Tunnelling and Underground Space Technology; 20: 333-343. 2005.

40. Farmer, I. W. Stress distribution along a resin grouted anchor. Int. J. Rock Mech. Min. Sci. Geomech. Abstr. 12: 347-351.1975.

41. Florence, A. L. & Schwer, L. E. Axisymmetric compression of a Mohr-Coulomb medium around a circular hole. Int. J. Numer. Anal. Meth. Geomech; 2: 367-379. 1978.

42. Freeman, T. J. The behaviour of fully-bonded rock bolts in the Kielder experimental tunnel. Tunnels & Tunnelling 10. pp. 37-40. 1978.

43. Ghose, A. K. & Ghosh, C. N. Design of support systems- A methodological approach. Proc. Int. Symposium on Rock Support, (eds. P.K. Kaiser & D.R. McCreath). 43-47. Sudbury, Canada, 1992.

44. Goel, R. K. & Jethwa, J. L. Prediction of support pressure using RMR classification. Proc. Indian Geotechnical Conf., Surat, India. 1991.

45. Goel, R.K. Correlations for Predicting Support Pressures and Closures in tunnels. Ph.D. Thesis, Nagpur University, India. 308 pp. 1994.

46. Goel, R. K., Jethwa, J. L. and Dhar, B. B. Effect of tunnel size on support pressure. Int. J. Rock Mech. Min. Sci. Geomech. Abstr. 33 (7): 749-755.1996.

47. Gokceoglu, C. & Aksoy, H. New approaches to the characterization of clay-bearing, densely joints and weak rock masses. Engineering Geology. Vol 58. pp. 1-23.2000.

48. Grasso, P., Mahtab, A. and Pelizza, S. Riqualificazione della massa rocciosa: un criterio per la stabilizzazione delle gallerie. Gallerie Grandi Opere Sotterranee 29, 35–41. 1989a.

49. Grasso, P., Mahtab A. and Pelizza S. Reinforcing a rock zone for stabilizing a tunnel in complex formations. Proc. Int. Cong. Progress and Innovation in Tunnelling, Vol 2, Toronto, 671-678. 1989b.

50. Graziani, A. & Ribacchi, R. Stato di Sforzo e di Deformazione intorno ad una Galleria sostenuta con Barre Passive, Atti XVIII Convegno Nazionale di Geotecnica, Rimini, AGI, 213-227. 1993

51. Grenon, M. & Hadjigeorgiou, J. Evaluating discontinuity network characterization tools through mining case studies. Soil Rock America 2003, Boston 1, 137–142. 2003.

52. Grimstad, E. & Barton, N. Updating the Q-system for NMT. Int. Symp. Sprayed Concrete, Fagernes, Norway, 46-66. 1993.

53. Hill, R. The mathematical theory of plasticity. Oxford Science Publications. 1950.

54. Hoek, E. & Brown, E.T. Empirical strength criterion for rock masses. J. Geothechnical Engng; 106: 1013-1035. 1980a.

55. Hoek E. & Brown E.T. Underground Excavations in Rock. London: Institution of Mining and Metallurgy 527 pages. 1980b.

56. Hoek, E. Strength of rock and rock masses, ISRM News Journal, 2(2), 4-16. 1994.

57. Hoek, E., Kaiser, P.K. and Bawden, W.F. Support of underground excavation in hard rock, A. A. Balkema. 1995.

58. Hoek, E & Brown, E. T. Practical estimates of rock mass strength. Int J Rock Mech Min Sci. 34(8): 1165-1186. 1997.

59. Hoek, E., Marinos, P. and Benissi, M. Applicability of the Geological Strength Index (GSI) classification for very weak and sheared rock masses. The case of the Athens Schist Formation. Bull. Engg. Geol. Env. 57(2), 151-160. 1998.

60. Hoek, E. Support for very weak rock associated with faults and shear zones. Proc. Int. Symp. Rock Support and Reinforcement Practice in Mining, Kalgoorlie, Australia, 1999.

61. Hoek, E. & Marinos, P. Predicting Tunnel Squeezing. Tunnels and Tunnelling International. Part 1 - November Issue. 45-51, Part 2 - December, 34-36. 2000.

62. Hoek, E. Big tunnels in bad rock. The Thirty-Sixth Karl Terzaghi Lecture. Journal of Geotechnical and Geoenvironmental Engineering. Vol. 127. pp. 726-740. 2001.

63. Hoek, E. Estimates of rock mass strength and deformation modulus. As a part of discussion papers. http://www.rocscience.com/hoek/Hoek.asp. Last accessed on November 2005

64. Hoek, E. Marinos, P, G. and Marinos, V. P. Characterization and engineering properties of tectonically undisturbed but lithologically varied sedimentary rock masses. Int J Rock Mech Min Sci. 42(2): 277-285. 2005.

65. Hoek E., Carranza-Torres C. T. and Corkum, B. Hoek-Brown failure criterion-2002 edition. Proc. 5th North American Rock Mechanics Symposium, Toronto, Canada, Vol. 1. 267–73. 2002.

66. Hollingshead, G. W. Stress distribution in rock anchors. Canadian Geotechnical Journal. 8: 588-592. 1971.

67. Indraratna, B. Application of fully grouted bolts in yielding rock. Ph.D Thesis.University of Alberta. 1987.

68. Indraratna, B. & Kaiser. P. K. Wall convergence in tunnels supported by fully grouted bolts. 28th U.S. Symp. Rock Mechanics. Tuscon, Arizona, 843-852. 1987.

69. Indraratna, B. & Kaiser, P. K. Analytical model for the design of grouted rock bolts. Int. J. Numer. Anal. Meth. Geomech; 14: 227-251. 1990a.

70. Indraratna, B. & Kaiser. P. K. Design for grouted rock bolts based on the convergence control method. Int. J. Rock Mech. Min. Sci. Geomech. Abstr. 27: 269-281. 1990b.

71. ISRM. (International Society for Rock Mechanics). ISRM Suggested method: Rock Characterization, Testing and Monitoring, (ed. E. T. Brown), London: Pergamon Press. 1981.

72. ITASCA Consulting Group, Inc. FLAC2D (Fast Lagrangian Analysis of Continua) Version 4.0. www. itascacg.com , Minneapolis. 2000. Last accessed on September 2005.

73. Jethwa, J.L., Dube, A. K., Singh, B. and Singh, B. Rock Load Estimation for Tunnels in Squeezing GroundConditions, RETC, San Francisco, 1981.

74. John, C. M., Detournay, E. and Fairhurst, C. Design charts for a deep circular tunnel under non-hydrostatic loading. 25th Symp. rock mechanics in rock mechanics in productivity and production. 849-856. 1984.

75. Kaiser, P. K., Guenot, A. and Morgenstern, N. L. Deformation of small tunnels; part 4: behaviour during failure. Int. J. Rock Mech. Min. Sci. Geomech. Abstr. 22: 141-152. 1985.

76. Kastner, H. Statik des tunnel-und Stollenbaues. Springer, Berlin- Göttingen. 1962.

77. Labiouse, V. Ground response curves for rock excavations supported by ungrouted tensioned rockbolts. Rock Mech. Rock Eng. 29 (2): 19–38. 1996.

78. Ladanyi, B. Use of long-term strength concept in the determination of ground pressure on tunnel linings. Proc. 3rd Cong. ISRM. Denver, Vol 2B, 1150-1156.1974.

79. Laubscher, D. H. Geomechanics Classification of Jointed Rock Masses-Mining Applications. Trans. Instn. Min. Metall. 86, A-1-A-7. 1977.

80. Littlejohn, G.S. & Bruce, D.A. Rock Anchors - State of the Art- Grouting engineering, Part 1, 2, and 3. Design, Construction, and Stressing and testing. 1975.

81. Lunardi, P. The design and construction of tunnels using the approach based on the analysis of controlled deformation in rocks and soils. Tunnels and Tunnelling Int., special supplement.May. 2000.

82. Marinos, P.G. & Hoek, E. GSI: A geological friendly tool for rock mass strength estimation, Proc. Int. Conf. Geotechnical & Geological Engineering (GeoEng 2000), 1422-1440, Melbourne, 2000.

83. Marinos. P, & Hoek, E. Estimating the geotechnical properties of heterogeneous rock masses such as flysch, Bull. Engg. Geol. Env. 60, 85-92. 2001.

84. Marinos, V., Marinos, P. & Hoek, E. The geological strength index: applications and limitations. Bull. Engg. Geol. Env. 64(1), 55-65. 2005.

85. Maple V 9.General purpose commercial mathematics software package. Waterloo Maple Inc. 2003.

86. Mathematica V 5.1. Computer algebra system package. Wolfram Research. 2004.

87. Mathis, J. I. & Page, C. H. Drifting in very poor rock-experience and analysis. Presented at the 101st annual Northwest mining association convention, Spokane, Washington, December 6-8. 1995.

88. McNiven, H. D & Ewoldsen, H. N. Rockbolting of tunnels for structural support- in two parts. Int. J. Rock Mech. Min. Sci. Geomech. Abstr. 6: 467-497. 1969.

89. Michelis, P. & Brown, E. T. A yield equation for rock. Canadian Geotechnical Journal. 23: 9-17. 1986.

90. Morales, T., Etxebarria, G., Uriarte, J. and Valderrama, I. Geomechanical characterization of rock masses in Alpine region: the Basque Arc (Basque-Cantabrian basin, Northern Spain). Engineering Geology. Vol 71. pp. 343-362. 2004.

91. Nitzsche, R. N. & Haas, C. J. Installation induced stresses for grouted roof bolts. Int. J. Rock Mech. Min. Sci. Geomech. Abstr. 13: 17-24. 1976.

92. Ogawa, T. & Lo, K. Y. Effect of dilatancy and yield criteria on displacement around tunnels. Canadian Geotechnical Journal. 24: 100-113. 1987.

93. Oreste, P. P. & Peila, D. Radial passive rockbolting in tunnelling design with a new convergence- confinement model. Int. J. Rock Mech. Min. Sci. Geomech. Abstr. 33: 443-454.1996.

94. Oreste, P. P. Nuovi modelli di calcolo delle stratture di rinforzo e precontenimento in galleria. Ph.D. Thesis. Politecnco di Torino. 1995.

95. Oreste, P. P. Il metodo convergenza-cofinamento: ruolo e limiti nella moderna progettazione geotecnica delle gallerie, Gallerie e grandi opere sotterranee. 66:34–50. 2002.

96. Oreste. P. P. Analysis of structural interaction in tunnels using the covergence–confinement approach. Tunnelling and Underground Space Technology; 18: 347-363. 2003.

97. Osgoui, R. & Ünal, E. Rock reinforcement design for unstable tunnel originally excavated in poor rock mass. Proc. World Tunnel Congress and 31st ITA Assembly. 291-296. Turkey. 2005a.

98. Osgoui, R. & Ünal, E. Characterization of Weak Rock Masses Using GSI and the Estimation of Support Pressure. 40th U.S. Rock Mechanics Symposium - June 25-29, Anchorage, Alaska. 2005b.

99. Osgoui, R. On the Assessment of the effect of the anisotropy in in-situ stress on support pressure in tunnels. Proc. Int. Symp. In-Situ Rock Stress, Trondheim, Norway. 2006a.

100. Osgoui, R. Ground Reaction Curve of reinforced tunnel using a new elasto-plastic model. Post Graduate Thesis. Politecnico di Torino. Italia. 2006b.

101. Özkan, I. Modified rock mass rating (M-RMR) system and roof behaviour model. Ph.D. Thesis. Middle East Technical University, Ankara. 370 pp. 1995.

102. Palmström, A. The volumetric joint count – A useful and simple measure of the degree of rock mass jointing. In: IAEG Congress, New Delhi. 221- 228. 1982.

103. Palmström, A. RMi – A rock mass characterization system for rock engineering purposes. Ph.D. Thesis, University of Oslo. 400 pp. 1995.

104. Palmström A. Characterizing rock masses by the RMi for use in practical rock engineering, Part 1: the development of the rock mass index (RMi). Tunnelling and Underground Space Technology; 11: 175–188. 1996.

105. Palmström A. Recent developments in rock support estimates by the RMi. Journal of Rock Mechanics and Tunelling Technology; 6(1): 1-19. 2000.

106. Palmström, A. Block size and shape. International workshop on Rock mass Strength, 17th March 2005 in Lulea, Sweden. 2005a.

107. Palmström, A. Measurements of and correlations between block size and rock quality designation (RQD). Tunnelling and Underground Space Technology; 20: 362-377. 2005b.

108. Palmström, A. & Broch, E. Use and misuse of rock mass classification systems with particular reference to the Q-system. Tunnelling and Underground Space Technology; 21: 575-593. 2006.

109. Pan, Y. W. & Chen, Y. M. Plastic zones and characteristics-line families for openings in elasto-plastic rock mass. Rock Mech. Rock Eng. 23: 275-292.1990.

110. Pande, G. N. & Gerrard, C. M. The bahavior of jointed rock masses under various simple loading states. Proc. 5th Cong. ISRM. Melbourne. 217-223. 1983.

111. Panet, M. & Guenot, A. Analysis of convergence behind the face of a tunnel. Proc. Tunnelling' 82. pp 197-204. Brighton. 1982.

112. Panet, M. Understanding deformations in tunnels. In comprehensive rock engineering, (ed. J. A. Hudson) Vol1, 663-690. Oxford: Pergamon. 1993.

113. Papanastassopoulou, F. Investigation of effect of rock bolts on stress distribution around underground excavations. Proc. Int. Symp. Rock Bolting (ed. O. Stephansson), Abisko, Sweden. 55-63. 1983.

114. Pariseau, W. G. & Duan, F. Progress and problems in cable bolt design. Proc. 7th Annual Workshop. Generic Mineral Technology Center. Mine system design and ground control. Virginia Polytechnical Institute and State University. Blacksburg. 23-34.1989.

115. Pariseau, W. G. & Moon, H. Elastic moduli of well-jointed rock masses. Proc. 6th Int. Conf. Numerical Methods in Geomechanics. Innsbruck. Austria. 1988.

116. Park, K, H. & Kim, Y, J. Analytical solution for a circular opening in an elastic–brittle–plastic rock. Int J Rock Mech Min Sci. 43: 616-622. 2006.

117. Peila, D. & Oreste, P. P. Axisymmetric analysis on ground reinforcing in tunnelling design. Computers and Geotechnics ; 17: 253-274. 1995.

118. Pelizza, S., Kim, S. and Kim, J. A study of strength parameters in the reinforced ground by rock bolts. Proc. World Tunnel Congress and 32nd ITA Assembly, Seoul, Korea. 06-0385. 2006.

119. Peng, S. S. & Guo, S. An improved numerical model of grouted bolt-roof rock interaction in underground openings. Rock support in mining and underground construction. Balkema.1992.

120. Press, W. H., Flannery, B. P., Teukolsky, S. A. and Vetterling, W. T. Numerical Recipies in C. The art of scientific computing (Second ed.). New York: Cambridge University Press. 1994.

121. Priest, S. D. & Hudson, J. A. Discontinuity spacing in rock. Int. J. Rock Mech. Min. Sci. Geomech. Abstr. 13: 135-148. 1976.

122. Protodyakonov, N. M. Firmness coefficient for estimation of rock loads. Anonymous reference. 1964.

123. Rabcewicz, L.V. The New Austrian Tunnelling Method. Water Power, Part 1, November 1964, pp. 511-515, Part 2. 1195-1197. 1964 & 1965.

124. Rocscience. Roclab Program: rock mass strength analysis using the Hoek-Brown failure criterion. Rocscience Inc., www.rocscience.com Toronto, Ontario, Canada. 2005a. Last accessed on September 2005.

125. Rocscience. A 2-D finite element program for calculating stresses and estimating support around the underground excavations. Geomechanics Software and Research, Rocscience Inc., www.rocscience.com Toronto, Ontario, Canada. 2005b. Last accessed on September 2005

126. Sakurai, S. Displacement measurements associated with the design of underground openings. Proc. Int. Symp. Field measurements in geomechanics, Zurich 2, 1163- 1178. 1983.

127. Senseny, P. E., Lindberg, H. E. and Schwer, L. E. Elastic-plastic response of a circular hole to repeated loading. Int. J. Numer. Anal. Meth. Geomech; 13: 459-476.1989.

128. Sharan, S. K. Elastic-brittle-plastic analysis of circular openings in Hoek-Brown media. Int J Rock Mech Min Sci. 40:817-824. 2003.

129. Sharan, S. K. Exact and approximate solutions for displacements around circular openings in elastic–brittle–plastic Hoek–Brown rock. Int J Rock Mech Min Sci. 42:542–549. 2005.

130. Sheorey, P. R. Support pressure estimation in failed rock conditions. Engineering Geology. Vol 22. pp. 127-140. 1985.

131. Singh, B., Jethwa, J. L., Dube, A. K. and Singh, B. Correlation between observed support pressure and rock mass quality. Tunnelling and Underground Space Technology; 7: 59-74. 1992.

132. Singh, B., Goel, R. K., Jethwa, J. L. and Dube, A. K. Support pressure assessment in arched underground openings through poor rock masses. Engineering Geology. Vol 48. pp. 59-81. 1997.

133. Sönmez, H. & Ulusay, R. Modifications to the geological strength index (GSI) and their applicability to stability of slopes. Int J Rock Mech Min Sci. 36:743–60. 1999.

134. Sönmez, H. & Ulusay, R. A discussion on the Hoek-Brown failure criterion and suggested modification to the criterion verified by slope stability case studies. Yerbilimleri (Earth sciences); 26:77–99. 2002.

135. Sönmez, H., Gokceoglu, C. & Ulusay, R. Indirect determination of the modulus of deformation of rock masses based on the GSIsystem. Int J Rock Mech Min Sci. 41: 849-857. 2004.

136. St John, C. M. & Van Dillen, D. E. Rockbolts: A new numerical representation and its application in tunnel design. Proc. 24th U.S. Symp. Rock Mech. Texas A & M University. 13-25. 1983.

137. Stille, H. Theoretical aspects on the difference between prestressesd anchor bolt and grouted bolt in squeezing rock. Proc. Int. Symp. Rock Bolting (ed. O. Stephansson), Abisko, Sweden. 65-73. 1983.

138. Stille, H., Holmberg, M. & Nord, G. Support of weak rock with grouted bolts and shotcrete. Int. J. Rock Mech. Min. Sci. Geomech. Abstr. 26 (1): 99-113. 1989.

139. Sülükçü, S. & Ulusay, R. Evaluation of the block punch index test with prime consideration on size effect, failure mechanism and its effectiveness in predicting rock strength. Int J Rock Mech Min Sci. 38:1091 – 1111. 2001.

140. Şen, Z. & Eissa, E. A. Volumetric rock quality designation. J. Geothechnical Engng; 117: 1331–1346. 1991.

141. Şen, Z. & Eissa, E. A. Rock quality charts for log-normally distributed block sizes. Int. J. Rock Mech. Min. Sci. Geomech. Abstr. 29: 1-12. 1992.

142. Tablore, J. La Mécanique des Roches. Dunod. Paris. 1957.

143. Terzaghi, K. Rock defects and load on tunnel supports. In: Proctor, R.V., White, T.C. (Eds.). Introduction to Rock Tunnelling with Steel Support.Youngstava, OH, USA. 1946.

144. Timoshenko, S. P. & Goodier, J. N. Theory of Elasticity. 3rd Edition. McGraw Hill, New York. 1970.

145. TUSC. Tunnelling and Underground Space Center. Technical University of Turin. Italy. 2006.

146. Tutluoglu, L. Rock Mechanics for Civil Engineers “MinE 527”. Lecture Notes. Middle East Technical University. Ankara. 2002.

147. Ulusay, R. & Gokçeoğlu, C. A new set procedure for the determination of the Block Punch Index and its possible uses in rock engineering. ISRM news Journal; 6(1): 50-54. 1999.

148. Ulusay, R., Gokçeoğlu, C. & Sülükçü, S. Draft ISRM suggested method for determining block punch strength index (BPI). Int J Rock Mech Min Sci. 38:1113 – 1119. 2001.

149. Ünal, E. Development of design guidelines and roof control standards for coal mine roofs, Ph.D. Thesis. The Pennsylvania State University. Department of Mineral Engineering. State College. 355 pp.1983.

150. Ünal, E. Rock reinforcement design and its application in mining. Proc. Int. Symposium on Rock Support, (eds. P.K. Kaiser & D.R. McCreath). 541-546. Sudbury, Canada, 1992.

151. Ünal, E. Modified rock mass classification: M-RMR system. Milestone in Rock Engineering: A Jubilee Collection; Z. T. Bieniawski, Editor; Balkema, 203-223. 1996.

152. Ünal, E. Workshop on rock mass classification in TUPRAG open-pit gold mine. Middle East Technical University. Ankara, 2002.

153. Venkateswarlu, V. Geomechanics classification of coal measure rocks vis-à-vis roof supports. Ph.D. Thesis. Indian School of Mines, Dhanbad. 1986.

154. Verman, M. Rock mass-tunnel support interaction analysis, Ph.D. Thesis. University of Roorkee, Roorkee, India. 1993.

155. Voegele, M. D. & Fairhurst. C. A numerical study of excavation support loads in jointed rock masses. The 23rd Symposium on Rock Mechanics. The University of California, Berkeley. 673-683. 1982.

156. Waner, S. & Costenoble, S. R. Numerical Integration-miscellaneous on-line topics for calculus applied to the real world, Department of Mathematics. Hofstra University. 2006.

157. Wang, Y. Ground response of a circular tunnel in poorly consolidated rock. J. Geothechnical Engng; 122: 703-708. 1996.

158. Ward. W. H., Tedd. P. & Berry. N. S. M. The Kielder experimental tunnel: final results. Géotechnique 33: 275-291. 1983.

159. Whittaker, B. N., Smith, S. F. and Matheson, G. D. Influence of in-situ stress field on the stability of mine tunnels. Proc. ISRM Symposium: Eurock'92 Rock Characterization, (ed. J. A. Hudson). 227-232. London. 1992.

160. Wickham, G. E. & Tiedmann, H. R. Research in ground support and its evaluation for coordination with system analysis in rapid excavation: report to the Advanced Research Projects Agency. Dept. of Defense, Contract No. Bureau of Mines H 021 0038 NTIS No. AD 743 100. 1972.

161. Wickham, G. E. & Tiedmann, H. R. Ground support prediction model- RSR Concept. Report to the Advanced Research Projects Agency. Dept. of Defense, Contract No. Bureau of Mines H 022 0075 NTIS No. AD 773 018. 1974.

162. Xueyi, S. Grouted rock bolt used in underground engineering in soft surrounding rock or in highly stressed regions. Proc. Int. Symp. Rock Bolting (ed. O. Stephansson), Abisko, Sweden. 93-99. 1983.

163. Yamatomi, J. & Amano, K. A study on the supporting capacity of grouted rock-bolts. Proc. Int. Symp. Mining Technology & Science. Mining Construction Section. China. 1985.

164. Yu, T. Z. & Xian, C. J. Behaviour of rock bolting as tunnelling support. Proc. Int. Symp. Rock Bolting (ed. O. Stephansson), Abisko, Sweden. 87-92. 1983.

165. Zienkiewicz, O. C. & Pande, G. N. Time dependent multi-laminate model of rock- a numerical study of deformation and failure of jointed rock masses. Int. J. Numer. Anal. Meth. Geomech; 1: 219-24. 1977.

APPENDIX A

MATHEMATICAL TREATMENTS USED IN ELASTO-PLASTIC SOLUTION

Determination of radial stress in the plastic zone

The following ordinary non-linear differential equation is to be solved:

$$\frac{d\sigma_r}{dr} - \frac{\sigma'_{ci}(m_b' \frac{\sigma_r}{\sigma'_{ci}} + s')^{a'}}{r} = 0 \qquad (5\text{-}19)$$

If $d\sigma_r = dy$, $dr = dx$, $\frac{m'_b}{\sigma'_{ci}} = c$, $\sigma'_{ci} = b$, $s' = d$, and $a' = a$

The Equation 5-19 can be written in the normal mathematical notation as:

$$\frac{dy}{dx} - \frac{b \cdot (c \cdot y + d)^a}{x} = 0$$

Using MATHEMATICA program (Mathematica V 5.1., 2004), the solution of the above equation is:

$$y = \frac{-d + [(ac - c)(-C_1 - b \ln x)]^{\frac{1}{1-a}}}{c} \qquad (A\text{-}1)$$

To find the constant (C_1), one must apply the boundary condition. If at $r = r_i$, $\sigma_r = 0$ or (at $x = x'$, $y = 0$), then:

$$C_1 = -b \ln x' - \frac{d^{1-a}}{(ac - c)} \qquad (A\text{-}2)$$

Substituting the Equation 3 into Equation 2 and simplifying yield:

$$y = \frac{\left[d^{1-a} - bc(a-1)\ln(\frac{x}{x'}) \right]^{\frac{1}{1-a}} - d}{c}$$

or

$$\sigma_r = \frac{\Gamma - s'}{\frac{m_b'}{\sigma_{ci}'}} \tag{5-20}$$

$$\Gamma = \left[s'^{1-a'} - m_b'(a'-1)\ln\left(\frac{r}{r_i}\right) \right]^{\frac{1}{1-a'}} \tag{5-21}$$

Determination of radial stress in the plastic zone considering the effect of the fictitious support pressure at tunnel boundary

In this case, only the boundary condition to be applied for Equation 5-19 must be changed to find the new function of radial stress.

If at $r = r_i$, $c_r = P_i$ or (at $x = x'$, $y = P$), the constant (C_1) can be determined as:

$$C_1 = -b\ln x' - \frac{(cp+d)^{1-a}}{ac - c} \tag{A- 3}$$

Substituting Equation A-3 into Equation A-1 and simplifying brings about:

$$y = \frac{\left[(cp+d)^{1-a} - bc(a-1)\ln(\frac{x}{x'}) \right]^{\frac{1}{1-a}} - d}{c}$$

or

$$\sigma_r = \frac{\frac{\Omega}{\sigma'_{ci}} - s'}{\frac{m'_b}{\sigma'_{ci}}} \tag{5-22}$$

$$\Omega = \left[(m'_b P_i + \sigma'_{ci} s')^{1-a'} - m'_b (a'-1) \sigma'^{1-a'}_{ci} \ln\left(\frac{r}{r_i}\right) \right]^{\frac{1}{1-a'}} \tag{5-23}$$

Numerical integration method used in elastic-plastic solution

In order to evaluate the integration stems from the solution of the differential equation of plastic strain (Equation 5-50 and 5-78), the use of one of numerical solutions is required. The Simpson's rule is chosen to solve the integration approximately (Waner & Costenoble, 2006). The integration which must be solved numerically is:

$$\left[\int_r^{r_e} r^{N_\psi - 1} \left[s'^{1-a'} + m_b{}' (1-a') \ln\left(\frac{r}{r_i}\right) \right]^{\frac{a'}{1-a'}} dr \right] \tag{A- 4}$$

The fundamental theorem of calculus gives us an exact formula for computing $\int_a^b f(x)\,dx$, provided that an antiderivative for f is found. This method of evaluating definite integrals is called the analytic method. However, there are times when this is difficult or impossible. In these cases, it is usually good enough to find an approximate or numerical solution, and there are some very straightforward ways to do this.

Simpson's rule is a Newton-Cotes formula for approximating the integral of a function *f* using quadratic polynomials (i.e., parabolic arcs instead of the straight line segments used in the trapezoidal rule). First, the interval [a, b] must be partitioned into intervals all of the same width with the use of an even number of intervals, so *n* will be even. In particular, let the function f be tabulated at points x_0, x_1, and x_2 equally spaced by distance $\frac{(b - a)}{n}$, and denote $f_n = f(x_n)$. Then Simpson's rule states that if n is even then

$$x_k = a + k\Delta x = a + k\frac{(b - a)}{n} \tag{A- 5}$$

$$\int_a^b f(x)dx \approx \frac{b-a}{3n}\left[\begin{matrix} f(x_0)+4f(x_1)+2f(x_2)+4f(x_3)+ \\ \ldots+2f(x_{n-2})+4f(x_{n-1})+f(x_n) \end{matrix}\right] \qquad \text{(A- 6)}$$

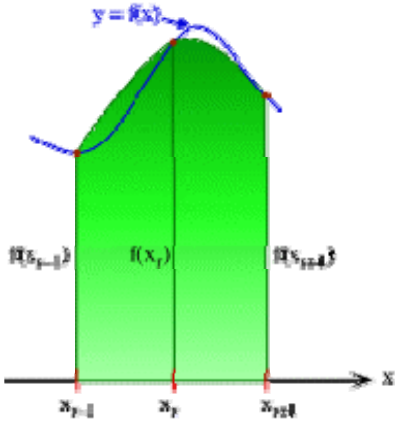

Figure A-1 The function *f*(*x*) (in blue) is approximated by a quadratic function *P*(*x*) (Waner & Costenoble, 2006)

It is necessary to approximate the areas in each strip and to draw a parabola through the three points $(x_{k-1}, f(x_{k-1}))$, $(x_k, f(x_k))$, and $(x_{k+1}, f(x_{k+1}))$, as shown in Figure A-1. It is then not too difficult to find the equation of this parabola (it has the form $y = Ax^2+Bx+C$), and from that to find the area underneath by integrating. The remarkably simple answer is:

$$\text{Area under parabola } \boldsymbol{P(x)} = \frac{b-a}{3n}\left[f(x_{k-1})+4f(x_k)+f(x_{k+1})\right] \qquad \text{(A- 7)}$$

When we add the area under the parabola over the first two strips to the area under the parabola over the 3rd and 4th strips, and so on, we get Simpson's rule.

Considering the parameters included in Table 5-2, the approximate result of the integration A-1 used in elasto-plastic solution will be 0.84451.

APPENDIX B

DETERMINATION OF THE EXTENT OF PLASTIC ZONE (YIELDING)

The categories I to III of the Equivalent Plastic Zones have been diagrammatically illustrated in Figure 5-14. A complete analysis of category I and a general discussion of categories II and III have been presented in section 5.15. The mathematical treatment of categories II and III is presented in detail here.

Determination of the Equivalent Plastic Zone Category II

The condition of major yielding, $\rho < r_i^* < (r_i+L_b)$, occurs when the extent of the plastic zone has propagated beyond the neutral point. In this situation, the plastic zone itself is divided by the neutral point into two zones. Consequently, only the plastic zone region that falls within the pick-up length of the bolt is effectively stabilized by the positive shear stresses.

Zone 1 : $r_i < r < \rho$

This region is the inner yielded zone confined between the tunnel boundary and the neutral point. The equivalent stresses in this region are given by equations identical to those of zone 1 of category I:

$$\sigma_r = \frac{\Gamma^* - s^*}{\frac{m_b^*}{\sigma_{ci}^*}} \tag{5-61}$$

$$\Gamma^* = \left[s^{*1-a} - m_b^*(a-1)\ln\left(\frac{r}{r_i}\right)\right]^{\frac{1}{1-a}} \tag{5-62}$$

$$\sigma_\theta = \sigma_r + \sigma_{ci}^*\left(m_b^* \frac{\sigma_r}{\sigma_{ci}^*} + s^* \right)^a \tag{5-63}$$

at $r = \rho$

then $\sigma_r = \sigma\rho$ .i.e :

$$\sigma_\rho = \frac{\Gamma^* - s^*}{\frac{m_b^*}{\sigma_{ci}^*}} \tag{B- 1}$$

$$\Gamma^* = \left[s^{*1-a} - m_b^*(a-1)\ln\left(\frac{\rho}{r_i}\right)\right]^{\frac{1}{1-a}} \tag{B- 2}$$

Zone 2 : $\rho < r < r_e^*$

This is the outer plastic zone beyond the neutral point in the anchor length where the negative shear stresses are created so as to ensure the equilibrium with the positive shear stresses formed on the pick-up length. The plastic stresses in this zone are obtained as follows. In order to determine the plastic stresses in this region first the stress equilibrium Equation 5-19 has to be solved using the boundary condition of at $r = \rho$, $\sigma_r = \sigma\rho$.

Therefore the stresses field will be:

$$\sigma_r = \frac{\frac{\xi}{\sigma_{ci1}} - s_1}{\frac{m_{b1}}{\sigma_{ci1}}} \tag{B- 3}$$

$$\xi = \left[(m_{b1}\sigma_\rho + \sigma_{ci1}s_1)^{1-a'} - m_{b1}(a'-1)\sigma_{ci1}{}^{1-a'}\ln\left(\frac{r}{\rho}\right)\right]^{\frac{1}{1-a'}} \tag{B- 4}$$

and

$$\sigma_\theta = \sigma_r + \sigma_{ci1}\left(m_{b1}\frac{\sigma_r}{\sigma_{ci1}} + s_1 \right)^{a'} \tag{B- 5}$$

where

$$m_{b1} = (1-\beta)m_b' ,\ s_1 = (1-\ \beta)s' \tag{B- 6}$$

$$\sigma_{ci1} = (1-\beta)\sigma_{ci}' ,\ c'_{ci} = S.c_{ci}$$

Zone 3 : $r_e^* < r < r_i + L_b$

This is the inner elastic zone within the reinforced region which surrounds the yielded zone. The equivalent elastic stresses in this zone are represented by the following equations:

$$\sigma_r = P_o\left[1-\left(\frac{r_e^*}{r}\right)^2\right]+\sigma_{re}\left(\frac{r_e^*}{r}\right)^2 \qquad \text{(B- 7)}$$

$$\sigma_\theta = P_o\left[1+\left(\frac{r_e^*}{r}\right)^2\right]-\sigma_{re}\left(\frac{r_e^*}{r}\right)^2 \qquad \text{(B- 8)}$$

The peak tangential and radial stresses at elastic-plastic boundary are obtained as:

$$\sigma_{\theta e} - \sigma_{re} = \sigma_{ci}\left(m_b\frac{\sigma_{re}}{\sigma_{ci}}+s\right)^a \qquad \text{(5-30)}$$

$$\sigma_{re} = P_o + \frac{m_b c_{ci}}{8} - \frac{1}{8}\sqrt{16P_o m_b\sigma_{ci} + m_b{}^2\sigma_{ci}{}^2 + 16\sigma_{ci}{}^2 s} \qquad \text{(5-32)}$$

Zone 4 : $r > (r_i + L_b)$

This is the outer undisturbed elastic zone beyond the reinforced zone. The elastic stress fields in this zone are given by:

$$\sigma_r = P_o\left[1-\left(\frac{r_i+L_b}{r}\right)^2\right]+\sigma_{L_b}\left(\frac{r_i+L_b}{r}\right)^2 \qquad \text{(B- 9)}$$

$$\sigma_\theta = P_o\left[1+\left(\frac{r_i+L_b}{r}\right)^2\right]-\sigma_{L_b}\left(\frac{r_i+L_b}{r}\right)^2 \qquad \text{(B- 10)}$$

where

$$\sigma_{L_b} = P_o\left[1-\left(\frac{r_e^*}{r_i+L_b}\right)^2\right]+\sigma_{re}\left(\frac{r_e^*}{r_i+L_b}\right)^2 \qquad \text{(B- 11)}$$

Equivalent Plastic Zone (EPZ)

At the elastic-plastic interface, the assumption of continuity of radial stress yields:

From elastic part:

$$\sigma_{re} = P_o + \frac{m_b c_{ci}}{8} - \frac{1}{8}\sqrt{16P_o m_b \sigma_{ci} + m_b{}^2\sigma_{ci}{}^2 + 16\sigma_{ci}{}^2 s} \qquad \text{(5-32)}$$

From plastic part:

$$\sigma_{re} = \frac{\frac{\xi}{\sigma_{ci1}} - s_1}{\frac{m_{b1}}{\sigma_{ci1}}} \qquad \text{(B- 12)}$$

$$\xi = \left[(m_{b1}\sigma_\rho + \sigma_{ci1}s_1)^{1-a'} - m_{b1}(a'-1)\sigma_{ci1}{}^{1-a'}\ln\left(\frac{r_e^*}{\rho}\right)\right]^{\frac{1}{1-a'}} \qquad \text{(B- 13)}$$

Equating and simplifying the above equations leads to the following equations:

$$\frac{r_e^*}{\rho} = e^J \qquad \text{(B- 14)}$$

where

$$J = \frac{(m_{b1}\sigma_\rho + \sigma_{ci1}s_1)^{1-a'} - \left[s_1\sigma_{ci1} + P_o m_{b1} + \frac{m_b m_{b1}\sigma_{ci}}{8} - \frac{m_{b1}}{8}(16P_o m_b\sigma_{ci} + m_b^2\sigma_{ci}^2 + 16\sigma_{ci}^2 s)^{\frac{1}{2}}\right]^{1-a'}}{m_{b1}(a'-1)\sigma_{ci1}{}^{(1-a')}} \qquad \text{(B- 15)}$$

where

$$\sigma_\rho = \frac{\Gamma^* - s^*}{\frac{m_b^*}{\sigma_{ci}^*}} \tag{B-1}$$

$$\Gamma^* = \left[s^{*1-a} - m_b^*(a-1)\ln\left(\frac{\rho}{r_i}\right)\right]^{\frac{1}{1-a}} \tag{B-2}$$

The above equationS can be written as follows to make the interest form

$$\frac{\rho}{r_i} = e^h \tag{B- 16}$$

$$h = \frac{s^{*\,1-a} - \Gamma^{*1-a}}{m_b^*(a-1)} \tag{B- 17}$$

The production of the Equations B-14 and B-16 yields normalized radius of the equivalent plastic zone (EPZ):

$$\frac{r_e^*}{r_i} = e^J \cdot e^h = e^{(J+h)} \tag{B- 18}$$

Determination of the Equivalent Plastic Zone Category III

The condition of excessive yielding, $r_e^* > (r_i + L_b)$, occurs either due to large *in-situ* stress in relatively poor rock or as a result of inadequate bolt length. In this situation, the bolt is completely embedded in the yielded rock and no anchorage is provided from the outer elastic zone.

Zone 1 : $r_i < r < \rho$

The equivalent radial and tangential stress fields for this inner plastic zone (pick-up length region) are depicted by the same equations corresponding to zone 1 of category II:

$$\sigma_r = \frac{\Gamma^* - s^*}{\frac{m_b^*}{\sigma_{ci}^*}} \tag{5-61}$$

$$\Gamma^* = \left[s^{*1-a} - m_b^*(a-1)\ln\left(\frac{r}{r_i}\right)\right]^{\frac{1}{1-a}} \tag{5-62}$$

$$\sigma_\theta = \sigma_r + \sigma_{ci}^*\left(m_b^* \frac{\sigma_r}{\sigma_{ci}^*} + s^* \right)^a \tag{5-63}$$

at $r = \rho$

then $\sigma_r = \sigma\rho$ .i.e :

$$\sigma_\rho = \frac{\Gamma^* - s^*}{\frac{m_b^*}{\sigma_{ci}^*}} \tag{B-1}$$

$$\Gamma^* = \left[s^{*1-a} - m_b^*(a-1)\ln\left(\frac{\rho}{r_i}\right)\right]^{\frac{1}{1-a}} \tag{B-2}$$

where:

$$m_b^* = (1+\beta)m_b',\ s^* = (1+\beta)s'$$

$$\sigma_{ci}^* = (1+\beta)\sigma_{ci}',\ c'_{ci} = S.c_{ci}$$

Zone 2 : $\rho < r < (r_i + L_b)$

This is the middle plastic zone which is confined to the anchor length of the bolted region. The stress fields are given by the same equations associated with the zone 2 of category II:

$$\sigma_r = \frac{\frac{\xi}{\sigma_{ci1}} - s_1}{\frac{m_{b1}}{\sigma_{ci1}}} \tag{B-3}$$

$$\xi = \left[(m_{b1}\sigma_\rho + \sigma_{ci1}s_1)^{1-a'} - m_{b1}(a'-1)\sigma_{ci1}^{\ 1-a'}\ln\left(\frac{r}{\rho}\right)\right]^{\frac{1}{1-a'}} \tag{B-4}$$

and

$$\sigma_\theta = \sigma_r + \sigma_{ci1}\left(m_{b1}\frac{\sigma_r}{\sigma_{ci1}} + s_1 \right)^{a'} \tag{B-5}$$

where

$$m_{b1} = (1-\beta)m_b',\ s_1 = (1-\beta)s' \tag{B-6}$$

$$\sigma_{ci1} = (1-\beta)\sigma_{ci}',\ c_{ci}' = S.c_{ci}$$

at $r = r_i + L_b$

then $\sigma_r = \sigma_L$

$$\sigma_L = \frac{\frac{\xi}{\sigma_{ci1}} - s_1}{\frac{m_{b1}}{\sigma_{ci1}}} \tag{B- 19}$$

$$\xi = \left[(m_{b1}\sigma_\rho + \sigma_{ci1}s_1)^{1-a'} - m_{b1}(a'-1)\sigma_{ci1}^{\,1-a'} \ln\left(\frac{r_i + L_b}{\rho} \right) \right]^{\frac{1}{1-a'}} \tag{B- 20}$$

Zone 3 : $(r_i + L_b) < r < r_e^*$

This region is the outer plastic zone beyond the reinforced region and its equivalent stresses are represented by:

$$\sigma_r = \frac{\frac{\eta}{\sigma_{ci}'} - s'}{\frac{m_b'}{\sigma_{ci}'}} \tag{B- 21}$$

$$\eta = \left[(m_b'\sigma_{L_b} + \sigma_{ci}'s')^{1-a'} - m_b'(a'-1)\sigma_{ci}'^{\,1-a'} \ln\left(\frac{r}{r_i + L_b} \right) \right]^{\frac{1}{1-a'}} \tag{B- 22}$$

$$\sigma_\theta = \sigma_r + \sigma'_{ci}\left(m'_b \frac{\sigma_r}{\sigma'_{ci}} + s' \right)^{a'} \tag{5-18}$$

where σ_L and σ_ρ are readily obtained from Equations B-19 and B-1 , respectively.

Zone 4 : $r > r_e^*$

This is the elastic region surrounding the plastic zone. The elastic stress fields are given by the same expressions pertaining to the zone 3 of category II:

$$\sigma_r = P_o\left[1 - \left(\frac{r_e^*}{r}\right)^2\right] + \sigma_{re}\left(\frac{r_e^*}{r}\right)^2 \tag{B-7}$$

$$\sigma_\theta = P_o\left[1 + \left(\frac{r_e^*}{r}\right)^2\right] - \sigma_{re}\left(\frac{r_e^*}{r}\right)^2 \tag{B-8}$$

Equivalent Plastic Zone (EPZ)

At the elastic-plastic interface, the assumption of continuity of radial stress yields:

From elastic part:

$$\sigma_{re} = P_o + \frac{m_b \sigma_{ci}}{8} - \frac{1}{8}\sqrt{16 P_o m_b \sigma_{ci} + m_b{}^2 \sigma_{ci}{}^2 + 16 \sigma_{ci}{}^2 s} \tag{5-32}$$

From plastic part:

$$\sigma_{re} = \frac{\dfrac{\eta}{\sigma'_{ci}} - s'}{\dfrac{m'_b}{\sigma'_{ci}}} \tag{B- 23}$$

$$\eta = \left[(m'_b \sigma_{L_b} + \sigma'_{ci} s')^{1-a'} - m'_b (a'-1) \sigma'^{\,1-a'}_{ci} \ln\left(\frac{r^*}{r_i + L_b} \right) \right]^{\frac{1}{1-a'}} \tag{B- 24}$$

Equating and simplifying the above equations leads to the following equations:

$$\frac{r_e^*}{r_i + L_b} = e^q \tag{B- 25}$$

where

$$q = \frac{(m_b'\sigma_L + \sigma_{ci}'s')^{1-a'} - \left[s'\sigma_{ci}' + P_o m_b' + \frac{m_b m_b' \sigma_{ci}}{8} - \frac{m_b'}{8}(16P_o m_b \sigma_{ci} + m_b^2\sigma_{ci}^2 + 16\sigma_{ci}^2 s)^{\frac{1}{2}} \right]^{1-a'}}{m_b'(a'-1)\sigma_{ci}'^{(1-a')}} \tag{B- 26}$$

where

$$\sigma_L = \frac{\frac{\xi}{\sigma_{ci1}} - s_1}{\frac{m_{b1}}{\sigma_{ci1}}} \tag{B-18}$$

$$\xi = \left[(m_{b1}\sigma_\rho + \sigma_{ci1}s_1)^{1-a'} - m_{b1}(a'-1)\sigma_{ci1}{}^{1-a'} \ln\left(\frac{r_i + L_b}{\rho}\right) \right]^{\frac{1}{1-a'}} \tag{B-19}$$

and

$$\sigma_\rho = \frac{\Gamma^* - s^*}{\frac{m_b^*}{\sigma_{ci}^*}} \tag{B-1}$$

$$\Gamma^* = \left[s^{*1-a} - m_b^*(a-1)\ln\left(\frac{\rho}{r_i}\right) \right]^{\frac{1}{1-a}} \tag{B-2}$$

The above equation can be written as follows to have the proper form

$$\frac{\rho}{r_i} = e^h \tag{B-16}$$

$$h = \frac{s^{*\,1-a} - \Gamma^{*1-a}}{m_b^*(a-1)} \tag{B-17}$$

and

$$\frac{r_i + L_b}{\rho} = e^t \tag{B- 27}$$

where

$$t = \frac{(m_{b1}\sigma_\rho + s_1\sigma_{ci1})^{1-a'} - (m_{b1}\sigma_L + s_1\sigma_{ci1})^{1-a'}}{m_{b1}(a'-1)\sigma_{ci1}^{\;1-a'}} \tag{B- 28}$$

Taking into account the Equations B-25, B-16, and B-27:

$$\frac{r_e^*}{r_i} = e^q \cdot e^h \cdot e^t = e^{(q+h+t)} \tag{B- 29}$$

APPENDIX C

SPREADSHEET IMPLEMENTATION OF THE PROPOSED ANALYTICAL SOLUTION

Table C-1 Spreadsheet implementing the proposed elasto-plastic solution

Design of the grouted bolts based on an elastic-plastic solution for circular tunnels in Hoek & Brown media [27 06 2006] Prepared by: Reza R Osgoui							**Middle East Technical University**	
Input and Output								
ri(m)	2		**Stresses analysis**					
Po (MPa)	15		**Stress in plastic zone**		**Strains and displacements Analysis**			
E(Gpa)	5.7		G(Mpa)	2192.30769	**Strains in elastic zone**			
ν	0.3		k(Mpa)	4750	εr	-1.05E-02		
σci	30				εθ	1.32E-02		
ψ	0		σθ(MPa)	1.30766968				
mb	1.7		M	2.96E-01				
s	3.90E-03		σre(MPa)	6.12E+00				
mb'	0.85				**Strains in plastic zone**			
s'	1.90E-03		**Ω**	0.057	elastic	εre	-8.95E-05	
a	0.5		σr(MPa)	0.0000	strains	εθe	2.09E-04	
S	1		re(m)	4.83361934				
σci'	30						Brown BC	
r(m)	2				plastic	εθp	1.40E-02	
a'	0.5		**Stress in elastic zone**		strains	εrp		
Nψ	1.0		σθ(MPa)	66.8779697				
λ(integrand)	0.73202		σr(MPa)	-36.8779697				
Pi(Mpa)	0.00					εrt	-8.95E-05	
γ(MN/m3)	2.40E-02				total strains	εθt	1.42E-02	
Maximum radial distance (to plot results)								
Rmax [m]:	10		(Rmax)					
Grouted rock bolt configurations and effect								
λ	0.6	*β*	0.121					
d (mm)	32.00	mb*	0.953					
Cb (kN)	280.00	σci*	33.619					
St (m)	1.00	s*	2.129E-03					
Sl (m)	1.00							
Lb (m)	3.00	mb1	0.747					
ρ(m)	3.27	σci1	26.381					
		s1	1.671E-03					

Table C-1 (continued)

Unsupported Tunnel case							
Boundary conditions							
ur1 [m]:	0.00979127						
ur1P [m]:	0.0098						
Solution for the elastic region							
point	r [m]	rho	sigr [MPa]	sigt [MPa]	ur [m]		
1	10.0000	2.069	12.9249	17.0751	0.0047		
2	9.7281	2.013	12.8073	17.1927	0.0049		
3	9.4562	1.956	12.6793	17.3207	0.0050		
4	9.1843	1.900	12.5399	17.4601	0.0052		
5	8.9123	1.844	12.3875	17.6125	0.0053		
6	8.6404	1.788	12.2205	17.7795	0.0055		
7	8.3685	1.731	12.0369	17.9631	0.0057		
8	8.0966	1.675	11.8345	18.1655	0.0058		
9	7.8247	1.619	11.6107	18.3893	0.0060		
10	7.5528	1.563	11.3623	18.6377	0.0063		
11	7.2809	1.506	11.0855	18.9145	0.0065		
12	7.0089	1.450	10.7759	19.2241	0.0068		
13	6.7370	1.394	10.4280	19.5720	0.0070		
14	6.4651	1.338	10.0353	19.9647	0.0073		
15	6.1932	1.281	9.5898	20.4102	0.0076		
16	5.9213	1.225	9.0815	20.9185	0.0080		
17	5.6494	1.169	8.4980	21.5020	0.0084		
18	5.3774	1.113	7.8239	22.1761	0.0088		
19	5.1055	1.056	7.0391	22.9609	0.0093		
20	4.8336	1.000	6.1183	23.8817	0.0098		
(pt_E)	(r_E)	(rho_E)	(sigr_E)	(sigt_E)	(ur_E)		
Solution for the plastic region							
point	r [m]	rho	sigr [MPa]	sigt [MPa]	Ω	λ(integrand)	ur [m]
1	4.8336	1.0000	6.1183	18.6771	5.2575	0.0000	0.0098
2	4.6845	0.9691	5.7309	17.8902	4.9283	0.0614	0.0103
3	4.5353	0.9383	5.3442	17.0910	4.5996	0.1209	0.0107
4	4.3862	0.9074	4.9585	16.2790	4.2718	0.1782	0.0113
5	4.2371	0.8766	4.5746	15.4540	3.9454	0.2334	0.0118
6	4.0879	0.8457	4.1929	14.6154	3.6210	0.2864	0.0124
7	3.9388	0.8149	3.8144	13.7631	3.2992	0.3370	0.0130
8	3.7897	0.7840	3.4399	12.8964	2.9809	0.3852	0.0137
9	3.6405	0.7532	3.0705	12.0151	2.6669	0.4310	0.0144
10	3.4914	0.7223	2.7075	11.1188	2.3583	0.4741	0.0151
11	3.3422	0.6915	2.3524	10.2071	2.0566	0.5146	0.0159
12	3.1931	0.6606	2.0071	9.2799	1.7631	0.5522	0.0168
13	3.0440	0.6297	1.6739	8.3367	1.4798	0.5868	0.0178
14	2.8948	0.5989	1.3552	7.3776	1.2090	0.6184	0.0188
15	2.7457	0.5680	1.0545	6.4025	0.9534	0.6467	0.0200
16	2.5966	0.5372	0.7757	5.4116	0.7164	0.6715	0.0212
17	2.4474	0.5063	0.5238	4.4055	0.5023	0.6927	0.0226
18	2.2983	0.4755	0.3050	3.3850	0.3162	0.7100	0.0242
19	2.1491	0.4446	0.1270	2.3517	0.1650	0.7232	0.0259
20	2.0000	0.4138	0.0000	1.3077	0.0570	0.7320	0.0279
(pt_P)	(r_P)	(rho_P)	(sigr_P)	(sigt_P)	(c_k1)		(ur_P)

Table C-1 (continued)

Grouted Bolts Effect Min.Yielding							
Boundary conditions							
ur1 [m]:	0.008861415						
ur1P [m]:	0.0089						
Solution for the elastic region							
point	r [m]	rho	sigr [MPa]	sigt [MPa]	ur [m]		
1	10.0000	2.286	13.3003	16.6997	0.0039		
2	9.7039	2.218	13.1950	16.8050	0.0040		
3	9.4079	2.151	13.0796	16.9204	0.0041		
4	9.1118	2.083	12.9528	17.0472	0.0043		
5	8.8157	2.015	12.8130	17.1870	0.0044		
6	8.5196	1.948	12.6583	17.3417	0.0046		
7	8.2236	1.880	12.4867	17.5133	0.0047		
8	7.9275	1.812	12.2954	17.7046	0.0049		
9	7.6314	1.744	12.0815	17.9185	0.0051		
10	7.3353	1.677	11.8411	18.1589	0.0053		
11	7.0393	1.609	11.5698	18.4302	0.0055		
12	6.7432	1.541	11.2620	18.7380	0.0057		
13	6.4471	1.474	10.9108	19.0892	0.0060		
14	6.1510	1.406	10.5076	19.4924	0.0063		
15	5.8550	1.338	10.0418	19.9582	0.0066		
16	5.5589	1.271	9.4996	20.5004	0.0070		
17	5.2628	1.203	8.8633	21.1367	0.0074		
18	4.9667	1.135	8.1098	21.8902	0.0078		
19	4.6707	1.068	7.2086	22.7914	0.0083		
20	4.3746	1.000	6.1183	23.8817	0.0089		
(pt_E)	(r_E)	(rho_E)	(sigr_E)	(sigt_E)	(ur_E)		
Solution for the plastic region							
point	r [m]	rho	sigr [MPa]	sigt [MPa]	Ω	λ(integrand)	ur [m]
1	4.3746	1.0000	6.1183	18.6771	5.8995	0.0000	0.0089
2	4.2496	0.9714	5.7168	17.8612	5.5171	0.0463	0.0092
3	4.1246	0.9429	5.3174	17.0350	5.1366	0.0909	0.0097
4	3.9996	0.9143	4.9206	16.1983	4.7587	0.1340	0.0101
5	3.8747	0.8857	4.5272	15.3509	4.3839	0.1754	0.0105
6	3.7497	0.8572	4.1377	14.4925	4.0129	0.2152	0.0110
7	3.6247	0.8286	3.7532	13.6232	3.6467	0.2531	0.0115
8	3.4997	0.8000	3.3745	12.7426	3.2860	0.2892	0.0120
9	3.3748	0.7714	3.0029	11.8508	2.9320	0.3234	0.0126
10	3.2498	0.7429	2.6397	10.9476	2.5860	0.3556	0.0132
11	3.1248	0.7143	2.2863	10.0330	2.2494	0.3858	0.0138
12	2.9998	0.6857	1.9447	9.1071	1.9240	0.4139	0.0145
13	2.8748	0.6572	1.6170	8.1700	1.6118	0.4398	0.0153
14	2.7499	0.6286	1.3056	7.2219	1.3152	0.4633	0.0161
15	2.6249	0.6000	1.0136	6.2631	1.0371	0.4845	0.0169
16	2.4999	0.5715	0.7446	5.2941	0.7809	0.5031	0.0178
17	2.3749	0.5429	0.5029	4.3153	0.5506	0.5190	0.0189
18	2.2500	0.5143	0.2937	3.3268	0.3514	0.5322	0.0200
19	2.1250	0.4858	0.1234	2.3275	0.1892	0.5424	0.0212
20	2.0000	0.4572	0.0000	1.3077	0.0716	0.5494	0.0226
(pt_P)	(r_P)	(rho_P)	(sigr_P)	(sigt_P)	(c_k1)		(ur_P)

Table C-1 (continued)

Grouted Bolts Effect Major.Yielding							
Boundary conditions							
ur1 [m]:	0.009601653						
ur1P [m]:	0.0096						
Solution for the elastic region							
point	r [m]	rho	sigr [MPa]	sigt [MPa]	ur [m]		
1	10.0000	2.110	13.0045	16.9955	0.0046		
2	9.7232	2.051	12.8892	17.1108	0.0047		
3	9.4463	1.993	12.7637	17.2363	0.0048		
4	9.1695	1.934	12.6266	17.3734	0.0050		
5	8.8926	1.876	12.4765	17.5235	0.0051		
6	8.6158	1.818	12.3118	17.6882	0.0053		
7	8.3390	1.759	12.1303	17.8697	0.0055		
8	8.0621	1.701	11.9299	18.0701	0.0056		
9	7.7853	1.642	11.7076	18.2924	0.0058		
10	7.5084	1.584	11.4604	18.5396	0.0061		
11	7.2316	1.526	11.1842	18.8158	0.0063		
12	6.9547	1.467	10.8743	19.1257	0.0065		
13	6.6779	1.409	10.5252	19.4748	0.0068		
14	6.4011	1.350	10.1297	19.8703	0.0071		
15	6.1242	1.292	9.6795	20.3205	0.0074		
16	5.8474	1.234	9.1637	20.8363	0.0078		
17	5.5705	1.175	8.5692	21.4308	0.0082		
18	5.2937	1.117	7.8790	22.1210	0.0086		
19	5.0169	1.058	7.0714	22.9286	0.0091		
20	4.7400	1.000	6.1183	23.8817	0.0096		
(pt_E)	(r_E)	(rho_E)	(sigr_E)	(sigt_E)	(ur_E)		
Solution for the plastic region							
point	r [m]	rho	sigr [MPa]	sigt [MPa]	Ω	λ(integrand)	ur [m]
1	4.7400	1.0000	6.1183	18.6771	5.8995	0.0000	0.0096
2	4.5958	0.9696	5.7168	17.8612	5.5171	0.0582	0.0101
3	4.4516	0.9392	5.3174	17.0350	5.1366	0.1145	0.0105
4	4.3074	0.9087	4.9206	16.1983	4.7587	0.1689	0.0110
5	4.1632	0.8783	4.5272	15.3509	4.3839	0.2211	0.0115
6	4.0190	0.8479	4.1377	14.4925	4.0129	0.2713	0.0121
7	3.8747	0.8175	3.7532	13.6232	3.6467	0.3192	0.0127
8	3.7305	0.7870	3.3745	12.7426	3.2860	0.3649	0.0133
9	3.5863	0.7566	3.0029	11.8508	2.9320	0.4082	0.0140
10	3.4421	0.7262	2.6397	10.9476	2.5860	0.4490	0.0147
11	3.2979	0.6958	2.2863	10.0330	2.2494	0.4873	0.0155
12	3.1537	0.6653	1.9447	9.1071	1.9240	0.5228	0.0164
13	3.0095	0.6349	1.6170	8.1700	1.6118	0.5556	0.0173
14	2.8653	0.6045	1.3056	7.2219	1.3152	0.5855	0.0183
15	2.7211	0.5741	1.0136	6.2631	1.0371	0.6122	0.0193
16	2.5768	0.5436	0.7446	5.2941	0.7809	0.6357	0.0205
17	2.4326	0.5132	0.5029	4.3153	0.5506	0.6558	0.0218
18	2.2884	0.4828	0.2937	3.3268	0.3514	0.6722	0.0233
19	2.1442	0.4524	0.1234	2.3275	0.1892	0.6848	0.0249
20	2.0000	0.4219	0.0000	1.3077	0.0716	0.6932	0.0268
(pt_P)	(r_P)	(rho_P)	(sigr_P)	(sigt_P)	(c_k1)		(ur_P)

Table C-1 (continued)

Grouted Bolts Effect Exceeding.Yielding							
Boundary conditions							
ur1 [m]:	0.009663988						
ur1P [m]:	0.0100						
Solution for the elastic region							
point	r [m]	rho	sigr [MPa]	sigt [MPa]	ur [m]		
1	10.0000	2.096	12.9785	17.0215	0.0046		
2	9.7248	2.038	12.8624	17.1376	0.0047		
3	9.4496	1.981	12.7361	17.2639	0.0049		
4	9.1743	1.923	12.5982	17.4018	0.0050		
5	8.8991	1.865	12.4474	17.5526	0.0052		
6	8.6239	1.808	12.2819	17.7181	0.0053		
7	8.3487	1.750	12.0997	17.9003	0.0055		
8	8.0734	1.692	11.8986	18.1014	0.0057		
9	7.7982	1.635	11.6758	18.3242	0.0059		
10	7.5230	1.577	11.4281	18.5719	0.0061		
11	7.2478	1.519	11.1517	18.8483	0.0064		
12	6.9726	1.462	10.8419	19.1581	0.0066		
13	6.6973	1.404	10.4931	19.5069	0.0069		
14	6.4221	1.346	10.0986	19.9014	0.0072		
15	6.1469	1.288	9.6498	20.3502	0.0075		
16	5.8717	1.231	9.1365	20.8635	0.0079		
17	5.5965	1.173	8.5457	21.4543	0.0082		
18	5.3212	1.115	7.8607	22.1393	0.0087		
19	5.0460	1.058	7.0607	22.9393	0.0091		
20	4.7708	1.000	6.1183	23.8817	0.0097		
(pt_E)	(r_E)	(rho_E)	(sigr_E)	(sigt_E)	(ur_E)		
Solution for the plastic region							
point	r [m]	rho	sigr [MPa]	sigt [MPa]	Ω	λ(integrand)	ur [m]
1	4.7708	1.0000	6.1183	18.6771	5.8995	0.1565	0.0100
2	4.6250	0.9694	5.7168	17.8612	5.5171	0.2027	0.0105
3	4.4791	0.9389	5.3174	17.0350	5.1366	0.2474	0.0109
4	4.3333	0.9083	4.9206	16.1983	4.7587	0.2905	0.0114
5	4.1875	0.8777	4.5272	15.3509	4.3839	0.3319	0.0119
6	4.0416	0.8472	4.1377	14.4925	4.0129	0.3716	0.0125
7	3.8958	0.8166	3.7532	13.6232	3.6467	0.4096	0.0131
8	3.7500	0.7860	3.3745	12.7426	3.2860	0.4457	0.0137
9	3.6041	0.7555	3.0029	11.8508	2.9320	0.4799	0.0143
10	3.4583	0.7249	2.6397	10.9476	2.5860	0.5121	0.0151
11	3.3125	0.6943	2.2863	10.0330	2.2494	0.5423	0.0158
12	3.1666	0.6638	1.9447	9.1071	1.9240	0.5704	0.0167
13	3.0208	0.6332	1.6170	8.1700	1.6118	0.5962	0.0176
14	2.8750	0.6026	1.3056	7.2219	1.3152	0.6198	0.0185
15	2.7292	0.5721	1.0136	6.2631	1.0371	0.6409	0.0196
16	2.5833	0.5415	0.7446	5.2941	0.7809	0.6595	0.0208
17	2.4375	0.5109	0.5029	4.3153	0.5506	0.6755	0.0221
18	2.2917	0.4804	0.2937	3.3268	0.3514	0.6886	0.0236
19	2.1458	0.4498	0.1234	2.3275	0.1892	0.6988	0.0253
20	2.0000	0.4192	0.0000	1.3077	0.0716	0.7059	0.0272
(pt_P)	(r_P)	(rho_P)	(sigr_P)	(sigt_P)	(c_k1)		(ur_P)

Table C-1 (continued)

Case I. re*<ρ< (a+L) minimal yielding			
			Pi Effect
	Y	0.783	**0.783**
	re*	4.375	**4.375**
Case II. ρ<re*< (a+L) major yielding			
	Γ*		0.079
	σρ		2.710
	h		0.493
	J		0.370
	re*		4.740
Case III. re*>(a+L) excessive yielding			
	Γ*	0.079	
	σρ	2.710	
	h	0.493	
	ξ	5.068	
	σL	6.722	
	t	0.423	
	q	-0.047	
	re*	4.771	

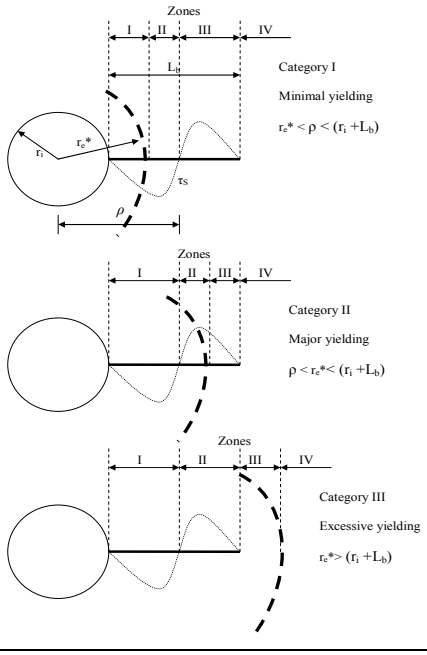

APPENDIX D

FLAC CODES FOR THE IMPLEMENTAION AND VERIFICATION OF THE ANALYTICAL MODEL

```
;FLAC CODES FOR IMPLEMENTATION AND VERIFICATION
;OF THE PROPOSED ELASTO-PLASTIC ANALYTICAL MODEL
;Performed by Ing. Reza Osgoui
;GENERATION OF THE MODEL AND GRIDS
config extra = 8
grid 120,120
gen 0,0 0,30 30,30 30,0 i=1,121 j=1,121
;Constitutive model for rock yield condition:
;HOEK-BROWN (Non-Associated flow rule)
model mohr
c hoek.fis
; FISH routine for Hoek-Brown failure surface
; the dilation angle is specified using hoek_psi
; (hoek_psi = fi for an associated flow rule)
;
def cfi
  loop i (1,izones)
    loop j (1,jzones)
      if state(i,j) > 0 then
         h_mm=hb_mmr
         h_ss=hb_ssr
      else
         h_mm=hb_mmi
         h_ss=hb_ssi
      end_if
```

```
      effsxx = sxx(i,j)  + pp(i,j)
      effsyy = syy(i,j)  + pp(i,j)
      effszz = szz(i,j)  + pp(i,j)
      tension(i,j)=0.5*hb_sc*(sqrt(h_mm^2+4*h_ss)-h_mm)
      temp1=-0.5*(effsxx+effsyy)
      temp2=sqrt(sxy(i,j)^2+0.25*(effsxx-effsyy)^2)
      s3=min(temp1-temp2,-effszz)
      if s3<0.0 then
        s3=0.0
      end_if
      h_lam=1+0.5*h_mm*hb_sc/sqrt(h_mm*hb_sc*s3+hb_sc^2*h_ss)
      fi=2*atan(sqrt(h_lam))/degrad-90
      friction(i,j)=fi
      sci=s3*(1-h_lam)+sqrt(h_mm*s3*hb_sc+hb_sc^2*h_ss)
      coe=0.5*sci/sqrt(h_lam)
      cohesion(i,j)=coe
      psi = hoek_psi
      dilation(i,j)=psi
    end_loop
  end_loop
end

def supstep
  cfi
  if ns=0 then
    ns=5
  end_if
  command
    step ns
    print k
  end_command
end

def supsolve
```

```
loop k (1,nsup)
  supstep
end_loop
end

set hb_sc=30 hb_mmi=1.7 hb_ssi=.0039 hb_mmr=.85 hb_ssr=.0019
set hoek_psi=0
set ns=5 nsup=4000
unmark
;GENERATION OF TUNNEL
gen arc 0,0 2,0 90
gen adjust
;BOUNDARY CONDITIONS ( constrains and pressure)
fix y j=1
fix x i=1
apply pressure=15 i=121
apply pressure=15 j=121
;ROCK MASS PROPERTIES (ELASTIC CONDITION)
prop dens=0.0020 bulk=4750 shear=2192
prop cohesion=200 friction=50
prop dilation=0 tension=200
;STRESS INITIALAZATION INSIDE THE ELEMENTS
ini syy=-15
ini sxx=-15
ini szz=-9
;CALCULATION STEPS
;(LITHOSTATIC CONVERGENCE IN ELASTIC CONDITION)
step 50000
;INITIATION OF THE VELOCITIES
ini xdis=0 ydis=0 xvel=0 yvel=0
supsolve
save selastic 1306.sav
;Assignmnet of the dispacement and velocities of
;the model(INITIAL CONDITION)
```

```
ini xdis=0 ydis=0 xvel=0 yvel=0
;EXCAVATION OF THE TUNNEL
model null reg 1 1



;EVALUATION OF PRESSURE ON TUNNEL PERIMETER
;FIXING OF NODES ON TUNNEL PERIMETER
fix x y mark
;ONE CALCULATION STEP TO READ INTERNAL PRESSURE
step 1
;CALLING FISH CODES
call find_rf.dat
def FIND_RF
  loop i(1,izones+1)
    loop j(1,jzones+1)
      if and (flags(i,j), 128) = 128 then
        ex_4(i,j)=xforce(i,j)
        ex_5(i,j)=yforce(i,j)
      end_if
    end_loop
  end_loop
end
FIND_RF
;FREEING NODES ON THE TUNNEL PERIMETER
free x y mark

fix x i=1 j=9
fix y j=1 i=9
;CALLING FISH CODES TO REDUCE INTERNAL PRESSURE
call app_rf.dat
def APP_RF

 loop ii(2,9)
  loop jj(2,9)
```

```
    if and (flags(ii, jj), 128) = 128 then
      xaf=-ex_4(ii, jj) * perc_car
      yaf=-ex_5(ii, jj) * perc_car
      command
        apply xforce xaf yforce yaf i=ii j=jj
      end_command
    end_if
  end_loop
end_loop

loop ii(1,1)
  loop jj(9,9)
    if and (flags(ii, jj), 128) = 128 then
      yaf=-ex_5(ii, jj) * perc_car
      command
        apply yforce yaf i=ii j=jj
      end_command
    end_if
  end_loop
end_loop


loop ii(9,9)
  loop jj(1,1)
    if and (flags(ii, jj), 128) = 128 then
      xaf=-ex_4(ii, jj) * perc_car
      command
        apply xforce xaf i=ii j=jj
      end_command
    end_if
  end_loop
end_loop

end
```

```
set perc_car=0.9
APP_RF
supsolve
save s901306.sav

set perc_car=0.8
APP_RF
supsolve
save s801306.sav

set perc_car=0.7
APP_RF
supsolve
save s701306.sav

set perc_car=0.6
APP_RF
supsolve
save s601306.sav

; THE SUPPORT PRESSUREAT THE TIME OF REINFORCEMENT
;INSTALATION IN FACE IS 60 % OF TOTAL PRESSURE
;installation of grouted rock bolts in radial form
struct prop=2 E=210000 area=.000804 yield=.28 sbond=.1131 kbond=11.11
struct cable begin grid 9,3 end 4.8296,1.2941 seg=15 prop=2
struct cable begin grid 7,7 end 3.5356,3.5356 seg=15 prop=2
struct cable begin grid 3,9 end 1.2941,4.8296 seg=15 prop=2

set perc_car=0.5
APP_RF
supsolve
save s501306.sav

set perc_car=0.4
```

```
APP_RF
supsolve
save s401306.sav

set perc_car=0.3
APP_RF
supsolve
save s301306.sav

set perc_car=0.2
APP_RF
supsolve
save s201306.sav

set perc_car=0.1
APP_RF
supsolve
save s101306.sav

set perc_car=0
APP_RF
supsolve
save s01306.sav

save supportedbolt 1306.sav
```

CURRICULUM VITAE

PERSONAL INFORMATION

Surname, Name: Rangsaz Osgoui, Reza
Nationality: Iranian (IR)
Date and Place of Birth: 9 June 1975 , Tehran
Marital Status: Single
Phone: +39 329 066 18 97
email: reza_tunnelling@yahoo.it

EDUCATION

Degree	Institution	Year of Graduation
PhD	Middle East Technical University (METU), Rock Mechanics, Mining Engineering Department.	2006
MSc (Second)	Politecnico di Torino, Tunnelling and Tunnel Boring Machines (TBMs)	2006
MSc	Tehran Azad University, Mining Engineering Department	2000
BSc	Tehran Azad University, Mining Engineering Department	1997

WORK EXPERIENCE

Year	Place	Enrollment
2006- Present	GEODATA , Torino	Consultant Engineer
2001-2005	METU Department of Mining Engineering	Research and Teaching Assistant

FOREIGN LANGUAGES

Advanced English, Advanced Turkish, Basic Italian

RECENT PUBLICATIONS

1. Osgoui, R. & Ünal, E. Rock reinforcement design for unstable tunnel originally excavated in poor rock mass. Proc. World Tunnel Congress and 31st ITA Assembly. 291-296. Turkey. 2005.

2. Osgoui, R. & Ünal, E. Characterization of Weak Rock Masses Using GSI and the Estimation of Support Pressure. 40th U.S. Rock Mechanics Symposium - June 25-29, Anchorage, Alaska. 2005.

3. Osgoui, R. On the Assessment of the effect of the anisotropy in in-situ stress on support pressure in tunnels. Proc. Int. Symp. In-Situ Rock Stress, Trondheim, Norway. 2006.

HOBBIES

Running (about 40 km per week), Ritmos Latino, Fitness.